Cyprus University of Technology

Faculty of Engineering and Technology

**Doctoral Dissertation**

# A STUDY OF ALTERNATIVE HYDROLOGICAL RESPONSE UNITS (HRU) CONFIGURATIONS IN THE CONTEXT OF GEOGRAPHICAL INFORMATION SYSTEMS (GIS) - BASED DISTRIBUTED HYDROLOGICAL MODELING

**Eleni Savvidou**

**Limassol, May 2018**

CYPRUS UNIVERSITY OF TECHNOLOGY

FACULTY OF ENGINEERING AND TECHNOLOGY

DEPARTMENT OF CIVIL ENGINEERING AND GEOMATICS

Doctoral Dissertation

# A STUDY OF ALTERNATIVE HYDROLOGICAL RESPONSE UNITS (HRU) CONFIGURATIONS IN THE CONTEXT OF GEOGRAPHICAL INFORMATION SYSTEMS (GIS) - BASED DISTRIBUTED HYDROLOGICAL MODELING

Eleni Savvidou

Limassol, May 2018

# Approval Form

Doctoral Dissertation

## A STUDY OF ALTERNATIVE HYDROLOGICAL RESPONSE UNITS (HRU) CONFIGURATIONS IN THE CONTEXT OF GEOGRAPHICAL INFORMATION SYSTEMS (GIS) - BASED DISTRIBUTED HYDROLOGICAL MODELING

Presented by

Eleni Savvidou

Supervisor: Assistant Professor Dimitrios Skarlatos, Faculty of Engineering and Technology, Cyprus University of Technology

Signature _____

Member of the committee: Professor Athanasios Loukas, Department of Civil Engineering, University of Thessaly

Signature _____

Member of the committee: Professor Phaedon C. Kyriakidis, Faculty of Engineering and Technology, Cyprus University of Technology

Signature _____

Cyprus University of Technology

Limassol, May 2018

## Copyrights

I would like to express my sincere gratitude to my research supervisor Dr. Dimitrios Skarlatos for the continuous support throughout my Ph.D study, for his patience, motivation, and immense knowledge and for allowing me to grow as a research scientist. His guidance helped me in all the time of research and writing of this thesis. I would also like to thank Dr. Antonis Koussis for his insightful comments and encouragement, and also for giving me direction to widen my research from various perspectives. My sincere thanks also go to Dr. Andreas Efstratiadis and Dr Ourania Tzoraki who provided me an opportunity to join their team as a research student, and who provided me with invaluable knowledge and skills and guided me to complete my research. Without they precious support it would not be possible to conduct this research. Last but not the least, I would like to thank my husband, my parents and sister for supporting me spiritually throughout writing this thesis and my life in general.

# ABSTRACT

A new methodology for delineating Hydrological Response Units (HRUs), based on the widely used runoff Curve Number (CN) concept, is proposed, aiming to provide a systematic and physically-consistent procedure for the delineation of HRUs in the context of hybrid semi-distributed hydrological models. Given that the hydrological and engineering community has great experience in estimating the CN parameter on the basis of easily-retrieved geographical information, a methodology for delineating HRUs is proposed and tested, based on distributed CN maps, along with guidelines for its optimal use. Their formulation is an extension of the standard SCS approach, with the use of an empirical expression accounting for three major physiographic characteristics, by means of indices of: (a) soil permeability, evaluated according to the hydraulic properties of the soil and the unsaturated zone, and the dominant geological formations; (b) land use/land cover characteristics, typically expressed in terms of vegetation density; and (c) drainage capacity, evaluated according to the geomorphological characteristics of the basin (mainly the terrain slope) and the existence of runoff retention structures.

The map of CN classes is eventually used within model parameterization, to identify the essential number and spatial extent of HRUs and, consequently, the number of control variables of the calibration problem.

The proposed approach aims, on the one hand, at reducing subjectivity introduced by the definition of HRUs and providing parsimonious modelling schemes, on the other. In particular, the modified CN-based parameterization: (1) allows the user to assign as many parameters as can be supported by the available hydrological information, (2) associates the model parameters with anticipated basin responses, as quantified in terms of CN-classes across HRUs, and (3) reduces the effort for model calibration, simultaneously ensuring good predictive capacity.

The proposed approach is demonstrated and tested in semi-arid river basins with intermitted low. In the hydrological simulation of the Nedontas River Basin, Greece, parameterizations of different complexities are employed in the HYDROGEIOS modelling framework. A modelling experiment with a varying number of HRUs, where the parameter estimation problem was handled through automatic optimization, showed

that the parameterization with three HRUs, i.e., equal to the number of flow records, ensured the optimal performance. Similarly, tests with alternative HRU configurations confirmed that the optimal scores, both in calibration and validation, were achieved by the CN-based approach, also resulting in parameters values across the HRUs that were in agreement with their physical interpretation. The approach is further tested in two other river basins, Yialias and Kouris river basins, Cyprus, two watersheds of different sizes that vary in terms of physiographic characteristics and meteorological stresses, ideal to evaluate the performance of the method in diverse environments. Different classification schemes were implemented in creating the CN sub-sets to delineate the final HRUs, in an attempt to emphasize the advantage of the association of each HRU response to the corresponding parameter values in terms of CN, thus, allowing for a more efficient and objective model set up, assuring the parameters' physical meaning and realistic representation of the hydrological behaviour of the basin. Hence, through a proper classification of CNs, the user can determine a priori a reasonable and relatively narrow range of feasible parameter bounds, which is of key importance towards ensuring effective and efficient calibrations. Finally, the sensitivity of the approach on each of the three major physiographic characteristics was investigated to provide further insight as to what impact each characteristic has on the HRU delineation processes, and thus, model performance.

**Keywords:** hydrological response units, distributed hydrological modeling, curve number, GIS, parameterization, calibration.

# TABLE OF CONTENTS

# LIST OF TABLES

LIST OF FIGURES

# LIST OF ABBREVIATIONS

| | |
|---|---|
| AGNPS | Agricultural Non-Point Source |
| AI | Artificial Intelligence |
| AMC | Antecedent Soil Moisture Condition |
| ANN | Artificial Neural Networks |
| AnnAGNPS | Annualized Agricultural Non-Point Source |
| ANSWERS | Area Non-Point Source Watershed Environment Response Simulation |
| ASA | Aggregated Simulation Area |
| BMP | Best Management Practices |
| CASC2D | CASCade of Planes in 2-Dimensions |
| CLC | Corine Land Cover |
| CN | Curve Number |
| CSA | Critical Source Area |
| DEM | Digital Elevation Model |
| EPIC | Erosion Productivity Impact Calculator |
| ER | Evapotranspiration |
| FL | Fuzzy Logic |
| FU | Functional Units |
| GA | Genetic Algorithms |
| GIS | Geographical Information System |
| GLUE | Generalized Likelihood Uncertainty Estimation |
| GSSHA | Gridded Surface Hydrologic Analysis |
| HAND | Height Above the Nearest Drainage |

| | |
|---|---|
| HEC-1/HEC-HMS | Hydrologic Engineering Centre Hydrologic Modelling System |
| HRU | Hydrologic Response Unit |
| HSG | Hydrological Soil Group |
| HSPF | Hydrological Simulation Program-FORTRAN |
| HSU | Hydrologically Similar Units |
| KINEROS2 | KINematic Runoff and EROSion |
| LU / LC | Land Use / Land Cover |
| MIKE SHE | Systéme Hydrologique Européen, |
| MUSCLE | Modified Universal Soil Loss Equation |
| NRCS | Natural Resources Conservation Service |
| PET | Potential Evapotranspiration |
| PRMS/MMS | Precipitation-Runoff Modelling System / Modular Modelling System |
| REA | Representative Elementary Area |
| REW | Representative Elementary Watershed |
| SCS | Soil Conservation Service |
| SRTM | Shuttle Radar Topography Mission |
| SWAT | Soil and Water Assessment Tool |
| TDA | Threshold Drainage Area |

# 1 Introduction

Based on their spatial scale of process representation, hydrological models are generally categorized from lumped to distributed. In the former, the watershed is considered as a single unit that responds homogeneously to its spatially-averaged meteorological inputs, while the model parameters are only associated with the macroscopic properties of the watershed as a whole. In this context, the only means to establish a lumped modelling scheme of satisfactory predictive capacity is to infer its parameters through calibration.

In contrast, distributed "physically-based" models explicitly account for the spatial heterogeneities of physiographic characteristics, meteorological inputs, hydrological processes and boundary conditions, via discretization of the model domain in finely-resolved computational units. The fundamental laws of hydraulics and semi-empirical hydrological formulae are applied at each spatial unit, which allows, in theory, to estimate all model parameters from field data.

The advantages and disadvantages of the two approaches have been widely discussed in the literature. The widely-accepted conclusion is that lumped models cannot represent the spatial variability of the basin processes, while fully-distributed models are data and time demanding. Nevertheless, despite their different backgrounds, both approaches suffer from uncertainties related to the estimation of their parameters. In fact, from the introduction of physically-based models, the hydrological community has criticized them as overly complex, over-parameterized and difficult to use, while challenging their ability to apply parameters that are directly measured in the field without some kind of calibration. The reasonable argument behind this criticism is that the physical properties are measured at the point scale, while the parameters are assigned to the grid-cell scale, thus by definition conceptual. Hence, given that distributed models are comprised by many parameters, they are vulnerable to the well-known shortcomings of calibration, i.e., the equifinality problem. However, it is argued that in some situations, the use of process-based models varies from necessary to most appropriate, especially when knowledge of flow paths or distributed state variables and/or preservation of physical constraints is important.

For many problems of everyday practice requiring flow predictions at a relatively small number of points across the river network, semi-distributed models are broadly recognized as a good compromise between lumped and fully-distributed approaches.

The key concept is to divide the watershed into a number of sub-basins and propagate the runoff generated from each sub-basin through the river network (and similarly for the subsurface processes). Although at the sub-basin scale, the modelling remains lumped (except for certain cases, in which sub-basins are further divided into smaller units), at the watershed scale, the heterogeneities are partially accounted for by assigning different meteorological inputs and different properties to each sub-basin. Another advantage of semi-distributed schemes is the representation of flow routing, which is of key importance when fine time steps are employed (e.g., in flood modelling).

The configuration of a semi- or fully-distributed model and the associated level of complexity are determined by the user. This task involves two separate tasks. In particular, the discretization of the watershed predetermines the aggregation patterns of spatial information, i.e., the size and shape of computational elements, and controls the associated topographic parameter values, such as slope, aspect, etc. On the other hand, different delineations of the stream network connectivity and hillslope size affect and can often misrepresent rainfall-runoff processes. Therefore, watershed subdivision has the potential to affect the predictions of hydrological modelling, a subject that has been handled in various ways, while the optimal level of watershed delineation that can provide an adequate representation of the spatial heterogeneity of a watershed is a subject that has received great attention in distributed hydrological modeling.

While it is common practice to partition a watershed into smaller units (e.g., sub-basins), it is not easy to identify a strictly optimal spatial scale. Nevertheless, it is accepted that the sub-watershed size should be adapted to the modelling objectives, as the latter determine the dominant hydrological processes to be considered in simulations. It is feasible to represent the landscape heterogeneity through small sub-watersheds; for large watersheds, however, a fine resolution is often prohibited, mainly by high data requirements. Therefore, in meso- and large-scale watersheds, significant simplifications and reductions are required, in order to aggregate spatial heterogeneity and associated parameters at various levels of watershed subdivision. Increasing the number of sub-watersheds definitely increases input data preparation, computational time and calibration effort; therefore, the sub-watershed-average inputs generated from gauging stations vary with different watershed subdivisions.

Over the years, many watershed subdivision practices have been developed and tested using a variety of well-established models. An obvious approach is to divide the watershed into its natural sub-watersheds, thus preserving the watershed's natural boundaries, flow-paths and channels for realistic water routing. The concepts of critical source area, threshold drainage area and aggregated simulation area have also been used to delineate sub-watersheds within semi-distributed models. Moving from semi- to fully-distributed modelling, more detailed concepts are employed, such as grid elements, Representative Elementary Areas (REAs) and Representative Elementary Watershed (REW).

In the above approaches, the river basin is represented as an assembly of discrete entities of pre-determined geometry (typically, sub-basins, in the case of semi-distributed schemes, and grid cells, in the case of fully-distributed ones), where the heterogeneity of its physical characteristics is not explicitly accounted for. Therefore, the model parameterization is dictated by the discretization, which may result in unjustifiable complexity, due to the large number of associated parameters.

From the mid-990s, attention has been given to physically-based parameterization approaches through the so-called Hydrologic Response Units (HRUs), which generally represent areas with similar land use and soil characteristics. Their implementation is quite simple, since there is no interaction or topological connection between the HRUs; thus, runoff from each HRU is calculated separately and summed together to determine the total runoff from each sub-basin. HRUs are defined as "distributed, heterogeneously structured areas with common land use and pedo-topo-geological associations controlling their unique hydrological dynamics" (Flügel 1995). The assumption of homogeneity is justified by the fact that the dynamics of hydrological processes within an HRU vary only by a small amount compared to the dynamics among different HRUs.

A variation of the above concept requires threshold specification for land cover, soil and slope classes, which is then used to delineate HRUs. The watershed is divided into several sub-basins that are further divided into discontinuous land masses, delineated through aggregation, according to user-defined thresholds for land use, soil type and slope ranges within each sub-watershed; this is followed by a GIS-based spatial overlay scheme, resulting in a "unique combination" HRUs with homogeneous characteristics, representing percentages of the sub-basin area that contribute differently to the entire

watershed responses. The use of thresholds results in apparent loss of information, so it is suggested to be applied only when the number of HRUs delineated results in acceptable computation costs. This approach has been adopted, among others, in SWAT. While the incorporation of HRUs has allowed SWAT the flexibility to adapt from field plots to entire river basins, the fact that HRUs are used in a non-spatial manner is regarded as a key weakness of the model.

An alternative definition of HRUs, is proposed as the product of separate partitions of the basin that account for different properties, such as land use, soil permeability, geology, slope, etc. This product is known as the common refinement of the partitions, while the related procedure in GIS is often called “union of layers”. Using an appropriate classification of the key watershed properties, the number of HRUs and, consequently, the number of parameters are manually adjusted. HRUs do not represent contiguous geographical areas, instead, they represent basin partitions with common characteristics, and thus common parameter values. The shape of this non-contiguous element is of no interest, since at each time step, the runoff generated by HRUs is integrated over sub-basins and propagated to their outlet. This approach has been adopted in their modelling system HYDROGEIOS, in an attempt to make schematization and parameterization two clearly independent procedures.

The key advantage of this approach is its flexibility, since there are no restrictions on the configuration of HRUs, while the availability of data (critical for calibration) does not influence the watershed schematization. However, the fact that the delineation of HRUs is disengaged from watershed schematization does not necessarily ensure efficient, physically-consistent and parsimonious parameterizations, as the modeler is still allowed to determine any combination of layers. In addition, by definition, the number of HRUs is equal to the product of different classes that are accounted for within the formulation of the aforementioned layers. If one wishes to reduce the number of HRUs, one must manually merge the initial HRUs, thus losing information and physical consistency. The above shortcoming was the motivation to develop an improved procedure for HRU delineation, based on the well-established curve number concept, which is even more flexible and, at the same time, easy to implement within any modelling scheme.

All approaches, despite their differences in delineating HRUs, make use of geographical layers of watershed properties that affect runoff dynamics, in order to define areas with approximately homogenous response, and thus parameterization.

The aim of this research is to provide a systematic and physically-consistent procedure for the delineation of HRUs in the context of hybrid semi-distributed hydrological modeling, by taking advantage of the runoff Curve Number concept (CN), which has been widely used as a representative indicator of the catchment's behaviour. Given that the hydrological and engineering community has great experience in estimating the CN parameter on the basis of easily-retrieved geographical information, a methodology for delineating HRUs is proposed and tested, based on distributed CN maps, along with guidelines for its optimal use. Their formulation is an extension of the standard SCS approach, with the use of an empirical expression accounting for three major physiographic characteristics, by means of soil permeability, land use/land cover characteristics and drainage capacity indices. The map of CN classes is eventually used within model parameterization, to identify the essential number and spatial extent of HRUs and, consequently, the number of control variables of the calibration problem. The proposed approach aims, on the one hand, at reducing subjectivity introduced by the definition of HRUs and providing parsimonious modelling schemes, on the other.

The main objective is to propose and test a methodology for delineating HRUs, based on a modified Curve Number (CN) approach. The CN-value accounts for three major physiographic characteristics of the river basin, by means of classes of:

a) soil permeability, evaluated according to the hydraulic properties of the soil and the unsaturated zone, and the dominant geological formations (different criteria are employed in urbanized areas);
b) land use/land cover characteristics, typically expressed in terms of vegetation density; and
c) drainage capacity, evaluated according to the geomorphological characteristics of the basin (mainly the terrain slope) and the existence of runoff retention structures.

A semi-automatic procedure in a GIS environment allows producing basin maps of distributed CN-values as the combination of the three classified layers. The map of CN-values is used in the context of model parameterization, to identify the essential number

and spatial extent of HRUs and, consequently, the number of control variables of the calibration problem.

The new approach aims at reducing the subjectivity introduced by the definition of HRUs, and simultaneously at providing parsimonious modelling schemes. In particular, the modified CN-based parameterization:

1) allows the user to assign as many parameters as can be supported by the available hydrological information
2) associates the model parameters with anticipated basin responses, as quantified in terms of CN-classes across HRUs, and
3) reduces the effort for model calibration, simultaneously ensuring good predictive capacity.

The proposed approach will be demonstrated and tested in semi-arid river basins with intermitted low. In the hydrological simulation of the Nedontas River Basin, Greece, parameterizations of different complexities are employed in the HYDROGEIOS modelling framework. A modelling experiment with a varying number of HRUs will be performed, where the parameter estimation problem was handled through automatic optimization. Additionally, the proposed CN-based method is contrasted with two other well-established HRU delineation strategies, i.e., the unique combination and the union of layers. The approach will be further tested in two other river basins, Yialias and Kouris river basins, Cyprus, two watersheds of different sizes that vary in terms of physiographic characteristics and meteorological stresses, ideal to evaluate the performance of the method in diverse environments. Different classification schemes will be implemented in creating the CN sub-sets to delineate the final HRUs in an attempt to emphasize the advantage of the association of each HRU response to the corresponding parameter values in terms of CN. Moreover, the sensitivity the proposed CN equation will be examined, regarding the weight each physiographic characteristic has on the estimation of the CN.

# 2 Theory

## 2.1 Hydrological modeling

Models are the purposeful simplification of reality (Hammond & McCullagh 1989) and the formal presentation of a theory (Harvey 1967). Models have long been implemented in the field of hydrology, aiming to conceptualize the hydrological cycle (Lacroix 1999) in an attempt to explain the natural processes that transform precipitation into runoff (Kite 1994). Hydrological models are increasingly used, not only to model hydrologic response, but also erosional response, sediment yield and water quality (Lacroix 1999), to forecast streamflow, estimate climate change and expand the understanding of hydrological processes.

### 2.1.1 Model types

According to their spatial scale of process representation, hydrological models are generally classified from lumped to distributed. In the first approach, the watershed is considered as a single unit that responds homogeneously to its spatially-averaged meteorological inputs. That model structure is quite simple, since the hydrological processes are conceptualized through hydraulic analogues (e.g., linear reservoirs), but given that the model parameters are only associated with the macroscopic properties of the watershed as a whole, they have limited physical background. In this context, the unique means to establish a lumped modelling scheme of satisfactory predictive capacity is to infer its parameters through calibration, aiming to reproduce as closely as possible the observed responses of the basin.

In contrast, distributed models explicitly account for the spatial heterogeneity across the watershed, in terms of physiographic characteristics, weather inputs, hydrological processes and boundary conditions. The representation of heterogeneity is employed via discretization of the model domain in finely-resolved computational units (e.g., grid cells). The fundamental laws of hydraulics and semi-empirical hydrological formulae are applied at each spatial unit, which allows, in theory, to directly estimate all model parameters from field data. Due to their bottom-up basis, which takes advantage of the significant advances in understanding the hydrological processes at the micro (point,

continuum)-scale, fully-distributed models are also identified as “physically-based” (Beven 1989).

Hydrologic watershed models can also be further defined as stochastic or deterministic based on the approach used for model input or parameter specification (Melone et al. 2005). This essentially characterizes their level of randomness or precision, as well as inclusion of modelling process techniques. Stochastic models will produce ‘probable outcomes’ obtained using known relationships among states and events, while deterministic models tend to be more ‘precise’ involving statistical distributions representing most, if not all, of their inputs or parameters, and therefore determining a range of outputs (Lacroix 1999; Melone et al. 2005). Although most models are in nature deterministic, stochastic models have a simple framework concept providing the possibility to describe heterogeneity with limited spatial or temporal details, and also provide decision makers with the ability to determine the level of uncertainty associated with various predictions (Daniel et al. 2011; Melone et al. 2005), which is very useful.

Another model classification arises from the nature of the algorithms employed by the model, which can be empirical, conceptual or physically-based (Melone et al. 2005). Empirical watershed models use functions to approximate or fit available data. They range from simple regression models to hydroinformatics-based models utilizing artificial intelligence (AI) techniques, such as Artificial Neural Networks (ANN), Fuzzy Logic (FL), and Genetic Algorithms (GA) (Daniel et al. 2011).

An ANN is an interconnected group of artificial neurons that uses mathematical modeling for information processing. In general, neural networks are adaptive systems, changing their structure according to the external information flowing through the network. In other words, ANNs are non-linear statistical modeling tools, used for modeling complex relationships between inputs and outputs (Haykin 1999). The internal structure of an ANN consists of neurons organized in layers, assigned with weight values for controlling the transfer of internal signals. These weight values are considered parameters of an ANN and have to be adjusted in an iterative training process, called training. During the training, the ANNs need input consisting of corresponding model input and output, so that after training, it can simulate or mimic the model (Kamp & Savenije 2007).

The FL method is based on the fuzzy sets theory (Zadeh 1965), where, instead of using known governing physical relationships, these are defined verbally. In classic set theory, an item can be assigned as a member of a set [1], or a non-member of a set [0]. In fuzzy set theory, the main idea is to define the fuzzy membership functions that define the relationships between the system input and outputs (Mahabir et al. 2003).

The GA method is a non-linear optimization search technique, based on the principle of natural selection and artificial survival of the fittest (Agrawal & Singh 2003). GAs employ three distinct operations; reproduction, crossover, and mutation, evolving the initial population to the next generation. The process is repeated for many generations until an optimal global solution is achieved, after a sufficient number of generations.

Most models, however, are conceptual in nature, with the level of functionality varying from one model to another depending on whether they were designed to be site specific or for general applications (Lacroix 1999). On the other hand, physically-based models rely on the understanding of the physics underlying the hydrological processes that control the response of the catchment and utilize physically based equation in order to describe these processes (Daniel et al. 2011)

Hydrological models encompassing time dimensions are most often distinguished as yearly, monthly, daily or smaller time frames. Models, however, can be formulated for specified events and are therefore subdivided into event-based streamflow simulations, simulating individual precipitation-runoff events focusing on infiltration and surface runoff, or continuous-process models explicitly accounting for all runoff components and also considering soil moisture distribution between storm events (Singh 1988; Singh 1989; Singh 1995; Melone et al. 2005).

The advantages and disadvantages of the different approaches have been widely discussed in the literature (Boyle et al. 2001; Ajami et al. 2004; Nalbantis et al. 2011). It is obvious that lumped conceptual models cannot represent the spatiotemporal variability of the hydrological processes at basin level, while fully-distributed models are data and time-demanding. Yet, the most important issue is that, despite their different backgrounds, both approaches suffer from uncertainties related with the estimation of their parameters. In fact, from the introduction of physically- or process-based models, the hydrological community has criticized them as overly complex and over-parameterized and difficult to use, while strongly disputing their ability to apply

parameters that are directly measured in the field (observable), without some kind of calibration (e.g. Beven, 1989; Eckhardt and Arnold, 2001; Fatichi et al., 2016; Refsgaard, 1997). The reasonable argument behind this criticism is that the physical properties are measured at the point scale, while the parameters are assigned to the grid-cell scale and are thus by definition conceptual. Hence, given that distributed models comprise so many parameters, they are too vulnerable against the well-known shortcomings of calibration, i.e. the equifinality problem (Beven & Binley 1992). However, it has been argued that in some situations the use of process-based models is necessary, while in a certain class of problems they are the most appropriate tool to use, especially in cases where knowledge of flow paths or distributed state variables and/or preservation of physical constraints is important (Fatichi et al. 2016).

For many problems of the everyday practice requiring flow predictions at a relatively small number of points across the river network, semi-distributed models are broadly recognized as a good compromise between lumped and fully-distributed approaches (Boyle et al. 2001). The key concept is to divide the watershed in a number of sub-basins and propagate the runoff generated from each sub-basin through the river network (and similarly for the subsurface water processes). Although at the sub-basin scale the modelling remains lumped (except for some specific cases, in which sub-basins are further divided in smaller units), at the watershed scale the heterogeneities are partially accounted for by assigning different meteorological inputs and different properties at each sub-basin. Another advantage of semi-distributed schemes is the representation of flow routing processes, which is of key importance when fine time steps are employed (e.g., in flood modelling).

The configuration of a semi- or fully-distributed model and the associated level of complexity are determined by the user. This task involves two separate issues, the discretization of the watershed and the parameterization of the model. The discretization refers to the delineation of the spatial units (typically, grid cells in the case of distributed, and sub-basins in the case of semi-distributed models), while the parameterization refers to the spatial assignment of the model parameters.

### 2.1.2 Watershed models

This section provides a description of the most commonly used and widely accepted watershed-scale hydrological models (Singh & Woolhiser 2002; Borah & Bera 2003; Kalin & Hantush 2003; Singh et al. 2006; Oogathoo 2006; Daniel et al. 2011), discussing their key strengths and weaknesses in different watershed applications while table 1 provides a summary of their main characteristics and features.

***AGNPS – Agricultural Non-Point Source / AnnAGNPS - Annualized Agricultural Non-Point Source***

The AnnAGNPS model (Young et al. 1995; Bosch et al. 1998), the current version of AGNPS, is a semi-empirical distributed continuous watershed model, developed to perform daily simulations of the sediment and nutrient transport from agricultural watersheds (< 3000 $km^2$), with output options for an event, monthly or annual basis. AnnAGNPS model can support runoff and erosion management, and nutrient movement by performing cost-benefit analysis, while it can perform simulations of numerous best management practices (BMPs), including ponds, vegetative filters strip, riparian buffers, and others (Kalin & Hantush 2003). The model can also be used for analyzing the long-term effects of hydrological changes and watershed management practices (Borah & Bera 2003). Mixed results have been reported by the application of AnnAGNPS in several studies: Baginska et al. (2003) reported satisfactory event flow predictions in Australia, Das et al. (2004) produced runoff results with acceptable accuracy in Ontario, while Suttles et al. (2003) and Yuan et al. (2001) produced adequately results when predicting long-term monthly and annual runoff. However, both studies (Suttles et al. 2003; Yuan et al. 2001) showed inadequately representation of the overland flow in riparian areas, nutrient and sediment load predictions were overestimated, while it was suggested that proper cell discretization could improve runoff estimates. Moreover, AnnAGNPS over-predicted event-based peak flow results (Shrestha et al. 2005), was not adequately formulated in simulating intense single-event storms (Borah & Bera 2003), was considered unsuitable for storm event analysis in the case of drastic variation in flow and constituent concentrations and loads (Borah et al. 2002), while it does not consider subsurface and groundwater processes, making the model use in BMPs impact analysis qualitative (Croley & He 2005b). In conclusion, key limitations of the AnnAGNPS model include: (a) inability to perform simulation of baseflow or frozen

soil conditions; (b) as the model does not account for the spatial distribution of precipitation, it does not provide a mass balance equation for water inflow and outflow; and (c) the runoff simulation is not entirely based on physical laws (Oogathoo 2006). Furthermore, the use of Curve Number (CN) method (explained in detail in Section 2.3.3.2), which does not consider time distribution, does not allow the model to reproduce measured runoff from specific storm events (Kawkins 1978; Wischmeier & Smith 1978; Beven 2000; Garen & Moore 2005; Croley & He 2005b), while additional limitations are realized, including (a) not explicitly accounting for antecedent moisture conditions in runoff calculations; and (b) difficulties in separating storm runoff from the total discharge hydrograph. These limitations can result in incorrect CN estimates for runoff and infiltration, on which sediment, nutrient and pesticide loadings are directly related, thus possibly producing inaccurate estimates for non-point source pollution rates (Croley & He 2005a).

***ANSWERS/ANSWERS-2000 – Area Non-Point Source Watershed Environment Response Simulation***

The ANSWERS model is comprised of two major response components, the hydrology component (Huggins & Monke 1966) and the upland erosion component (Foster & Meyer 1972). The model divides the watershed area into square grid elements of less than 10000 m side-length, where all watershed characteristics are considered homogeneous. ANSWERS-2000 is an expanded version of the ANSWERS model (Beasly et al. 1980) that uses breakpoint precipitation data and simulates runoff events on a 30-second time step, with a daily time-step between the events. Simulations are performed on watersheds of medium size (5-30 $km^2$) where surface hydrological processes dominate, providing a surface runoff hydrograph at both the outlet of the watershed and at any other points selected by the user (Dillaha et al. 2004). Both models were designed for ungauged river basins, as well as for evaluating the effectiveness of agricultural and urban watershed BMPs in the decrease of sediment and nutrient transport to the river network during surface runoff events (Kalin & Hantush 2003; Dillaha et al. 2004). Connolly et al. (1997) used ANSWERS to predict runoff at a watershed outlet, generating accurate simulations for various surface cover conditions; runoff predictions, however, were less accurate when low intensity events were simulated compared to higher intensity events. Dillaha et al. (2004) used ANSWERS-

2000 on two US-watersheds in Georgia with good performance in runoff, sediment and nitrate predictions, and on a 11.53-km$^2$ watershed in Virginia with good performance in the largest storm simulations while cumulative predictions of runoff volume, sediment yield and nitrate were within 40% of the measured values. Bai et al. (2004) showed that the model performed satisfactorily in simulating runoff during non-snow seasons, with Oogathoo (2006) pointing out that a key weakness of ANSWERS models is their inability to simulate interflow, baseflow contribution and groundwater contributions to snow pack and snowmelt, suggesting that the model is less suitable for areas with high baseflow contribution, winter snow accumulation and snow melt. Another key weakness noted by Borah & Bera (2003) is that ANSWERS is not sufficiently formulated for intense single-event storm simulations, with possible numerical problems inherent in its outcome, while ANSWERS-2000 does not include channel erosion and sediment transport routines, thus, the sediment and chemical components of the models are not suitable for watershed applications. Both models utilize also the CN methods and deal with the same limitations as the AGNPS and AnnAGNPS identified earlier (Beven 2000; Garen & Moore 2005; Croley & He 2005a).

### *GSSHA - Gridded Surface Hydrologic Analysis / CASC2D - CASCade of Planes in 2-Dimensions*

CASC2D (Julien & Saghafian 1991) is a physically-based model developed for surface runoff predictions in arid and semi-arid watershed, performing water and sediment simulations in 2D over land grids and 1D channels, that can be either single-event or long-term continuous simulations. The model divides the watershed into grid cells with water and sediment being routed from one to the next one. GSSHA (Downer & Ogden 2004; ERDC 2013) is an improvement of CASC2D in terms of stability and efficiency, while the added ability of performing simulations of saturated and unsaturated groundwater allows the model to be applied in a variety of climates and catchments. As GSSHA is a component within the U.S. Department of Defence Watershed Modelling System (Aqauveo 2014), it was developed for providing hydrological prediction in the widest range of places and conditions, including urban watersheds with complex spatial configurations. Moreover, the GSSHA has improved in terms of simulating major hydrologic storage units and predicting sediment transport in streams, particularly during large rainfall events (Downer & Ogden 2004). Both models were tested in an

experimental watershed with GSSHA producing more accurate sediment discharge for selected storm events (Ogden et al. 2001; Downer & Ogden 2004). However, Kalin & Hantush (2003) indicate key limitations, including the potential of producing very poor sediment results, suggesting that erosion in channels is not transport-limited, thus the volume of the produced sediment is greater that the volume the flow can carry. Moreover, Borah & Bera (2003) notes that the numerical schemes of the model are computationally intensive and data demanding while, when the number of model grid cells is larger than 100000, simulation times become prohibitive, narrowing the applicability of the model in medium to large-size watershed. This however, is not a disadvantage nowadays, considering the advances in computer science and technology.

***HEC-1/HEC-HMS – Hydrologic Engineering Centre Hydrologic Modelling System***

HEC-1 model was developed for simulating hydrological processes on watershed ranging from 1-$km^2$ to 100000-$km^2$ in size, producing runoff hydrographs at one or multiple points within complex basin configurations for gauged and hypothetical rainfall events (Feldman 1995). The model is superseded by HEC-HMS (Scharffenberg 2008; USACE 2013; Bennie et al. 1997), providing a variety of options for precipitation-runoff simulation and routing processes, integrated hydrological analysis components, data storage and management capabilities, graphics and reporting facilities. Both models have been widely used for flood modelling and impact analysis of land use changes (Oogathoo 2006). Duru & Hjelmfelt (1994) used the kinematic-wave method of the mode and with limited calibration, showed good model performance on runoff predictions, while land use impacts on the hydrological cycle were evaluated accurately, while Sui (2005) applied successfully the HEC-1 model simulating runoff in an ungagged watershed in Canada. However, Oogathoo (2006) notes that important features are excluded; the simulation time-step is constant making the model unsuitable for components that require a more detailed analysis, and also, with the main objective of the model being flood modelling, the method used for the baseflow simulation is simple, thus, the loss component is not accounted for in the absence of rainfall, i.e. the soil does not dry out and recover its loss potential. Other model limitations include: uncoupled models for evapotranspiration-infiltration and infiltration-baseflow processes, no interactions between the aquifers, although flow can be separated within the dendritic stream network is allowed, it has limited capability, and finally, lack of

downstream flow influence or reversal with the potential of backwater, but only if contained within the reach (USACE 2013).

***HSPF – Hydrological Simulation Program-FORTRAN***

HSPF (Donigian et al. 1995; USEPA 2008) is a semi-distributed, continuous model that performs simulations of hydrologic and associated water quality processes on pervious and impervious soils, in streams as well as in well-mixed impoundments simulating water as overland, hypothermic and groundwater flow. The model has incorporated the hydrologic response unit concept (HRUs) concept, based on homogeneous climate and storage capacity factors, while simulations can be performed for periods of a few minutes to hundreds of years. HSPF has been generally used for the assessment of the effects of land use change, reservoir operations, water flow diversions as well as non-point source treatment alternatives (Kalin & Hantush 2003), while it is also suitable for mixed agricultural and urban watersheds (Borah & Bera 2003). Key strengths of the models include: (a) a comprehensive representation of the watershed characteristics, stream processes and pollutant sources; (b) flexibility and adaptability of the model to a wide range of watershed types and conditions; and (3) well-designed code modularity and structure (AquaTerra 2011). However, as the model conceptualises overland areas as levelled water detention storage while using storage-based or non-linear equation to model routing processes, it does not adequately simulate intense single-event storms, more so in large sub-basins and long channels (Borah & Bera 2003; Oogathoo 2006). Moreover, HSPF is high data demanding while no comprehensive parameter estimation guidelines are provided, resulting in a strenuous and long calibration process (Saleh & Du 2004), while user training is usually required (AquaTerra 2011).

***KINEROS2 – KINematic Runoff and EROSion***

KINEROS2, adopted as part of the Automated Geospatial Watershed Assessment Tool (AGWA) software system (Miller et al. 2007; Guertin et al. 2008), is represented by a cascade of planes and channels, used to determine the effects of different artificial features, e.g. small detention reservoirs, urban development structures, or lined channels, on flood hydrographs and sediment yield (Woolhiser et al. 1990). The model is limited to Hortonian flow processes and cannot be applied to long-term simulations. Moreover, it lacks an evapotranspiration component, crucial for the water mass balance calculation (Kalin & Hantush 2003). With a complete set of hydrology and sediment

components, however, the model is considered to be a useful tool for the analysis of single, severe or design storms, and for the evaluation of watershed management practices (Borah & Bera 2003). KINEROS2 was tested on an USDA experimental watershed in Iowa (Kalin & Hantush 2003), with robust results in erosion and sediment transport simulations. Although the model was designed for arid and semi-arid environments (Al-Qurashi et al. 2007), several research studies have shown that the model can successfully perform erosion and sediment transport simulations, and also characterise the runoff response due to land use changes in arid and semi-arid watersheds. For example, Lajili-Ghezal (2004) applied the model in a Tunisian semi-arid watershed resulting in satisfactory runoff predictions from ungauged watersheds and evaluations of future land use plans, while Miller et al. (2007) used the model in Arizona, and successfully assessed the increased event runoff volumes and flash flood response. Al-Qurashi et al. (2007), however, were less successful in a model application in Oman, where, despite the extensive and high-resolution input data and the use of automatic calibration procedure, the model performance in validation was poor. Moreover, Borah & Bera (2003) note that the model simulates well runoff and sediment yield in watershed with an area up to 10 $km^2$.

***MIKE SHE – Systéme Hydrologique Européen,***

MIKE SHE is a distributed and physically-based model performing simulations of major hydrologic processes, with process model for evapotranspiration, overland, unsaturated and groundwater flow, and their interactions (Graham & Butts 2005). Spatial distribution of basin properties, climate input and hydrological response is represented horizontally, though an orthogonal grid network, and vertically through a column of horizontal layers at each grid cell (Abbott et al. 1986a). The model is suitable for simulation of storm or long-term events with a variable time step, while its modular structure provides the capability of data exchange between the model components as well as the addition of new process model components, based on data availability (Abbott et al. 1986b). MIKE SHE is considered to be one of the most comprehensive watershed models, incorporating virtually all of the phases of the hydrologic cycle (Kalin & Hantush 2003), while it can also simulate wetlands, and pesticide and nutrient management. The model has been applied successfully for river basin management and modeling (Christensen 2004), integrated surface and groundwater modeling (Demetriou

& Punthakey 1999; Sahoo et al. 2006), land use change and anthropogenic effects (Refsgaard 1996), and irrigation (Jayatilaka et al. 998; Singh et al. 1999; Mishra et al. 2005). Thompson et al. (2004) applied the model in a wetland in England and showed good simulation results reproducing the seasonal dynamics of groundwater and ditch water levels, while Sahoo et al. (2006) applied the model in a mountainous region in Hawaii simulating satisfactorily storm events. Moreover, Demetriou & Punthakey (1999) used the model in an Australian watershed with complex hydro-geological characteristics, producing accurate model prediction of water transfer from aquifers, drainage and supply systems and land surface, while Singh (1999) showed that the model can be used for water resources management and irrigation planning. Similar to the GSSHA model, MIKE SHE is also computationally intensive, prohibiting its application to medium to large-size watersheds, and is subject to computational instability due to the use of approximate numerical solutions in flow equations (Borah & Bera 2003).

***PRMS - Precipitation-Runoff Modelling System / MMS Modular Modelling System***

PRMS (Leavesley et al. 1983; Leavesley & Stannard 1995) is a modular-design, deterministic, distributed model that performs simulations of watershed water movement driven by precipitation and snowmelt, through overland, hypodermic and base flow, on a daily and sub-daily time-step over the course of a storm. PRMS divides the watershed into sub-units based on its physiographic characteristics and precipitation distribution, using two levels of partitioning. Firstly, the basin is divided into HRUs, based on watershed characteristics where water and energy balances are computed daily. The sum of all HRU responses, weighted on a unit-area basis, produces the daily watershed streamflow response. The second partitioning level is available for storm hydrograph simulations, where the watershed is conceptualized as a series of interconnected rectangular flow planes and channel segments. Surface runoff is therefore routed over the flow planes and into the channel segments, and channel flow is routed thought the watershed channel system. An HRU is considered to be the equivalent of a flow plane or it can be further delineated into several flow planes. PRMS was redesigned to form the basis of the US Geological Survey (USGS) Modular Modeling System (MMS) supporting the integration of models and tools at different level (Leavesley & Stannard 1995), including individual process models, tightly and

loosely coupled models, as well as fully integrated support systems (Leavesley et al. 2000). With regards to this aspect, Hunt & Steuer (2000) and Steuer & Hunt (2001) applied the model to examine the effect of land-cover change and urbanization on groundwater recharge, feeding the results into the USGS groundwater model, Modular Three-Dimensional Finite-Difference Groundwater Flow Model (MODFLOW) applied for further studies. Moreover, Hobson (2005) coupled MMS with a stochastic weather generator in an attempt to provide a framework for weather variables and streamflow simulation. The model was also effectively applied for evaluation of the effects of climate and water resources variations, water management (Leavesley et al. 2000) as well as flood modeling, including the representation of flood wave propagation in single precipitation events (Borah & Bera 2003). This model capability was demonstrated by Valeo et al. (2007) who analyzed the effects of climate change on flooding, while Yates et al. (2000) used the model with historical radar precipitation and forecast data for flash flood simulation on a partially burned watershed. Key limitations of PRMS/MMS (Borah & Bera 2003) include: (a) not sufficient formulation for single rainfall events, i.e. using one-dimensional flow equations, with possible numerical problems inherent in its outcome; and (b) in storm simulations the model is limited to hydrology and overland sediment components.

***SWAT - Soil and Water Assessment Tool***

SWAT (Arnold et al. 1993; Neitsch et al. 2005; Gassman et al. 2007) is a physically-based, continuous-time watershed model operating on a daily time step, designed to predict the impact of management practices on water and sediment yields in ungauged watersheds. SWAT divides the watershed into sub-basins and further into HRUS based on common land use, soil and slope characteristics. The sub-watershed delineation is based on a defined threshold drainage area, while the HRU delineation is based on aggregation using user-defined thresholds for land use, soil type and slope range within each subwatershed, followed by a GIS-based spatial overlay scheme. HRUs can be therefore seen as discontinuous land masses consisting of homogeneous characteristics, representing percentages of the sub-watershed area. HRUs are used in a non-spatial manner, meaning that they are not identified spatially within simulations. Alternatively, a watershed can only be divided into sub-watersheds characterized by dominant land use, soil and slope. In this approach, lateral flow paths between sub-watersheds are

considered, essential for establishing an appropriate routing structure through the watershed. SWAT core strengths include simulations of agricultural and forest watersheds (Kalin et al. 2003; Borah & Bera 2003), based on which it has been adopted as part of the USEPA's Better Assessment Science Integrating Points and Nonpoint Sources (BASINS) System (USEPA 2015) and AGWA (Miller et al. 2007; Guertin et al. 2008) software systems. Primary applications of SWAT include the calibration and/or sensitivity analysis, hydrologic and water quality evaluation, climate change effects, variation in configuration or data input effects, with the foundation strength being the combination of simplified upland and channel processes incorporated in the model (Gassman et al. 2007). SWAT has been evaluated on watersheds with a wide range of conditions, producing satisfactory results (Kang et al. 2006; Gebremeskel et al. 2005; Hao et al. 2004; Bärlund et al. 2007; Kaur et al. 2004; Gosain et al. 2006; Mishra et al. 2007; Bouraoui et al. 2005; Gikas et al. 2005) across many of which, and has shown flexibility is surface runoff simulations. Du et al. (2005) used the model and produced satisfactory results in simulating surface and subsurface flows, water table dynamics and more, while many studies demonstrate the use of SWAT as an evaluation tool for climate change impacts on streamflow (Stone et al. 2001; Eckhardt & Ulbrich 2003; Thomson et al. 2003). SWAT also incorporates the calculation of Total Maximum Daily Loads (TMDLs) and the simulation of numerous BMPs and conservation practices (Santhi et al. 2006; Chaplot et al. 2004; Gassman et al. 2007; Kang et al. 2006); These examples have highlighted the flexibility and robustness of SWAT but also some weaknesses, most notably the use of non-spatial aspects of HRUs (Oogathoo 2006; Gassman et al. 2007). As a result, SWAT cannot represent explicitly riparian buffer zones, wetlands, and other BMPs, while flow and pollutant routing within a given subwatershed is ignored (Gassman et al. 2007), while additional limitations are incorporated associated with the use of the CN method, as identified earlier (Beven 2000; Garen & Moore 2005; Croley & He 2005a).

**Table 1:** Main characteristics and features of watershed models [D=Distributed, SD=Semi-distributed, C=Continuous, E=Event-based, Pu=Public, Pr=Proprietary] (Source: Daniel et al., 2011)

| Model | Suited applications | Main components | Runoff | Subsurface flow | Spatial scale | Temporal scale | Watershed representation | Availability |
|---|---|---|---|---|---|---|---|---|
| AnnAGNPS | Agriculture watersheds; widely used for evaluating a wide variety of conservation practices and BMPs | Hydrology, sediment, nutrients and pesticide transport, DEM used to generate grid and stream network | CN, TR-55 for peak flow | Darcy's equation | D | C- daily or sub-daily steps | Homogeneous land areas, reaches, and impoundments | Pu |
| ANSWERS-2000 | Medium size agriculture watersheds; ungagged watershed; used for evaluation of BMPs effectiveness | Runoff; infiltration, water/river routing, drainage, river routing, chemical/nutrient transport | Manning equation | Darcy's equation | D | C | Grid/cells | Pu |
| GSSHA/ CASC2D | Agriculture or urban watersheds; diverse modeling capabilities in a variety of climates and watersheds with complex spatial datasets | Spatially varying rainfall; rainfall excess and 2-D flow routing; soil moisture, channel routing, upland erosion, & sediment transport | 2-D diffusive wave equations | No component | D | E; C | 2D square overland grids; 1D channels | Pr |
| HEC-1/ HEC-HMS | Urban watersheds; widely used for flood modeling and land use change impacts | Precipitation, losses, baseflow, runoff transformation and routing | CN, kinematic wave equations | No component | SD | E | Dendritic network or grid | Pu |
| HSPF | Both agriculture and urban watersheds; diverse water quality and sediment transport at any point of the watershed | Runoff/water quality constituents, simulation of pervious/impervious areas, stream channels and mixed reservoirs | Empirical outflow | Interflow outflow, percolation; groundwater outflow | SD | C | Pervious/impervious land areas, stream channels and mixed reservoirs; 1D sim. | Pu |

| | | | | | | | | |
|---|---|---|---|---|---|---|---|---|
| KINEROS2 | Urban environments and studying impacts of single sever or design storm even; applied to agriculture watersheds | Distributed rainfall inputs, rainfall excess, overland flow, channel routing, sediment transport, interception, infiltration, surface runoff & erosion | Kinematic wave equations | No component | D | E; C; variable steps | 2D rectangular overland grids; 1D channels; 1D unsaturated/3D saturated flow | Pu |
| MIKE SHE | Wide range of spatial and temporal scales; modular design facilitates integration of other models; advanced capabilities for water quality, parameter estimation and water budget analysis | Interception, overland/channel flow, unsaturated/saturated zones, snow-melt; aquifer/river exchange, advection/dispersion of solutes, geochemical processes, plant growth, soil erosion and irrigations | 2D diffusive wave equations | 3D groundwater flow | D | E; C; variable steps | 2D rectangular/square overland grids; 1D channels; 1D unsaturated/ 3D saturated flow | Pr |
| PRMS/ MMS | Agriculture watershed; modular design facilitates integration of other models (e.g. climate models) | Hydrology and surface runoff, channel flow, channel reservoir flow, soil erosion, overland and sediment transport | Kinematic wave equations | No component | D | E | Flow planes, channel segments, channel reservoir; 1D sim. | Pu |
| SWAT | Agriculture watersheds; used for calculating TMDLs and simulating a wide variety of conservation practices and other BMPs | Hydrology, weather, sedimentation, soil temperature and properties, crop growth, nutrients, pesticides, agricultural management, channel/reservoir routing | CN for runoff; SCS TR-55 for peak flow | Lateral subsurface flow/ground flow | SD | C; daily steps | Sub-basins based on climate, HRU, ponds, groundwater, and main channel | Pu |

## 2.2 Watershed delineation

The configuration of a semi- or fully-distributed model and the associated level of complexity are determined by the user. This task involves two separate tasks, the discretization of the watershed, i.e., the model schematization, and the model parameterization. The former refers to the delineation of the spatial units (typically, grid cells in the case of distributed and sub-basins in the case of semi-distributed models), while the later refers to the spatial assignment of the model parameters (Efstratiadis et al. 2008; Nalbantis et al. 2011).

During the long history of hydrological models, these two topics have been handled in many different ways. In particular, the discretization of the watershed predetermines the aggregation patterns of spatial information, i.e. the size and shape of computational elements, and controls the associated topographic parameter values such as slope, aspect etc. On the other hand, different delineations of the stream network connectivity and hillslope size affect and can often misrepresent rainfall-runoff processes on hillslopes and across channels. Consequently, the watershed subdivision has the potential to affect the output of hydrological modeling (Zhang et al. 2013). This relates to the ongoing theoretical debate about the optimal level of watershed discretization that adequately represents the spatial heterogeneity of a watershed (Beven 1993), a subject that has received considerable attention in the literature from the early steps of distributed modelling. For instance, Hromadka (1986) states that "Arbitrary subdivision of the watershed into subareas should generally be avoided. … an increase in the watershed subdivision does not necessarily increase the modeling 'accuracy' but rather transfers the model's reliability from the calibrated unit hydrograph and lag relationships to the unknown reliability of the several flow routing submodels used to link together the several subareas".

While it is common practice to partition a watershed into smaller units (e.g., sub-basins), it is not easy to identify a strictly optimal spatial scale. It is accepted that, for a given watershed and a given data set, the sub-watershed size should be adapted to the modelling objectives, as the latter determine the dominant hydrological processes considered in the simulation (Dehotin & Braud 2008). It is feasible to represent the landscape heterogeneity through small sub-watersheds; for large watersheds, however, a

fine resolution is often prevented, mainly by high data requirements. Therefore, when hydrological models are employed in meso- and large-scale watersheds, significant simplifications are required, in order to aggregate the spatial heterogeneity and its associated parameters at various levels of watershed subdivision (Cho & Olivera 2009).

Increasing the number of sub-watersheds definitely increases input data preparation, computational time and calibration effort; therefore, the sub-watershed-average inputs generated from discrete gauging stations vary with different watershed subdivisions (Han et al. 2014). Few works have been reported in the literature to explain the variations in the distributed model inputs as a result of various levels of watershed subdivision. For instance, Li et al. (2014) report that the precipitation input pattern in the hydrological modelling was significantly affected by watershed subdivision. Savenije (2010) proposed an approach between complex distributed and simple lumped modeling, aiming to find the right level of simplicity while avoiding over-simplification. H**e** presented a process-based, but conceptual approach, where topography is used as a key for classification, retaining maximum simplicity whilst taking into account observable landscape characteristics. A new terrain descriptor, the Height Above the Nearest Drainage (HAND) based on SRTM-DEM data (Rennó et al. 2008) has also been employed in landscape classification, revealing strong correlation between soil water conditions and topography, while Donnelly et al. (2016) found the strongest relationships to be between upstream area, proportion of upstream agricultural land, elevation, mean precipitation, and mean temperature. Gharari et al. (2011) assessed the performance and sensitivity of HAND-based landscape classification framework compared with other several classification indicators. They reported that HAND and surface slope appeared to be the stronger indicators for different dominant hydrological processes.

Over the years, several watershed subdivision approaches have been developed and tested using a variety of well-established hydrological models aiming to examine the effects of watershed subdivision on hydrologic model outputs. From the obvious approach in semi-distributed models to divide the watershed into its natural sub-watersheds based on topography extracted from a Digital Elevation Model (DEM), or by using concepts such as the Critical Source Area (CSA), Threshold Drainage Area (TDA) and Aggregated Simulation Area (ASA); to more detained delineation concepts

employed in fully distributed models, such as grid elements, representative elementary areas (REA), and representative elementary watershed (REW).

### 2.2.1 Sub-basins

An obvious approach is to divide the watershed into its natural sub-watersheds based on topography extracted from a Digital Elevation Model (DEM). This configuration preserves the watershed's natural boundaries, flow-paths and channels for realistic water routing. Boyd et al. (1979; Goodrich et al. (1988); Goodrich (1992); Norris (1992); Norris & Haan (1993); Bingner et al. (1997); Zhang et al. (2004); and Wingfield (2008) are only a few examples of research investigating the effects of different subdivision schemes on model performance.

Boyd et al. (1979) developed the WBNM–Watershed Bounded Network Model and showed that the estimated peak flow fluctuated at low subdivision schemes applied on ten watersheds (2.6 $km^2$–13.6 $km^2$) in New South Wales, but stabilized at 5 subbasins, above which all model subdivisions gave good results. Goodrich et al. (1988) demonstrated that simulation accuracy was unaffected for large storm simulations in Walnut Gulch watershed in Arizona, while for smaller storms, simulations did not account for greater impact of infiltration processes on runoff, which reduced model accuracy for decreasing subdivision levels. Goodrich (1992) showed that variations in drainage density affect the accuracy of the model runoff predictions.

Norris (1992) showed that peak flow estimates for the single sub-watershed scheme of a 31.08-$km^2$ watershed was about 35% less that the peak flow estimates for the 3 and 6 sub-watershed schemes; with 3 or more subdivisions of the watershed, the peak flow estimates stabilized within a range of acceptable variation. Norris & Haan (1993) used HEC-1 and demonstrated that, as watershed subdivision increased in the Little Washita watershed (152.3 $km^2$) in Oklahoma, the estimated peak flow increased as well, before rapidly decreasing after 5 subdivisions. It was concluded the number of sub-watersheds can have a significant impact on peak flow estimates; peak flow estimates increase as the number of sub-watersheds increased. However, beyond an optimum sub-watershed threshold number, there is no significant improvement in the modeling accuracy.

Bingner et al. (1997) showed that total runoff volume varied by only 5% with different subdivisions of the Goodwin Creek watershed (21.3 $km^2$) in Mississippi using SWAT.

In contrast, annual sediment yield produced from upland areas appear to be very sensitive to the subdivision level. Decreasing sub-watershed size increases sediment yield. This variability was attributed to the effects of increasing level of aggregation on average sub-watershed slopes and on the watershed proportion that was delineated as cropland. An upper limit to sub-watershed size was required in order to adequately simulate sediment yield. Zhang et al. (2004) applied the SCA-SMA–Sacramento Soil Moisture Accounting model and demonstrated that the subdivided model performed consistently better than the lumped model for both low and high flood events of Blue River basin (1232 $km^2$) in Oklahoma. Wingfield (2008) examine watershed subdivision effects on components of the runoff hydrograph of five watersheds in Texas, USA (9.9 $km^2$-199.4 $km^2$) using HEC-HMS and showed that no subdivision scheme consistently performed better than any other for each of the hydrograph components.

A watershed can be divided into sub-watersheds based on a Critical Source Area (CSA), a threshold for stream generation. CSA is the minimum upstream drainage area required for a source channel or stream to be initiated and maintained. It is specified as a percentage of the total area of the watershed and controls the number and size of sub-watersheds. Higher CSA values produce a less dense stream network and therefore fewer sub-watersheds (Di Luzio & Arnold 2004). The concept of CSA in watershed division into sub-watersheds has been applied amongst others by Thieken et al. (1999), FitzHugh & Mackay (2000), Kalin et al. (2003), Arabi et al. (2006), Muleta et al. (2007), Kumar & Merwade (2009) and Cho et al. (2010).

A similar concept to CSA to delineate watersheds in sub-watershed is Threshold Drainage Area (TDA). TDA specifies which cells of the watershed are defined are stream cells and which defined as land cells draining into the stream cells. Higher TDA values produce fewer and larger sub-watersheds while smaller TDA values produce more and smaller sub-watersheds. Nour et al. (2008) used different TDA values to delineate Willow watershed (15.62 $km^2$) in Canada by using an Artificial Neural Network approach and showed that streamflow predictions were unaffected by watershed subdivision.

Instead of sub-watersheds, Kite (1997) introduced the concept of Aggregated Simulation Areas (ASA) in the hydrological model SLURP–Semi-distributed Land Use Runoff Process. A watershed can be delineated based on CSA values into spatial units

known as ASAs, for which the land use classes are known. ASAs are essentially sub-watersheds having one main outlet (Kite 1997; Lacroix 1999). Lacroix (1999) concluded that a subdivision scheme of least 20 ASAs of the Wolf Creek basin (183.3 $km^2$) in Canada were necessary to predict adequately water balance components, while runoff predictions continued to improve up to approximately 500 ASAs with each ASA covering about 0.2% of the total watershed area.

### 2.2.2 Grid elements

Equally spaced grids is another, more detailed, watershed delineation concept where the watershed is subdivided in grid elements, each representing the dominant land use and soil type. The effects of grid-cell size on surface runoff were investigated by (Molnár & Julien 2000) using the CASC2D distributed hydrologic model on Goodwin Creek watershed (21$km^2$) and Hickahala-Senatobia watershed (560 $km^2$) in Mississippi. Square grid-cell sizes ranging from 127 to 914 meters were tested and results showed that flow on overland cells is more sensitive to variations in grid-cell size compared to channel flow. Moreover, coarse gird-cell sizes can be used for rainfall-runoff simulations and are more appropriate when simulating high-intensity and long-duration events. Manguerra & Engel (1998) suggest that such concept may only be required when site-specific water impoundments are present such as reservoirs or ponds, in the cases of large watersheds when significant channel losses or abstractions are expected, or when detailed visualization of the spatial distribution of a certain output parameter is desired.

Bathurst (1986) considers grid spacing and time step to be the two most important structural parameters in distributed hydrologic modeling. Although increasing the size of the two parameters minimizes computing requirements, it also increases the possibility of inaccurate watershed representation and therefore inaccurate hydrological response. Bathurst (1986) applied the SHE hydrologic model on the Wye watershed (10.55 $km^2$) and concluded that dividing the watershed into grid element that are no larger than 1% of the total watershed area would ensure homogeneity in each element.

Tao & Kouwen (1989) investigated the impact of spatial DEM resolution on the Grand River watershed (3520 $km^2$) in Canada with two different grid cell sizes (5 km×5 km and 10 km×10 km), concluding that model results are not significantly affected by grid

size changes. A similar investigation was performed by Bruneau et al. (1995), using the TOPMODEL on the Coetdan watershed (12 $km^2$) in France, suggesting that the optimum grid-cell size for hydrologic modeling is 50 m. The effect of DEM grid size was also examined by Zhang & Montgomery (1994) on land surface representation and hydrological simulations on two watersheds, the Mettman Ridge (0.3 $km^2$) and the Tennesse Valley (1.2 $km^2$), USA. Results showed that computed topographic parameters and simulated hydrographs are significantly affected by DEM grid size. Zhang & Montgomery (1994) concluded that a grid size that is smaller than the hillslope length was required in order to simulate adequately the hillslope hydrological processes.

### 2.2.3 Representative Elementary Area (REA)

Wood et al. (1988) introduced the Representative Elementary Area (REA) concept and proved that it can exist in the context of hydrological modeling. According to Wood et al. (1988), a watershed can be considered as being composed of numerous (infinite) points at which evaporation, infiltration and runoff form the local water balance fluxes. In a continuous representation, the heterogeneity of the actual watershed in is replaced with a spatially integrated representative watershed or an assemblage of such representative sub-watersheds. Within such integrated representations, the hydrologic variables at every location are related to its average value provided from associated probability distributions. Each mathematical point of the continuum is associated with the area over which the average values are taken. This area acts as the smallest discernible point that is representative of the continuum and is defined as the REA. Variations in topography, soils and rainfall can be therefore represented by REAs without much loss in output quality (Wood et al. 1988).

Wood et al. (1988) experimented on the Cooweeta River basin (17 $km^2$) in North Carolina where the point hydrologic response was modeled and then aggregated to form the watershed hydrologic response. A modified version of the TOPMODEL was applied within each 30-m pixel comprising the watershed and pixel output was averaged to form each sub-watershed output. Results showed that at smaller scales (< 1 $km^2$), sub-watershed response is highly variable with regards to actual patterns of topography, soil, land use and rainfall characteristics. At larger scales (> 1 $km^2$) further sub-watershed aggregation had only little impact on the simulated results. REA was therefore defined

to be 1 $km^2$ for this watershed. Further studies showed that the size of REA is mainly affected by topography, with soil and rainfall variability having only small effect.

The concept was also investigated by Sasowsky & Gardner (1991) who utilized the hydrologic model SPUR–Simulating Production and Utilization of Ranglands on the Walnut Gulch watershed (146 $km^2$) in Arizona and showed that 37 and 66 subdivisions produced similar results and performed better than the 3 sub-watershed scheme.

### 2.2.4 Representative Elementary Watershed (REW)

The concept of a Representative Elementary Watershed (REW) in integrated hydrological modeling was introduced by Reggiani et al. (1998, 1999, 2000) and Reggiani & Rientjes (2005). In this approach, the point-scale equations of mass, momentum and energy conservation are integrated over the REW and mapped on the large scale. The approach is leaning towards specifying the fluxes across the volume boundaries instead of trying to increase the process description detail within the REW. The concept was applied on the River Geer watershed in Belgium (494 $km^2$) where 73 REW were delineated based on Strahler's $2^{nd}$ stream order (Reggiani & Rientjes 2005).

## 2.3 Hydrologic Response Units

From the mid-990s, attention has been given to physically-based parameterization approaches through the so-called Hydrologic Response Units (HRUs), which generally represent areas with similar land use and soil characteristics. Their implementation is quite simple, since there is no interaction or topological connection between the HRUs; thus, runoff from each HRU is calculated separately and summed together to determine the total runoff from each sub-basin.

### 2.3.1 Definition and Origin

The concept of hydrological response units was first introduced by Leavesley et al. (1983), who delineated topographic-stream-segment-based HRUs for storm hydrograph simulations through the PRMS hydrologic model. In this approach, the watershed is conceptualized as a series of interconnected rectangular flow planes where surface runoff flows over before entering the channel segments, from where is routed thought the watershed channel system. An HRU is considered to be the equivalent of a flow

plane or delineated as several flow planes. However, the key assumption of homogeneity in HRUs was asserted by Flügel (1995), who defined HRUs as "distributed, heterogeneously structured areas with common land use and pedo-topo-geological associations controlling their unique hydrological dynamics". Such approach is justified by the fact that the dynamics of hydrological processes within an HRU vary only by a small amount compared to the dynamics among different HRUs. The concept of homogeneous HRUs was applied on the River Bröl basin (216 $km^2$), Germany, using the PRMS/MMS model (Leavesley & Stannard 1995). A total of 23 HRUs were delineated and tested using a 20-year hydro-meteorological data series of daily values. It was found that HRUs are a reliable means for regional hydrological watershed modeling, allowing spatial up- and down-scaling (Flügel 1997; Flügel 1995). Bongartz (2003) compared to topographic-based (Leavesley et al. 1983) and homogeneous HRUs (Flügel 1995), and reported that, for watersheds with areas less than 200 $km^2$, homogeneous HRUs provided better representation of the watershed processes.

Similar concepts with the HRUs are the Hydrologically Similar Units (HSU) (Karvonen et al. 1999) and the Functional Units (FU) (Argent et al. 2007) concepts. HSUs aggregate areas that have hydrologically similar behavior, including land use, soil type, vegetation and slope. Each HSU is represented by a cross-section termed characteristic profile. Water balance over each characteristic profile is calculated independently and the influence of a specific characteristic profile on the total runoff is generated by accounting the surface area of the corresponding HSU. The scale of HSUs is smaller than the scale of HRUs. In the FU concept (Argent et al. 2007), the watershed in divided in FUs based on land use, management, location, hydrological response or other spatial features. The FU concept is not significantly different from the HRU concept.

### 2.3.2 HRU homogenous delineation approaches

A variation of the homogeneous HRU concept requires threshold specification for land cover, soil and slope classes, which is then used to delineate HRUs (Srinivasan et al. 2000; Neitsch et al. 2002). More specifically, the watershed is divided in several sub-basins that are further divided in discontinuous land masses, delineated through aggregation, according to user-defined thresholds for land use, soil type and slope ranges within each sub-watershed; this is followed by a GIS-based spatial overlay

scheme, resulting into “unique combination” HRUs with homogeneous characteristics, representing percentages of the sub-basin area that contribute differently to the entire watershed responses. The process is illustrated in Figure 1 below. In this example, a rectangular sub-basin of size 30 cells (5x6) is assumed, with four, three and two different classes of land cover, soil type and slope categories, respectively (Fig. 1a). By applying an assumed threshold of 20% of the total cells (i.e. 6 cells) for land cover, 30% of the total cells (i.e. 9 cells) for soil type, and 20% of the total cells (i.e. 6 cells) for terrain slope categories, any land cover, soil type and slope category occupying less than six, nine and six cells, respectively, in the sub-basin will be lumped with adjacent areas. As a result, land cover category 3and soil type category 2 will be lumped with the adjacent dominant cells, as they fall below the specified threshold (Fig. 1b). A spatial overlay is then performed (Fig. c) so that cells that have the same combination of land cover, soil type and slope category are given a unique HRU identification number (Table 2 and Fig. 1d). From this example, it can be observed that there is an apparent loss of information, as land cover category 3 and soil type category 2 do not exists for model calculations. It can be argued that, in the matter of achieving balance between watershed representation and computational efficiency, some compromises are required. It is therefore suggested that thresholds should only be applied when the number of HRUs delineated (function of drainage area and the thresholds) results in acceptable computation costs (Gitau 2003). Moreover, it must be emphasized that not all HRUs are contiguous in nature (e.g. HRU number 2 in Fig. 1d), as, although in may appear that only one cell (HRU number 6) separates the three other cells that belong to HRU number 2; this non-contiguity pattern can be more pronounced on a sub-basin scale.

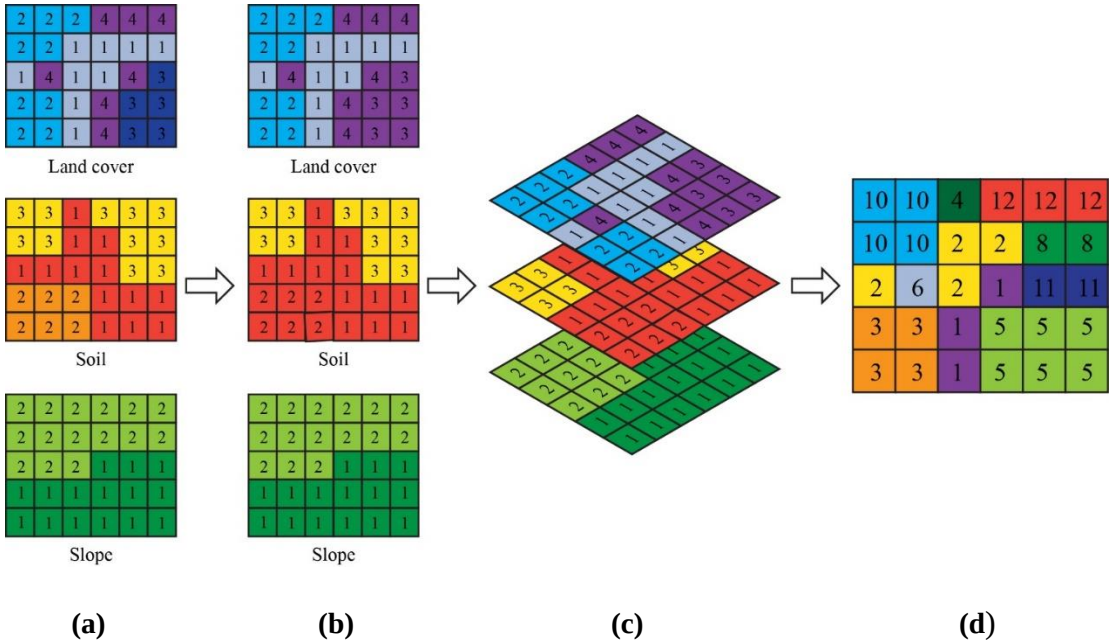


**Figure 1:** Illustration of the unique combination HRU delineation algorithm: (a) Layer of geographic information for land cover, soil, and slope; (b) lumped categories within each map after applying a threshold of 20, 30, and 20% for land cover, soil, and slope, respectively. Note: lumped areas have similar cell background; (c) layer overlay; and (d) final HRU distribution according to Table 2

**Table 2:** Unique combination of land cover, soil, and slope of the HRUs delineated in Figure 1

| | HRU Unique Combination ID | | | | | | | | | | | |
|---|---|---|---|---|---|---|---|---|---|---|---|---|
| | 1 | 2 | 3 | 4 | 5 | 6 | 7 | 8 | 9 | 10 | 11 | 12 |
| Land cover | 1 | 1 | 2 | 2 | 4 | 4 | 1 | 1 | 2 | 2 | 4 | 4 |
| Soil | 1 | 1 | 1 | 1 | 1 | 1 | 3 | 3 | 3 | 3 | 3 | 3 |
| Slope | 1 | 2 | 1 | 2 | 1 | 2 | 1 | 2 | 1 | 2 | 1 | 2 |

This unique combination HRU concept has been adopted and widely used by SWAT (Arnold et al. 1993; Neitsch et al. 2005). While the incorporation of HRUs has allowed SWAT the flexibility to adapt from field plots to entire river basins, the fact that HRUs are used in a non-spatial manner, i.e. they are not identified spatially within simulations, is regarded as key weakness of the model (Gassman 2008; Gassman et al. 2007).

However, in most distributed hydrological models, the river basin is assumed to be an assembly of discrete entities (typically grid cells), with different properties, that contribute differently to its responses. Some of these properties are in fact parameters, since they cannot be determined by field measurements at the small-scale (although

physically-based approaches treat them as known properties rather than as unknown quantities; cf. Refsgaard, 1997). Thus, HRUs denote spatial elements of pre-determined geometry, while the parameterization of the hydrological processes is dictated by the model discretization (Efstratiadis et al., 2008; Nalbantis et al., 2011; Daniel et al., 2011). A well-known example is the HEC-HMS model, which considers different parameters per sub-basin, thus the number of parameters increase linearly with the number of sub-basins.

Efstratiadis et al. [(Efstratiadis et al. 2008)] proposed an alternative definition of HRUs, as the product of separate partitions of the basin that account for different properties, such as land use, soil permeability, geology, slope, etc. This product is known as the common refinement of the partitions, while the related procedure in GIS will be next referred to as the "union of layers". This approach has been adopted in their modelling system HYDROGEIOS, in an attempt to make schematization and parameterization two clearly independent procedures. Using an appropriate classification of the key watershed properties, the number of HRUs and, consequently, the number of parameters are manually adjusted. In particular, the number of HRUs is determined as the product of the parent layer classes, i.e., $N = \prod n_j$, where $n_j$ is the number of classes corresponding to the $i$-th layer. The process is illustrated in Figure 2 below. Using the same 30 cell-rectangular sub-basin example as before with four, three and two different classes of land cover, soil type and slope categories, respectively (Fig. 2a), the final number of classes of each watershed properties is adjusted based on the desired number of HRUs. Assuming that the available hydrological information allows for the configuration of only four HRUs, as this is subject to the classical conflict between accuracy in the representation of process heterogeneity and model parsimony (Section 2.3.3.5), the number of classes corresponding to the watershed properties must be adjusted accordingly. Given that $N = 4$, the product of the number of land use classes $n_1$, soil type classes $n_2$ and terrain slope classes $n_3$; must then be equal to four, i.e. $n_1 \times n_2 \times n_3 = 4$. As shown in Fig. 2b, the four, three and two different classes of land cover, soil type and slope categories, respectively, have been adjusted to two, two and one class, respectively, in order for their product to be equal to four, i.e. $2 \times 2 \times 1 = 4$ (Fig. 2b). A spatial overlay is then performed (Fig. 2c), so that cells that have the same combination of land cover, soil type and slope category produce a different HRU (Fig.

2d). Similarly, with the unique combination example illustrated in Figure. 1, an apparent loss of information is observed. However, in this case, the user can control beforehand which land cover, soil type or terrain slopes are lumped in the process, while the final number of HRUs is also predetermined.

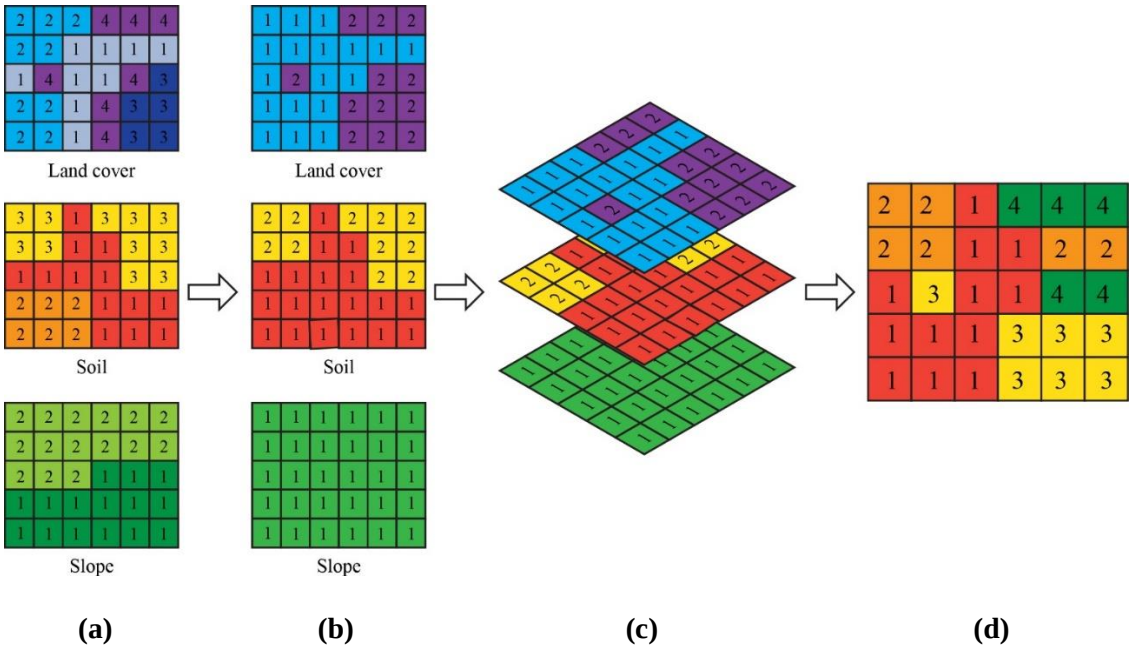


**Figure 2:** Illustration of the union of layers HRU delineation method: (a) Layer of geographic information for land cover, soil, and slope; (b) adjusted category classes land cover, soil, and slope, based on the desired final HRU number; (c) layer overlay; and (d) final HRU distribution

In contrast to classical parameterization approaches, HRUs do not represent contiguous geographical areas (while sub-basins are by definition contiguous). Instead, they represent basin partitions with common characteristics, and thus common parameter values. The intersection of the sub-basin and HRU layers represents the minor geographical elements in the modelling procedure, driven by the rainfall and Potential Evapotranspiration (PET) of the corresponding sub-basin and responding according to the parameter values of the corresponding HRU. The shape of this non-contiguous element is of no interest, since at each time step, the runoff generated by HRUs is integrated over sub-basins and propagated to their outlet. The key advantage of this approach is its flexibility, since there are no restrictions on the configuration of HRUs, while the availability of data (critical for calibration) does not influence the watershed schematization, i.e., the delineation of sub-basins: one may consider a large number of sub-basins, in order to provide a detailed spatial representation of runoff across the

watershed, while keeping a parsimonious parameterization. However, the fact that the delineation of HRUs is disengaged from watershed schematization does not necessarily ensure efficient, physically-consistent and parsimonious parameterizations, as the modeler is still allowed to determine any combination of layers. In addition, by definition, the number of HRUs is equal to the product of different classes that are accounted for within the formulation of the aforementioned layers. If one wishes to reduce the number of HRUs, one must manually merge the initial HRUs, thus losing information and physical consistency. The above shortcoming was the motivation to develop an improved procedure for HRU delineation, based on the well-established curve number concept, which is even more flexible and, at the same time, easy to implement within any modelling scheme.

### 2.3.3 Advantages and Limitations

This section provides a review of five HRU research topics that highlight the advantages and limitation of the HRU delineation concept;

(a) the effect of HRU definition thresholds applied for land use, soil and slope, on hydrologic model predictions;
(b) the limitation of hydrologic models to fully account for slope variability in the HRU level, therefore being less accurate on upland catchment simulations;
(c) the non-spatial nature of HRUs, meaning that they are not identified spatially within simulations;
(d) the output shape of HRUs and how realistically represents the watershed terrain; and finally,
(e) the parameter uncertainty inherited thought the HRU configuration.

#### 2.3.3.1 *Definition Thresholds*

The emphasis on the effect of watershed subdivision has led to a more complete understanding of the hydrological cycle and is considered crucial to the investigation of how accurate model input parameters describe the watershed structure and how land use, soil type and slope alter the water cycle components (Zhang et al. 2013). Spatial discretization most commonly divides a watershed in HRUs (Xu et al. 2011) and the effect of HRU definition in watershed modeling has been the question of many modelers, as they create or revise hydrological models, and the main goal of many

research studies yielding conflicting results. The effects of watershed subdivision in HRUs has been investigated on the accuracy or behavior of various semi-distributed model outcomes, including runoff (Mamillapalli et al. 1991; Manguerra & Engel 1998), streamflow (Haverkamp et al. 2003; Setegn et al. 2008; Rouhani et al. 2009; Githui & Thayalakumaran 2011; Cho et al. 2010), sediment yield and sediment generation (FitzHugh & Mackay 2001; Chen & Mackay 2004; FitzHugh & Mackay 2000; Muleta et al. 2007), sediment and nutrient concentrations (Jha et al. 2004; Arabi et al. 2006), best management practices (BMPs) implementation (Arabi et al. 2006), water balance components such as evapotranspiration, percolation and soil waters content (Tripathi et al. 2006), as well as parameter uncertainty (Gong et al. 2010; Kumar & Merwade 2009). Table 3 summarizes the characteristics of these studies, including the location and size of the watershed(s) investigated, the subdivision schemes applied, the land use, soil and slope thresholds used for the HRU definition and finally the main findings and conclusions.

Mamillapalli et al. (1996) examined the effects of increasing level of discretization and HRUs using different soil and land use combinations and showed that, in general, increased watershed subdivision and finer HRU delineation within each sub-watershed increases the runoff accuracy. Accuracy increased up to the 20 sub-watershed scheme of average sub-watershed size 215 $km^2$. Beyond that level, accuracy improvements plateaued. Although coarser aggregation levels resulted in decreases in accuracy, increasing the number of HRUs by lowering the land use and soil thresholds successfully compensated for the decreased number of sub-watersheds. In contrast, Manguerra & Engel (1998) found that runoff predictions were insensitive to sub-watershed and/or HRU variations. They examined the effects of watershed subdivision on total runoff predictions and showed that only slight improvements in runoff prediction were apparent with increased discretization in the sub-watershed/HRU approach, but generally runoff prediction was concluded to be insensitive to sub-watershed and/or HRU variations. This seems to be due to the agricultural nature of the watersheds modeled, which were relatively flat with small variations in land use and soil, while Mamillapalli et al. (1996) modeled a watershed with great variations in climatic, land use, soil and topographic characteristics, producing significant areas of low and high potential runoff.

**Table 3:** Summary of HRU definition research studies [dom. = dominant]

| Reference | Location | No. of Basins | Size ($km^2$) | No of Subwatersheds | No of HRUs | LU - Soil - Slope Definitions | Findings |
|---|---|---|---|---|---|---|---|
| Mamillapalli et al. (1996) | Texas USA | 1 | 4297 | 4, 8, 14, 20, 24, 29, 35, 40, 54 | 1 | dom. - dom. - no<br>20% - 40% - no<br>15% - 30% - no<br>10% - 20% - no<br>5% - 10% - no | Runoff accuracy - Increased up to20 subwatersheds (215$km^2$) and 5%-10% HRU definition |
| Manguerra & Engel (1998) | Animan Science & Greenhill Indiana USA | 2 | 3.28<br>113.38 | 1 | 1, 3, 6, 16, 26; | dom, - dom, - no | Runoff accuracy – Increased (slightly) with increased subdivision |
| Haverkamp et al. (2003) | Weiherbach & Dietzhoelze, Germany; Bosque River, Texas USA | 3 | 6.3;<br>81.7;<br>4297.0 | 3,5,6,9,14,17,20,25,27,35,52,54,60,78,99,127, 163,297 | 1 | dom. - dom. - no;<br>10% - 5% - no | Streamflow accuracy - Increased up to 78 subwatersheds (1$km^2$) using the dominant LU and Soil, and up to 9 subwatersheds (9$km^2$) using the HRU definition |
| FitxHugh & Mackay (2000, 2001) | Pheasant Brach, Winsconsin USA | 1 | 47.3 | 3, 5, 1, 23, 47, 73, 97, 181 | 29, 64, 138, 244, 425, 638, 831, 1384 | 10% - 10% - no | Streamflow and Runoff - Insensitive to subdivision<br>Sediment yield- Insensitive to subdivision<br>Sediment generation - Decreased with increased subdivision |
| Chen & Mackay (2004) | Pheasant Brach, Winsconsin USA | 1 | 47.3 | 5<br>25<br>95<br>179 | 5, 13, 23, 79;<br>25, 75, 181, 769;<br>95, 350, 626, 998;<br>179, 675, 1095, 1569 | dom. - dom. - no;<br>20% - 15% - no;<br>10% - 10% - no;<br>5% - 5% - no | Streamflow - Insensitive to subdivision<br>Sediment yield and generation - Decreased |

| | | | | | | | |
|---|---|---|---|---|---|---|---|
| | | | | | | | with increased subdivision |
| Jha et al. (2004) | Iowa, USA | 4 | 1929; 4776; 10829; 17941 | 5, 11, 17, 27, 35, 47, 53; 3, 11, 17, 27, 37, 47; 3, 9, 17, 27, 37, 47; 3, 9, 15, 23, 35 | 1 | 0% - 0% - no | Streamflow, Sediment and Nutrient accuracy - Increased (slightly) with increased subdivision Streamflow - Insensitive to subdivision Sediment and Nutrient (N,P) yield - Decreased with increased subdivision (optimal subwatershed sizes 3%, 2% and 5% of the total drainage area for sediment yield, N and inorganic P respectively) |
| Arabi et al. (2006) | Dreisback & Smith Fry, Indiana, USA | 2 | 6.23 7.30 | 1, 2, 5, 8, 11, 19, 29, 51, 103; 1, 4, 8, 12, 20, 33, 63, 89 | 73, 91, 138, 180, 204,301, 359, 470, 647; 95, 159, 239, 278, 358, 429, 577, 676 | 0% - 0% - no | Sediment and Nutrient (N,P) yield - Decreased with increased subdivision BMPs - sensitive to subdivision level (optimal subwatershed size 4% of the total drainage area for BMP evaluation) |
| Tripathi et al. (2006) | Nagwan wateshed, India | 1 | 90.23 | 1, 12, 22 | 1 | dom. - no - no | Water balance - Insensitive to subdivision Runoff - Insensitive to subdivision ET, Percolation and Available Soil Content - Vary with increased subdivision |

| | | | | | | | |
|---|---|---|---|---|---|---|---|
| Muleta et al. (2007) | Big Creek, Illinois USA | 1 | 133 | 9, 75, 118 | 9, 75, 118;<br>22, 217, 352 | dom. - dom. - no;<br>20% - 20% - no | Streamflow and Sediment accuracy - Increased with increased subdivision<br>Streamflow - Insensitive to subdivision<br>Sediment yield and generation - Decreased with increased subdivision |
| Setegn et al. (2008) | Lake Tana Basin, Ethiopia | 1 | 15096 | DNF | 1 | dom. HRU<br>20% - 10% - 20%<br>10% - 20% - 10%<br>10% - 10% - 20%<br>20% - 20% - 10%<br>25% - 30% - 20% | Streamflow accuracy - increased with increased subdivision up to 34 subwatersheds (444km$^2$) and 214 HRUs (10%-20%-20%) |
| Rouhani et al. (2009) | Grote Nete River, Belgium | 1 | 384 | 1, 4, 9, 21, 40, 65 | 1, 42, 71, 169, 280, 392 | dom. HRU | Streamflow accuracy - increased with increased subdivision up to 21 subwatersheds (18km$^2$)<br>Daily slow flow - insensitive to subdivision<br>Daily total flow - increased with increased subdivision |
| Kumar & Merwade (2009) | St. Joseph River, USA | 2 | 2800;<br>700 | 10, 12, 24, 36, 58, 97;<br>7, 9, 15, 17, 23, 41 | 124, 145, 320, 391, 750, 1209;<br>97, 110, 209, 273, 401, 558;<br>107, 139, 266, 305, 365, 722;<br>62, 98, 133, 164, 216, 310; | dom. HRU | Streamflow - Insensitive to subdivision<br>Significant parameters - narrow uncertainty range across subdivisions<br>Non-Significant parameters - wide uncertainty range across subdivisions |

| | | | | | | | |
|---|---|---|---|---|---|---|---|
| Gong et al. (2010) | Upper Daning River, China | 1 | 2010 | 7, 9, 13, 19, 23, 37, 55 | 1 | 0% - 0% - 0% | Parameter uncertainty – narrow range across subdivisions<br>Streamflow accuracy - increased up to 13 subwatersheds (155km$^2$)<br>Sediment yield accuracy - increased up to 55 subwatersheds (37km$^2$) |
| Cho et al. (2010) | Little River, Georgia USA | 1 | 15.7 | 3, 11, 17, 29, 35, 54, 96, 180 | 331,656,830,1074,1176,1422,1826, 2326 | 0% - 0% - no | Streamflow - Insensitive to subdivision<br>Sediment and Nutrient yield - Decreased with increased subdivision |

Haverkamp et al. (2003) developed a statistical approach/tool, called SUSTAT, based on entropy, with the objective to identify the appropriate level of discretization for optimizing the accuracy of model results. It was concluded that the HRU approach produced more accurate streamflow predictions, resulting in higher entropy values, as opposed to using just a single dominant land use and soil type. Similarly to Mamillapalli et al. (1996), model efficiency increases up to a certain number of sub-watersheds, beyond which model accuracy improves insignificantly; for the Dietzhoelze watershed is was 78 sub-watersheds with the dominant land use and soil approach, and 9 sub-watersheds with the HRU approach. Results proved that the SUSAT tool identified within an acceptable limit the appropriate level of subdivision.

Both FitzHugh & Mackay (2000, 2001) and Chen & Mackay (2004) applied SWAT to study the effects of watershed subdivision on streamflow and sediment prediction. FitzHugh & Mackay (2000) showed that increasing subdivision did not seriously affect streamflow or outlet sediment, mainly due to the transport-limited nature of the watershed. However, it caused sediment generation to decrease substantially (by 44%). This revealed a non-linear relationship between sediment generation (MUSCLE equation) and land use and soil attributes, as well as the HRU area used to capture land use and soil variability in the sub-watershed. Based on this analysis, FitzHugh & Mackay (2000) developed two simple indexes that can be directly incorporated into a GIS and predict sediment generation estimates prior to model running. FitzHugh & Mackay (2001) also found that sediment yield varied at the outlet of the watershed when source-limited and transport-limited watershed scenarios were compared.

Chen & Mackay (2004) discuss the results obtained by FitzHugh & Mackay (2000, 2001) and state that they do not adequately explain the reasons why runoff and sediment yield respond differently to spatial data aggregation, compared to sediment generation. Based on this finding, the hypothesis emerged that the effect of spatial aggregation is observed partly due to the model structure, and therefore sub-models for runoff and sediment yield have different responses to the same change in spatial representation. Chen & Mackay (2004) tested this hypothesis focusing on the effect of model structure in relation to watershed subdivision. Similar to FitzHugh & Mackay (2000, 2001), it was concluded that annual streamflow was found to be unaffected by increased watershed subdivision, while sediment yield decreased as the number of HRUs

increases within a given watershed delineation. Regarding sediment generation, results showed an initial increase at the coarse watershed configurations. A decrease was then observed as the number of HRUs increased to 1569. This was attributed to the averaging of the topographic attributes, variations in the statistical distribution of the detachment factors of sediment, and the linear scaling of the MUSCLE equation outputs from the HRUs to the sub-watershed level. HRUs neglect the non-linear relationship between the runoff energy and sediment generation in the MUSCLE equation, causing the sediment generation to decrease when the HRU area is decreased. It is therefore concluded that model structure plays a significant role in the response of the model to spatial data aggregation. Integration of MUSCLE, which assumes a topographically based spatial connectivity and non-spatial HRUs, is conceptually incompatible (Chen & Mackay 2004).

Jha et al. (2004) evaluated the impact of watershed subdivision on flow, sediment yield and nutrient losses predictions. Moreover, they developed a guideline for identifying an appropriate sub-watershed scale for efficiently simulating watershed behavior and for reducing input data preparation and thus computational evaluation efforts without significantly compromising the accuracy of the simulation. Similarly to previous studies (FitzHugh & Mackay 2000; Chen & Mackay 2004), results showed that streamflow was not significantly affected by increased subdivision, while the opposite result was found regarding sediment yield and nutrient concentrations predictions. The optimal threshold sub-watershed sizes with respect to the total drainage area were found to be approximately 3%, 2% and 5% for accurately simulating sediment yield, nitrate (N) and inorganic phosphorous (P), respectively. Small sub-watershed sizes did not significantly increase the simulation accuracy

Arabi et al. (2006) investigated the effect of watershed subdivision on the evaluation of Best Management Practices (BMPs) regarding sediment and nutrients within a watershed. BPM were applied at the HRU levels and simulations were performed for all subdivision schemes, with and without the representation of BMP. Results showed that sediment, total P, and total N predictions were highly influenced by the level of subdivision without BMP representation, agreeing with findings of previous studies (FitzHugh & Mackay 2000; Chen & Mackay 2004; Jha et al. 2004). After implementation of the BMPs, predicted reduction of sediment and nutrient yields were

insignificant with coarser delineations, but reduction became apparent with finer delineations. It was therefore concluded that evaluation of the BMPs impacts on sediment and nutrient yield is very sensitive to the watershed delineation level. The optimal sub-watershed size was identified to be approximately 4% of the total watershed area, to adequately represent the influence of these BMPs using SWAT.

Tripathi et al. (2006) expressed the need to study the watershed subdivision effects on water balance components, including evapotranspiration (ET), percolation and soil water content; since no previous research extended beyond modelling runoff and sediment yield. A perfect water balance was achieved for the watershed under all subdivision schemes. Results show no variation in the total runoff prediction with increased subdivision, while variations were observed for other water balance components: ET (5%-48%), percolation (2%-26%) and soil water content (0.3%-22%). Thus, based on this study, it is concluded that watershed subdivision has a significant effect on the water. It is therefore concluded that waters balance components are highly affected by watershed subdivision.

Muleta et al. (2007) examined the sensitivity of SWAT output to spatial scale and showed that finer watershed discretization, in both sub-watersheds and HRUs, increases model accuracy for both streamflow and sediment yield. Similar with FitzHugh & Mackay (2000), Chen & Mackay (2004) and Jha et al. (2004), streamflow and its components were found to be relatively insensitive to watershed subdivision, while sediment generation and sediment yield decreases with increases in watershed subdivision. It was also found, unlike previous studies (FitzHugh & Mackay 2000), that parameters derived from topography, land use and soil are responsible for sediment generation, while channel slope and length properties along with topography, land use and soil properties are responsible for sediment processes in the channel. Therefore, sediment yield significantly varies even when outlet channel properties remain the same. Moreover, sediment yield was found to be sensitive to human activities conducted in the subwatersheds, indicating that SWAT is capable to evaluate consequences of alternative watershed management practices

Setegn et al. (2008) examined the impact of watershed subdivision and HRUs on SWAT streamflow predictions and concluded that the 34 sub-watershed delineations resulted in the best representation of the hydrological processes and best model efficiency. Further

increases in sub-watershed number produced no significant changes in streamflow simulation. HRU analysis showed that the 10%-20%-10% combination resulting in 214 HRUs gave the best streamflow estimation, while the single HRU option produced unsatisfactory results. Increasing the HRU threshold definitions decreases evapotranspiration since less land use classes are included in the simulations. It is concluded that HRU characteristics and therefore HRU definition is the key factor affecting streamflow, which was confirmed by the model sensitivity analyses, which showed that flow is more sensitive to HRU definition thresholds than sub-watershed delineation.

A similar research was performed by Rouhani et al. (2009), who examined the effect of sub-watershed number as well as the spatial distribution of aerial rainfall on streamflow components prediction. Streamflow and it components was only moderately affected by different delineation level. These results are in line with Mamillapalli et al. (1996), but in contrast with Jha et al. (2004). The 21-sub-watershed model yielded the highest accuracy, while model performance decreased with further increase in subdivision. This was explained by the fixed parameter number applied to the different subdivision schemes. Daily slow flow components remained unaffected by the different subdivisions in contrast with daily total flow. Moreover, increased subdivision models are less able to simulate extreme flow effectively.

Kumar & Merwade (2009) stated that there is lack of information regarding the impact of watershed subdivision and soil data resolution on SWAT model calibration and parameter uncertainty. It was found that calibrated parameters were different for all 24 subdivision configurations, although their effect on model output was minimal. Parameter uncertainty analysis showed that significant parameters exhibit very narrow uncertainty range across different subdivision configurations in comparison with non-significant parameters. It was also concluded that fewer significant parameter could reduce model parameter uncertainty and accelerate the calibration process. With regards to model output, cross–validation showed that streamflow predictions are not affected by the level of subdivision, highlighting the non-unique nature of calibrated parameters in hydrologic modeling.

Parameter uncertainty in watershed subdivision was also considered by Gong et al. (2010). Previous studies only used one set of tested parameter values for simulating

different subdivision schemes (Manguerra & Engel 1998; Arabi et al. 2006; Tripathi et al. 2006). Gong et al. (2010) discusses that, due to parameter uncertainty, equifinality always occurs in hydrology (Beven 1993, 2006). Consequently using the same set of parameters in different subdivision schemes is inappropriate. Gong et al. (2010) aim to identify an appropriate subdivision scheme while considering parameter uncertainty. Different parameter values were obtained for each subdivision scheme, and considering that model structure and inputs were the same for all subdivisions, differences in model outputs will primarily be caused by parameter uncertainty. Results showed that the 13 sub-watershed scheme produced the most accurate results. Differences in parameter uncertainty were relatively small among subdivision schemes.

Cho et al. (2010) investigated the effects of watershed subdivision and different filter strip width (FILTERW) configurations and showed that streamflow predictions remained stable for all subdivision schemes and FILTERW configurations, with only a 0.8% variation between the minimum and maximum streamflow prediction. Predicted sediment and nutrient concentrations from upland areas decreased with increased subdivision level. The impact of different HRU number and parameters on flow and ET was investigated by Githui & Thayalakumaran (2011). Results showed that evapotranspiration is not affected by the number of HRUs or by the parameter transfer between models. Flow on the other hand was influence by both the number of HRUs and model parameterization. In general, the 11-HRU model performed better that the 98-HRU model in simulating flow and ET. More detailed watershed discretization is necessary for better quantification of the water balance.

From the literature described above and summarized in Table 3, it can be observed that many different sizes of watersheds have been modeled, applying multiple subdivision schemes, each having a specific study goal and producing conflicting results. Moreover, each study used a unique combination of data inputs and calibration techniques. Therefore, they are not fully comparable and it is difficult to draw universal conclusions, mainly due to the specificity of each investigation. However, some important conclusions are obtained and will be used as guidelines for further research.

Findings regarding the effect of subdivision level on model accuracy show that simulation that included the HRU delineation yielded better results compared to simulation performed only at the sub-watershed level. It was also observed that, in most

cases, accuracy increased with increased subdivision up to a certain sub-watershed size, usually a moderate one. This relates to the less sensitive two-tiered subdivision scheme employed by SWAT, where a watershed within only a few sub-watersheds can actually have many HRUs and therefore capture spatial variability. This is why, by incorporating HRUs, high model accuracy is achieved without increased subdivision in the sub-watershed level. In the HRU level however, studies that experimented with multiple HRU definitions observed that, within the same sub-watershed configurations, accuracy in the simulation increases as more and more land use, soil and slope combinations are simulated, choosing smaller definition thresholds (Mamillapalli et al. 1991; Chen & Mackay 2004; Setegn et al. 2008). The same conclusion was drawn from studies that compared the use of dominant land use and soil option, or the dominant HRU option, with multiple HRUs using definition thresholds (Manguerra & Engel 1998; Haverkamp et al. 2003; Muleta et al. 2007).

Regarding the effect on watershed subdivision on model output, it was indicated by many studies that runoff and streamflow predictions were insensitive to increased subdivision (FitzHugh & Mackay 2000; Gong et al. 2010; Jha et al. 2004; Tripathi et al. 2006; Muleta et al. 2007; Kumar & Merwade 2009; Cho et al. 2010; Githui & Thayalakumaran 2011), while sediment generation, sediment yield and nutrient concentration prediction exhibited a decrease up to a certain subdivision level, after which they stabilized (FitzHugh & Mackay 2000; Gong et al. 2010; Jha et al. 2004; Muleta et al. 2007; Cho et al. 2010). Moreover, it was observed that water balance remains unaffected by increased subdivision (Tripathi et al. 2006), while water balance components such as evapotranspiration, percolation and soil water content vary (Tripathi et al. 2006; Githui & Thayalakumaran 2011). Finally, significant simulation parameters varied by only a narrow range across subdivision (Kumar & Merwade 2009; Gong et al. 2010), in opposition with non-significant simulation parameters (Kumar & Merwade 2009).

#### 2.3.3.2 *Slope Factor*

To account for the lack of sub-daily meteorological data, physiological attributes of plants and physical soil properties, many hydrological models have adopted the Soil Conservation Service – SCS (now called the Natural Resources Conservation Service –

NRCS) Curve Number method (NRCS 1972), the most common method for predicting runoff.

The curve number, CN, is a conceptual parameter, ranging from 1 to 100, attempting to capture in a single value the physiographic characteristics of a catchment that are associated with runoff generation. The method is widely used in the context of the homonymous rainfall-runoff modelling approach, and depends on soil and land characteristics, as well as on the soil moisture present in the soil profile before the start of a rainfall event.

The SCS runoff equation is:

$$Q = \frac{(P - I_a)^2}{(P - I_a) + S} \tag{1}$$

where:

$Q$ = runoff (mm)

$P$ = rainfall (mm)

$S$ = potential maximum retention after runoff begins (mm)

$I_a$ = initial abstraction (mm)

Initial abstraction $(I_a)$ includes all losses before runoff such as water retained in surface depressions, water intercepted by vegetation, evaporation, and infiltration. Although $I_a$ can vary greatly, it is largely correlated with soil and land cover parameters, and is therefore approximated by the empirical equation:

$$I_a = \alpha S \tag{2}$$

where $\alpha$ is the percentage of initial abstractions. A 20% of initial abstractions is applied, i.e. $\alpha$ = 0.2 as recommended by literature (Ponce & Hawkins 1996).

Substituting Eq. (2) in Eq. (1) allows the use of a combination of $S$ and $P$ to produce a unique runoff amount:

$$Q = \frac{(P - 0.2S)^2}{P + 0.8S} \text{ for } P > 0.2S \tag{3}$$

$$Q = 0 \qquad \text{for } P \leq 0.2S$$

Finally, *S* is associated to the soil land cover conditions of the river basin through the CN parameter

$$S = \frac{25400}{\mathrm{CN}} - 254 \tag{4}$$

In particular, the CN parameter is determined from NRCS lookup tables accounting for several combinations of land use/land cover characteristics and four hydrological soil groups (HSGs). Table 4 below shows the HSG classification (A, B, C and D) based on their minimum infiltration rate, while Table 5 shows the runoff curve number according to SCS for urban areas, cultivated and other agricultural lands and arid and semi-arid rangelands, for each HSG. These reference CN values have been obtained experimentally from rainfall and runoff measurements over a wide range of geographic, soil, and land management conditions. Moreover, the method considers three antecedent soil moisture conditions (AMC), depending on the cumulative 5-day antecedent rainfall and the season category, dormant or growing: AMC I: dry conditions corresponding to 5-day antecedent rainfall less than 13 mm for dormant and less than 35 mm for growing season, AMC II: moderate conditions corresponding to 5-day antecedent rainfall of 13-38 mm for dormant and 35-53 mm for growing season, and AMC III: wet conditions corresponding to 5-day antecedent rainfall less than 38 mm for dormant and more than 53 mm for growing season. The reference CN values shown in Table 5 are for AMC II conditions and the typically-used ratio of initial abstraction losses, i.e. 20 % of maximum potential retention (henceforth referred to as reference conditions). The CN parameter can be adjusted for AMC I and AMC III based on the following equations:

$$\mathrm{CN_I} = \frac{4.2\ \mathrm{CN_{II}}}{10 - 0.058\ \mathrm{CN_{II}}} \tag{5}$$

$$\mathrm{CN_{III}} = \frac{23\ \mathrm{CN_{II}}}{10 + 0.13\ \mathrm{CN_{II}}} \tag{6}$$

The adjustment of the CN parameter to dry and wet conditions compared to the moderate soil moisture conditions can also be seen in Figure 3.

**Table 4:** NRCS Hydrologic Soil Group classification (Source: USDA, 1986)

| HSG | Description | Soil texture |
|---|---|---|
| A | Low runoff potential and high infiltration rates even when thoroughly wetted and consist chiefly of deep, well to excessively drained sand or gravel. High rate of water transmission (<7.50 mm/hr) | Sand, loamy sand, or sandy loam |
| B | Moderate infiltration rates when thoroughly wetted and consist chiefly of moderately deep to deep, moderately well to well drained soils with moderately fine to moderately coarse textures. Moderate rate of water transmission (3.75-7.50 mm/hr) | Silt loam or loam |
| C | Low infiltration rates when thoroughly wetted and consist chiefly of soils with a layer that impedes downward movement of water and soils with moderately fine to fine texture. Low rate of water transmission (1.30-3.75 mm/hr). | Sandy clay loam |
| D | High runoff potential and very low infiltration rates when thoroughly wetted and consist chiefly of clay soils with a high swelling potential, soils with a permanent high water table, soils with a claypan or clay layer at or near the surface, and shallow soils over nearly impervious material. Very low rate of water transmission (0-1.30 mm/hr). | Clay loam, silty clay loam, sandy clay, silty clay, or clay |

**Table 5:** Runoff curve number according to SCS for urban areas, cultivated and other agricultural lands and arid and semi-arid rangelands for rainfall type II (Source: Koutsoyiannis 2011; USDA 1986)

| Land cover description | Curve number for hydrologic soil group | | | |
|---|---|---|---|---|
| | A | B | C | D |
| *Urban areas* | | | | |
| Open space (lawns, parks, golf courses, cemeteries, etc. | | | | |
| Poor condition (grass cover < 50%) | 68 | 79 | 86 | 89 |
| Fair condition (grass cover 50% to 75%) | 49 | 69 | 79 | 84 |
| Good condition (grass cover >75%) | 39 | 61 | 74 | 80 |
| Impervious areas: | | | | |
| Paved parking lots, roofs, driveways, etc. | 98 | 98 | 98 | 98 |
| Paved streets with curbs and storm sewers | 98 | 98 | 98 | 98 |
| Paved streets with open ditches | 83 | 89 | 92 | 93 |
| Gravel roads | 76 | 85 | 89 | 91 |
| Dirt roads | 72 | 82 | 87 | 89 |
| Western desert urban areas: | | | | |
| Natural desert landscaping | 63 | 77 | 85 | 88 |
| Artificial desert landscaping | 96 | 96 | 96 | 96 |
| Urban districts: | | | | |
| Commercial and business - 85% impervious | 89 | 92 | 94 | 95 |
| Industrial - 72% impervious | 81 | 88 | 91 | 93 |
| Residential districts by average lot size: | | | | |

| | | | | |
|---|---|---|---|---|
| 1/8 acre or less (town houses) - 65% impervious | 77 | 85 | 90 | 92 |
| 1/4 acre - 38% impervious | 61 | 75 | 83 | 87 |
| 1/3 acre - 30% impervious | 57 | 72 | 81 | 86 |
| ½ acre - 25% impervious | 54 | 70 | 80 | 85 |
| 1 acre - 20% impervious | 51 | 68 | 79 | 84 |
| 2 acres - 12% impervious | 46 | 65 | 77 | 82 |
| *Cultivated agricultural lands* | | | | |
| Fallow* | 74-77 | 83-86 | 88-91 | 90-94 |
| Row crops* | 61-72 | 70-81 | 77-88 | 80-91 |
| Small grain* | 58-65 | 69-76 | 77-84 | 80-88 |
| Close-seeded or broadcast legumes or rotation meadow* | 51-66 | 67-77 | 76-85 | 80-89 |
| *Other agricultural lands* | | | | |
| Pasture, grassland, or range – continuous forage for grazing* | 39-68 | 61-79 | 74-86 | 80-89 |
| Meadow – continuous grass, protected from grazing and generally mowed for hay | 30 | 58 | 71 | 78 |
| Brush – brush-weed-grass mixture with brush the major element* | 30-48 | 48-67 | 65-77 | 73-83 |
| Woods – grass combination* | 32-57 | 58-73 | 72-82 | 79-86 |
| Woods* | 30-45 | 55-66 | 70-77 | 77-83 |
| Farmsteads – buildings, lanes, driveways, and surrounding lots | 59 | 74 | 82 | 86 |
| *Arid and semi-arid rangelands* | | | | |
| Herbaceous – mixture of grass, weeds, and low-growing brush* | - | 62-80 | 74-87 | 85-93 |
| Oak-aspen –mixture of oak brush, aspen, mountain mahogany, bitter brush, and maple* | - | 30-66 | 40-74 | 48-79 |
| Pinyon-juniper – pinyon, juniper, or both; grass understory* | - | 41-75 | 61-85 | 71-89 |
| Sagebrush with grass understory* | - | 35-67 | 47-80 | 55-85 |
| Desert shrubs – saltbush, greasewood, creosote bush, black bush, bursage, palo verde, mesquite, and cactus* | 49-63 | 68-77 | 79-85 | 84-88 |

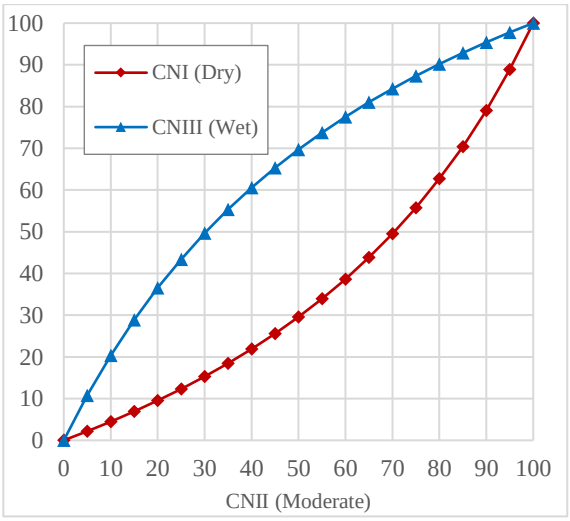


**Figure 3:** CN parameter adjustment for dry and wet soil moisture conditions, compared to the moderate soil moisture conditions

The CN method however, does not take into account the effect of slope (Huang et al. 2006; Xu et al. 2011). Slope is a factor that affects dramatically the hydrological processes of a watershed. On steeper slopes, reduction of the initial abstraction, a decrease in infiltration, and a reduction of the recession time of overland flow results in increased surface runoff (Huang et al. 2006). The curve numbers obtained from the NRCS handbook are assumed to correspond to a 5% slope, while most studies do not account for the slope when determining the CN, and therefore the surface runoff. Some hydrological models, such as SWAT, allow the users to adjust the CN values by slope. This adjustment must be done before inputting the CN values and according to the average slope of the watershed investigated. Using the CN method without including the slope factor has many disadvantages, especially in regions with various landforms and steep slopes. Using slope as a factor for HRU delineation and adjusting the CN values accordingly would improve the accuracy runoff simulation (Xu et al. 2011).

Huang et al. (2006) stresses the need for an appropriate method to predict runoff from steep land, as it is considered essential for the delineation of sensitive areas in order to protect them and to develop suitable agricultural practices that will reduce runoff and soil loss. Despite the extent of cultivation on hillslope areas, very few attempts have been made to incorporate a slope factor into the CN method. One of these attempts is the slope-adjusted $CN_2$, named $CN_{2a}$ by Sharpley & Williams (1990), which is obtained by:

$$CN_{2a} = \frac{1}{3}(CN_3 - CN_2)(1 - 2e^{-13.86a}) + CN_2 \quad (7)$$

Where $CN_2$ and $CN_3$ are the SCS CN values for soil moisture condition 2 (average) and soil moisture condition 3 (wet), and a ($m \cdot m^{-1}$) is the slope. $CN_{2a}$ is used instead of $CN_2$ in the subsequent runoff calculations. Note that the method assumes that $CN_2$ obtained from the SCS handbook table corresponds to a 5% slope.

The slope adjusted $CN_{2a}$ equation was evaluated and by Huang et al. (2006). Based on the assumption that the $CN_2$ values corresponds to a 5% slope, Huang et al. (2006) proposed an optimized slope adjusted equation:

$$CN_{2s} = 0.8794(CN_3 - CN_2)(1 - 1.0311e^{-0.611a}) + CN_2 \quad (8)$$

Initial simulations showed that runoff increased significantly with slope. Simulations that applied the standard SCS CN method underestimated large runoff events and overestimated small events, while the difference between observed and estimated runoff depth increased with slope. The optimized and non-optimized forms of the slope-adjusted CN method were then applied in Erosion Productivity Impact Calculator (EPIC) model, and in both simulations the runoff prediction was improved for steep slopes. However large runoff events were still underestimated, and small ones overestimated. Based on the relationship between observed and theoretical CN values and slope, Huang et al. (2006) developed a new CN slope-adjusted equation:

$$CN_{2a} = CN_2 \frac{322.79 + 15.63a}{a + 323.52} \quad (9)$$

where slope a ($m \cdot m^{-1}$) should be between 14% and 140%. The developed equation produced the best predicted runoff depth values. Huang et al. (2006) concluded that the CN slope-adjusted equation seems to be the most suitable for runoff prediction in the Loess Plateau steep areas. However, it needs to be validated and possibly improved for other sites.

The CN slope-adjusted equation developed by Huang et al. (2006) was applied by Xu et al. (2011) when the effect of multiple factors in watershed discretization was investigated in the Ansai watershed (1334$km^2$) of the Loess Plateau in China, with an average slope of 23,9%. Since previous research (Jha et al. 2004; Tripathi et al. 2006) has shown that the level of watershed subdivision has no impact on runoff predictions,

the watershed was divided into 21 sub-watersheds in ArcSWAT based on the precipitations station distributions. The sub-watersheds were further delineated using two approaches. The first one was the typical HRU approach using land use and soil type combinations. The second was the so called land type units approach, in which the units were delineated based on land use, vegetation condition, soil type and slope. For both delineation approaches both land use and soil thresholds were set to 0%, 5% and 12%, to exclude the influence of the number of units on runoff simulation, resulting in 256, 83 and 60 HRUs and 1547, 285 and 85 land type units respectively. SWAT was used to simulate runoff for both delineation approaches, in which curve numbers were assigned and adjusted. Comparing the two approaches, the land type unit produced better results than the HRUs. The runoff curve number for each kind of land type unit was defined by land use type, soil type, the hydrological condition of vegetation and modified by slope, reducing the uncertainty of the parameters and therefore represent more accurately watershed runoff.

The effect of slope is also dominant in the concept of Variable Source Area (VSA) watersheds, where surface runoff is generated by only a small portion of the watershed and expands with an increasing amount of rainfall. The VSA hydrology concept was proposed by the original developers of the CN method (Hawkins 1979). However, it was never implemented in the CN method as used by the NRCS. Attempts were therefore made to adjust the CN method by assigning different CNs for wet and dry portions to correspond with VSAs (White et al. 2009), and also to fully reinterpret the original CN method (Schneiderman et al. 2007; Hawkins 1979).

In watersheds dominated by VSA hydrology, HRU definition is shown to be inappropriate for describing the spatial and temporal behavior of hydrological processes (Schneiderman et al. 2007). In VSA watersheds surface runoff is generated by only a small portion of the landscape that is characterized by shallow, low conductive soils, large contributing areas, mild slopes, or any combination of the three. Although SWAT includes slope classes in HRU delineation, which somehow addresses the above issues, there is currently no method of including upslope contributing area in the HRU definition (White et al. 2011).

White et al. (2011) developed and tested a CN-free version of SWAT based on a simple water balance approach (SWAT-WB) that replaced the CN method of runoff generation

(SWAT-CN). Both methods were applied on two watersheds. The Gumera watershed (1270 $km^2$) in Blue Nile, Ethiopia and Town Brook watershed (37 $km^2$) Catskill Mountains, New York. The Gumera watershed was delineated in 656 HRUs in 25 sub-watersheds with SWAT-WB and 117 HRUs in 24 sub-watersheds with SWAT-CN, while the Town Brook watersheds in 180 HRUs in 3 sub-watersheds with SWAT-WB and 172 HRUs in 3 sub-watersheds with SWAT-CN. Results showed better streamflow predictions with SWAT-WB compared to SWAT-CN in simulations performed in the Gumera watershed, while in the Town Brook watershed both models produced approximately equally accurate predictions. The spatial distribution of runoff-generating areas for the two watersheds differed greatly between the two models. SWAT-WB predicted the water table heights distribution on a hillslope in the watershed significantly better, capturing more realistically the spatial distribution of runoff dynamics. Effective water and land management schemes will therefore be easier to successfully implement in watersheds dominated by saturation-excess runoff generation such as VSA watersheds.

#### 2.3.3.3 *Topology Limitation*

One of the major weaknesses of HRUs, as observed by many research studies, is their non-spatial nature. HRUs are discontinuous land masses consisting of homogeneous land use, soil, and management characteristics, representing percentages of the sub-watershed area. They are used in a non-spatial manner, meaning that they are not identified spatially within simulations. Topography is not considered within the HRU and terrain parameters are identical for all HRUs within a given sub-watershed (Pai et al. 2012).

Gassman (2008) observed that the incorporation of the non-spatial HRUs in SWAT is being regarded as both a strength and weakness. It provided flexibility and supported the model to adapt to virtually any watershed with a broad variety of hydrologic conditions and with minimal computational costs of simulations (Gassman et al. 2007).

However, in watershed hydrologic modeling, fluxes are transferred from an up-gradient modelling unit to a down-gradient modeling unit and finally to the stream. The direction and amount of water yield from one modelling unit to another depends on topographic parameters of the watershed such as hillslope and aspect. Existing methods of HRU

delineation lack topological connectivity across units and do not consider the topography of the watershed. It is therefore not possible to establish an appropriate flux routing structure through the investigated watershed in the HRU level (Khan et al. 2013; Haverkamp et al. 2003). Moreover, riparian buffer zones, wetlands and other BMPs cannot be explicitly represented, while flow and pollutant routing within a given sub-watershed is ignored (Gassman et al. 2007).

The lack of topological connectivity in the HRU approach is even more apparent in hydrological modelling of upland catchments. As mentioned in previous sections, in upland catchments, the upslope areas typically have shallow conductive soils and higher rainfall. Such catchment conditions generate significant runoff that is transmitted to medium and low slopes, either as a deep drainage or lateral flux, i.e. surface or sub-surface runoff. Hydrologic modelling of hillslope areas under varying geomorphic setting is crucial in understanding the behavior of hydrologic response (Bogaart & Troch 2006; Hilberts et al. 2007; Lyon & Troch 2007).

In the HRU approach, the size of the aggregated spatial structures is larger than the hillslope length that affects adequate representation of the hillslope hydrologic processes, especially for upland catchments (Khan et al. 2013). Hillslope hydrologic processes are more sufficiently represented when the aggregated entities, e.g. HRUs, are smaller than the length of the hillslope (Zhang & Montgomery 1994). Since hillslope hydrological processes control the runoff generation mechanisms in the watershed, an appropriate representation of those processes is essential. The lack of topological connectivity of HRUs is therefore a major disadvantage, as it is necessary to transfer fluxes from the upper HRUs to the lower HRUs, and finally to the stream network (Khan et al. 2013).

Khan et al. (2013) and Khan, Tuteja, & Sharma (2011) delineated contiguous topologically connected HRUs for the Maclaughlin (459 $km^2$), Delegate (1364 $km^2$) and Bombala (1135 $km^2$) upland catchments of the Snowy River in NSW, Australia. The catchment was first divided in four landforms, using thresholds derived from topographical and geomorphological attributes using a range of indices. The catchment was also divided in sub-watersheds according to Strahler's stream-order convention. The two delineations were overlaid and the common area was termed as HRUs. Soil moisture movement modelling across multiple cross-sections of the Maclaughlin

catchment was performed using the HRUs delineation. Results were compared with those using a single landform, and with those using pixel level landscape representations. It was shown that HRU based simulations were very close to the pixel based, while single landform simulations appeared to be significantly different. Khan, Tuteja, & Sharma (2011) validated the HRU delineation approach against in-situ observations and high resolution aerial photographs. Landform delineation was found consistent with in-situ observations, while HRU delineation of high topographic relief Maclaughlin catchment and low topographic relief Little River catchment was found consisted with the image analysis of high resolution images.

#### 2.3.3.4 *Output Shape*

In the recent years, there have been many applications of hydrologic modelling for identifying priority pollutant contributing areas at the sub-watershed and HRU level. These applications acknowledge the disproportional nature of pollutant contribution areas in a watershed and try to spatially identify those areas that are considered hotpots of pollution. Their ultimate aim is to target conservation practices instead of random implementation and to achieve maximum pollutant reduction.

Agricultural conservation practices are applied at the field scale. Therefore, conservation targeting at a field scale is key to watershed pollution management. HRU outputs, however, do not provide the right spatial scale in order to transfer model results to actionable items for watershed pollution management. Pai et al. (2012) attempted to simplify HRU output by aggregating and mapping it to field scale boundaries within a watershed. A tool called Field_SWAT was also developed, allowing watershed managers and conservations agencies to visualize the pollutant contributing areas to user-defined boundaries, such as fields, in order to target implementation of conservation practices. The developed tool aggregates HRU output into a user-defined field boundary using multiple aggregation techniques, mean, mode, geometric mean and area-weighted mean. This tool does not generate any new model simulation. It simply transfers HRU output to user-defined field boundaries using one of the aggregation techniques.

The tool was tested in Second Creek watershed (189 $km^2$) in Arkansas. The watershed was delineated using ArcSWAT and HRUs were defined without applying any

thresholds for land use, soil and slope, resulting in 218 HRUs. Annual runoff and sediment outputs were simulated using SWAT. The Field_SWAT was then run using a field layer GIS shapefile with 89 polygons, manually delineated using aerial photography, representing arbitrarily selected fields and other land parcels in the test watershed. Based on statistical and visual analysis of the results obtained from both HRUs and Field_SWAT, it was observed that the abstract HRU outputs were best mapped to field outputs with the area-weighted aggregation method. Field_SWAT could potentially be a useful tool for targeting conservation practices at field scale and communicating model outputs to watershed managers and interested stakeholders (Pai et al. 2012).

Investigating the HRUs output shape from a different perspective, Sanzana et al. (2013) attempted to produce a more realistic representation of the HRU polygons. HRUs are generally defined in a GIS environment, by intersecting raster or vector layers of land uses, soil types and sub-watersheds as well as polyline layers representing river drainage networks and ditches. The overlapping of these layers may result in a mesh with topological and numerical problems, not accurately representative of the watershed terrain.

A pre-processing is therefore necessary to improve the HRUs mesh, so that negative effects on the performance of hydrological modeling are avoided. Sanzana et al. (2013) developed a set of computer-assisted mesh generation tools that produce a more regular and physically meaningful HRU mesh that is appropriate for hydrological modelling. The main issues addressed by these tools, implemented in GRASS-GIS, are: the high heterogeneity in geometric and morphometric properties within the HRUs, the correction of concave polygons or polygons containing holes inside, the segmentation of very large polygons, and the bad estimations of the perimeter of units and the distances amongst them. The issues addressed are based on the third level of a watershed discretization methodology proposed by Dehotin & Braud (2008)

The HRU mesh generation tools were applied and tested in the Mercier subwatershed (7 $km^2$) and the Chaudanne sub-watershed (4.1 $km^2$) of the Yzeron watershed (150 $km^2$) in France. The mesh-improvement process produced more HRUs of smaller size, which are considered to be more homogeneous and representative of the watershed terrain. In total, 117 polygons were improved in the Yzeron watershed (8 to remove holes, 43 for

homogeneity of slopes, 20 to improve convexity, and 46 to reduce area) increasing the final number of HRU polygons from 2208 to 2518 in Mercier sub-watershed and from 2573 to 2945 in Chaudanne sub-watershed.

The overland flow path in the two sub-watersheds was represented using both the original HRU delineation and the HRU-improved mesh. The improvements led to significant changes, both in the extension and trajectory of the overland flow paths. A more realistic physical representation was obtained with the HRU-improved mesh, which is assumed to enhance the simulation of surface and sub-surface flows when incorporated in a hydrological model (Sanzana et al. 2013).

#### 2.3.3.5 *Parameter uncertainty*

Parameter uncertainty is an inherent characteristic of all processes involved in hydrological modelling, including the HRUs, especially in deterministic conceptual watershed modelling, where model parameters are estimated via calibration. Uncertainty is a result of model complexity as well as multiple error sources, interacting in an unknown manner, causing the automatic calibration approach also to behave in an unknown way, with the user having no knowledge of the internal workings. Aside from apparent errors in raw measurements and data-processing, a major source of uncertainty can be the insufficient representation of the hydrological processes or, in opposition, overly-complex representations that cannot be supported by the field measurements and information regarding the physical systems to be modelled (Butts et al. 2004; Refsgaard 1997; Wagener, D. P. Boyle, et al. 2001). Parameter uncertainty is also strongly associated with the concept of "equifinality" (Beven & Binley 1992), which refers to the ability to achieve a successful model outcome by using different parameter sets, based on different model configuration, initial conditions, calibration data and fitting criteria. Due to equifinality, it is therefore impossible to distinguish one optimal model structure or parameter set that will reproduce best the hydrological processes across the watershed.

To quantify the uncertainty of the predictions of deterministic conceptual modelling, various mathematical techniques have been developed and embedded in the calibration process, looking for internal routes to the model output that corresponded? to multiple parameter sets and were consistent with the physical behavior of the river (Freer et al.

1996b; Kuczera & Parent 1998; Thiemann et al. 2001; Vrugt et al. 2002; Beven & Binley 1992). Their application, however, indicate that, most of the time, the uncertainty of model predictions is equivalent to the statistical uncertainty of the measured model outputs.

Then again, the application of distributed "physically-based" models, where the fundamental hydraulics laws and semi-empirical hydrologic formulae are applied at each spatial unit, enables, in theory, to directly derive all model parameters from field measurements. This is however significantly restrained by the heterogeneity of processes across the watershed as well as the unknown scale-dependence of model parameters (Beven 1989; Wagener, D. P. Boyle, et al. 2001), while their ability to apply model parameters based on field measurements, without some form of calibrations, has been strongly disputed (e.g. Beven, 1989; Eckhardt and Arnold, 2001; Fatichi et al., 2016; Refsgaard, 1997) due to the equifinality problem (Beven & Binley 1992). In attempt to overcome this, optimization is employed for only a small portion of parameters each time (Beven 2001; Madsen 2003; Vrugt et al. 2004; Muleta & Nicklow 2005; Refsgaard 1997; Eckhardt & Arnold 2001). More specifically, Jakeman & Hornberger (1993) suggest that only five or six parameters can be identified based on a single hydrograph, otherwise parameter uncertainty related to poor identifiability can negatively affect the prediction s of hydrological models (Wagener, D. P. Boyle, et al. 2001).

With distributed physically based schemes being data and time-demanding, and lumped conceptual models unable to represent the spatial and temporal variability of the hydrological processes within the river basin, the introduction of conceptual semi-distributed models for streamflow estimation have been recognized as a good compromise between the two aforementioned approaches (Boyle et al. 2001; Ajami et al. 2004; Nalbantis et al. 2011), providing a satisfactory representation of the basin comprising the level of detail for an engineering application within the network-type configuration and at the same time being computationally efficient. In any case, absence of interior calibration data, then, increases model complexity, resulting, once again, in uncertainty in the model predictions (Efstratiadis et al. 2008).

In the context of (semi-)distributed hydrological modeling, HRU configuration is also subject to the conflict between accuracy in the representation of process heterogeneity,

dictating the required number of HRUs, and model parsimony, associated with the number of parameters inferred through calibration. In other words, the process of HRU delineation, i.e. the number and spatial extent of HRUs across the river basin, is directly related to the number of control variable of the calibration problem. As the river basin is assumed to be an assembly of discrete entities with different properties that contribute differently to its responses, HRUs therefore denote spatial elements of pre-determined geometry, and with parameterization of the hydrological processes dictated by the model discretization, a large number of unknown parameters is resulted, increasing linearly with the number or sub-basins (Efstratiadis et al. 2008; Nalbantis et al. 2011; Daniel et al. 2011). Theoretically, as the number of parameters increases, one should expect obtaining better calibration results, i.e. closer fitting to the observed data. However, in practice, the increase of model parameters induces more complexity to the calibration problem, which is far from a straightforward optimization task. In fact, as a result of interrelated uncertainties and errors in all aspects of hydrological modelling and calibration (Efstratiadis & Koutsoyiannis 2010), the outcome of automatic optimization procedures may be a model of poor predictive capacity, typically because of algorithmic weaknesses (e.g., trapping to local optima).

Efstratiadis et al. (2008) in a different HRU approach (Section 2.3.2), rather than "units" of contiguous geographical areas, defined HRUs as the product of separate basin partitions, i.e. common refinement of partitions, accounting for different characteristics such as soil permeability, land cover, terrain slope etc. Through an appropriate classification of the above basin characteristics, the number of HRUs is adjusted and, consequently, so is the number of the parameters that associated with the soil hydrological processes, retaining therefore some physical meaning that allow a better identification of their prior uncertainty (i.e. upper and lower parameter bounds, used in calibration). The HYDROGEIOS modelling framework (Efstratiadis et al. 2008; Nalbantis et al. 2011) has adopted the "union of layers' HRU delineation concept, in an attempt to handle model schematization and parameterization as two independent procedures. With the HRUs representing basin partitions with common characteristics, and therefore common parameter values, the approach is very flexible, with no restriction in the number and shape of HRUs, while data availability, that is crucial for the calibration procedure, does not affect the schematization of the watershed. If data

availability for model calibration is limited, a small number of HRUs can be defined to represent the spatial heterogeneity of the basin and related hydrological processes, while more HRUs can be defined as more data become available, in order to identify the spatial distribution of model parameters. However, the fact the HRUs delineation is disengaged from the watershed schematization does not necessarily ensure an efficient and parsimonious parameterization.

# 3 Methodology

## 3.1 Scope and Objectives

The objective of this section is to propose and test a systematic method for delineating HRUs), based on the widely used runoff Curve Number (CN) concept, in the context of hybrid semi-distributed hydrological modeling The HRUs will be delineated based on distributed CN maps produced with a semi-automatic GIS procedure, and will account for three major physiographic characteristics of the river basin, by means of classes of: (a) soil permeability, evaluated according to the mechanical properties of the soil and the unsaturated zone, and the dominant geological formations; (b) land use/land cover characteristics, typically expressed in terms of vegetation density; and (c) drainage capacity, evaluated according to the geomorphological characteristics of the basin and the existence of runoff retention structures. The map of CN classes is eventually used within model parameterization, to identify the essential number and spatial extent of HRUs and, consequently, the number of control variables of the calibration problem. The proposed approach aims, on the one hand, at reducing subjectivity introduced by the definition of HRUs and providing parsimonious modelling schemes, on the other. In particular, the modified CN-based parameterization: (1) allows the user to assign as many parameters as can be supported by the available hydrological information, (2) associates the model parameters with anticipated basin responses, as quantified in terms of CN-classes across HRUs, and (3) reduces the effort for model calibration, simultaneously ensuring good predictive capacity.

## 3.2 The standard CN approach and its shortcomings

The Curve Number (CN) has been widely used in hydrology, mostly within the homonymous event-based flood modelling approach, developed by the Soil Conservation Service (SCS) (NRCS 1972) (see also Section 2.3.3.2). SCS (now the Natural Resources Conservation Service (NRCS) introduced this conceptual parameter in an attempt to capture the physiographic characteristics that affect runoff generation in a single value, ranging from 1–100 (the larger this value, the larger the runoff ratio) and in order to determine the key parameter of the modelling procedure, called the maximum potential retention. According to the standard SCS-CN method, CN depends on soil and land characteristics, as well as on the soil moisture present in the soil profile

before the start of a rainfall event. In particular, it considers three Antecedent Soil Moisture (AMC) conditions (Type I: dry, Type II: moderate, Type III: wet), depending on the cumulative five-day antecedent rainfall and the season (dormant or growing). CN values for AMC II conditions and the typically-used ratio of initial abstraction losses, i.e., 20% of maximum potential retention (henceforth referred to as reference conditions), are determined from detailed look up tables by NRCS (NRCS 2004), accounting for combinations of numerous land use/land cover characteristics and four hydrological soil types (A, B, C, D), which are further classified according to their hydrological conditions (good, fair, poor) (Table 4). The reference CN values have been extracted experimentally from rainfall and runoff measurements over a wide range of geographic, soil and land management conditions (Table 5). It is noted that according to recent suggestions, the hypothesis of three discrete AMC types was revised, in order to better represent the inherent variability of the soil moisture, thus considering CN as a random variable and the two extreme conditions, i.e., AMC-I and AMC-III, as bounds of the distribution. Moreover, a much lower initial abstraction ratio, of 5%, is now generally recommended (Soulis & Valiantzas 2012; Banasik et al. 2014).

An important shortcoming of the standard CN method is that it does not take into account the effect of slope. In fact, the reference CN values provided in the standard SCS tables were mainly identified from small agricultural watersheds with mild slopes, considering that the rainfall-runoff transformation is only affected by the soil and land cover characteristics. However, in the general case, the relief characteristics also affect greatly the hydrological response of a watershed. Steep slopes cause a reduction of initial abstractions, a decrease in infiltration and a reduction of the recession time of overland flow, which in turn results in increased surface runoff (Montgomery & Dietrich 2002). Today, it is accepted that the reference CN values are applicable for terrain slopes around 5%, and several researchers have proposed empirical formulae for adjusting the CN values to slope (Huang et al. 2006; Xu et al. 2011; Deshmukh et al. 2013; Verma et al. 2017).

Moreover, the classification of soil types does not cover adequately the entire range of permeability characteristics of the geological formations that are dominant in several areas worldwide. For instance, a number of Mediterranean watersheds lie in highly permeable terrain (e.g., limestone, dolomite, karst), resulting in very low runoff rates

(Merheb et al. 2016). According to the typical classification by SCS, these should be classified in to Group A, representing sand, loamy sand or sandy loam types of soils. Reported experience with the use of the NRCS approach for flood estimations in such basins indicates that the associated CN values were quite overestimated; in fact, much lower values, of about 30–40, should be employed to represent the significant infiltration losses (Efstratiadis, Koussis, et al. 2014).

A common difficulty with CN derivation from NRCS tabular data is the subjectivity involved in the determination of representative parameter values, through combining land cover classes and hydrological soil groups across different hydrological conditions. The estimations are mainly based on qualitative information rather than on numerical criteria, while for several common cases, the recommended values range too widely (particularly for soil types of Category A). Therefore, quite different interpretations may be given for similar land cover and soil characteristics, thus resulting in significant uncertainty in the determination of CN values.

## 3.3 Analytical Method for CN Assessment

An analytical method for assessing the reference CN value over an area of interest is proposed, in order to facilitate spatial calculations in GIS environments. Accounting for the aforementioned shortcomings, some modifications with respect to the standard CN approach are employed. In particular, the proposed classification is based on the categorization of three (instead of two) physiographic characteristics, each one comprising five classes, i.e., water permeability (hydraulic conductivity) of soil and near-surface geologic strata, henceforth referred to as permeability, land use/cover and drainage capacity (Table 9). Input geographical data for the production of the associated thematic layers in rural areas may include hydro-lithological or soil maps, land use/cover maps, terrain slope maps and any other relevant information. In urban or suburban areas, information about building features may also be accommodated as any other relevant urban features.

Permeability classifications in rural areas account for the mechanical properties of the soil and the unsaturated zone (e.g., horizontal and vertical hydraulic conductivity) that affect infiltration, interflow and percolation mechanisms. Based on hydro-lithological or soil maps and depending on the predominant soil type underlying geological formation

and structures (for urban or suburban areas), the permeability class is first described as very high, high, moderate, low or very low (Table 6). In urban areas, the corresponding classification is defined by the density of structures, building features and open space development. A ranking from 1–5 is then assigned, where an index of one refers to very high-permeability substrata (e.g., karst) and five to very low-permeability substrata (e.g., dense rocks). Residential areas range from Classes 3–5, according to their built density.

Vegetation classes are formulated on the basis of land characteristics related to retention mechanisms, soil roughness and filtration capacity, e.g., due to root zone growth. Based on a relevant land use map (e.g., CORINE Land Cover Map), the vegetation class of the area of interest is first described as dense, moderate, undergrowth, sparse or zero (Table 7). A ranking from 1–5 is then assigned, where and index of one refers to dense vegetation class (e.g., evergreen forests) and five to bare soil. It is recommended that burned areas be classified under one category with respect to their original condition; for instance, a burned coniferous forest should be classified as a moderate vegetation class, thus assigning a rank of two instead of one.

The drainage capacity of the area of interest depends on geomorphological characteristics (topography, slope), the development of the river network and the existence of runoff regulation systems across the area of interest (e.g., land reclamation works, retention structures, sewer networks). The drainage capacity class is first described as negligible, low, moderate, high and very high, and then a ranking from 1–5 is assigned (Table 8). In the absence of other information, these ranks may be exclusively assigned on the basis of five terrain slope categories, since this is an easily-retrieved property through typical DEM processing. A rank of one is assigned to practically horizontal areas, while five is assigned to slopes over 30%.

**Table 6:** Permeability classes based on soil and geological characteristics of the basin and the predominant structure type.

| Ranking | Permeability class | Ground features | Geological or hydrolithological characteristics | Structure features |
|---|---|---|---|---|
| 1 | Very High | Very light and well drained soils | Strongly karstified carbonate formations, extensive development e.g. fractured limestones, dolomites, marbles | |
| 2 | High | Sandy and gravelly soils, with a small percentage of silt and clay | Fluvial deposits, inconsistent conglomerates, breccia triadic | Very small settlements |
| 3 | Moderate | Thick sandy soils, silts and silty soils, sandy clay | Granular alluvial deposits, schists, cohesive conglomerates, platy or fine grained limestone alternating with schist formations | Sparsely built areas, significant garden development, urban parks |
| 4 | Low | Fine clay soils, soils from clay, soils poor in organic material | Flysch, metamorphic, plutonic and volcanic rocks, granular non-alluvial deposits (alternating sands, marls, clays, conglomerates, marly limestones, sandstones), granular molasse deposits | Moderately built areas with lawns and small gardens |
| 5 | Very Low | Shallow soils that swell when wetted, plastic clays | Compact rock of negligible permeability (granites) | Shopping centers, densely built areas |

**Table 7:** Vegetation classes based on land use/cover characteristics

| Ranking | Vegetation class | Land use/cover characteristics |
|---|---|---|
| 1 | Dense | Forests (conifers, broadleaf) |
| 2 | Moderate | Transitional forests, orchards, olive groves, riparian vegetation |
| 3 | Low | Pastures, crops, vineyards, grassland, scrub |
| 4 | Sparse | Fallow land, non-irrigated arable land, dunes, wetlands, scattered construction |
| 5 | Zero | Bare or rocky soil, artificial surfaces (roads, buildings) |

**Table 8:** Drainage capacity classes based on the average slope and related ground features

| Ranking | Drainage capacity class | Average slope* | Other features |
|---|---|---|---|
| 1 | Negligible | 0 % | Inadequate drainage system, frequent and extensive bedsores, unformatted hydrographic network |
| 2 | Low | 1-2 % | Significant surface degradation, occasional bedsores, poorly shaped river network |
| 3 | Moderate | 2-10 % | Small surface degradation, rare flooding, shallow, small drainage corridors |
| 4 | High | 10-30 % | Negligible soil degradations, very well shaped hydrographic network, existence of drainage network |
| 5 | Very High | >30 % | Mountainous terrain |

* Rounded to the nearest integer, i.e. the first class corresponds to slopes <0.5 %, the second to gradients between 0.5 to 2.5 % and so on.

According to the above classifications, the dominant classes of permeability, land use/cover and drainage capacity, as well as the corresponding indices $i_{\mathrm{PERM}}$, $i_{\mathrm{VEG}}$ and $i_{\mathrm{SLOPE}}$, ranging from 1–5 (Table 9), are assigned for the given area (if necessary, non-integer values may also be assigned to ensure more detailed classifications). Based on these characteristic values, the following empirical relationship is proposed, to estimate the representative value of CN (for AMC II conditions and 20% of maximum potential retention):

$$\mathrm{CN} = 10 + 9 \times i_{\mathrm{PERM}} + 6 \times i_{\mathrm{VEG}} + 3 \times i_{\mathrm{SLOPE}} \quad (10)$$

It should be emphasized that the modified classification and the empirical formula (10) are not in contrast with the standard procedure by NRCS (NRCS 2004). For instance, the lowest recommended CN value by NRCS is 30, while in the proposed approach, it is slightly smaller (CN = 28), in order to account for terrains with substantial infiltration losses (e.g., karst basins). According to NRCS, for pasture areas under good conditions, the CN varies from 39–80, for soil Groups A and D, respectively, while in the proposed approach, if a vegetation class between moderate and low is considered (thus, setting $i_{\mathrm{VEG}}$ = 2.5), the feasible range of CN is from 37–85. Similarly, for woods under good conditions, the recommended CN values vary from 30–77, while in the proposed approach, if a dense vegetation class is considered ($i_{\mathrm{VEG}}$ = 1), CN can range from 28–76.

The quantification of the three individual components of CN within Eq. (10) allows its direct implementation in a GIS environment, as explained in the next section. The

detailed tabular data by NRCS can be used in parallel to assign proper permeability, vegetation and drainage capacity classes over the area of interest.

**Table 9:** Coding of physiographic characteristics for the estimation of parameter CN for reference conditions (AMC type II and initial abstraction ratio 20 %).

| Permeability Class | $i_{\mathrm{PERM}}$ | Vegetation Class | $i_{\mathrm{VEG}}$ | Drainage Capacity Class | $i_{\mathrm{SLOPE}}$ |
|---|---|---|---|---|---|
| Very High | 1 | Dense | 1 | Negligible | 1 |
| High | 2 | Moderate | 2 | Low | 2 |
| Moderate | 3 | Low | 3 | Moderate | 3 |
| Low | 4 | Sparse | 4 | High | 4 |
| Very Low | 5 | Zero | 5 | Very High | 5 |

## 3.4 GIS-Based Procedure for Extracting CN Maps

Although the proposed methodology is applicable at any spatial scale, i.e., from the grid cell to much larger areas (e.g., watersheds, sub-basins), it is recommended to employ it at fine spatial resolutions and then aggregate to larger scales, by taking advantage of GIS facilities. The developed GIS procedure employs the empirical formula (10) at the grid-cell scale, where the input data for CN estimation are provided by means of raster data for the three aforementioned indices. Based on the CN values calculated for each cell of the reference surface, a raster map can be produced showing the spatial distribution of the CN parameter. The configuration process of the CN parameter map within a GIS environment is shown in Figure 4, where raster layers of permeability, vegetation density and slope indices, with values from 1–5, are overlaid, to produce a raster map of distributed values of CN for the reference area of interest.

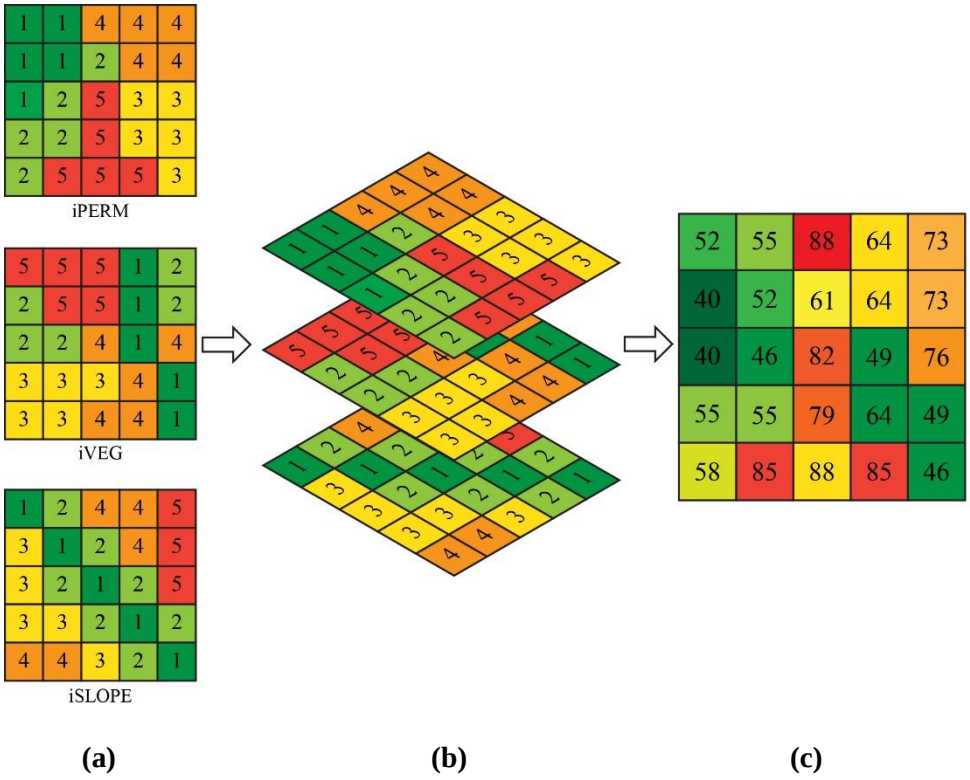


**Figure 4:** (a) Layer of geographic information for permeability classes (iPERM), vegetation density classes (iVEG) and drainage capacity classes (iSLOPE); (b) layer overlay; (c) CN parameter map

## 3.5 Validation based on observed flood events

Within the context of DEUCALION research project (Efstratiadis, Koukouvinos, Michaelidi, et al. 2014; Efstratiadis, Koussis, et al. 2014), involving the assessment and improvement of modelling tools and associated engineering practices in ungauged basins that are typically affected by flash floods, a number of flood events in nine pilot basins in Greece and two in Cyprus has been analysed. Common characteristics of most of the basins were the relatively small scale (up to ~150 km$^2$), the quite significant extent of highly-permeable geological formations and the steep slopes. The key task was the evaluation of the NRCS-CN method for extracting the effective rainfall, combined with the unit hydrograph theory, and the development of empirical formulas within this procedure to better represent the peculiarities of Mediterranean catchments that are mainly affected by flash floods (Efstratiadis, Koussis, et al. 2014).

At each catchment and for each event, it was attempted to retrieve the “optimal” initial abstraction ratio and unit hydrograph shape parameters and to determine the associated

CN value. The CNs across the examined flood events exhibited significant variation, which is primarily (but not exclusively) explained by the variability of initial soil moisture conditions. A summary of the results is provided in Table 10. For each basin, the average CN value from the examined events, adjusted for Type II conditions and initial abstraction ratio 20%, is contrasted with the estimated CN by the proposed GIS procedure. In most cases, the estimated CN fits quite well with the empirically-derived ones. These are subject to significant uncertainties, both because of the limited data sample, as well as the assumptions made when extracting them from observed flood data (Kowalik & Walega 2015; Soulis & Valiantzas 2012; Banasik et al. 2014). Clearer evidence of the good agreement of the proposed approach with the hydrological behavior of the examined catchments results from the high correlation of the estimated CNs with the observed average runoff coefficients; the latter are easily computed as the ratio of flood runoff to rainfall, and thus, they are not prone to arbitrary assumptions. As shown in Figure 5, a power-type relationship is fitted, which is consistent with the nonlinearity of the SCS-CN procedure.

**Table 10:** Summary of flood data analysis at the pilot catchment of the DEUCALION project.

| Basin | Area ($km^2$) | Examined Events | Average Runoff Coefficient | Average Observed CN (Adjusted) | Reference CN |
|---|---|---|---|---|---|
| Nedontas | 120.8 | 11 | 0.121 | 53 | 61 |
| Karveliotis | 15.3 | 10 | 0.171 | 52 | 65 |
| Alagonia | 20.9 | 10 | 0.350 | 74 | 70 |
| Lousios | 166.3 | 11 | 0.156 | 70 | 63 |
| Sarantapotamos | 144.6 | 12 | 0.059 | 62 | 48 |
| Oinoe | 51.2 | 12 | 0.012 | 52 | 45 |
| Chalandri stream | 5.2 | 1 | 0.215 | 88 | 62 |
| Drafi | 15.7 | 10 | 0.094 | 52 | 54 |
| Lykorema | 7.9 | 11 | 0.101 | 78 | 52 |
| Peristerona (Cyprus) | 77.1 | 14 | 0.407 | 72 | 71 |
| Xeros (Cyprus) | 68.5 | 10 | 0.279 | 70 | 66 |

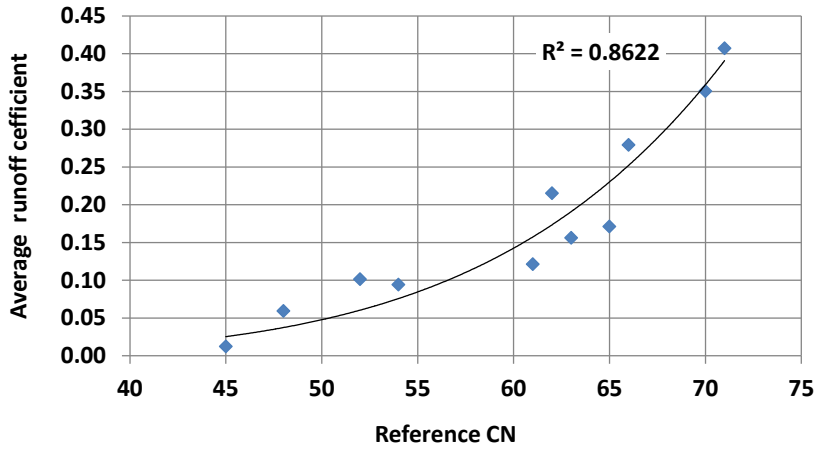


**Figure 5:** Scatter plot of reference CN values and average flood runoff coefficients.

## 3.6 HRU delineation approaches based on CN classes

Although the aforementioned method had been initially developed for estimating CN values, in order to be used next within the NRCS-CN event-based scheme, the proposed method emphasises its use within the parameterization of distributed hydrological models (and not their governing equations, which may follow or not the aforementioned method in rainfall-runoff calculations). In this context, the original CN concept was expanded as the "hydrological identity" of the area of interest, i.e., from the grid cell to the basin scale. The analytical formula (10) when combined with the GIS-based procedure allows a detailed representation of the spatial heterogeneity of physiographic characteristics of a river basin, in terms of CN classes. Following, the raster layer of CNs can be used for delineating HRUs, under the assumption that cells with identical CN values exhibit similar hydrological behavior. In this respect, HRUs can be configured as clusters of such cells, to be represented by the same response model, and thus, the total number of model parameters becomes directly proportional to the number of CN classes across the river basin.

Such a detailed configuration is not always effective, since it results in a large number of HRUs and, consequently, an even larger number of parameters. An obvious way to reduce the number of parameters is through aggregation of the initially formulated HRUs, by considering sub-sets of CNs instead of individual classes. In that case, a representative (e.g., weighted-average) value of the CN is obtained, based on the area that each CN class occupies. Evidently, the parameterization becomes more flexible and

more subjective, as the user needs to define both the desirable number of aggregated CN classes and the associated ranges of CN values. In the hypothetical example of Figure 6, the delineation of two HRUs is illustrated, by using CN = 63 as the threshold.

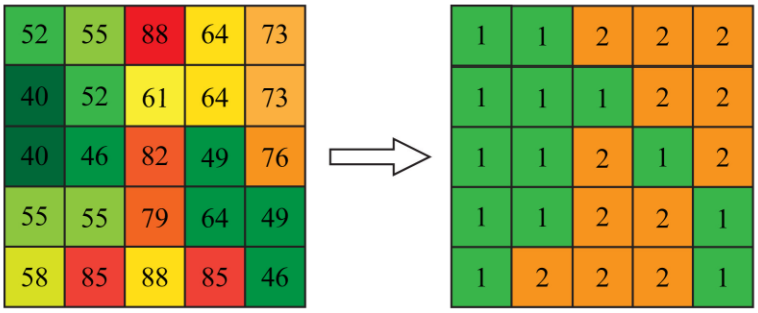


**Figure 6:** HRU delineation based on the CN map: (a) CN parameter classes and (b) configuration of two HRUs, using CN = 63 as the threshold to determine the associated CN classes.

## 3.7 Which is the recommended Number of HRUs?

The proposed CN-based approach for delineating HRUs can be applied to any fully- or semi-distributed model, provided that the parameters involved within the simulated processes are mapped at the HRU scale. Under this assumption, the number of HRUs is a critical decision, since it is directly associated with the number of parameters to be inferred through calibration and, consequently, the model complexity.

As already discussed, the configuration of HRUs is subject to the classical conflict between accuracy in the representation of process heterogeneity, which in turn dictates the required number of HRUs, and model parsimony (Efstratiadis & Koutsoyiannis 2010). In the case of lumped conceptual schemes, the assumption is that only a few parameters can be identified from observed flow data. For instance, Jakeman and Hornberger (1993b), who investigated numerous parameterizations, concluded that for a wide range of basins with a temperate climate, only a “handful” of parameters can be consistently estimated from rainfall-runoff data; this empirical “rule” has been also confirmed by other researchers, using different models (Fenicia et al. 2014; Wheater et al. 1986). In order to provide a more rigorous justification, Wagener et al. (2001b) stated that the level of structural complexity that can be supported by the information provided by the observations can be simply defined as the number of parameters that can be

identified. In an attempt to improve the identifiability of parameters in the case of more complex schemes (e.g., semi-distributed) that may use a large number of parameters, Efstratiadis and Koutsoyiannis (2010) have proposed the introduction of multiple criteria, each one explaining only a "handful" of them. In particular, they suggested retaining a ratio of about 1:5–1:6 between the number of performance criteria and the number of parameters to be calibrated, to ensure a parsimonious representation of the calibration problem in a multi-objective context.

However, the question of how many parameters should be applied primarily depends on the spatial heterogeneity of the modelled processes across the specific study area. If the basin is homogenous, a simple model with few parameters can ensure good fitting to the observed data. For instance, Fenicia et al. (2016) found sufficient the use of only two ''handfuls'' (specifically, 11) as the parameters to represent ten observed hydrographs across a river basin.

Nevertheless, based on the broader hydrological experience, it is reasonable to associate the number of HRUs with the available discharge information across the river basin. As a general empirical rule, in order to represent the process heterogeneity with the least model complexity, it is proposed that the number of HRUs should be close to the number of the observed responses across the basin. Traditionally, these refer to streamflow data, yet they may also refer to other response data types, at the point scale (e.g., groundwater level observations), as well as remotely-retrieved distributed data, such as soil moisture and evapotranspiration (Pollacco et al. 2013; Silvestro et al. 2015). Therefore, if $N$ response time series are available from different sources, then up to $N$ CN parameter classes should be considered, in order to formulate the corresponding HRU classes. Obviously, this recommendation presupposes that both the quantity and quality of the observed data are satisfactory and also that the measurement sites are appropriately distributed across the basin. The spatial distribution of the monitored data used in calibration is a critical issue. Ideally, these data should be uncorrelated, to ensure the maximization of the available information (Wagener, D.P. Boyle, et al. 2001). In practice, in the typical case of multisite streamflow data, the above criterion is fulfilled (not absolutely, but as much as possible) if the monitoring stations are well distributed across the river network and, more precisely, if they are located at points capturing the heterogeneity of the watershed.

In general, the proposed parameterization strategy results in different combinations of the areas covered by the associated HRUs upstream of each station, which allows one to account implicitly for the spatial variability of the catchment characteristics, which are represented through the HRU concept. Therefore, the calibration of the *N* sets of model parameters (one per each HRU) will be based on the combined hydrological information embedded in the observed data by the *N* stations. Note that this approach is far from classical practices of semi-distributed modelling, where different parameters are assigned to the entire sub-watershed area upstream of each flow monitoring station (Ajami et al. 2004). If such an area is highly heterogeneous, the resulting parameter values will reflect totally different hydrological behaviors, thus losing physical interpretation. In contrast, the CN-based approach assumes that the parameter values of a given HRU represent a specific hydrological behavior, which is quantified in terms of the representative (e.g., spatially averaged) value of the associated CN class. This is considered another advantage of the proposed approach, since, through a proper classification of CNs, the user can also determine a priori a reasonable (i.e., physically-consistent) and relatively narrow range of feasible parameter bounds, which is of key importance in ensuring effective and efficient calibrations (Efstratiadis & Koutsoyiannis 2010). Moreover, the user can macroscopically evaluate the model performance on a quantitative basis, by contrasting the statistical behavior of the simulated runoff with the expected physical behavior, as summarized in terms of CN information.

# 4 Initial Testing of the proposed method

## 4.1 Scope and Objectives

The objective of this section is to test the proposed method in the hydrological simulation of the Nedontas River Basin. The simulation suite used was the HYDROGEIOS model, which is based on the HRU concept and is very flexible in the formulation of HRUs. The formulation of the HRUs was evaluated against alternative parameterizations and their impact on model calibration and predictive capacity. In this context, two calibration experiments are employed:

***Calibration Experiment 1: Varying the number of HRUs***

In the first experiment, the CN map of the basin is used to delineate from one up to five HRUs, thus providing configurations of varying complexity

***Calibration Experiment 2: Contrasting alternative HRU delineation approaches***

In the second experiment, the proposed CN-based method is contrasted with two other well-established HRU delineation strategies, i.e., the unique combination and the union of layers (Section 2.3.2).

## 4.2 Modeling Approach - HYDROGEIOS modelling framework

The modelling approach is based on the HYDROGEIOS software, which is a GIS-based tool implementing conjunctive simulation of surface and groundwater processes across river basins that may also be human-modified. The software supports daily and hourly time steps, in order to represent fine-scale hydrological processes, particularly floods (Efstratiadis, Koukouvinos, Dimitriadis, et al. 2014).

The water fluxes are represented on the basis of a semi-distributed schematization of the river basin, which is divided into sub-basins, which are interconnected through the hydrographic network. The latter propagates the surface runoff generated from sub-basins, where precipitation and PET time series are assigned as meteorological inputs. The model parameterization is based on the HRU concept. At each basin partition, i.e., the intersection of sub-basin and HRU, a conceptual model that transforms precipitation

into actual evapotranspiration, percolation to the groundwater system and surface runoff is epmployed. Within HYDROGEIOS, the standard NRCS-CN approach was not used, since it is not applicable for continuous simulation.

Moreover, the choice of HYDROGEIOS for employing and evaluating the proposed CN-based delineation method was also made because the model is very flexible in the formulation of HRUs, in contrast to other tools that imply several constraints on the configuration of geographical inputs.

### 4.2.1 Model formulation and input data

The conceptual model of HYDROGEIOS is based on a river basin scale, network-type schematization of the physical and artificial components of the hydrosystem that are represented in the form of thematic layers: the hydrographic network, the surface hydrological system, the underground hydrological system and the water sources management system. The individual layers are connected through the river nodes [surface hydrological system → hydrographic network], river segments [hydrographic network → underground hydrological system], springs [underground hydrological system → surface hydrological system], boreholes [underground hydrological system → hydrographic network] and aqueducts [hydrographic network → water management system]. The configuration of the above model components and the required input data (geographical and hydrological) are explained next.

***Hydrographic network***

For given nodal inflows, i.e. surface and groundwater runoff, the allocation of hydrological fluxes across the river network is expressed in terms of a graph optimization problem, to account for human interventions, i.e. surface and groundwater abstractions, as well as losses due to infiltration (Efstratiadis et al. 2008; Nalbantis et al. 2011). The schematization of the hydrographic network (i.e. the main watercourse and tributaries) is implemented through a two-step process. At first, the initial network is formulated within a GIS environment, based on a DEM of the river basin (Fig. 7a), by adjusting the flow accumulation parameter. A low flow accumulation parameter will produce a dense hydrographic network. This is usually an iterative process until the desired network is formed. The initial network is formed with nodes only at the outlet of the basin and at the junctions of the river segments; additional control points are added

across the network corresponding to flow monitoring stations, inflow nodes, abstraction points, etc. (Fig. 7b). Input data to the river nodes are the co-ordinates $(x, y)$, the elevation $(z)$, the inflow time series (if any) and the observed discharge time series (if any). The network topology is fully defined by the upstream and downstream nodes of each river segment (also referred to as river branch or watercourse), i.e. the course between two nodes. While one or more river segments can contribute upstream of each node, only one segment may be initiated downstream. The final, tree-type, hydrographic network, must end at a final node, which is the basin outlet (Fig. 7c). Input data to the river segments are the length $L$, and the infiltration coefficient $\delta$, a dimensionless parameter of the surface hydrology model representing the percentage of the total surface runoff that recharges the groundwater system. Water inflow and outflow only occur at the river nodes while along the river segments the discharge is considered to be stable.

In hourly simulations, routing phenomena are also represented, by re-solving the problem from upstream to downstream. In the case of relatively steep slope channels, a kinematic-wave model is employed, implementing a temporal transfer of the hydrograph from the upstream to the downstream node, while in the case of mild slopes, a Muskingum diffusive-wave scheme is employed, implementing a non-linear transformation of the input hydrograph (Koussis 2009; Koussis 2010). For the linear kinematic-wave model, the travel time through each river segment $K$ is defined, while for the Muskingum diffusive-wave scheme along with travel time parameter, a weight parameter $X$, is also defined. In the case of the one-dimensional hydraulic analysis model, additional information is required such as the geometry of the segment cross section, the stage-discharge relationship, the longitudinal slope, the Manning coefficient, etc.

***Surface hydrological system***

The water fluxes across the surface hydrological system are represented on the basis of a semi-distributed schematization of the river basin, which is divided in sub-basins that are interconnected through the hydrographic network. The watershed of the river basin is delineated by defining a single outlet node from the hydrographic network, while sub-basins upstream of each node are created so that each river segment crosses a unique sub-basin (Fig. 7d). The parameterization of the surface hydrological system is based on

the HRU concept, indicating spatial units of the basin with common geomorphological and hydrological characteristics. Thus, the surface hydrological processes and associated model parameters are considered homogeneous within each HRU.

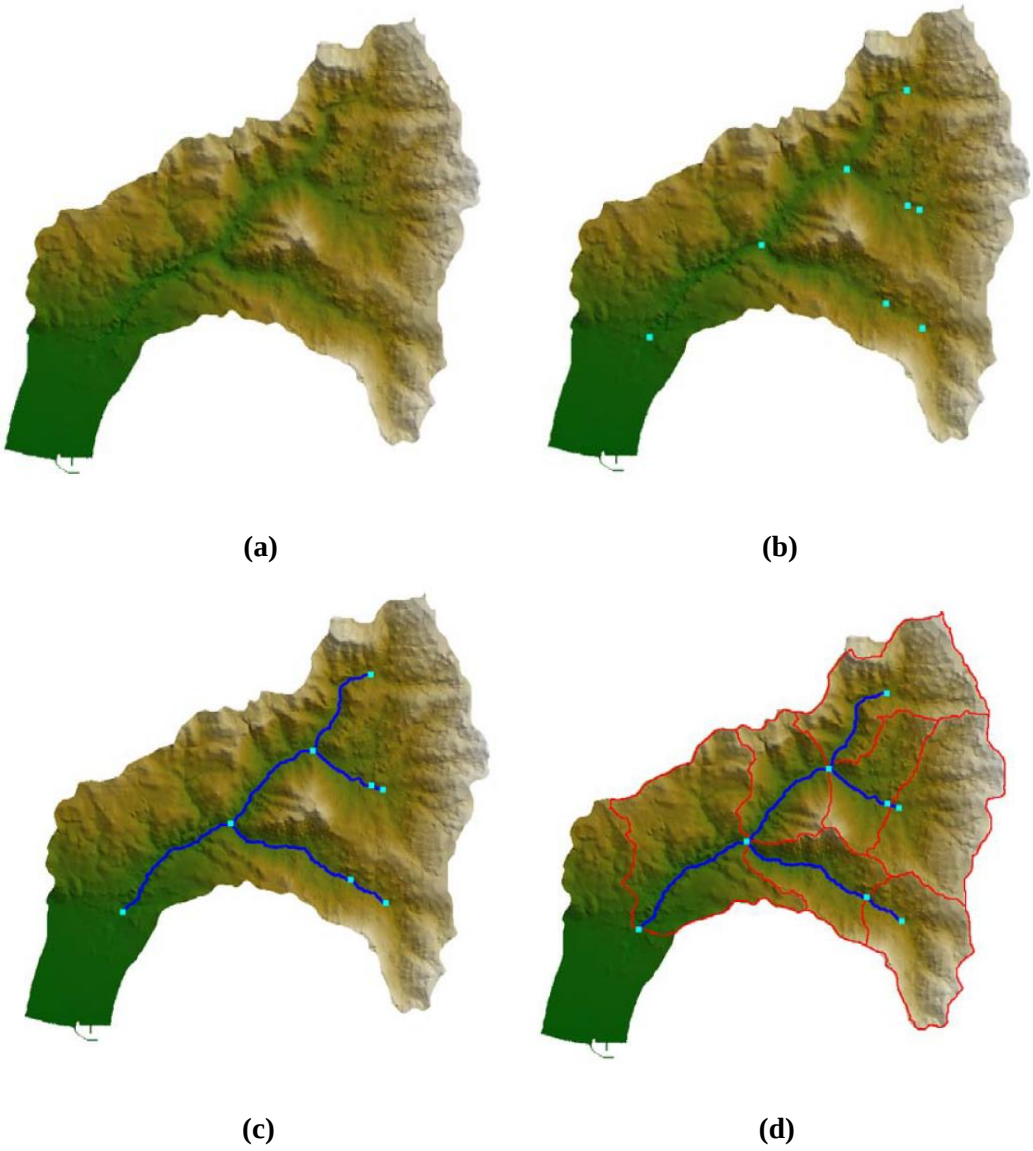


**Figure 7:** Geographic information layers used for the schematization of the hydrographic network and the surface hydrological system: (a) Digital Elevation Model, (b) nodes of the hydrographic network, (c) segments of the hydrographic network, and (d) sub-basins

As meteorological inputs are assigned to each sub-basin, all calculations are implemented on a derivative layer, produced from the intersection of the sub-basin and the HRU layers. A conceptual precipitation-runoff model is employed, transforming precipitation into actual evapotranspiration, percolation to the groundwater system and surface runoff over the sub-basin. The total runoff of each sub-basin, obtained by adding

to the surface runoff the discharge of any spring that may be included in the sub-basin, is considered to be instantaneously transferred as point inflow to the corresponding downstream node. Surface runoff is transferred as point inflow to the corresponding downstream node. The related processes are conceptualized through the surface hydrology model (also referred to as soil moisture model) described in Section 4.2.2. Input data to each sub-basin include the sub-basin area A, the mean elevation H, the length of the main river tributary segment passing through the sub-basin L, and the mean slope S. A linear reservoir scheme is employed to propagate the surface runoff generated from each sub-basin to the corresponding outlet node hydrograph, that uses a recession coefficient $\theta$, and the time of concentration $t_c$, is estimated by the empirical relationship Giandotti based on the sub-basin input data.

***Groundwater hydrological system***

The hydrological processes of the saturated zone, also referred to as the aquifer, are represented by conceptual groundwater reservoirs connected by virtual transfer elements. The formulation of the groundwater network is based on a multi-cell approach where the aquifer is resolved into non-rectangular cells that formulate a network of conceptual tanks and associated flow elements**.** According to (Rozos & Koutsoyiannis 2005), the multi-cell mathematical concept derives from the finite volume method, provided that the cell edges are parallel or normal to the equipotential contours and the line joining the centroids of adjacent cells is perpendicular to their common edge. It has been proven that this approach allows the description of complex geometries based on the physical characteristics of the groundwater system, through parsimonious structures (Rozos & Koutsoyiannis 2006).

According to the available information, the cell discretization can be based on (a) the geometry of the sub-basins (Fig. 8a): in the case where no other information is available, the groundwater cells geometry matches the geometry of the sub-basins, and each cell collects the infiltration of the corresponding sub-basin that discharges either through a virtual spring in the sub-basin or downstream, depending on the boundary conditions; (b) the geometry of the aquifer: in the case where information is available on the aquifer boundaries resulting in a conceptual model with a very small number of cells, taking into account the geometry of the aquifer; (c) the properties of the aquifer (Fig. 8c): resulting in a conceptual model, in which the number of cells equals the number of the

homogenous regions of the aquifer, based on hydraulic and/or geographic properties; and (d) the hydraulic condition of the aquifer (Fig. 8b): in the case where sufficient information is available regarding the aquifer flow conditions, the cell discretization can be based on the flow lines, resulting in a physically based model and the parameters can be calibrated based on piezometric observations.

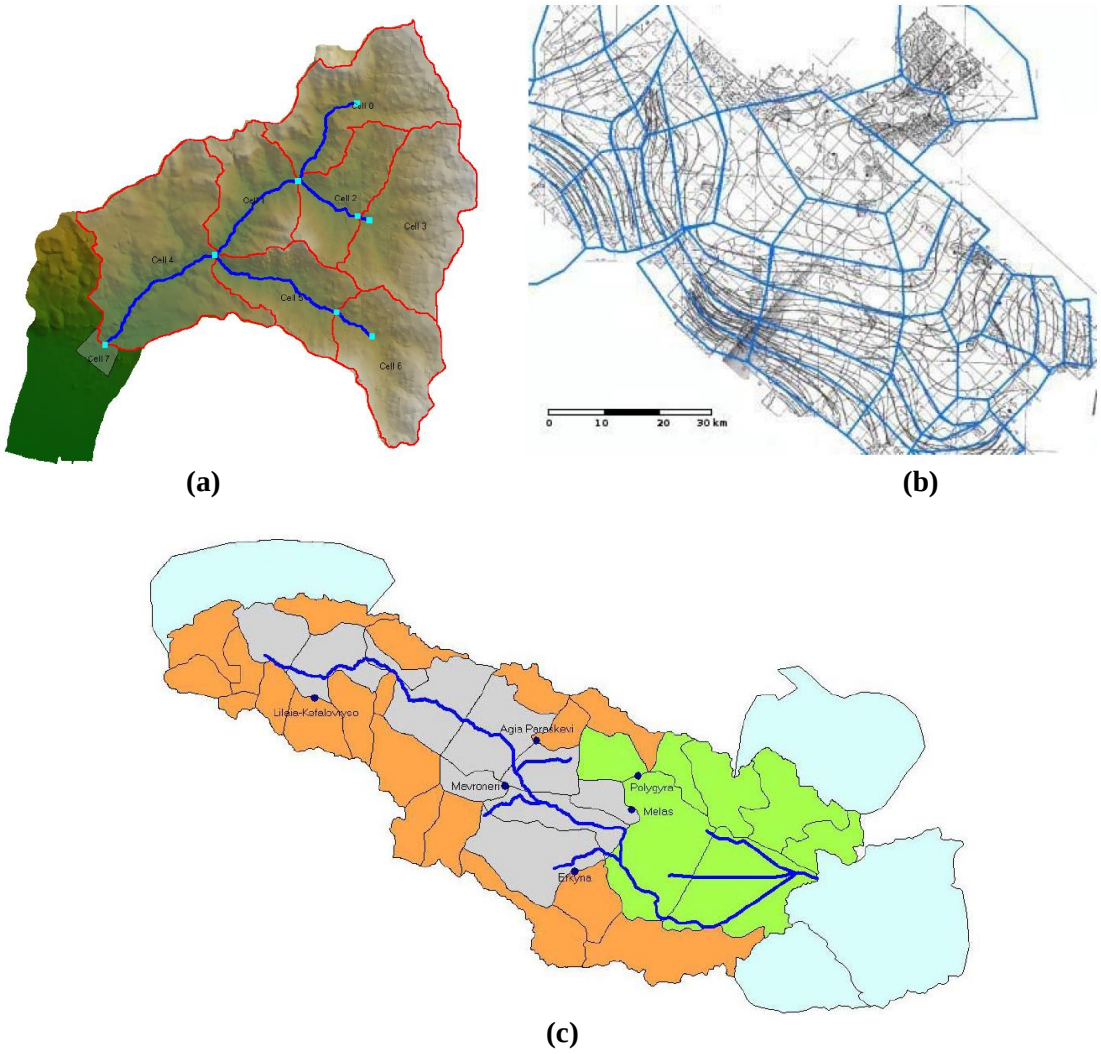


**Figure 8:** Groundwater cell discretization based on (a) the geometry of the sub-basins, (b) the hydraulic condition of the aquifer, and (c) the properties of the aquifer

The parameterization of the groundwater processes has therefore a physical meaning, and as a result, the computational effort is significantly reduced, especially when compared to typical finite difference or finite element schemes. Input properties of the groundwater cells are the top elevation, $w_i^{max}$, and bottom elevation, $w_i^{min}$, of each cell, and the water tables at the beginning of the simulation, $w_{i0}$. Regarding the boundary conditions, the user can define the common edge between two neighboring cells as

impervious or not, to prohibit or allow, respectively, the water exchange between them. Based on the input properties and boundary conditions, feasible water routes through the aquifer are identified. The geometrical properties of the groundwater cells are automatically generated within a GIS environment, including the centroid coordinates of each cell, $(x_i, y_i)$, the distances, $l_{ij}$, and common edge lengths, $\beta_{ij}$, between adjacent cells, the area of each cell, $F_i$, as well as all unions and intersections with the surface geographical layers. Two parameters are assigned to each groundwater cell, specific yield capacity, $S_y$, and hydraulic conductivity, K. Distributed stresses, namely inflows due to infiltration underneath each river segment, areal inflows due to percolation and abstractions due to pumping, are propagated across the groundwater network, outputs of which are point outflows to the river network through springs (baseflow) and underground losses to neighbouring basins or the sea. Spring properties include the discharge altitude, the interconnected cell, while a hydraulic conductivity parameter is assigned to each spring. The related processes are conceptualized through the groundwater model described in Section 4.2.3.

***Water management system***

HYDROGEIOS can also be applied to human-modified basins thought a system-oriented water management scheme that represents the allocation of the hydrological fluxes under anthropogenic interventions. The major hydraulic works, the corresponding water uses and constrains and their interactions with the physical system are coarsely depicted, represented the following components: junction nodes, representing points of water supply and demand; irrigation nodes representing water extraction to meet irrigation needs (a fixed percentage of which is considered to return back to the network through the drainage network); borehole groups, i.e. water abstraction systems (wells) from groundwater resources, lying on neighboring locations and serving the same use are conceptualized as clusters, with the pumping capacity estimated as the sum of the individual pumping capacities of the boreholes constituting the cluster; and aqueducts, i.e. water transfer projects connecting pairs of nodes, may conduct water to the hydrographic network or abstract it to satisfy demands. These components are connected to the hydrographic network and the aquifer, thus forming a single natural and artificial (conceptual) network referred to as hydrosystem. The properties of the hydrosystem include discharge and pumping capacities, target priorities, demand time

series and unit transportation costs. In the case of multiple water resources and conveyance paths, priorities and costs are assigned to express preferences regarding the allocation of abstractions. When a demand can be satisfied through different abstractions, actual or hypothetical unit costs (monetary unit per transmitted water volume unit) can be imposed to the corresponding aqueducts, for example, a positive and a zero-unit cost for groundwater and surface water abstractions, respectively, will force the model to abstract water from the river network rather that from groundwater. The preservation of target priorities and the minimization of costs are both ensured via the flow allocation model (Graham et al., 1986; Kuczera, 1989; Fredericks et.al., 1998; Dai and Labadie, 2001; Efstratiadis et al., 2004).

### 4.2.2 Surface hydrology model

The surface hydrology model is employed at each basin partition, i.e. the intersection of sub-basin and HRU, transforming precipitation into actual evapotranspiration, percolation to the groundwater system and surface runoff over the sub-basin. A schematic layout of the modelling components and associated fluxes is shown in Figure 9. The model comprises three conceptual storage mechanisms: (a) an interception tank $S_{1t}$, on the ground, which transforms precipitation into direct evaporation, overland flow and infiltration, using two parameters: interception capacity r and maximum infiltration rate $i_0$; (b) an upper soil moisture accounting tank $S_{2t}$, which receives infiltration and produces evapotranspiration through the upper soil, excess runoff due to soil saturation, horizontal flow through the soil (interflow), and vertical flow to the deeper zone, considered as constant ratio of infiltration; this component uses four parameters: field capacity k, threshold up to interflow θ, recession rate for interflow λ, and percentage of infiltration β; (c) a lower soil moisture accounting tank $S_{3t}$, which receives vertical flow from the upper tank to produce deep evapotranspiration and percolation to the saturated zone (represented by the groundwater model), using a sole parameter:. the recession rate for percolation μ. In total, seven parameters are assigned to each HRU, while an additional parameter is considered for each sub-basin, by means of the recession rate of a linear reservoir routing scheme; the latter is employed to propagate the runoff produced across each sub-basin (i.e. the aggregated runoff from all common HRU partitions) to its outlet. Water losses along the river network are modelled by assigning

infiltration parameters to particular reaches, which represent constant ratios of discharge that are conducted to the groundwater system. All surface hydrology model parameters are summarised in Table 11, Section 4.2.4.

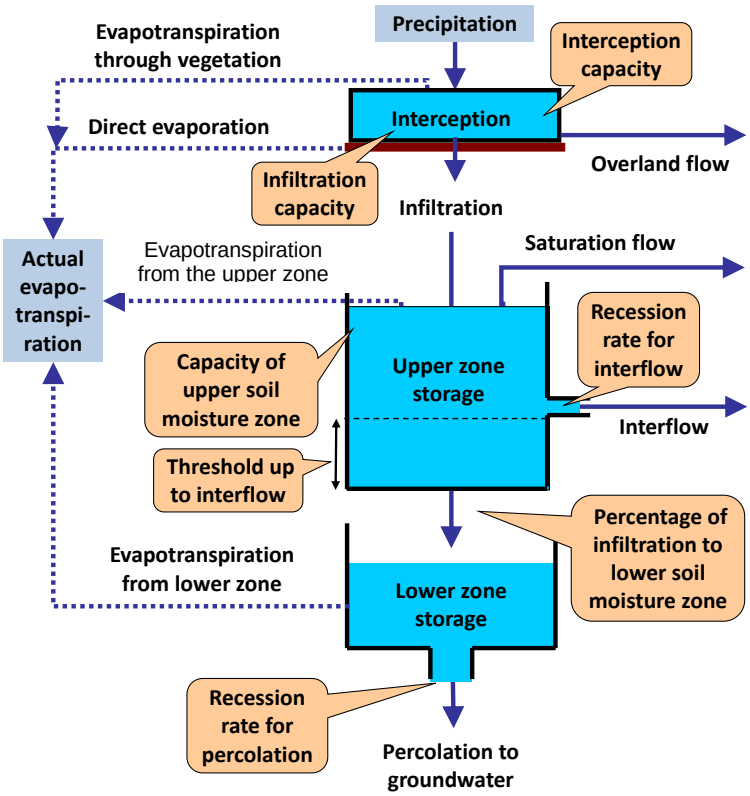


**Figure 9:** Representation of modelling components and associated fluxes within basin partitions. Model inputs, i.e. precipitation and PET, vary across sub-basins, while model parameters, shown in callouts, vary across HRUs.

As illustrated in Figure 9, model inputs are the aerial precipitation $P_t$ and potential evapotranspiration $E_{Pt}$, while outputs are the total soil moisture of the three conceptual storage tanks $S_t$, the surface runoff $Q_t$, the actual evapotranspiration $E_t$, and the percolation $G_t$. At each time step t, $[t, t + \Delta t]$ where $\Delta t$ is the simulation time interval (i.e. daily or hourly), the water balance equation is:

$$S_{t+1} = S_t + (P_t - Q_t - E_t - G_t)\Delta t \qquad (11)$$

where for a given value of soil moisture for each storage tank at the beginning of the simulation, the above formulae is solved based on some assumptions regarding the unknown variables $Q_t$, $E_t$, and $G_t$.

The total surface runoff is allocated to three components:

$$Q_t = Q_{Dt} + Q_{St} + Q_{It} \quad (12)$$

where:

$Q_{Dt}$ = direct runoff: excess of precipitation conducted through the impervious areas of the basin to its outlet within the time interval without any infiltration into the soil.

$Q_{It}$ = interflow (hypodermic flow): time-lagged lateral drainage of the unsaturated zone, represented as an outflow from the horizontal hole of the upper zone storage tank

$Q_{St}$ = saturation flow: soil moisture excess of the upper zone storage tank (if it exists) contributes to the streamflow as quick runoff due to saturation, at the end of the simulation step.

Real evapotranspiration, which is by definition less than or equal to potential evapotranspiration is allocated into three components:

$$E_t = E_{Ct} + E_{Dt} + E_{St} \quad (13)$$

where:

$E_{Ct}$ = crop evapotranspiration: minimum amount between the available moisture retained in flora and the corresponding potential evapotranspiration.

$E_{Dt}$ = direct evaporation: amount of precipitation evaporated quickly, from the water retained on the surface, before infiltrating into the soil and cannot exceed the interception capacity or the potential evapotranspiration

$E_{St}$ = soil evapotranspiration: the evapotranspiration deficit between the actual and potential evapotranspiration, satisfied by the actual moisture in the upper and lower unsaturated storage zones (using different mechanisms for the two zones). Specifically, the whole moisture amount in the upper zone is assumed available for evapotranspiration, whereas the lower zone moisture is partially available.

Finally, percolation to groundwater $G_t$ is the vertical water transfer from the upper unsaturated to the lower saturated soil zones, represented as an outflow from the outlet at the bottom of the lower-zone storage tank.

Given that at each time step $t$, $[t, t + \Delta t]$ where $\Delta t$ is the simulation time interval, aerial precipitation $P_t$ potential evapotranspiration $E_{Pt}$, ground water retention $S_{1t}$, and soil moisture in the upper, $S_{2t}$, and lower, $S_{3t}$, unsaturated zones are known variables for the

three conceptual storage tanks, initial soil moisture values are required at $t = 0$. However, since simulation begins at the start of the hydrological year (i.e. before the beginning of the wet season. in October in Greece), negligible initial soil moisture can be assumed, i.e. $S_{1t} = 0,\ S_{2t} = 0,\ S_{3t} = 0$.

To realistically represent the routing of the flow produced on the ground surface ($I_t = Q_{Dt} + Q_{St}$) to the outlet of each sub-basin, a transformation is applied based on the linear reservoir model with a time time lag, as shown in Figure 10 below. The reservoir, with infinite capacity, receives as input the surface runoff of the basin, $I_t$ , while the outflow is the space-time transformation to runoff, $Q_t$ at the outlet node of the basin (hydrograph). Flow retention is represented by the reservoir storage $S_t$.

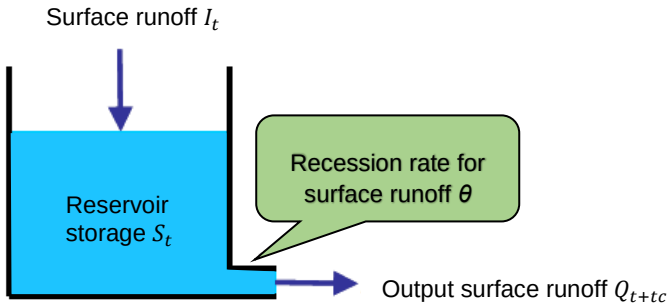


**Figure 10:** Illustration of the linear reservoir model for the routing of the sub-basin surface runoff

The linear reservoir model has two parameters assigned to each sub-basin: the recession rate of surface runoff, $\theta$, defined by the user or estimated through calibration, and the time lag, $t_c$, considered to be equal to the concentration time estimated by the empirical relationship of Giandotti (Giandotti 1934):

$$t_c = \frac{4\sqrt{A} + 1.5L}{0.8\Delta z} \qquad (14)$$

where:

$t_c$ = time of concentration (h)

A = sub-basin area (km$^2$)

L = length of the main river tributary segment passing through the sub-basin (km)

Δz = difference in altitude between the mean sub-basin height and height at the sub-basin outlet (m)

### 4.2.3 Groundwater model

HYDROGEIOS groundwater hydrological processes are based on a multi-cell approach, where the aquifer is resolved in non-rectangular cells, represented in the model by conceptual groundwater reservoirs (tanks) connected by virtual transfer elements. The stress components of groundwater tanks include: (a) areal inflows due to percolation through basin partitions (sub-basin/HRU intersection); (b) inflows due to infiltration underneath each river segment; and (c) point outflows due to pumping from each well (represented by boreholes). The first two stress components represent water inflows to the groundwater system due to natural recharge of the aquifer from precipitation, while the third component represents water outflow due to human intervention.

Percolation rates are outputs of the surface hydrological model, so the model integrates the equivalent depths from each sub-basin/HRU intersection on the corresponding cell area. If $F_{ijk}$ is the common area (intersection) of sub-basin $i$, HRU $j$, and groundwater cell $k$, $g_{ij}$ is the percolation amount from the intersection of sub-basin $i$ and HRU $j$, and $F_k$is the area of groundwater cell $k$, then the percolation amount at the specific cell is calculated by the following relationship:

$$g_k = \frac{1}{F_k} \sum_{i=1}^{NB} \sum_{i=j}^{NH} g_{ij} F_{ijk} \tag{15}$$

where $NB$ and $NH$ is the number of sub-basin and HRUs respectively.

Infiltration and pumping rates on the other hand, are outputs of the water management model. Regarding infiltration, the model estimates the river segment losses supplying each tank. Given that $\Delta_i$ is the volume of losses along river segment $i$, $L_{ik}$ is the partial length of river segment $i$ over groundwater cell $k$, and $L_i$ is the total length of the river segment I, the amount of percolation charging groundwater cell k is calculated by the following relationship:

$$\delta_\kappa = \frac{1}{F_k}\sum_{i=1}^{NR} \Delta_i L_{ik}/L_i \tag{16}$$

where $NR$ is the number of river segments. Similarly, for the estimation of the pumping amount per groundwater cell $w_k$, the sum of the borehole abstractions of corresponding to groundwater cell $k$ is calculated, and then divided by the corresponding cell area $A_k$.

For given stresses, the flow field problem is solved based on a simplified version of the scheme introduced by Rozos and Koutsoyiannis (2005), which proved suitable the simulation of aquifers with high parameter uncertainty, such as karst. The state variable of the model are the hydraulic heads and are calculated as follows:

$$h_i \begin{cases} w_i^{min} + w_i & w_i \le b_i \\ w_i^{max} + (w_i - b_i)\theta & w_i > b_i \end{cases} \tag{17}$$

where:

$w_i$= the water level in tank i

$w_i^{min}$= the bottom absolute level of tank i

$w_i^{max}$= the top bottom absolute level of tank i

$\theta$= the ration of specific yield to confined storage coefficient ($\theta >> 1$)

$b_i$= the layer thickness $\left(w_i^{max} = w_i^{min} + b_i\right)$

The upper branch of Eq. (17) corresponds to phreatic conditions, while the lower branch corresponds to confined conditions. Therefore, the layer thickness $b_i$ also represents the threshold between the confined and phreatic (unconfined) conditions. For a giver water level $w_i$, the water volume contained in the groundwater tank is calculated as:

$$\mathrm{V_i} = \mathrm{w_i F_i} \tag{18}$$

where $\mathrm{F_i}$ is the base area of the tank i, which is equal to the area of the corresponding cell i, multiplied by the specific yield $S_y$, a dimensionless model parameter, assigned to the cell i:

$$F_i = S_{yi} A_i \tag{19}$$

A low specific yield value indicates a small tank base area and therefore a large water level increase is required to store a given amount of groundwater volume, while conversely, a high specific yield value indicates a large tank vase area and therefore a small water level increase is required to store the same amount of groundwater volume. Another property of the groundwater water tank, and also a model parameter, is the hydraulic conductivity $K$, measured in (m/s).

A constant head condition is represented by assigning groundwater tanks with very large base area, forcing the corresponding water level to remain practically constant and near to the prescribed boundary value. Similarly, springs are modelled by assuming such dummy groundwater tanks, for which the slight water level changes are directly transformed to outflow hydrographs. Simulation of the groundwater losses is also implemented by a similar representation, conducted to neighboring river basins or the sea.

Groundwater flows are implemented through conceptual conducts $(\mathrm{i},\mathrm{j})$, where the indices denote adjacent interconnected tanks. The discharge is calculated using a Darcian formula as follows:

$$\mathrm{Q_{ij}} = \mathrm{K_{ij}A_{ij}}\frac{\mathrm{h_i} - \mathrm{h_j}}{\mathrm{I_{ij}}} \tag{20}$$

where:

$\mathrm{A_{ij}}$= cross sectional area, equal to the common plane area between cells i and j, assumed constant within each time interval

$\mathrm{I_{ij}}$= length between the centroids of cells i and j

$\mathrm{K_{ij}}$= conductivity parameter, computed as the arithmetic or geometrical mean of the corresponding tank conductivities

$\mathrm{h_i}$= the head value of tank i

$\mathrm{h_j}$= the head value of tank j

Equations (17) and (20) formulate an equations system that is solved through explicit or implicit numerical schemes, both implemented in HYDROGEIOS. In order to ensure numerical stability, a proper number of time intervals within a simulation step must be defined.

### 4.2.4 Calibration framework

The HYDROGEIOS conjunctive model, in its general form, comprises seven parameters per HRU, one parameter per sub-basin, one parameter per river segment and two parameters per groundwater cell (Table 11). In order to reduce the number of parameters, especially for the groundwater processes, for which it is often difficult to gather detailed spatial information (e.g. piezometric data), it is recommended to group cells with common hydraulic properties.

**Table 11:** List of model parameters

| Parameter | Symbol | Units | Model component |
|---|---|---|---|
| Interception capacity | r | mm | HRU |
| Infiltration capacity | $i_0$ | mm | HRU |
| Field capacity | k | mm | HRU |
| Threshold up to interflow | $\theta$ | mm | HRU |
| Recession rate for interflow | $\lambda$ | - | HRU |
| Percentage of infiltration | $\beta$ | - | HRU |
| Recession rate for percolation | $\mu$ | - | HRU |
| Recession rate for surface runoff | $\theta$ | - | Sub-basin |
| Time of concentration | $t_c$ | h | Sub-basin |
| Infiltration coefficient | $\delta$ | - | River segment |
| Specific yield | $S_y$ | - | Groundwater cell |
| Conductivity | K | m/s | Groundwater cell |

For the automatic estimation of the unknown model parameters, a calibration module is embedded that provides a set of statistical and empirical criteria for model fitting to multiple responses, such as river and spring discharge, and for several options concerning the definition of the feasible search space. These criteria include:

(a) typical statistical metrics, such as efficiency, i.e. the coefficient of efficiency or Nash-Sutcliffe index (Eq. 21) (Nash & Sutcliffe 1970) and bias, i.e. average bias (Eq. 22), standard deviation bias (Eq. 23) and coefficient of variation bias (Eq. 24), aiming to ensure as close a fit as possible of the simulated hydrographs to the observed ones;

$$\mathrm{EFF} = 1 - \left( \sum_{t=1}^{T} (y_t - y'_t)^2 \Big/ \sum_{t=1}^{T} (y_t - \bar{y})^2 \right) \tag{21}$$

$$\text{AVERBIAS} = \frac{\bar{y}' - \bar{y}}{y} \tag{22}$$

$$\text{SDEVBIAS} = \frac{\sigma_y' - \sigma_y}{\sigma_y} \tag{23}$$

$$\text{CAVRBIAS} = \frac{\frac{\sigma_y'}{\bar{y}} - \frac{\sigma_y}{\bar{y}}}{\frac{\sigma_y}{\bar{y}}} \tag{24}$$

where:

$y_t$ = observed flow values ($m^3/s$)

$y_t'$ = simulated flow values ($m^3/s$)

T = flow time period (s)

$\bar{y}$ = mean values of the observed flow values ($m^3/s$)

$\bar{y}'$ = mean values of the simulated flow values ($m^3/s$)

$\sigma_y$ = standard deviations of the observed flow values ($m^3/s$)

$\sigma_y'$ = standard deviations of the simulated flow values ($m^3/s$)

(b) zero-flow penalties (Eq. 25), emphasizing flow intermittencies that are easily observable, and very important from a water management perspective;

$$e_0 = \sqrt{\frac{1}{T_0}\sum_{t=1}^{T} z_t^2} \tag{25}$$

where $z_t$ is an auxiliary variable calculated as:

$$z_t = \begin{cases} y_t \text{ if } y_t' = 0 \\ y_t' \text{ if } y_t = 0 \\ 0 \text{ else} \end{cases} \tag{26}$$

and $T_0$ is the number of time steps for which the model fails to reproduce an observed floe interruption or, in the opposite, erroneously yield zero discharge.

(c) trend penalties (Eq. 27), to prohibit generating unrealistic flow or groundwater level patterns, in case of non-observable model variables, based on the Mann-Kendall rank correlation test (Kottegoda, 1980, p. 32-34) as follows: given a sample $(x_1, x_2, \dots, x_N)$, the statistic:

$$T = r/\sqrt{\sigma_r^2} \tag{27}$$

is a standard normal variable where:

$$r = 4P/[N(N-1)], \quad \sigma_r^2 = 2(2N+5)/[9N(N-1)] \tag{28}$$

and P is the number of all pairs $\{x_i, x_j, j > i\}$ with $x_i > x_j$. For a two-tailed test and for a level of significance a, the null hypothesis of no trend presence if $|T| < z_a/2$ is rejected. In that case, a penalty value equal to $|T| - z_a/2$ is assigned.

A modified efficiency index is also applied, that accounts for flow values above the observed mean, thus forcing fitting to flood fluxes. According to the available information, the user may use multiple criteria aggregated in a weighted objective function. For every criterion corresponding to a specific variable $f_i$, is assigned a non-negative weight coefficient $w_i$. By aggregating m criteria, results a universal error measure or overall error index, $F_{(\theta)}$, of the unknown parameters $\theta = (\theta_1, \theta_2, \dots, \theta_v)$, forming the objective function of the optimization problem:

$$F_\theta = \sum_{i=1}^{m} w_i f_i(\theta) \tag{29}$$

Conventionally, all the measures are defined so that the solution to the optimization problem, which corresponds to the optimal values of the parameters, $\theta^* = (\theta_1^*, \theta_2^*, \dots, \theta_n^*)$, minimizes the objective function. It is obvious that, by applying different weight coefficients, a different optimal solution can be obtained. The objective function and the parameter bounds are inputs to a complex calibration problem, which is handled through the advanced global optimization technique of the evolutionary annealing-simplex algorithm (Efstratiadis & Koutsoyiannis 2002; Rozos et al. 2004; Tsoukalas et al. 2016).

## 4.3 Study area and data

The study area is the Nedontas River Basin, upstream of the monitoring station "Latomeio (quarry) Baka", which is located in the southeastern part of Peloponnesus, Greece, and drains into the Gulf of Messenia (Figure 11). The basin is surrounded by Taygetos Mountain and has a drainage area of 118.4 km$^2$ and an average elevation of 770 m, reaching a maximum elevation of 1715 m and a minimum of 93 m at the Latomeio Baka outlet. Terrain slope ranges from almost flat on the lowland and riverside areas to 76% on the steep mountain slopes, with the mean slope calculated at

22%. Nedontas originates in the western slopes of Taygetos and is mainly formed by three tributaries: its headwaters comprise the Nedousa and Alagonia tributaries, as well as spring flows in their sub-basins; the upper reach of Nedontas is joined by the lower reach of Karveliotis stream emanating from the SE area of the basin. The length of the main river course is about 26 km; the river discharges to the Gulf of Messenia, traversing the city of Kalamata, a regional economic center of SW Peloponnese, with 55,000 inhabitants.

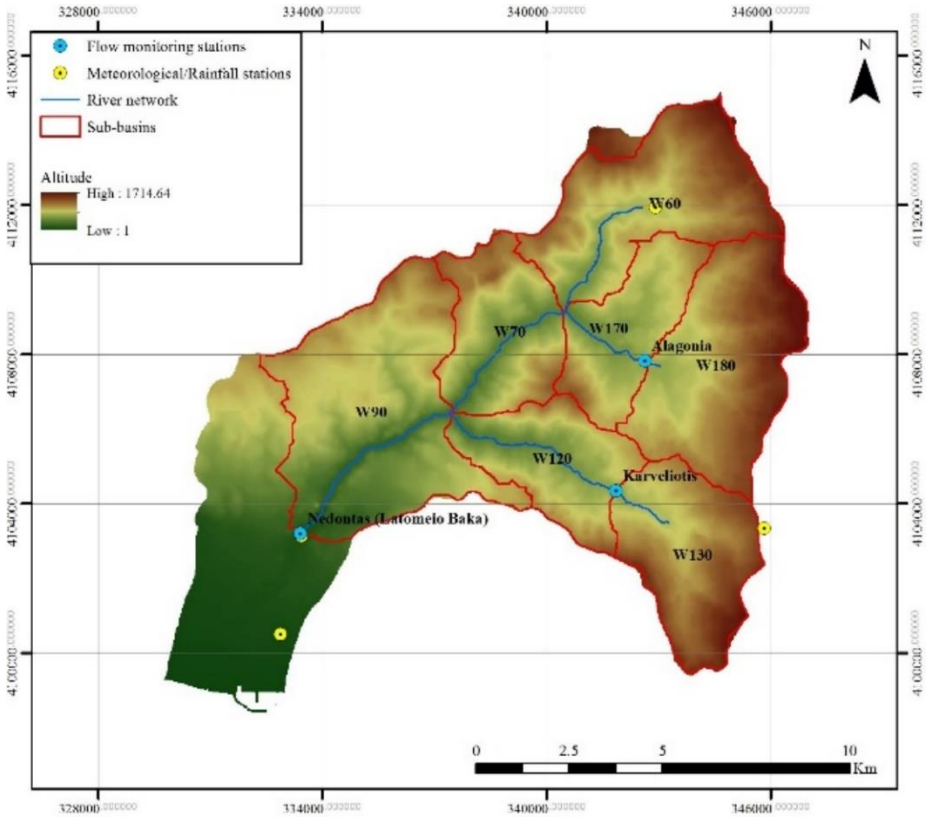


**Figure 11:** Digital map of Nedontas river basin, also showing monitoring stations (meteorological and hydrometric) and main modelling components (sub-basins, reaches).

The broader area is characterized by a mild Mediterranean climate influenced by orography, with long dry summers from April–October and wet winters from November–March. Mean annual temperature ranges from 13 °C–19 °C, with July being the hottest month (26.4 °C) and January the coldest (10.2 °C). Mean annual precipitation varies from 600 mm at the south, 1500 mm on the mountain range and 800–1200 mm in the central and northern plains and hilly areas (Koutsoyiannis et al. 2008). The river discharge is characterized by significant seasonal variability, since

during the dry period, the flow is occasionally interrupted. On a mean annual basis, the runoff arriving at the outlet is approximately 550 mm (2.1 $m^3/s$).

In the context of the aforementioned project (DEUCALION, see Section 3.5), the basin was equipped with a telemetry-based hydro-meteorological network, comprising four meteorological and three flow-gauging stations, installed at the basin outlet (Latomeio Baka) and upstream on the two main tributaries, Alagonia and Karveliotis (Efstratiadis et al. 2013). The input time series were meteorological and flow data for a three-year period (September 2011–April 2014), provided at 10- and 15-min intervals, respectively. The input geographical layers were a 25-m resolution DEM, to delineate the river network and associated sub-basins and to calculate their geometrical properties, as well as maps of classified geological formations and land cover. The geographical layers were used to formulate the CN map and define the HRUs.

## 4.4 Model setup

The study area was divided into seven sub-basins, by setting a flow accumulation threshold of 10 $km^2$ and by setting additional nodes at the three flow station sites, as illustrated in Figure 11. Their main properties are summarized in Table 12. Spatially-averaged precipitation time series of hourly resolution were extracted at the sub-basin scale, using the Thiessen polygon method.

**Table 12:** Nedontas sub-basins properties

| Sub-basin | Name | Area ($km^2$) | Mean elevation (m) | Stream length (m) | Mean slope (%) |
|---|---|---|---|---|---|
| W60 | Nedousa | 19.47 | 1008.9 | 4296.3 | 23.06 |
| W180 | Alagonia | 20.72 | 1092.4 | 497.5 | 18.26 |
| W130 | Karveliotis | 14.92 | 1096.5 | 1721 | 21.17 |
| W170 | Downstream of Alagonia | 10.91 | 739.4 | 2807.4 | 20.26 |
| W120 | Downstream of Karveliotis | 11.81 | 710.1 | 5755.2 | 25.87 |
| W70 | Downstream of Nedousa | 12.53 | 741.9 | 4588.8 | 26.97 |
| W90 | Latomeio Baka | 28.02 | 654.8 | 5920.9 | 18.41 |

Processing of the raw rainfall and temperature data included the removal of unreasonable or infeasible values (e.g. false negative rainfall) followed by aggregation of the 10-minute data to obtain hourly precipitation and mean hourly temperature time series. Finally, missing hourly values for both meteorological stresses were filled in through linear regression analysis from observed data from neighboring stations.

Spatially-averaged values were extracted at the sub-basin scale using the Thiessen polygon method (Fig. 12) and corrected for elevation assuming an annual rain slope value of 0.75 mm/m and a temperature decrease rate of 0.0065°C/m. These values were employed to "transfer" the point rainfall and temperature observations from the elevation of the meteorological stations to the average elevation of each sub-basin. For hourly PET estimations, monthly PET values were calculated over all sub-basins using the simplified Penman-Monteith formula (Tegos et al. 2013):

$$E = \frac{aR_a + b}{1 - cT_a} \tag{30}$$

where:

$R_a$= extraterrestrial solar radiation, a function of latitude and time $(kJ/m^2)$

$T_a$= temperature (°C)

a, b, c = regional parameters

According to Tegos et al. (2013) the optimal values of the parameters for the region of Kalamata are: $a$ = 0.000053 kg/kJ, $b$ = 0.064 kg/m$^2$ and $c$ = 0.0253°C$^{-1}$, and were used to calculate the monthly PET values for each sub-basin as a function of monthly temperature, followed by an empirical disaggregation approach where the daily PET values are assumed to be proportional to the ratio of the daily to monthly temperature, which was then divided by 24 to obtain the hourly values.

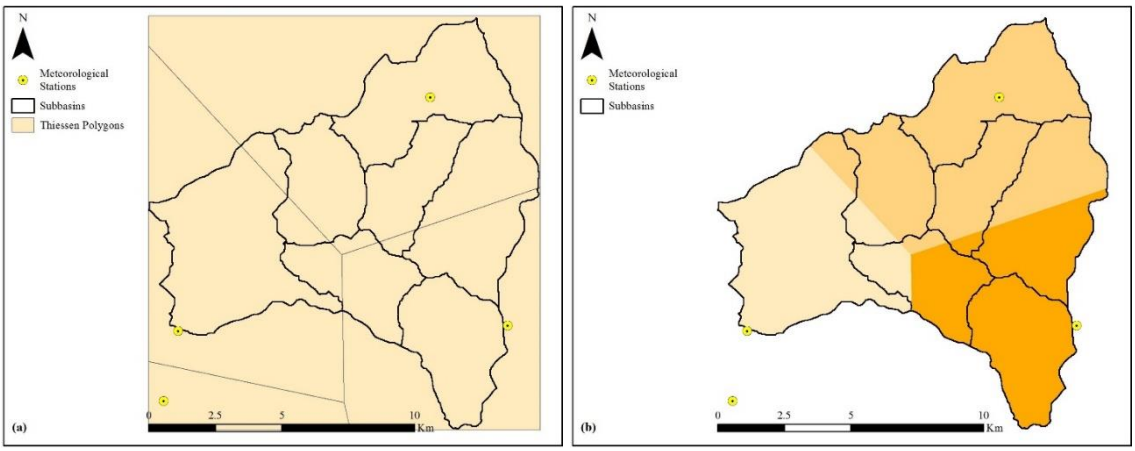


**Figure 12:** Nedontas river basin (a) Thiessen polygons for daily rainfall and evapotranspiration, (b) spatially-averaged rainfall and evapotranspiration per sub-basin.

The raw hydrometric data included stage data in 15-minute intervals at the three gauging stations, which had to be pre-processed in order to remove negative values and be adjusted to an offset stage value that corresponds to dry conditions. To construct the 15-minute discharge timeseries, either a theoretical hydraulic formula was used (e.g. Manning's equation), or an empirical stage-discharge relationships was established, i.e. rating curves (Efstratiadis et al. 2013). Considering only sporadic flow measurements available during the low-flow period, a theoretical relationship was applied, taking advantage the favourable hydraulic and geometrical characteristics of the cross-sections at the three gauging stations where stage recorders are installed. Under the assumption that the observed stage corresponds to the critical flow depth in a very wide cross-section, the discharge was estimated as follows:

$$q = w\, g^{1/2}\, y_c^{3/2} \tag{31}$$

where:

$y_c$= critical flow depth

w = flow width of the cross-section

g = acceleration of gravity (9.81 m/s$^2$)

Further analysis using the FLOW3D software (http://www.flow3d.com/) proved that Eq. (31) underestimated the high flows. With the combination of the two approaches, the final 15-minute discharge time-series were obtained, aggregated to hourly time-series (Efstratiadis et al. 2013).

The groundwater network was formulated by considering a conceptual groundwater tank underneath each sub-basin and allowing hydraulic connections between adjacent tanks, as well as with a hypothetical tank located downstream of the basin, to implement the underground losses to the sea, which are a quite significant portion of the water balance of the basin.

In all experiments, the simulation period was divided into a 10-month calibration period (September 2011–June 2012) and a 22-month validation period (July 2012–April 2014). Given that the simulation begins on 1 September, the beginning of the wet season in Greece, negligible initial soil moisture in the upper and lower soil moisture tanks is assumed. For the groundwater tanks, reasonable initial level values were assigned, based

on preliminary analyses and also taking advantage of macroscopic information (e.g., elevation of springs).

The model parameters were assigned as follows: (a) seven parameters for the rainfall-runoff component of each HRU; (b) one recession parameter for each sub-basin (seven in total); (c) one hydraulic conductivity for each groundwater cell (eight in total); and (d) a single leakage coefficient assigned to the downstream river segment accumulating the runoff losses due to infiltration (for the rest of the segments, infiltration losses were not considered). In the context of calibration experiments, the number of parameters that were associated with HRUs was varied, while the number of the rest of parameters was kept the same, i.e., 16. For the non-calibrated parameters, approximate estimates were provided, to ensure realistic fluctuations of the associated fluxes; for instance, a common specific yield was assigned to all groundwater cells, equal to 10%

The unknown parameters of each HRU configuration scheme were calibrated against the observed flows at the three monitoring stations. In order to evaluate the model performance in calibration and validation, common error measure was used, comprising a weighted sum of the coefficients of efficiency, high-flow efficiencies and a trend penalty to control the generation of unreasonable trends in the groundwater level behaviour. Note that according to common hydrological practices (Freer et al. 1996a; Moriasi et al. 2007)], efficiency values greater than 50% indicate a rainfall-runoff model of satisfactory predictive capacity, while a value of 30% indicates a marginally acceptable model (Freer et al. (Freer et al. 1996a) proposed this limit as the threshold for distinguishing behavioral solutions within the GLUE (Generalized likelihood uncertainty estimation) method). For the following calibration experiments, efficiency values above 75–80% are considered “satisfactory”, while efficiency values lower than 30% were characterized as “unsatisfactory”.

## 4.5 Preparation of the CN Maps

For the preparation of the CN map, to be next considered as the background for the delineation of HRUs, maps of classified geological formations, land cover maps, as well as a raster map of terrain slopes were used. Specifically:

Geological formations and information on the tectonic and lithological elements of the river basin were extracted from geological maps, published by the Institute of Geology

& Mineral Exploration of Greece. As shown in Figure 13a, the basin includes two major geological formations, i.e., Tripolis geotectonic units, on the western part, and Phyllite-Quartzite series, on the eastern. The Tripolis formations that occupy the largest part of the hilly and lowland areas mainly consist of limestones and marbles, alternating with crystalline slate. Limestone is porous, and through the centuries, rain and snow water have caused erosion, forming caves with stalagmites, stalactites and other karst landforms. In this respect, waters that have penetrated the karstified rocks either outflow from springs in the mountainous areas or are conducted to the sea, as underwater estuaries called “Anavoli”. On the other hand, the Phyllite-Quartzite series are extended over the mountain areas (Taygetos) and consists of Permian-Lower Triassic rocks of low to moderate permeability. The other three formations occupy only a small area in the SE part of the basin (Pindos formation, consisting of Upper Cretaceous-Paleocene rocks, Tyros layers, consisting of Carboniferous-Upper Triassic rocks, and Postalpine sediments, consisting of Quaternary, Holocene and Pliocene rocks).

Land-cover classes, illustrated in Figure 13b, were derived from the CORINE Land Cover 2000 map of the European Environmental Agency. These include broad-leaved forest (37%), coniferous forest (23%), transitional woodland-shrub (16%), pastures (10%), sclerophyllous vegetation (7%), mixed forest (3%), land principally occupied by agriculture, with significant areas of natural vegetation (3%), olive groves (<1%), complex cultivation patterns (<1%) and industrial or commercial units (<1%). In general, vegetation favors interception and infiltration, thus resulting in reduced overland flow. Given that a quite extended part of the basin, mainly in the NE, was burned in 2007, an updated map, provided by the National Observatory of Athens, Institute for Astronomy, Astrophysics, Space Applications & Remote Sensing, was also used for to represent the land cover characteristics during the simulation period. As explained in Section 3.3, these areas were classified under one category with respect to their original condition.

Finally, for the classification of drainage capacity, the terrain slope map (Fig. 13c) was used, which has been automatically extracted through the DEM.

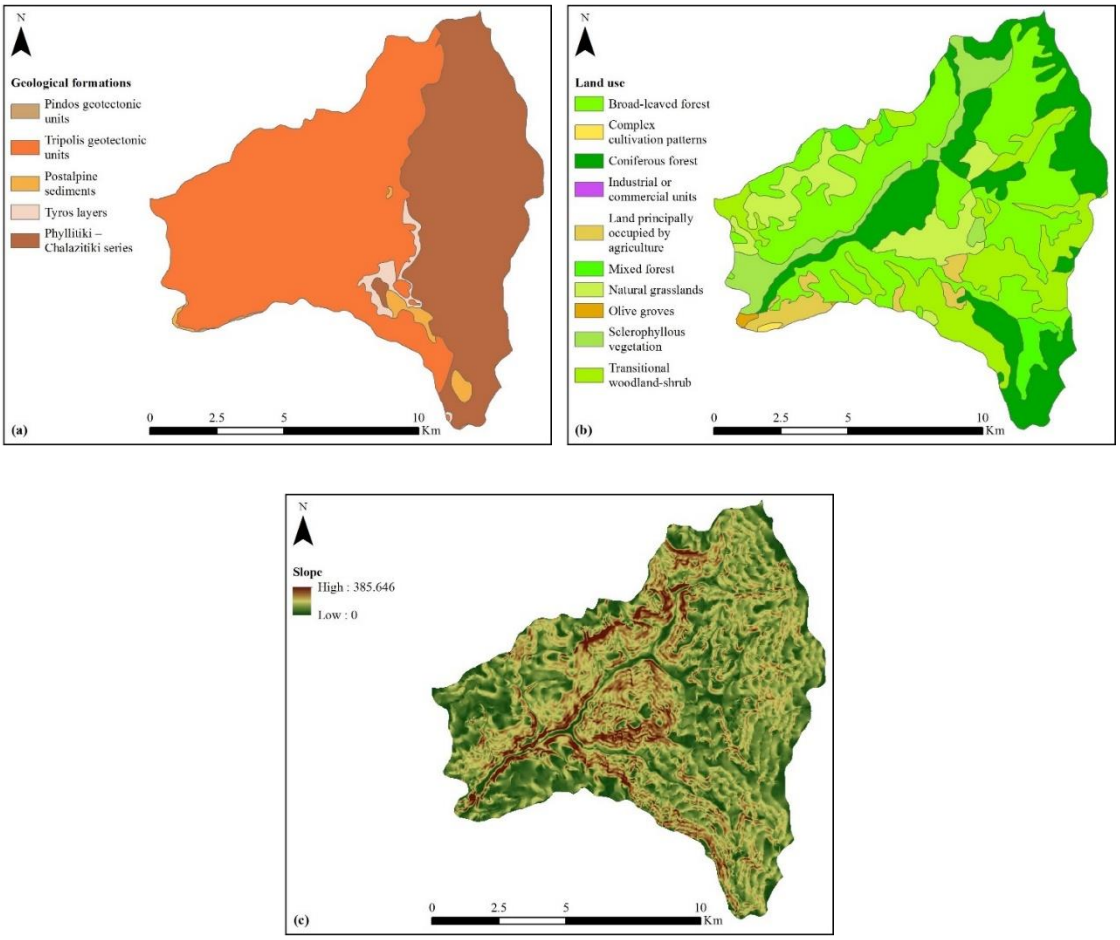


**Figure 13:** Nedontas river basin (a) geological formations, (b) land cover classes, (c) terrain slope (%).

The raster map of CNs, shown in Figure 15, has been produced by overlaying the raster layers of $i_{\mathrm{PERM}}$, $i_{\mathrm{VEG}}$ and $i_{\mathrm{SLOPE}}$, (Figs. 14a, 14b and 14c respectively) and then employing Eq. (10). The values of the three indices were assigned according to the guidelines of Table 9, accounting for the dominant classes of permeability, vegetation and drainage capacity, which were estimated on the basis of the aforementioned geological, land use and terrain slope information, respectively. The derived map (Fig. 15) contains 18 classes, ranging from CN = 37, for areas with high permeability, dense vegetation and very low slope, to CN = 91, for bare areas with low permeability and very high slope.

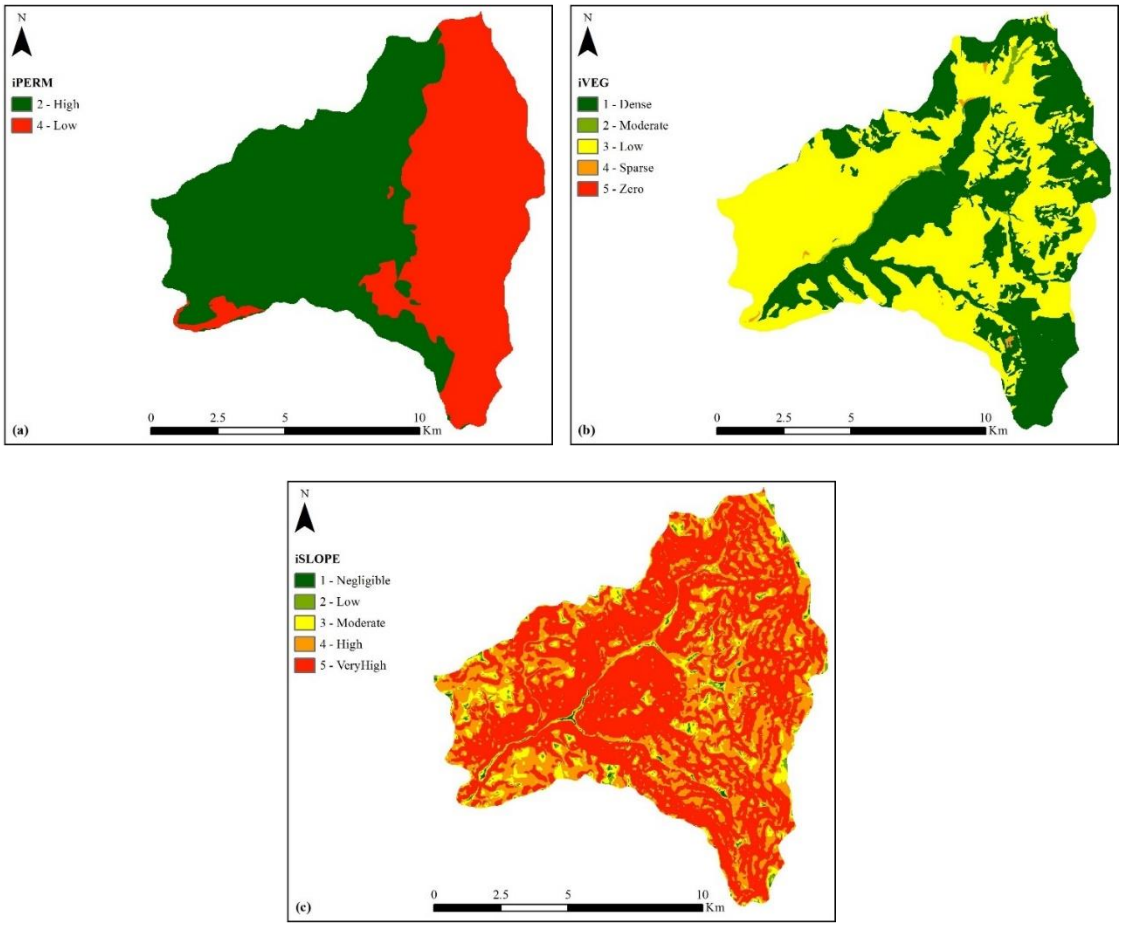


**Figure 14:** Nedontas river basin (a) water permeability classes (iPERM), (b) vegetation density classes (iVEG), (c) drainage capacity classes (iSLOPE).

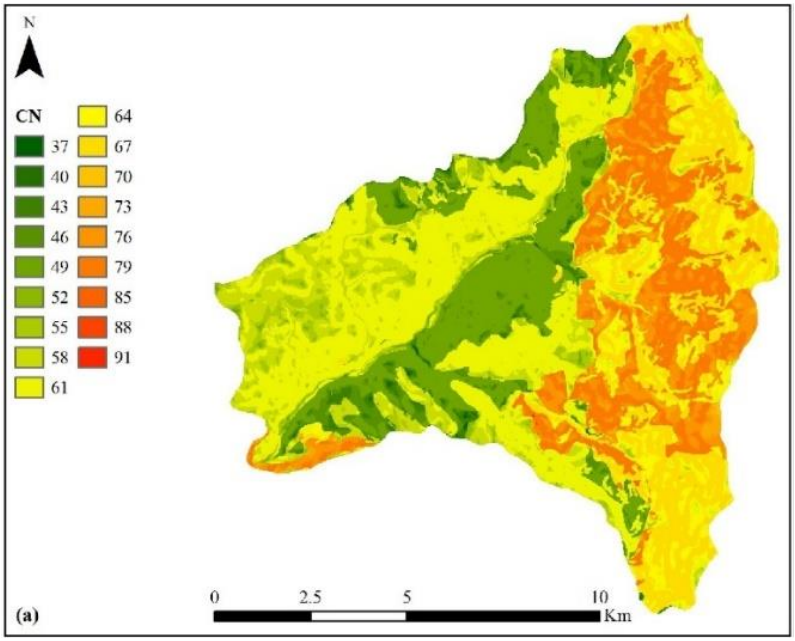


**Figure 15:** CN parameter map of the Nedontas river basin initial map of 18 CN classes

## 4.6 Calibration Experiment 1: Varying the number of HRUs

In order to test the key hypothesis that the number of HRUs should equal or close to the number of the available flow records (in that case, three), the calibration problem was run considering five alternative parameterizations, from one to five HRUs, as shown in Figure 17. Obviously, regarding the model schematization, the same semi-distributed structure was used, comprising seven sub-basins and associated meteorological inputs. It is noted that the single-HRU formulation with semi-distributed inputs is referred to as the semi-lumped modelling approach (Ajami et al. 2004). For the surface hydrological processes' representation, seven parameters were assigned to each HRU; thus, for each configuration, the total number of control variables is $7N$, where $N$ is the number of HRUs. Therefore, the simplest parameterization, the semi-lumped (homogenous) basin, required the estimation of seven parameters, while for the scenario with five HRUs, 35 unknown parameters of the surface hydrological module were considered.

The parameter estimation problem was handled through of a fully-automatic optimization approach, using the evolutionary annealing-simplex algorithm across an extended search space, defined by the physical bounds of the associated set of parameters (7, 14, 21, 28 or 35). To ensure unbiased results, all calibrations were carried out by assigning the same initial conditions and the same values for the rest of the parameters (groundwater conductivities, sub-basin routing rates, infiltration coefficient), as specified through preliminary calibrations. Moreover, to avoid getting trapped in local optima, thus resulting in sub-optimal model performance, several independent optimizations were employed for each parameterization, finally selecting the best solution. To take into account the increasing computational burden of optimization against the number of control variables, a maximum budget of $2000N$ trials was set. Thus, for the lumped approach, up to 2000 function evaluations were allowed for each optimization run, while for the more complex configuration ($N = 5$), the budget was increased up to 10,000 function evaluations (Table 13). It is important to note that within this first experiment, no manual interventions were allowed, as done in the context of the second experiment, which provided much improved results (Section 4.7). A schematic layout of the processes followed in the calibration experiment 1 is showed in Figure 16.

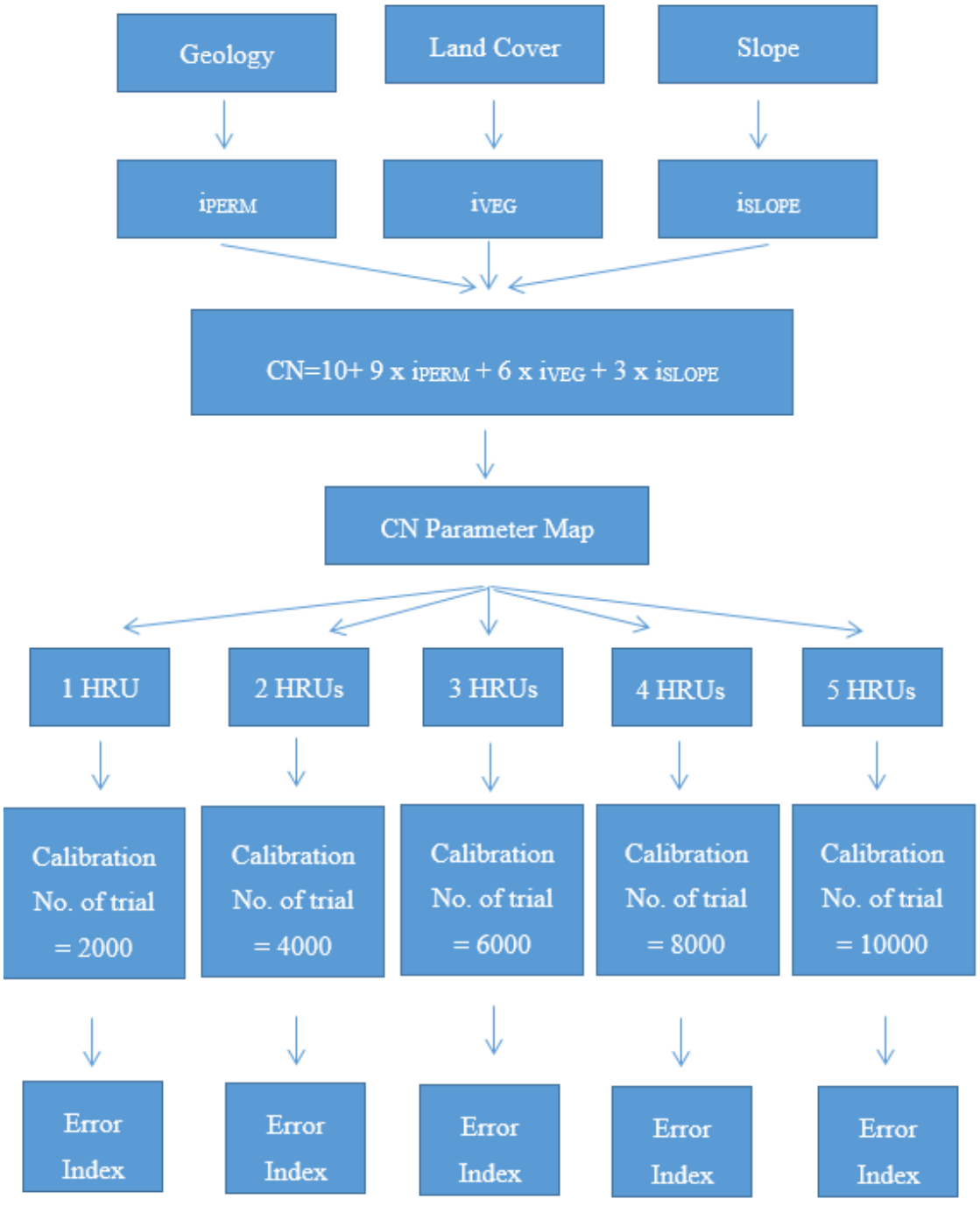


**Figure 16:** Schematic layout of the processes followed in the calibration experiment 1

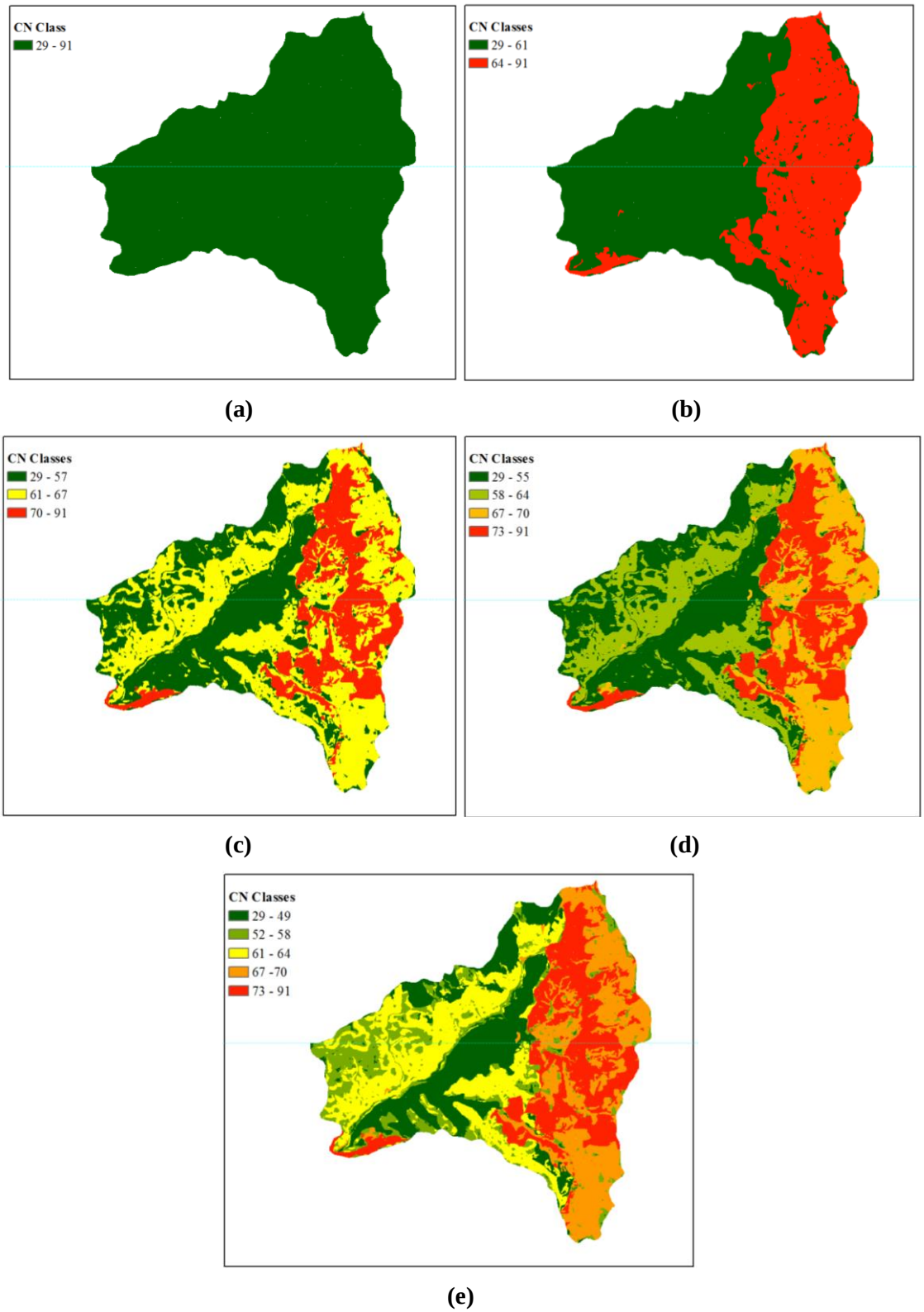


**Figure 17:** HRU delineation based on (a) one, (b) two, (c) three, (d) four and (d) five CN classes.

The overall model performance, in terms of the error measure for both the calibration and validation periods, is shown in Table 13, while analytical results of the optimal efficiency and high flow efficiency values obtained by each simulation at each monitoring station are summarized in Table 14.

**Table 13:** Overall model performance, expressed in terms of the composite error function, considering alternative parameterizations, by means of the number of HRUs

| No. of HRUs | CN Classes | No. of HRU parameters | No. of run trials | Error Index (F) in calibration | Error Index (F) in Validation |
|---|---|---|---|---|---|
| 1 | 29 - 91 | 7 | 2000 | 2.465 | 3.674 |
| 2 | 29 – 61<br>64 - 91 | 14 | 4000 | 2.072 | 3.043 |
| 3 | 29 – 57<br>61 – 67<br>70 – 91 | 21 | 6000 | 1.985 | 2.675 |
| 4 | 29 – 55<br>58 – 64<br>67 – 70<br>73 – 91 | 28 | 8000 | 2.094 | 3.621 |
| 5 | 29 – 49<br>52 – 58<br>61 – 64<br>67 – 70<br>73 – 91 | 35 | 10000 | 2.390 | 3.519 |

**Table 14:** Optimal values of efficiency and high flow efficiency for varying numbers of HRUs.

| Hydrometric Station | Calibration period | | Validation period | |
|---|---|---|---|---|
| | Efficiency | High Flow Eff. | Efficiency | High Flow Eff. |
| | One HRU | | | |
| Basin outlet – Latomeio Baka | 0.524 | 0.297 | 0.591 | -0.521 |
| Monitoring station – Karveliotis | 0.672 | -0.166 | 0.687 | 0.218 |
| Monitoring station – Alagonia | 0.662 | 0.054 | 0.708 | 0.416 |
| | Two HRUs | | | |
| Basin outlet – Latomeio Baka | 0.798 | 0.810 | 0.560 | -0.793 |
| Monitoring station – Karveliotis | 0.887 | 0.676 | 0.712 | 0.259 |
| Monitoring station – Alagonia | 0.674 | 0.083 | 0.722 | 0.496 |
| | Three HRUs | | | |
| Basin outlet – Latomeio Baka | 0.672 | 0.722 | 0.706 | -0.067 |
| Monitoring station – Karveliotis | 0.892 | 0.761 | 0.809 | 0.571 |
| Monitoring station – Alagonia | 0.721 | 0.248 | 0.736 | 0.571 |

| | | | | |
|---|---|---|---|---|
| | | Four HRUs | | |
| Basin outlet – Latomeio Baka | 0.773 | 0.814 | 0.643 | -0.407 |
| Monitoring station – Karveliotis | 0.869 | 0.631 | 0.738 | 0.285 |
| Monitoring station – Alagonia | 0.673 | 0.145 | 0.724 | 0.513 |
| | | Five HRUS | | |
| Basin outlet – Latomeio Baka | 0.716 | 0.762 | 0.567 | -0.563 |
| Monitoring station – Karveliotis | 0.819 | 0.521 | 0.793 | 0.622 |
| Monitoring station – Alagonia | 0.737 | 0.160 | 0.672 | 0.495 |

It is clear that the best overall model performance is achieved by the simulation with the three HRUs, both in calibration and validation, with overall index errors of 1.985 and 2.675, respectively. Only in two cases did other parameterizations result in more efficient results: at the outlet, the simulation with the four HRUs achieved efficiency and high flow efficiency values of 77.3% and 81.4%, respectively, and the simulation with the two HRUs achieved efficiency and high flow efficiency values of 79.8% and 81.0%, respectively, compared to the lower values of 67.2% and 72.2%, respectively, of the simulation with the three HRUs. However, in all other cases, the efficiency and high flow efficiency values achieved by the simulation with the three HRUs were higher, further confirming the fundamental hypothesis that the best compromise, in terms of model performance against computational effort, is ensured by considering the parameterization with three HRUs, which equals the number of available hydrographs.

## 4.7 Calibration Experiment 2: Contrasting alternative HRU delineation approaches

The CN-based approach with three HRUs was compared to existing HRU delineation methodologies, herein referred to as unique combination and union of layers (Section 2.3.2). A schematic layout of the processes followed in the calibration experiment 2 is showed in Figure 18.

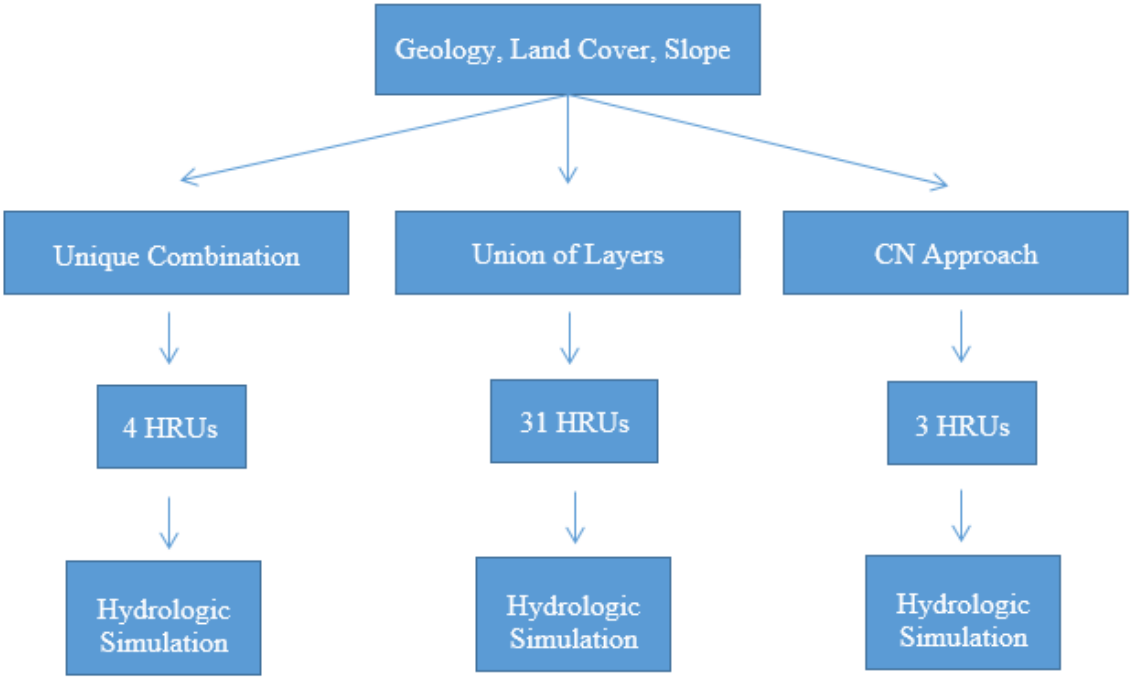


**Figure** 18: Schematic layout of the processes followed in the calibration experiment 1

The former accounts for user-defined thresholds for land use, soil type and slope range within each sub-watershed, followed by a spatial overlay scheme, 20%, 10% and 20% thresholds used for land use, soil and slope, respectively (Winchell et al. 2013). This means that any land use, soil and slope occupying less than or equal to the area percentage threshold defined in each sub-basin will be lumped with the adjacent dominant cells. A spatial overlay was then performed, and cells having the same combination of land use, soil and slope categories were given a unique HRU combination number, resulting in 31 HRUs (Figure 19a). In the union of layers delineation, HRUs are defined as the product of separate partitions accounting for different watershed properties. In this case, the product of the two dominant geological formations, corresponding to low and high permeability, and the two dominant land uses, corresponding to forests and meadow-pastures, was considered, thus obtaining four HRUs (Figure 19b).

Due to the different HRU delineations, the number of parameters associated with the rainfall-runoff module varied greatly (Table 15), specifically 31 × 7 = 217 for the unique combination (233 in total), 4 × 7 = 28 for the union of layers (44 in total) and 3 × 7 = 21 for the proposed CN approach (37 in total). The calibration problem was carried out through a hybrid strategy, combining human experience and automatic

optimization tools (Boyle et al. 2000; Mazi et al. 2004a; Mazi et al. 2004b; Rozos et al. 2004). It was an iterative process seeking progressive improvements of a relatively small group of parameters within a realistic value range and satisfactory predictive capacity for all model responses. Trial calibrations were initially employed that allowed large parameter variations. Following, several optimization runs were carried out by modifying the bounds of the feasible parameter search space, while trying different combinations of criteria weights. Then, focused was set on the optimization of the HRU parameters and on the most significant groundwater parameters, to attain a good fit of the hydrograph at the basin outlet, especially during high flows, and a satisfactory fit of the spring discharges. Once an initial good fit was achieved, the calibration focused on the improvement of specific aspects of the model responses, while ensuring a realistic water balance.

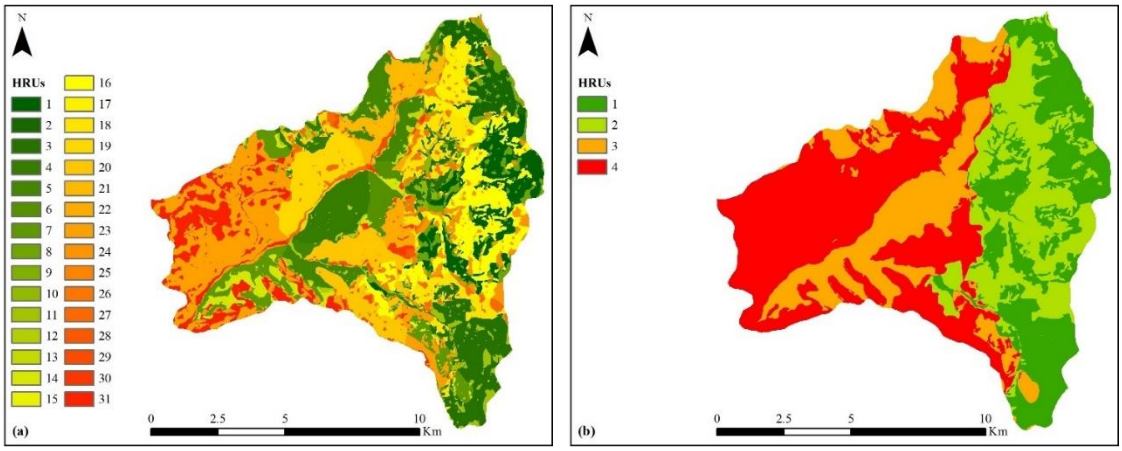


**Figure 19:** HRU delineation of Nedontas river basin (a) Unique combination method – 31 HRUs; (b) Union of Layers method – 4 HRUs; (c) CN method – 3 HRUs.

The optimized metrics are summarized in Table 16, whereas Figures 20–22 contrast the observed and simulated hydrographs at the three monitoring sites. At the basin outlet (Fig. 20), a very good fit is achieved by all parameterizations, for both calibration and validation period. Overall, the highest efficiency values are obtained by the proposed CN approach, with 81.4% and 80.2% for calibration and validation, respectively, compared to 80.1% and 77.1% obtained by the simulations performed with the union of layers and 76.8% and 71.9% with the unique combination. As shown in Figure 20, the simulations preserve the important features of the hydrographs, such as the high flows over the winter and zero flows over the summer periods for the calibration periods.

Although the high flow efficiency values are very good for the calibration period, none of the models succeeds at simulating the part of the hydrograph between March and June 2013 well (yet, this may be attributed to systematic measurement errors, since the recession limb appearing at the upstream stations is not shown at the outlet). The CN approach and the unique combination parameterization simulate the low flows well, while the union of layers overestimates the low summer flow both for the calibration and the validation periods.

The best performance by all parameterizations was achieved for the Karveliotis station (Fig. 21), located in the eastern part of the basin (calibration value first, validation value second): 89.2% and 83.7% for the CN approach, 90.8% and 81.3% for the unique combination and 65.5% and 76.2% for the union of layers delineation (Table 16). High flow efficiency with the CN approach was satisfactory both for calibration and validation (78.9% and 57.9%, respectively). Although the models preserved quite well the overall behavior of the hydrographs, some of the high flow events were somewhat underestimated, while the union of layers approach also underestimated the summer flows.

For Alagonia station (Fig. 22), located in the NE part of the basin, the efficiency values, although lower, were still very satisfactory, with 79.7% in calibration and 75.3% in validation for the simulation with the CN approach for the HRU delineation, 75.4% and 68.0%, respectively, with the unique combination delineation, and 65.8% and 72.6%, respectively, with the union of layers delineation (Table 16). High flow efficiency was satisfactory across the full simulation period only with the CN approach; the other two parameterizations produced mixed results. The CN-based and unique combination approaches better capture the high flows in the calibration period, while all modes simulated the low summer flows well.

Note that although the same calibration strategy was employed for the three HRU approaches, the computational time and human effort spent differed markedly. Table 15 provides a qualitative expression of this effort, which is mainly associated with the time needed for manual interventions within the hybrid calibration procedure. It is also associated with the number of individual optimizations, using small sub-sets of parameters or different ranges of their feasible bounds, in an attempt to achieve an acceptable model performance and simultaneously ensuring realistic hydrological

behaviors. The unique combination delineation required at least triple the effort to achieve satisfactory performance, compared to the union of layers and CN approaches, while preserving a realistic set of parameters turned out to be a very tedious task.

**Table 15:** Number of HRUs and their parameters resulted from each delineation approach.

| | Unique Combination | Union of Layers | CN approach |
|---|---|---|---|
| No. of HRUs | 31 | 4 | 3 |
| No. of HRU parameters | 217 | 28 | 21 |
| Total No. of parameters | 257 | 68 | 61 |
| Optimization effort* | ~3 | ~1.5 | 1 |

* Ranging from one to five, where 1 indicates minor and 5 major optimization effort.

**Table 16:** Optimal values of efficiency and high flow efficiency for the three HRU delineation approaches.

| Hourly runoff | Calibration period | | Validation period | |
|---|---|---|---|---|
| | Efficiency | High Flow Eff. | Efficiency | High Flow Eff. |
| | | Unique combination | | |
| Basin outlet – Latomeio Baka | 0.768 | 0.809 | 0.719 | 0.068 |
| Monitoring station – Karveliotis | 0.908 | 0.663 | 0.813 | 0.580 |
| Monitoring station – Alagonia | 0.754 | 0.253 | 0.680 | 0.141 |
| | | Union of layers | | |
| Basin outlet – Latomeio Baka | 0.801 | 0.757 | 0.771 | 0.195 |
| Monitoring station – Karveliotis | 0.655 | 0.693 | 0.762 | 0.368 |
| Monitoring station – Alagonia | 0.658 | 0.090 | 0.726 | 0.411 |
| | | CN based | | |
| Basin outlet – Latomeio Baka | 0.814 | 0.816 | 0.802 | 0.241 |
| Monitoring station – Karveliotis | 0.892 | 0.789 | 0.837 | 0.579 |
| Monitoring station – Alagonia | 0.797 | 0.300 | 0.753 | 0.440 |

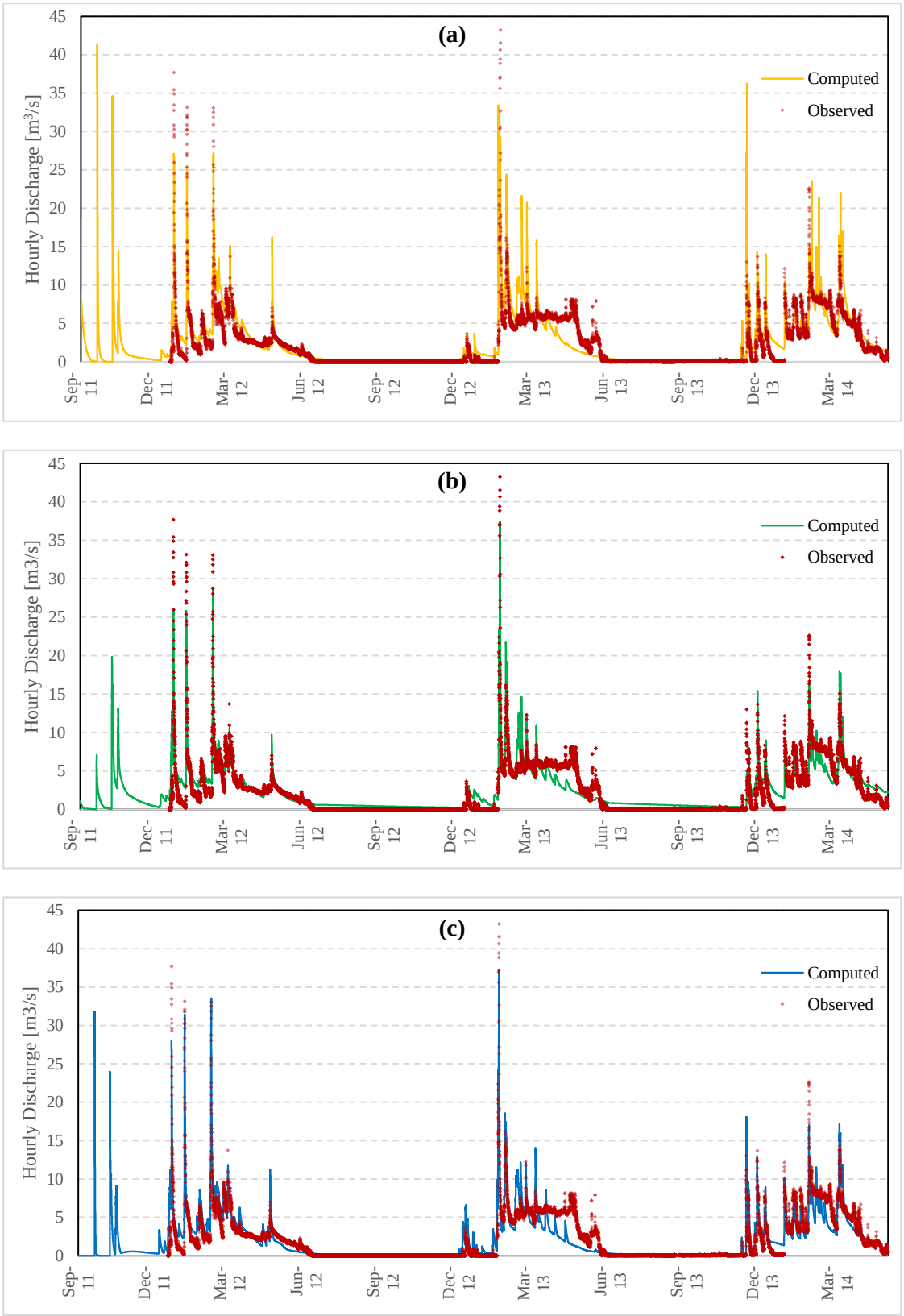


**Figure 20:** Computed vs. observed discharge series at the basin outlet (Latomeio Baka) for HRU delineation with (a) unique combination; (b) union of layers; (c) CN approach

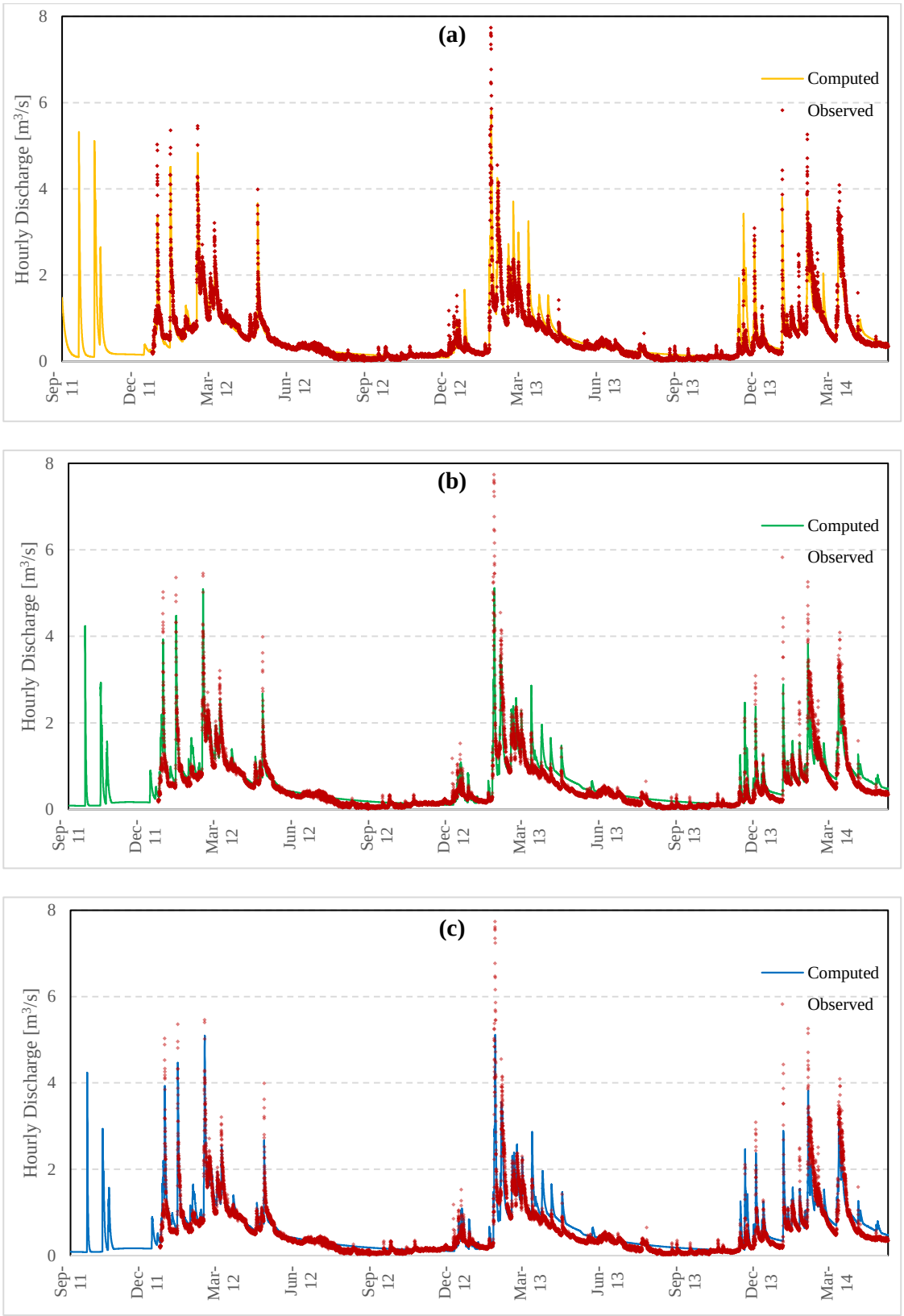


**Figure 21:** Computed vs. observed discharge series at Karveliotis monitoring station for HRU delineation with (a) unique combination; (b) union of layers; (c) CN approach.

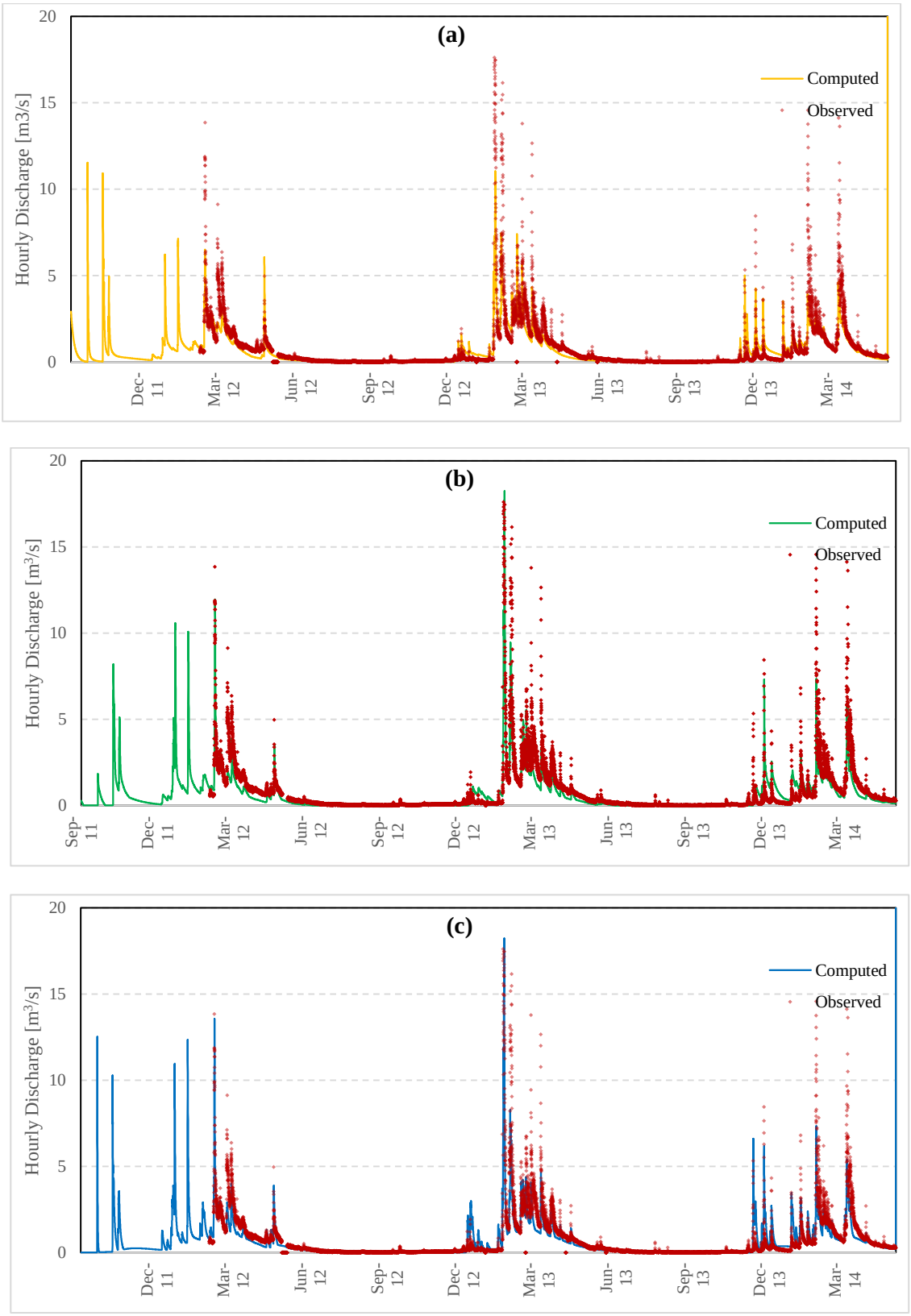


**Figure 22:** Computed vs. observed discharge series at Alagonia monitoring station for HRU delineation with (a) unique combination; (b) union of layers; (c) CN approach.

The overall conclusion is that neither an increased number of parameters, nor an increased calibration effort resulted in improved model performance. Therefore, it was confirmed that a too detailed parameterization actually induces more complexity to the calibration problem, which is far from a straightforward task. Actually, as a result of interrelated uncertainties and errors in all aspects of hydrological modelling and calibration (Efstratiadis & Koutsoyiannis 2010), an automatic optimization procedure cannot ensure a good predictive capacity, typically due to algorithmic weaknesses (e.g., trapping to local optima). In this context, it was not surprising that the optimal performance in calibration, and particularly in validation, was achieved by the most parsimonious parameterization, considering three HRUs.

## 4.8 Investigation of model results for CN-based parameterization

Table 17 shows the optimal values of the seven parameters assigned to the three corresponding HRUs, derived through the second calibration experiment. A low CN indicates areas with significant permeability, dense vegetation and very low drainage capacity, which do not favor the generation of overland flow. On the other hand, a high CN indicates areas with low water permeability, sparse vegetation and a high drainage capacity, producing significant runoff. Therefore, it is not surprising that the maximum infiltration ratio, which is associated with soil permeability, is higher for the HRUs with low CNs. On the other hand, soil capacity seems to be addressed by terrain slope characteristics, as plain areas of the basin have much larger capacities than the mountainous ones. Recession rates for percolation and the percentage of infiltration to the lower zone are also associated with permeability; thus, the infiltration rates through the high-permeability soils are significant. The good correspondence of the CN values with the physical characteristics of the HRUs allow the user to define a priori suitable parameter bounds and therefore facilitate the calibration procedure, while ensuring physically-consistent parameters.

Table 18 summarizes the annually-averaged water balance of the basin for the entire simulation period, ending in April 2014. A significant part of precipitation is lost to underground runoff (23.2%), while mean evapotranspiration losses are 34.3%. These values differ by 10–20% at the end of a hydrologic year (mid-autumn), with increased values of actual evapotranspiration and decreased values of underground losses.

Percolation reaches 35.9% of precipitation, whereas surface runoff is 22.8%. The mean annual runoff coefficient is estimated to be around 33.0%.

**Table 17:** Nedontas river basin calibrated HRU parameters of the simulation with the CN-based HRU delineation.

| HRU | CN 37-58 | CN 61-67 | CN 70-91 |
|---|---|---|---|
| Total Area ($km^2$) | 40.2 | 54.8 | 22.9 |
| Max. infiltration ratio (mm/h) | 80.0 | 61.3 | 39.4 |
| Interception capacity (mm) | 50.0 | 39.4 | 5.0 |
| Soil capacity up to spill (mm) | 393.5 | 377.0 | 50.0 |
| Perc. of infiltration to the lower zone (%) | 78.8 | 54.083 | 5.292 |
| Soil capacity up to interflow (mm) | 500.0 | 428.4 | 110.6 |
| Recession rate for interflow (%) | 0.426 | 0.231 | 2.571 |
| Recession rate for percolation (%) | 0.187 | 0.116 | 0.055 |

**Table 18:** Nedontas river basin simulated water balance of the simulation with the CN-based HRU delineation.

| Variable | Mean annual value (mm) | Mean annual value ($hm^3$) |
|---|---|---|
| Precipitation | 1690.3 | 200.1 |
| Evapotranspiration | 623.0 | 73.8 |
| Percolation | 607.1 | 71.9 |
| Surface runoff | 385.5 | 45.6 |
| Spring runoff | 249.6 | 29.6 |
| Underground losses | 343.7 | 49.9 |
| Soil storage change | 183.6 | 21.7 |
| Groundwater storage change | 29.3 | 3.5 |
| Outlet runoff | 557.2 | 66.0 |

| Overall Balance | |
|---|---|
| Output variable | Percentage of precipitation (%) |
| Evapotranspiration | 34.3 |
| River outflow | 30.7 |
| Underground losses | 23.2 |
| Storage change | 11.7 |

# 5 Implementation and verification

## 5.1 Scope and Objectives

The objective of this section is to verify the CN approach for HRU delineation in two other river basins, Yialias and Kouris river basins, in Cyprus, two watersheds of different sizes that vary in terms of physiographic characteristics and meteorological stresses, ideal to evaluate the performance of the method in diverse environments.

***Verification Test 1: CN Classification Methods Analysis***

Different classification schemes will be implemented in creating the CN sub-sets to delineate the final HRUs in an attempt to emphasize the advantage of the association of each HRU response to the corresponding parameter values in terms of CN, thus, allowing for a more efficient and objective model set up, assuring the user of the parameters physical meaning and realistic representation of the hydrological behaviour of the basin.

***Verification Test 2: CN Equation Sensitivity Analysis***

The sensitivity of the CN equation will be examined, by varying the coefficients of the three indices, $i_{PERM}$, $i_{VEG}$, and $i_{SLOPE,}$ forming the equation, to provide further insight as to what impact each index has on the HRU delineation processes, and thus, model performance.

The verification experiments, like the calibration experiments, were performed in the HYDROGEIOS modelling framework, previously described in Section 4.2.

## 5.2 Study area and data

The island of Cyprus is located in the southeastern part of the Mediterranean Sea (33°E, 35°N) and, with an area of 9251 $km^2$, it is the third largest island in the Mediterranean Sea. The topography of the island is dominated by two mountain ranges: the Troodos range located in the central part of the island reaching an altitude of 1952 m, and the Pentadaktylos range located in the north of the island reaching an altitude of 1085 m. In between the two ranges lie the Morphou and Messaoria plains, while coastal areas and

river valleys have fertile lands created from the deposition of sediments of rivers, all of which are intermittent streams with limited flow, gushing during winter time.

The study areas are the Yialias and Kouris river basins. The Yialias river basin is the second largest basin in Cyprus; it is located on the central-eastern part of the island and drains into the Gulf of Famagusta (Fig 23a). The Yialias river is the second longest? river with a total length of 88 km, originating in the northeastern slopes of Troodos, at the Macheras mountains. The river flows north of Ayia Varvara village and continues between Nisou and Pera Chorio villages, at which point all the river water infiltrates in very large natural galleries, enriching the aquifers underneath for many kilometers. The river then reappears and passes through Dali village, continues west of Potamia village, and runs through the valley of Mesaoria and towards the Famagusta Gulf. The study area is the part of the basin upstream of the monitoring station "Potamia" and has a drainage area of 112.6 km$^2$, with an average elevation of 422 m; the elevation ranges from a maximum of 1409 m down to 197 m. Terrain slope ranges from almost flat on the lowland and riverside areas to 43° on the steep mountain slopes, with the mean slope calculated at 7°.

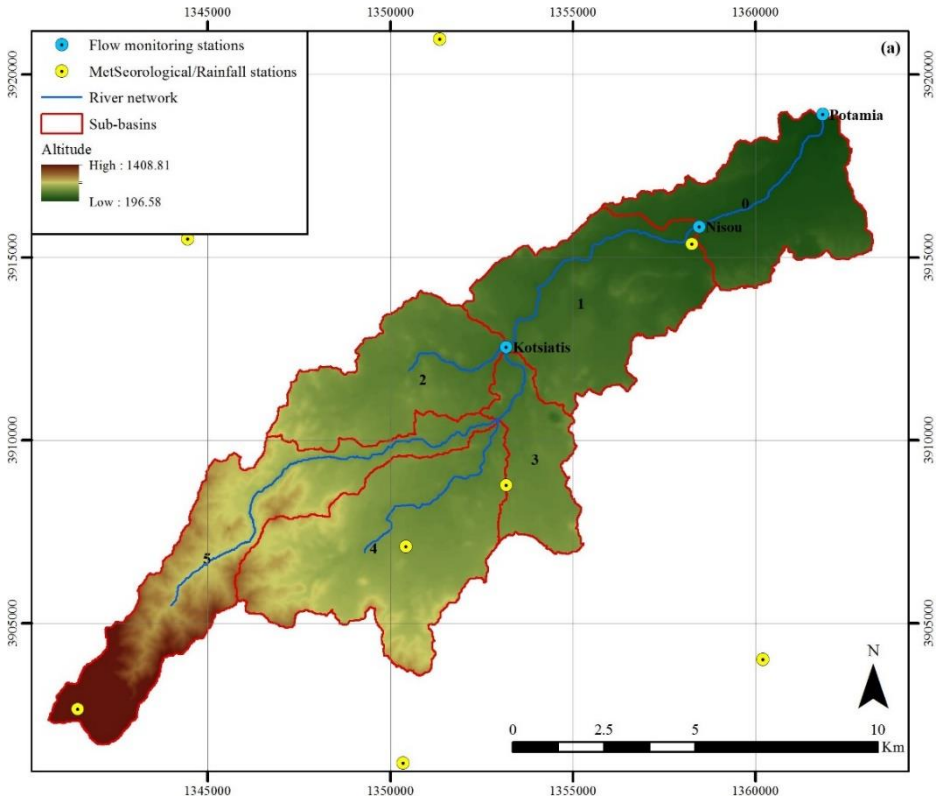

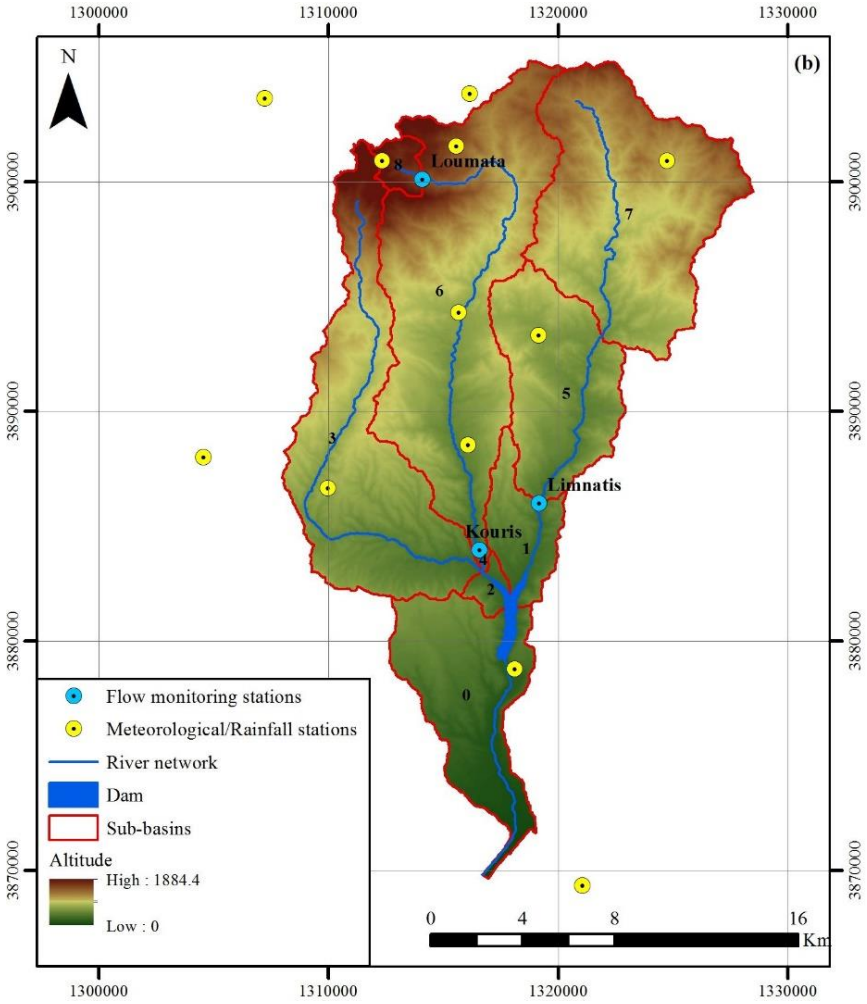


**Figure 23:** Digital map of (a) Yialias river basin and (b) Kouris river basin, also showing monitoring stations (meteorological and hydrometric) and main modelling components (sub-basins, reaches).

The Kouris river basin is located on the southern side of the Troodos mountain range and drains into the Gulf of Episkopi (Fig 23b). The basin has a drainage area of 338 $km^2$, with an average elevation of 750 m, reaching a maximum elevation of 1884 m dropping to 0 m the outlet of the basin. The terrain slope ranges from almost 0° on the lowland and riverside areas to 48° on the steep mountain slopes, with the mean slope calculated at 15°. The Kouris catchment is drained by three rivers, Kouris (38 km), which is the main river of the catchment with an average yearly runoff of 36 $Mm^3$ over the last 30 years, Kryos (20.3 km) and Limnatis (26.3 km). The rivers originate in the southern slopes of Troodos and flow into the Kouris Reservoir (dam was built in 1989), with 115 $km^3$ capacity and 110 m height, covering an area of 3.6 $km^2$. The rivers'

response to rainfall is quite fast with the maximum surface runoff appearing downstream the Kouris catchment after only several hours.

Cyprus has a Mediterranean climate influenced by orography, with hot dry summers from May to September and mild wet winters from November to March. The air temperature is greatly affected by the relief of the island that causes the temperature to drop by 5$^{o}$C per 1000 m of altitude increase, while marine influences result in cooler summers and warmer winters near coastal areas. The mean annual temperature ranges from 14$^{o}$C to 18$^{o}$C, with July and August being the hottest months (29$^{o}$C in flat areas and 22$^{o}$C in the mountains) and January the coldest (10$^{o}$C in flat areas and 3$^{o}$C in the mountains). The mean annual precipitation varies from 450 mm at the southwestern windward slopes of Troodos range to 1100 mm on the mountain top. On the leeward slopes precipitation decreases northwards and eastwards to 300-350 mm in the central plain and the flat southeastern areas of the island.

Daily precipitation and PET time-series were provided from the Cyprus Department of Meteorology and daily discharge time-series from the Cyprus Water Development Department. Data from ten meteorological/rainfall stations and three flow-gauging stations, Kotsiatis, Nisou and Potamia monitoring stations, were used for the Yialias study area, while data from twelve meteorological/rainfall stations and three flow-gauging stations, Loumata, Limnatis and Kouris monitoring stations, were used for the Kouris study.

For the preparation of input geographical layers, a 30-m resolution SRTM-DEM (USGS 2014) was used to delineate the river network and associated sub-basins and to calculate their geometrical properties of the two study areas, as well as maps of classified geological formations and land cover. The geographical layers were used to formulate the CN map and define the HRUs.

## 5.3 Model set up

Yialias river basin was divided into six sub-basins, while Kouris river basin was divided into nine sub-basins while. In both cases, additional nodes were set at the three flow-measuring station sites, as illustrated in Figure 23a. The main properties of the sub-basins are summarized in Tables 19 and 20 for Yialias and Kouris river basin, respectively

**Table 19:** Yialias sub-basin properties.

| Sub-basin | Name | Area ($km^2$) | Mean elevation (m) | Stream length (m) | Mean slope (°) | Mean slope (%) |
|---|---|---|---|---|---|---|
| 0 | Sub-basin 0 | 17.06 | 240.8 | 5247.4 | 2.87 | 5.04 |
| 1 | Sub-basin 1 | 21.48 | 296.8 | 7970.9 | 4.06 | 7.15 |
| 2 | Sub-basin 2 | 15.52 | 385.8 | 3568.3 | 5.03 | 8.88 |
| 3 | Sub-basin 3 | 8.68 | 370.2 | 2670.3 | 3.92 | 6.94 |
| 4 | Sub-basin 4 | 26.42 | 465.2 | 6408.4 | 7.43 | 13.31 |
| 5 | Sub-basin 5 | 23.46 | 664.8 | 12731.6 | 15.26 | 28.08 |

**Table 20:** Kouris sub-basin properties.

| Sub-basin | Name | Area ($km^2$) | Mean elevation (m) | Stream length (m) | Mean slope (°) | Mean slope (%) |
|---|---|---|---|---|---|---|
| 0 | Sub-basin 0 | 40.12 | 267.6 | 13428.1 | 8.93 | 16.19 |
| 1 | Sub-basin 1 | 14.47 | 400.6 | 5155.9 | 14.20 | 25.82 |
| 2 | Sub-basin 2 | 3.21 | 310.6 | 2203.9 | 15.63 | 28.72 |
| 3 | Sub-basin 3 | 69.54 | 732.5 | 25783.8 | 15.14 | 27.63 |
| 4 | Sub-basin 4 | 0.49 | 291.1 | 951.8 | 15.00 | 27.34 |
| 5 | Sub-basin 5 | 39.73 | 576.8 | 8964.4 | 14.57 | 26.56 |
| 6 | Sub-basin 6 | 94.69 | 897.8 | 24339.5 | 16.37 | 30.05 |
| 7 | Sub-basin 7 | 75.10 | 970.2 | 13261.8 | 18.10 | 33.28 |
| 8 | Sub-basin 8 | 4.28 | 1608.4 | 1436.0 | 16.20 | 29.59 |

Spatially-averaged hydrological inputs, i.e. daily precipitation and PET time series, were extracted at the sub-basin scale, using the Thiessen polygon method as shown in Figures 24 and 25 for Yialias and Kouris river basin, respectively. Instead of Thiessen polygon, a GIS interpolation would have been a more appropriate method for the extraction of the spatially-averaged hydrological, such as the Inverse Distance Weighted (IDW) tool, Natural Neighbor, or Kriging.

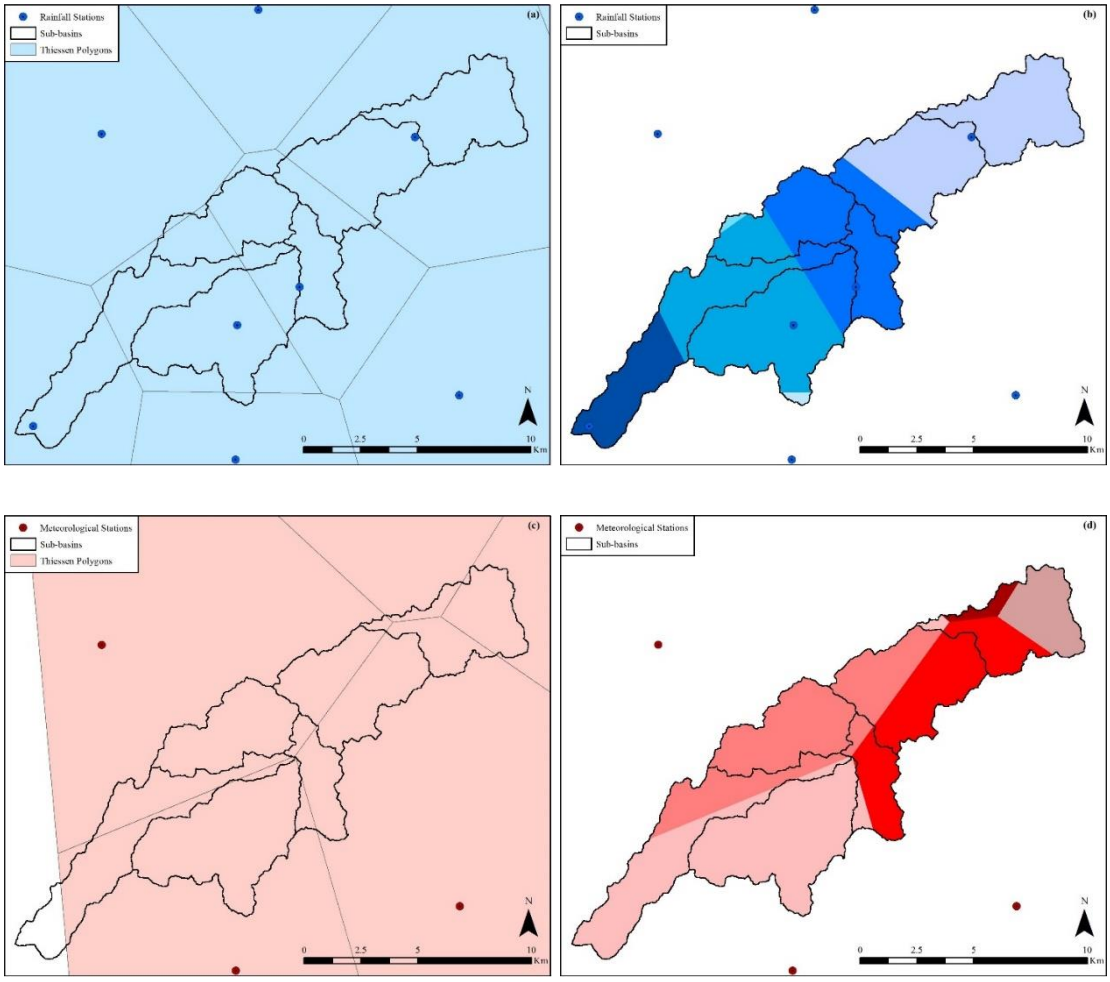


**Figure 24:** Yialias river basin (a) Thiessen polygons for daily rainfall, (b) spatially-averaged rainfall per sub-basin, (c) Thiessen polygons for daily evapotranspiration, (b) spatially-averaged evapotranspiration per sub-basin.

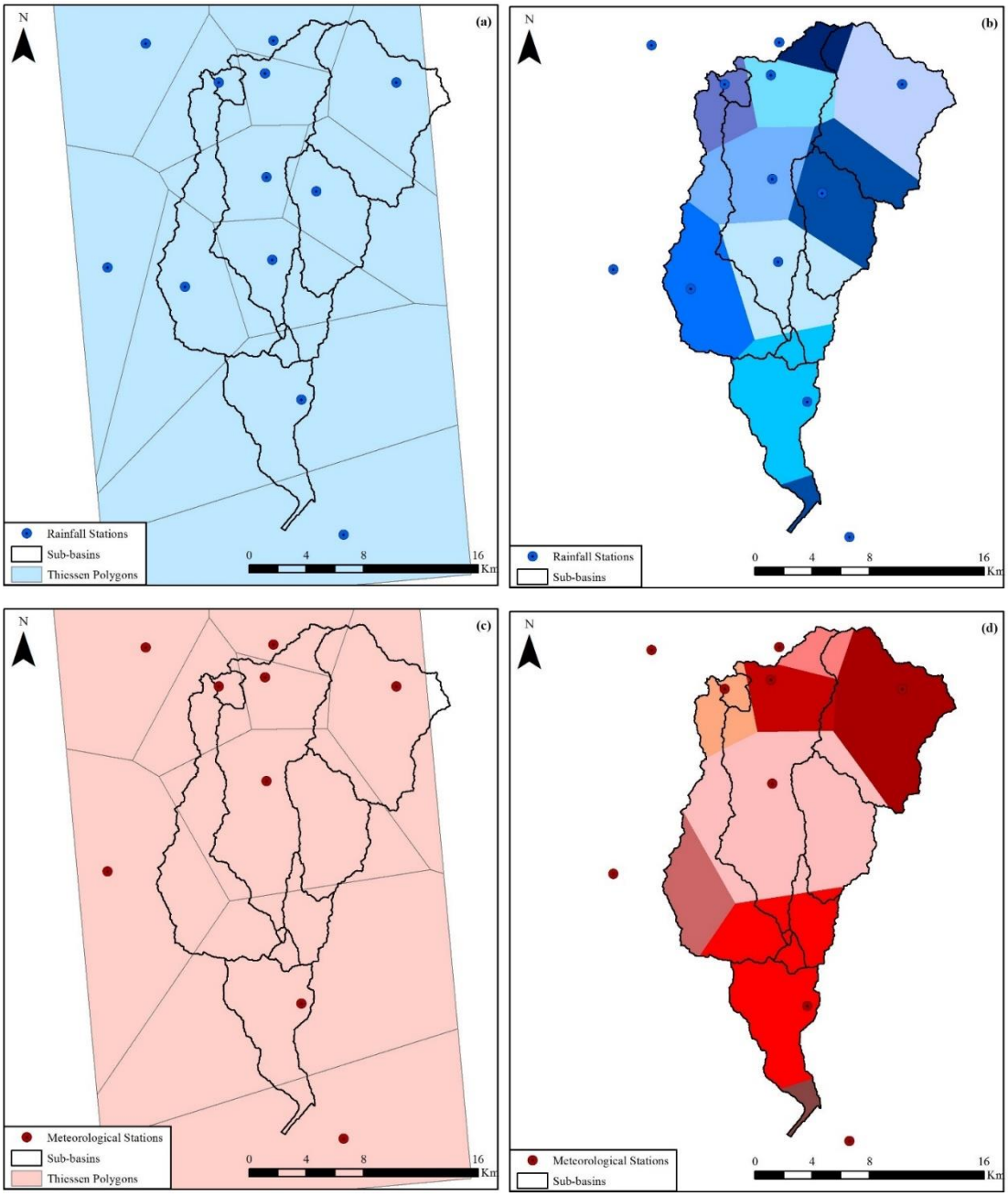


**Figure 25:** Kouris river basin (a) Thiessen polygons for daily rainfall, (b) spatially-averaged rainfall per sub-basin, (c) Thiessen polygons for daily evapotranspiration, (b) spatially-averaged evapotranspiration per sub-basin.

In all experiments, precipitation and evapotranspiration input series, initial conditions and settings were kept the same. The simulations were performed on a daily time step for a 12-year time period for Yialias river basin (October 1998 – September 2010), and for a 25-year time period for Kouris river basin. For the Yialias river basin the control period was split up in a 6-year calibration period (October 1998 – September 2004) and a 6-year validation period (October 2004 – September 2010), with a complete discharge observation time-series for all three monitoring stations, Kotsiatis, Nisou and Potamia. For the Kouris river basin the control period was split up in a 12-year calibration period (October 1985 – September 1997) and a 13-year validation period (October 1997 – September 2010), however, the discharge observation time-series of the three monitoring stations were not available for the entire control period. In particular, discharge observation time-series from the Loumata monitoring station were available for an 11-year period, from October 1990 to September 2001; from the Limnatis monitoring station were available for the entire 25-year control period, from October 1985 to September 2010; and from the Kouris monitoring station were available only for a 3-year period, from October 2007 to September 2010, which were only used for validation purposes. With the simulations commencing in the beginning of October, i.e. before the beginning of the wet season, negligible initial soil moisture was assumed in the upper and lower soil moisture tanks.

The model parameters for daily simulations were assigned as follows: (a) seven parameters for the rainfall-runoff component of each HRU; (b) one recession parameter for each sub-basin; and (c) one leakage coefficient assigned to the downstream river segments accumulating the runoff losses due to infiltration, while a zero value was set for the rest of the segments. With the number of HRUs remaining constant, although the delineation was based on a different classification method each time, the three simulation modes set up in HYDROGEIOS, the same number of model parameters was assigned: 21 ($3 \times 7$) HRU parameters, 6 (6 x 1) sub-basin parameters, and 6 (6 x 1) river segment parameters were assigned (33 in total) for the Yialias river basin, and 21 ($3 \times 7$) HRU parameters, 9 (9 x 1) sub-basin parameters, and 9 (9 x 1) river segment parameters were assigned (39 in total) for the Kouris river basin.

For each simulation mode of the Yialias river basin, the unknown model parameters were calibrated against the daily time series of observed discharge of the Kotsiatis,

Nisou and Potamia monitoring stations, and for each simulation mode of the Kouris river basin, the unknown model parameters were calibrated against the daily time series of observed discharge of the Loumata, Limnatis and Kouris monitoring stations. For the calibration of the Yialias model parameters the coefficient of efficiency or Nash-Sutcliffe index (Nash & Sutcliffe 1970) was used, as well as a variation of it, calculated only for the observed and simulated flow values that are above the mean value of the observed time series, in order to preserve the high flows of the hydrograph, while for the calibration of the Kouris model parameters the coefficient of efficiency or Nash-Sutcliffe index was used along with the bias of the mean. As mentioned in Section 4.4, according to common hydrological practices (Freer et al. 1996a; Moriasi et al. 2007)], efficiency values greater than 50% indicate a rainfall-runoff model of satisfactory predictive capacity, while a value of 30% indicates a marginally acceptable model (Freer et al. 1996a). For the following verification experiment, efficiency values above 55–60% are considered "satisfactory", while efficiency values lower than 30% were characterized as "unsatisfactory".

Parameter optimization was carried out by employing a hybrid strategy, combining human experience and automatic tools (Boyle et al. 2000; Rozos et al. 2004; Mazi et al. 2004a; Mazi et al. 2004b), aiming at a realistic set of parameters that would ensure satisfactory predictive capacity for all model responses. A similar strategy was used for all three models, through progressive improvements of a relatively small group of parameters. A 'rough' calibration was initially employed that allowed large parameter variations; several optimization runs were carried out by modifying the bounds of the feasible parameter search space, while trying different combinations of criteria weights. The calibration was then focused on the optimization of the HRU parameters in order to attain a good fit of the hydrograph at the monitoring stations.

## 5.4 Preparation of the CN Maps

For the delineation of HRUs, distributed geographical data were used, by means of classified geological formations and land cover maps, as well as the raster map of terrain slopes. For Yialias river basin these are illustrated in Figures 26a, 26b and 26c, respectively, and for Kouris river basin in Figures 27a, 27b and 27c, respectively. Specifically:

Geological formations and information on the tectonic and lithological elements of the two river basins were extracted from geological maps, published by the Cyprus Geological Survey Department (Table 21). Both basins are divided into two geological Terranes: the Troodos Terrane or the Troodos Ophiolite complex characterized by very low to moderate permeability, and the Circum Troodos Sedimentary Succession characterized by high and very high permeability.

As shown in Figures 26a and 27a, the Troodos Ophiolite complex dominates the central part of the island (southwestern half of Yialias basin and northern half of Kouris basin) having a characteristic domal structure. It constitutes the geological core of the island, consisting of the following stratigraphic units (in ascending order): Plutonics (mantle sequence and cumulates), Intrusives, Volcanics and Chemical sediments (Perapedhi Formation). The mantle sequence is composed mainly of harzburgite and serpentinite, derived from the residuals after the partial melting of the upper mantle, and are completely impermeable, while the cumulate rocks are produced from the crystallization and crystal concentration at the floor of magma chambers, and include dunite, wehrlite, pyroxenite that have low permeability, as well as gabbro and plagiogranites characterized with moderate permeability. The intrusive rocks are composed by sheeted dykes (diabase) of moderate permeability, formed by the magma solidification in the channels, followed by a suite of volcanic rocks consisting of two series of pillow lavas (lower and upper) of basaltic composition characterized by low permeability. Between these two rock sequences occurs a transitional zone, the basalt group dominated by dykes while lava pillows are less. Finally, the impermeable Perapedhi formation, composed of the chemical sediment umber, as well as radiolarites and radiolaritic shales, the first sediment deposits over the ophiolite rocks, resulted from hydrothermal activity and sea floor sedimentation.

The Circum Troodos Sedimentary Succession is a zone of autochthonous sedimentary rocks, that ranges in age from the Upper Cretaceous to the Pleistocene (79 Ma to recent), and covers the valley of Mesaoria (northeastern half of Yialias basin) as well as the southern part of the island (southern half of Kouris basin) (Figs. 26a and 27a), consisting of the Kannaviou, Moni, Kathikas, Lefkara, Pakhna, Kalavasos, Nicosia, Apalos-Athalassa-Kakkaristra, Fanglomerate, Terrace, and Alluvium-Colluvium Formations. The Lefkara Formation is composed of carbonate sediments consisting of

pelagic marls and karstic chalks with characteristic white colour, with or without cherts, followed by the Pakhna Formation consisting mainly of yellowish marls as well as porous calcarenite layers and conglomerates. Both formations are characterized by high permeability. Following the isolation of the Mediterranean Sea from the Atlantic Oceans and the evaporation of Mediterranean Sea water was the evaporates deposition of the Kalavasos Formation composed of karstic gypsum and gypsiferous marks, while with their re-connection the high permeable Nicosia Formation was deposited first containing grey and yellow siltstones and calcarenite layers, marls and sandy marls, followed by the Apalos-Athalassa-Kakkaristra and the Fanglomerate Formations that included clastic deposits such as gravels, sand and silt, both characterized by very high permeability. Similarly, the Alluvium-Colluvium Formation developed in brad valleys and river deltas, consisting of sands, silts, clay and gravel.

**Table 21:** Geological formations corresponding permeability classification

| Lithology | Formation | Epoch/Sequence | Period | iPERM |
|---|---|---|---|---|
| *Circum Troodos Sedimentary Succession* | | | | |
| Sands, silts, clays and gravels | Alluvium-Colluvium | Holocene | Quaternary | 5 |
| Gravels, sands and silts | Fanglomerate | Pleistocene | | 5 |
| Biocalcarenites, sandstones, sandy marls and conglomerates | Apalos-Athalassa-Kakkaristra | Pleistocene | | 5 |
| Biocalcarenites, sandstones, silts, gravels, sandy marls, marls, limestones and conglomerates | Nicosia | Pliocene | Neogene | 4 |
| Chalks, marls, marly chalks, chalky malrs and calcarenites | Pahkna | Middle Micocene | | 4 |
| Chalks, marls, marly chalks, chalky marls with cherts in places as bands or modules | Lefkara | Oligocene/ Eocene/ Palaeogene | Paleogene | 4 |

*Troodos Ophiolite*

| | | | | | |
|---|---|---|---|---|---|
| Hydrothermal and deep-water sediments: umbers, manganoan shales, pink radiolarian shales and mudstones | Perapedhi | | Campanian | | 1 |
| Olivine- and pyroxene-phyric, pillow lavas with occasional sheet flows, dykes and hyaloclastites, commonly altered to zeolite facies | Upper Pillow Lavas | Volcanic Sequence | | | 2 |
| Pillowed and sheet lava flows with abundant dykes and silts, altered to zeolite facies and in places stained with green celadonite | Lower Pillow Lavas | | | | 2 |
| Diabase dykes (>50%) with pillow lava screens, altered to greenschist facies | Basal Group | | | | 3 |
| Diabase dykes up to 3m wide, aphyric and clinopyroxene- and plagioclase-phyric altered to greenschist facies | Sheeted Dykes (Diabase) | Intrusive Sequence | Upper Cenomanian - Lower Campanian | Upper Cretaceous | 3 |
| Trondhjemites, granophyres, diorites, quartz-diorites and micro-granodiorites | Plagiogranite | Plutonic Sequence | | | 3 |
| Isotropic grabbros, uralite grabbros, olivine gabbros and layered melagabbros | Gabbro | | | | 3 |
| Websterites, clinopyroxenites, orthopyroxenites and plagioclase-bearing pyroxenites | Pyroxenite | | | | 2 |
| Wehrlites and plagioclase-bearing wehrlites, massive or layered | Wehrilite | | | | 2 |
| Dunites with subordinate clinopyroxene-dunites | Dunite | | | | 2 |
| Tectonized harzburgites with minor dunites and lherzolites | Harzburgite | Mantle Sequence | | | 1 |
| Pervasively serpentinized, tectonized harzburgites with minor dunites and lherzolites | Serpentinite | | | | 1 |

Land cover classes were derived from the CORINE Land Cover 2006 map (CLC2006), produced by the European Environmental Agency (Table 22). For Yialias river basin (Fig. 26b) land cover classes mainly include coniferous forest (26%), non-irrigated arable land (19%), sclerophyllous vegetation (13%), complex cultivation patterns (10%), olive groves (10%), discontinuous urban fabric (9%), permanently irrigated land (5%), transitional woodland-shrub (2%), annual crops associated with permanent crops (2%) and industrial or commercial units (1%). In general, vegetation favors interception and infiltration against overland flow, thus resulting to smoother flood hydrographs. For Kouris river basin (Fig. 27b) these mainly include coniferous forest (29%), sclerophyllous vegetation (20%), complex cultivation patterns (14%), land principally occupied by agriculture, with significant areas of natural vegetation (9%), vineyards (5%), annual crops associated with permanent crops (4%), discontinuous urban fabric (3%), transitional woodland-shrub (3%), non-irrigated arable land (2%), fruit trees and berry plantations (2%), natural grasslands (2%), olive groves (2%) and permanently irrigated land.

**Table 22:** CORINE land cover classes and corresponding vegetation density classification.

| Description | Category | Code | iVEG |
|---|---|---|---|
| Discontinuous urban fabric | Artificial surfaces | 112 | 5 |
| Industrial or commercial units | | 121 | 5 |
| Road and rail networks and associated land | | 122 | 5 |
| Mineral extraction sites | | 131 | 5 |
| Dump sites | | 132 | 5 |
| Sport and leisure facilities | | 142 | 5 |
| Non-irrigated arable land | Agricultural areas | 211 | 4 |
| Permanently irrigated land | | 212 | 3 |
| Vineyards | | 221 | 3 |
| Fruit trees and berry plantations | | 222 | 2 |
| Olive groves | | 223 | 2 |
| Annual crops associated with permanent crops | | 241 | 3 |
| Complex cultivation patterns | | 242 | 3 |
| Land principally occupied by agriculture | | 243 | 3 |
| Broad-leaved forest | Forest and semi-natural areas | 311 | 1 |
| Coniferous forest | | 312 | 1 |
| Natural grasslands | | 321 | 3 |
| Sclerophyllous vegetation | | 323 | 2 |
| Transitional woodland-shrub | | 324 | 2 |
| Beaches, dunes, sands | | 331 | 4 |
| Bare rocks | | 332 | 5 |
| Sparsely vegetated areas | | 333 | 3 |
| Burnt areas | | 334 | 5 |
| Water bodies | Water bodies | 512 | 4 |
| Sea and ocean | | 523 | 4 |

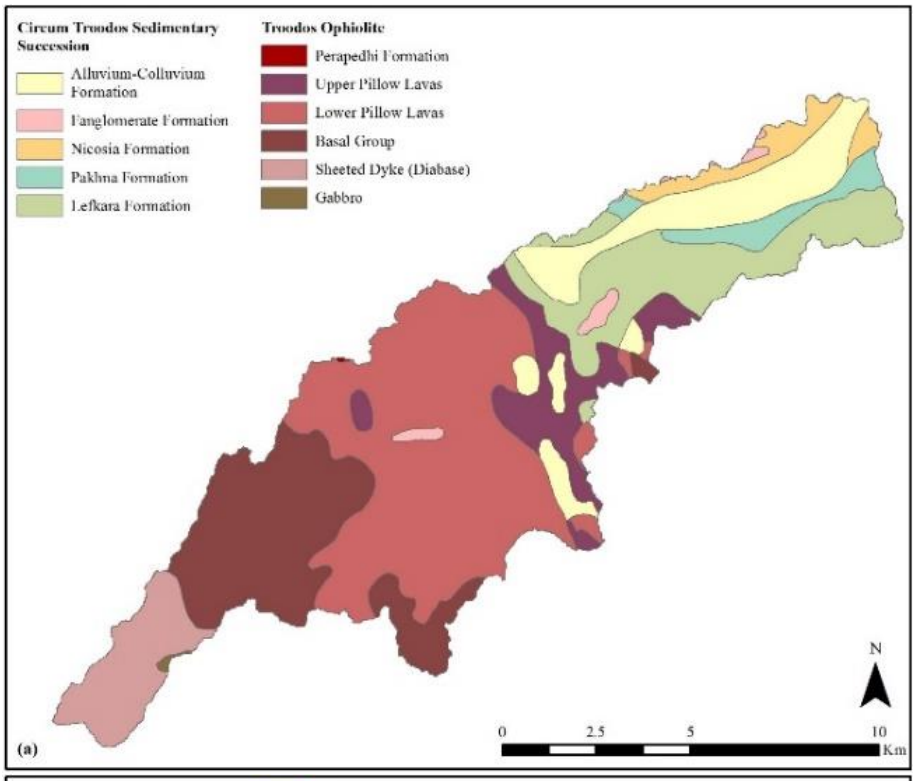
Circum Troodos Sedimentary Succession
Alluvium-Colluvium Formation
Conglomerate Formation
Nicosia Formation
Pakhna Formation
Lefkara Formation
Troodos Ophiolite
Perapedhi Formation
Upper Pillow Lavas
Lower Pillow Lavas
Basal Group
Sheeted Dyke (Diabase)
Gabbro
N
0
2.5
5
10
Km
(a)

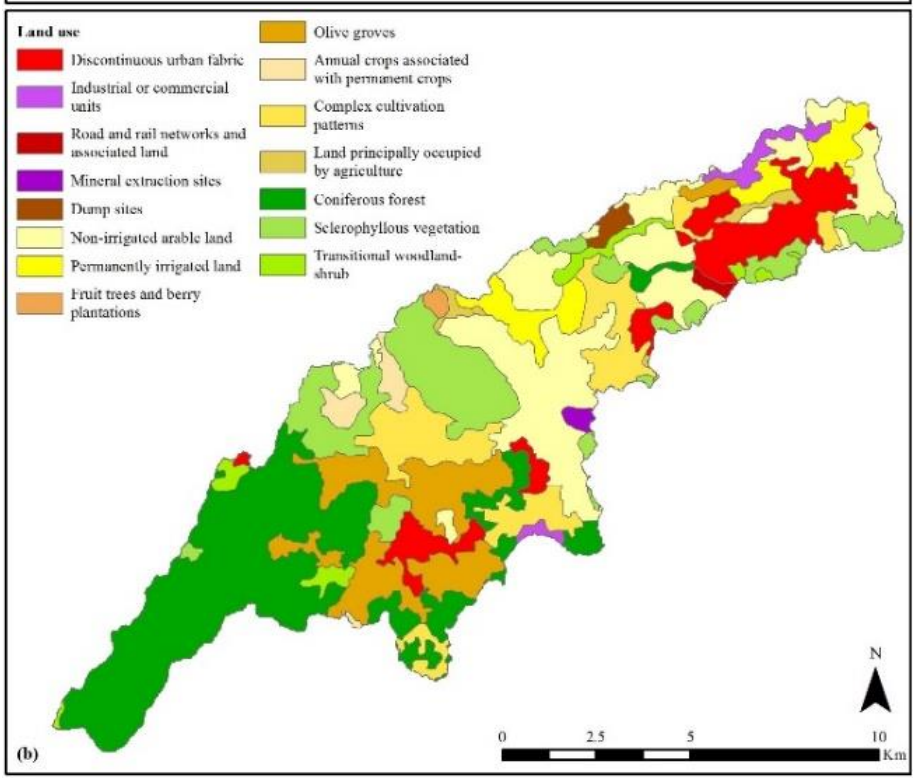
Land use
Discontinuous urban fabric
Industrial or commercial units
Road and rail networks and associated land
Mineral extraction sites
Dump sites
Non-irrigated arable land
Permanently irrigated land
Fruit trees and berry plantations
Olive groves
Annual crops associated with permanent crops
Complex cultivation patterns
Land principally occupied by agriculture
Coniferous forest
Sclerophyllous vegetation
Transitional woodland-shrub
N
0
2.5
5
10
Km
(b)

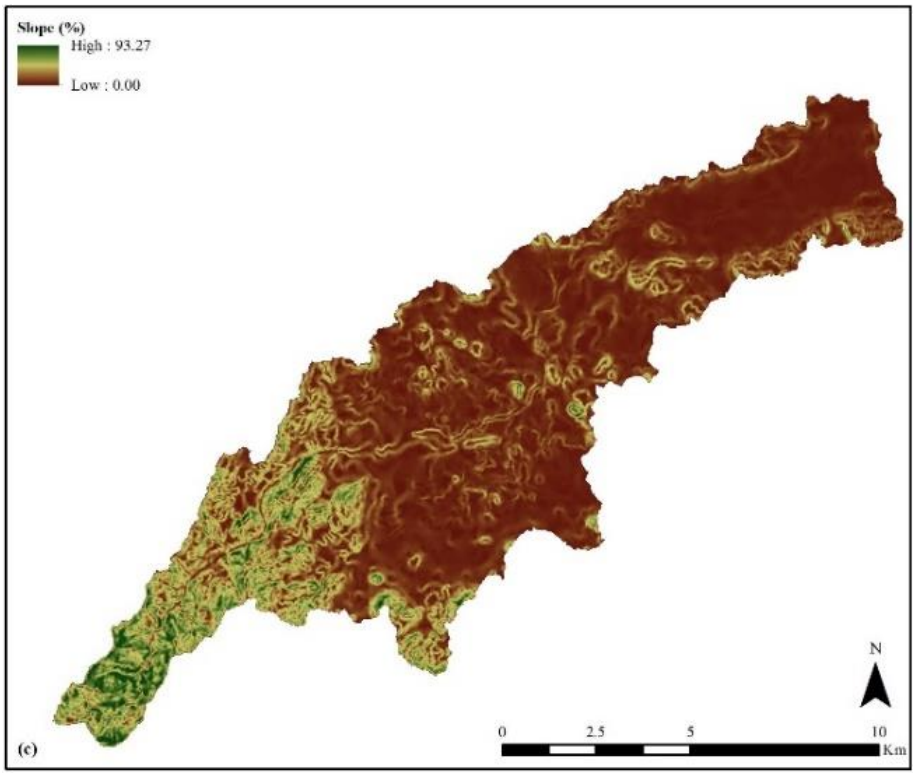


**Figure 26:** Yialias river basin (a) geological formations, (b) land cover classes, (c) terrain slope (%).

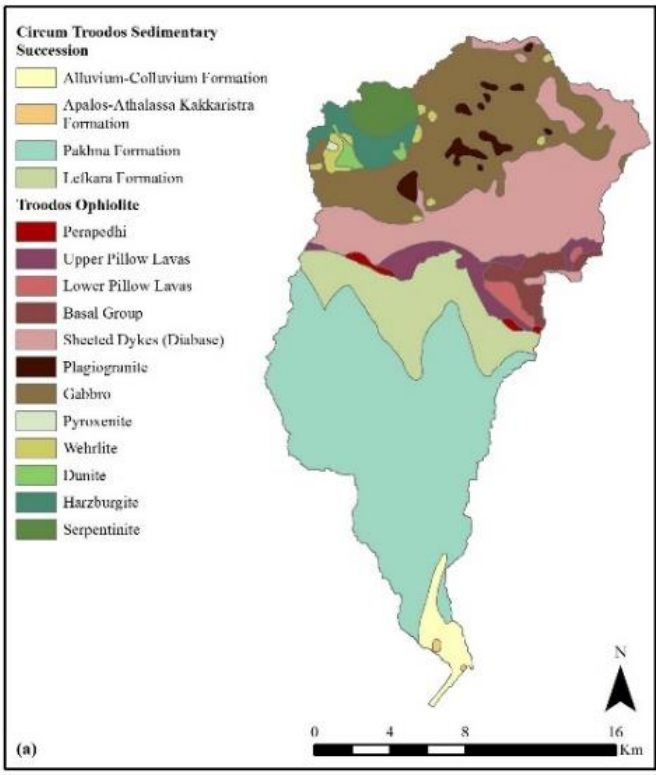
Circum Troodos Sedimentary Succession
Alluvium-Colluvium Formation
Apalos-Athalassa Kakkaristra Formation
Pakhna Formation
Lefkara Formation
Troodos Ophiolite
Perapedhi
Upper Pillow Lavas
Lower Pillow Lavas
Basal Group
Sheeted Dykes (Diabase)
Plagiogranite
Gabbro
Pyroxenite
Wehrlite
Dunite
Harzburgite
Serpentinite
N
0
4
8
16
Km
(a)

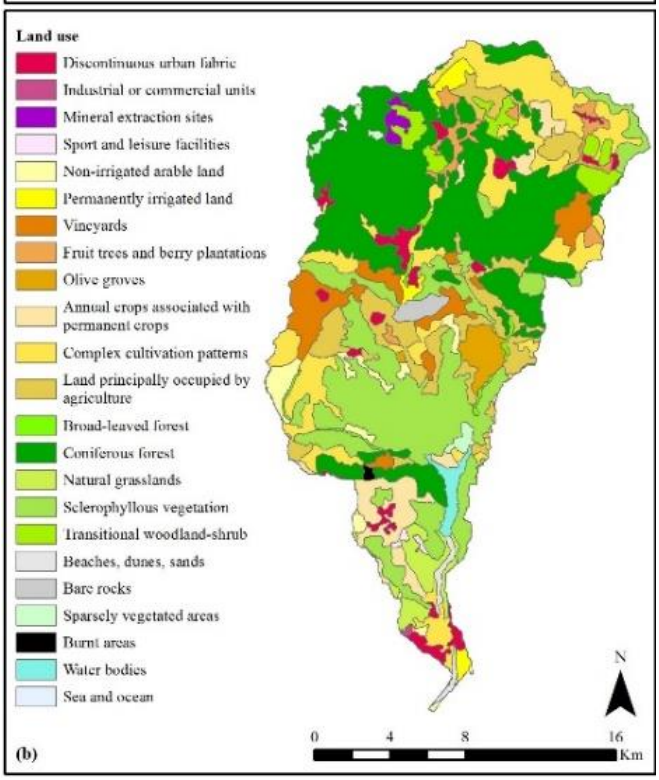
Land use
Discontinuous urban fabric
Industrial or commercial units
Mineral extraction sites
Sport and leisure facilities
Non-irrigated arable land
Permanently irrigated land
Vineyards
Fruit trees and berry plantations
Olive groves
Annual crops associated with permanent crops
Complex cultivation patterns
Land principally occupied by agriculture
Broad-leaved forest
Coniferous forest
Natural grasslands
Sclerophyllous vegetation
Transitional woodland-shrub
Beaches, dunes, sands
Bare rocks
Sparsely vegetated areas
Burnt areas
Water bodies
Sea and ocean
N
0
4
8
16
Km
(b)

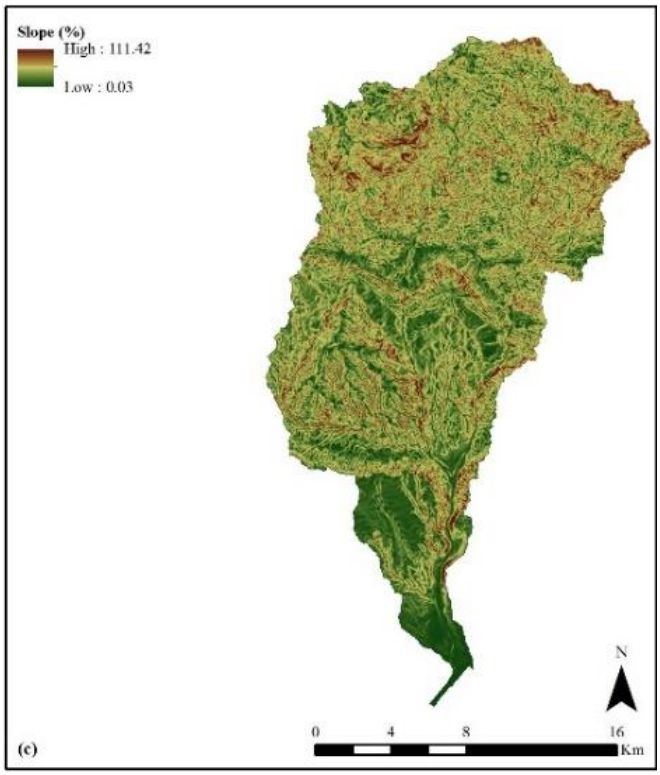


**Figure 27:** Kouris river basin (a) geological formations, (b) land cover classes, (c) terrain slope (%).

The raster layers of $i_{\mathrm{PERM}}$, $i_{\mathrm{VEG}}$ and $i_{\mathrm{SLOPE}}$ for Yialias and Kouris river basins can be seen in Figures 28a, 28b and 28c and Figures 29a. 29b and 29c for respectively. The values of the three indices were assigned based on the classifications provided by Tables 21 and 22 accounting for the dominant classes of soil permeability and vegetation density respectively, as well as the terrain slope map. The $i_{\mathrm{PERM}}$ classification for each geological formation and $i_{\mathrm{VEG}}$ classification for each land cover for the Yialias and Kouris river basins can be seen in the last column of tables 21 and 22 respectively.

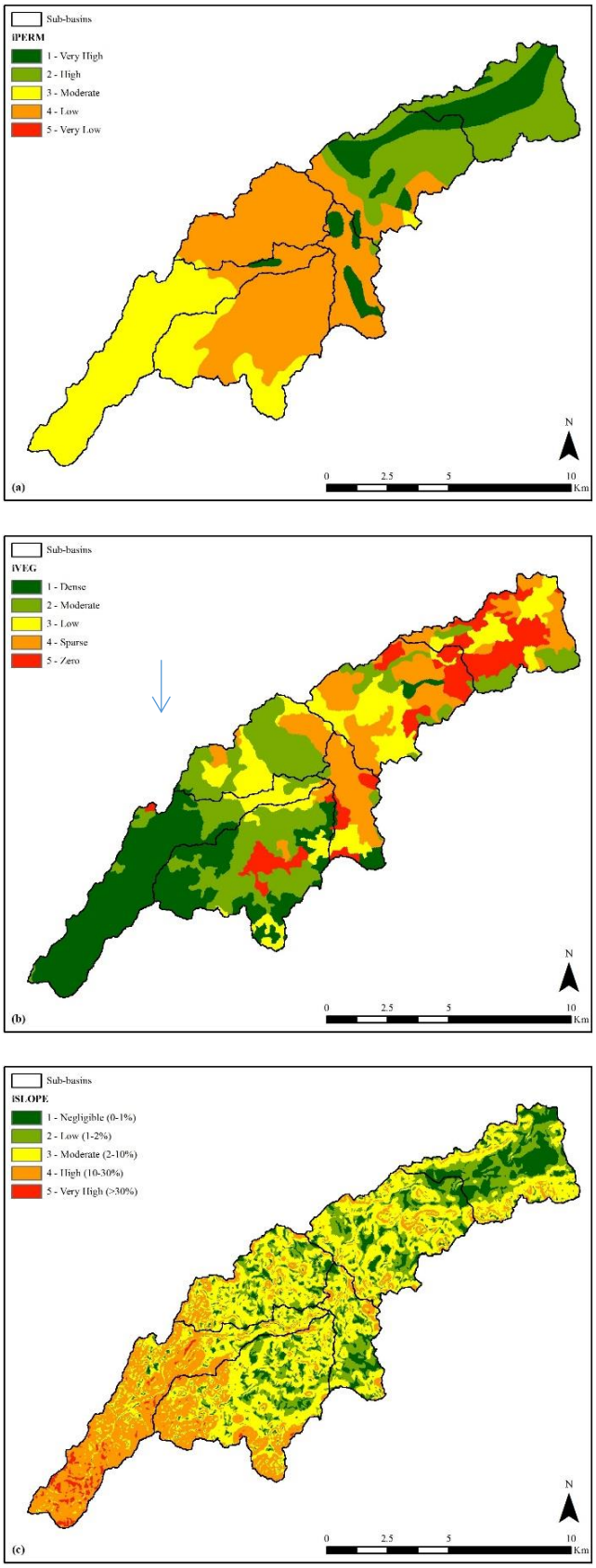


**Figure 28:** Yialias river basin (a) water permeability classes (iPERM), (b) vegetation density classes (iVEG), (c)drainage capacity classes (iSLOPE), (d) CN-parameter map.

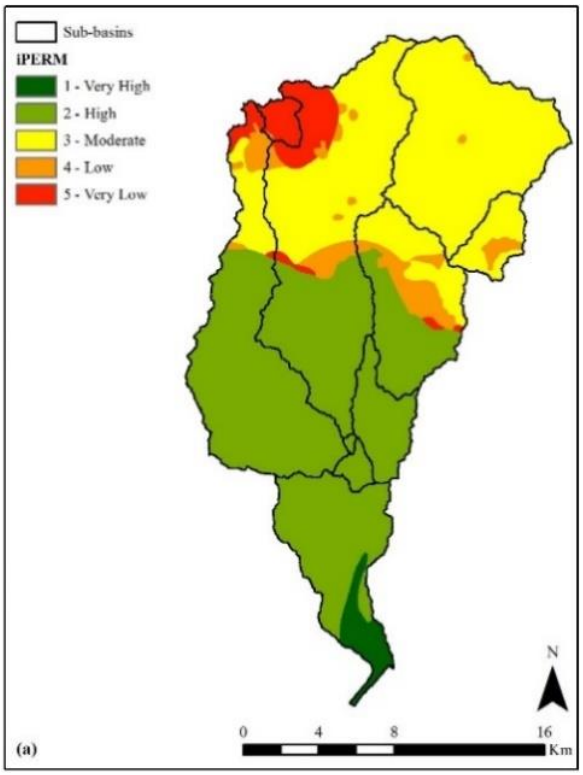
Sub-basins
iPERM
1 - Very High
2 - High
3 - Moderate
4 - Low
5 - Very Low
N
0
4
8
16
Km
(a)

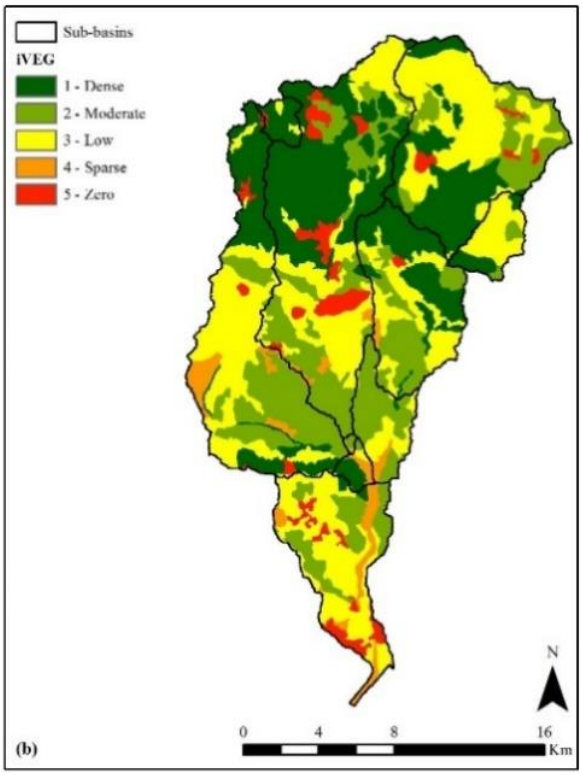
Sub-basins
iVEG
1 - Dense
2 - Moderate
3 - Low
4 - Sparse
5 - Zero
N
0
4
8
16
Km
(b)

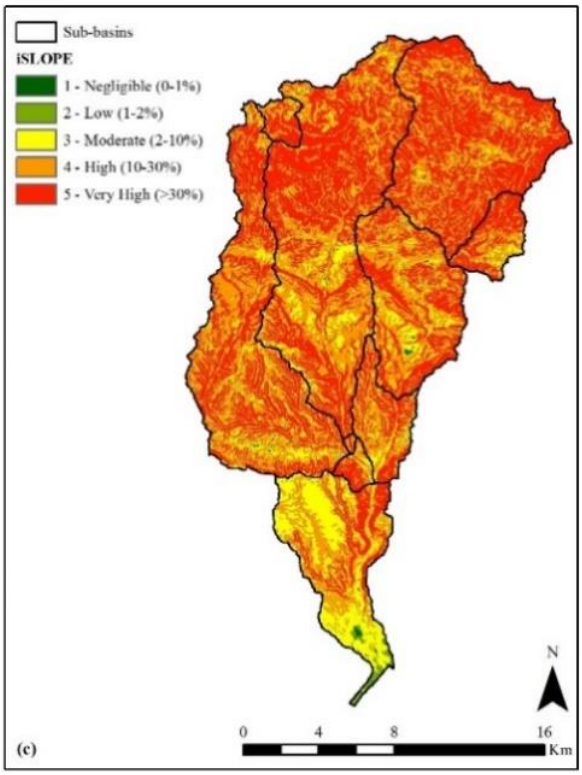


**Figure 29:** Kouris river basin (a) water permeability classes (iPERM), (b) vegetation density classes (iVEG), (c)drainage capacity classes (iSLOPE), (d) CN-parameter map.

## 5.5 Verification Experiment 1: CN Classification Methods Analysis

In this experiment, different classification schemes were implemented in creating the CN sub-sets to delineate the final HRUs in an attempt to emphasize the advantage of the association of each HRU response to the corresponding parameter values in terms of CN, thus, allowing for a more efficient and objective model set up, assuring the user of the parameters physical meaning and realistic representation of the hydrological behaviour of the basin. A schematic layout of the processes followed in the verification experiment 1 is showed in Figure 30.

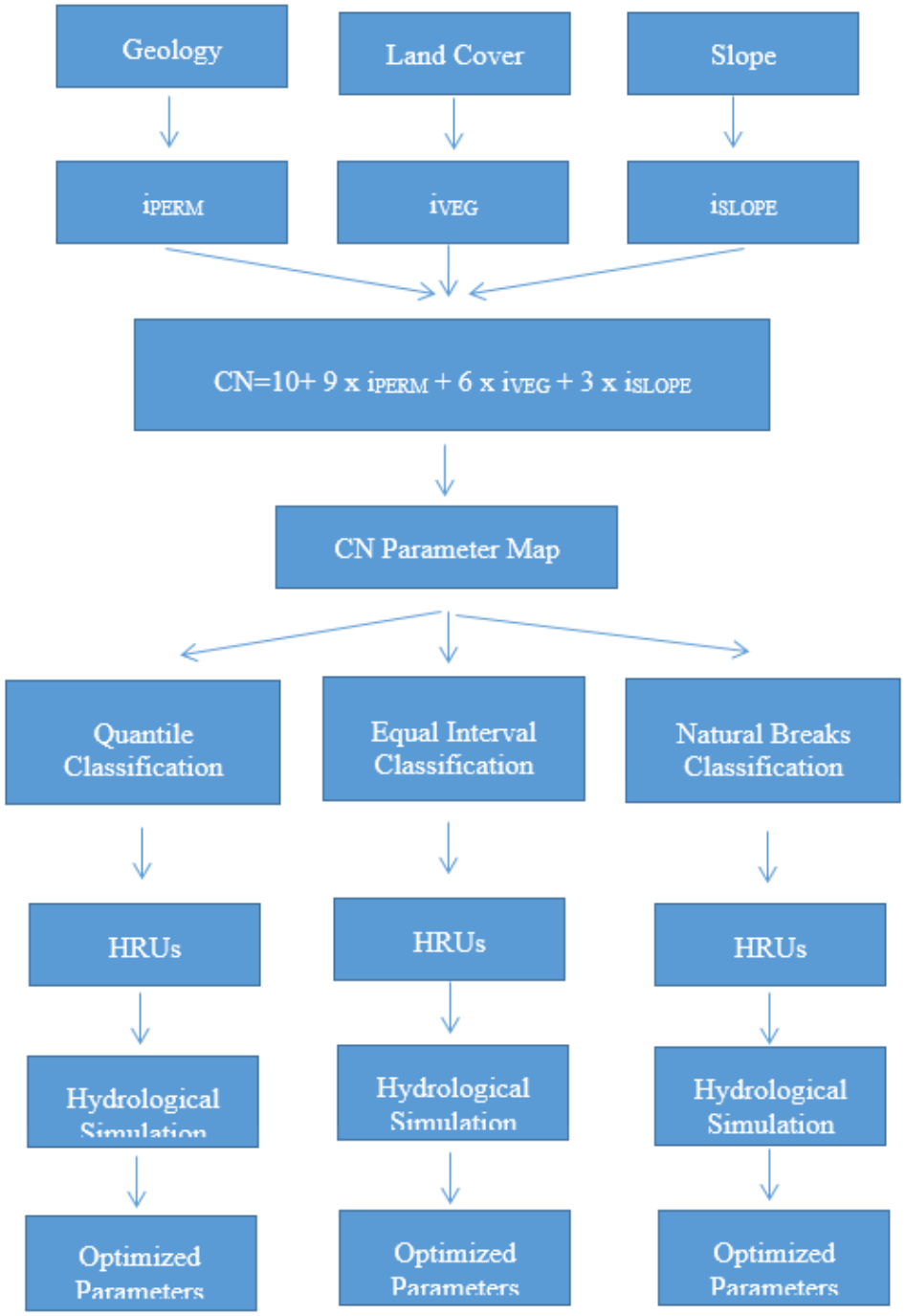


**Figure 30:** Schematic layout of the processes followed in the verification experiment 1

Based on the raster layers of $i_{\mathrm{PERM}}$, $i_{\mathrm{VEG}}$ and $i_{\mathrm{SLOPE}}$ for Yialias (Fig. 28) and Kouris (Fig. 29) river basins, CN parameter maps were produced: for Yialias basin it comprised 20 individual CN-classes (Fig. 31), ranging from CN = 34 to CN = 91, while for Kouris basin it comprised 22 individual CN-classes (Fig. 32), ranging from CN = 37 to CN = 100.

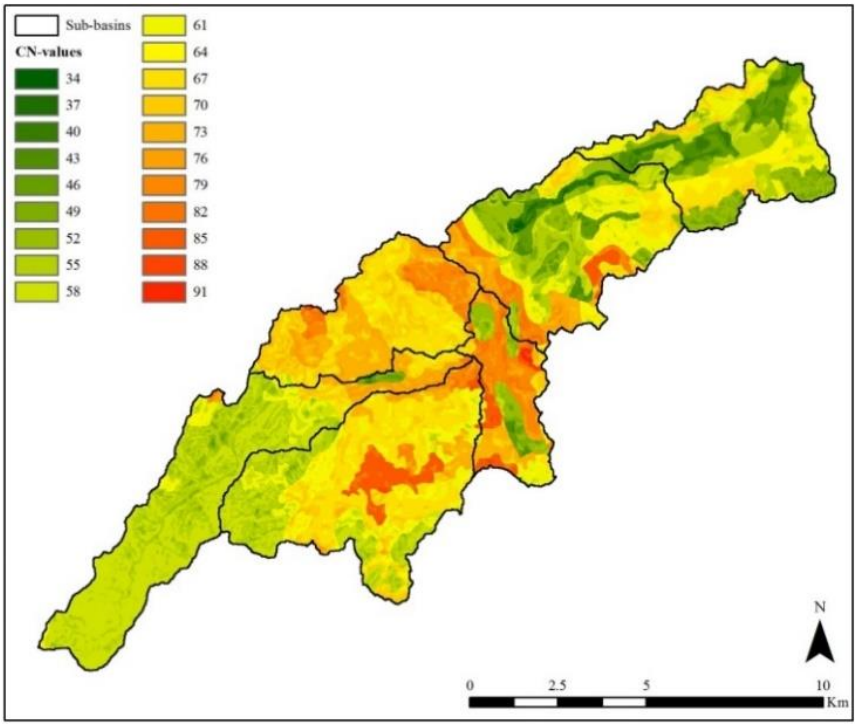


**Figure 31:** CN-parameter map of Yialias river basin

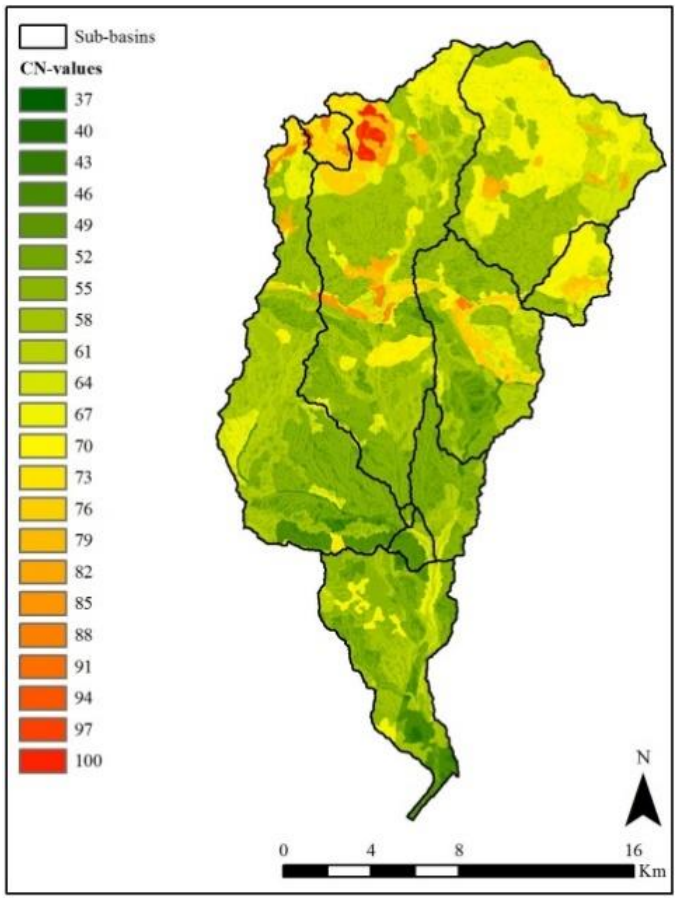


**Figure 32:** CN-parameter map of Kouris river basin

According to the recommended general principle, the number of HRUs delineated should be close to the number of discharge monitoring stations. Therefore, considering that hydrometric data are available from three discharge monitoring stations, both for Kouris and Yialias river basins, the CN-classes produced for each basin are aggregated in three sub-sets, based on which corresponding HRUs were formulated. In this section, three different data classification methods were applied and tested for the CN aggregation to delineate the HRUs; the quantile data classification, the equal intervals data classification, and the natural breaks, also referred to as “jenks”, data classification. The resulted HRUs for Yialias river basin based on the quantile, equal interval and natural breaks classification methods are illustrated in Figures 33a, 33b and 33c respectively, while the resulted HRUs for Kouris river basin methods are illustrated in Figures 34a, 34b and 34c respectively.

***Quantile classification***

In the quantile classification, each class contains equal, or approximately equal, number of features, depending on dataset:

$$\text{number of features per class} = \frac{\text{total number of features}}{\text{number of classes}}$$

Each class is therefore approximately equally represented in the final map. The three CN sub-set classes resulting from the quantile classification and used to delineate the three HRUs were CN 34-58, CN 61-67 and CN 70-91 for the Yialias river basin (Fig. 33a) and CN 37-55, CN 58-64 and CN 67-100 for the Kouris river basin (Fig. 34a)

***Equal interval classification***

In the equal interval classification, the entire range of data values (max-min) is divided in equal-sized sub-ranges, emphasizing the amount of data value relative to other values:

$$\frac{\text{range of data}}{\text{number of classes}} = \frac{(\text{max value} - \text{min value})}{\text{number of classes}}$$

The three CN sub-set classes resulting from the equal interval classification and used to delineate the three HRUs were CN 34-52, CN 55-73 and CN 76-91 for the Yialias river basin (Fig. 33b) and CN 37-58, CN 61-79 and CN 82-100 for the Kouris river basin (Fig. 34b)

***Natural break (Jenks) classification***

In the natural breaks classification, data are classified based on natural grouping inherent in the dataset, with class breaks identified that best group similar values, maximising the difference between classes. The classification is based on the Jenks Natural Break algorithm (De Smith et al 2015).

The three CN sub-set classes resulting from the natural breaks classification and used to delineate the three HRUs were CN 34-55, CN 58-67 and CN 70-91 for the Yialias river basin (Fig. 33c) and CN 37-61, CN 64-73 and CN 76-100 for the Kouris river basin (Fig. 34c). The resulted CN sub-set classes vary between the three classifications and should be considered during the calibration procedure so that the HRU parameters are physically consistent to these CN sub-sets.

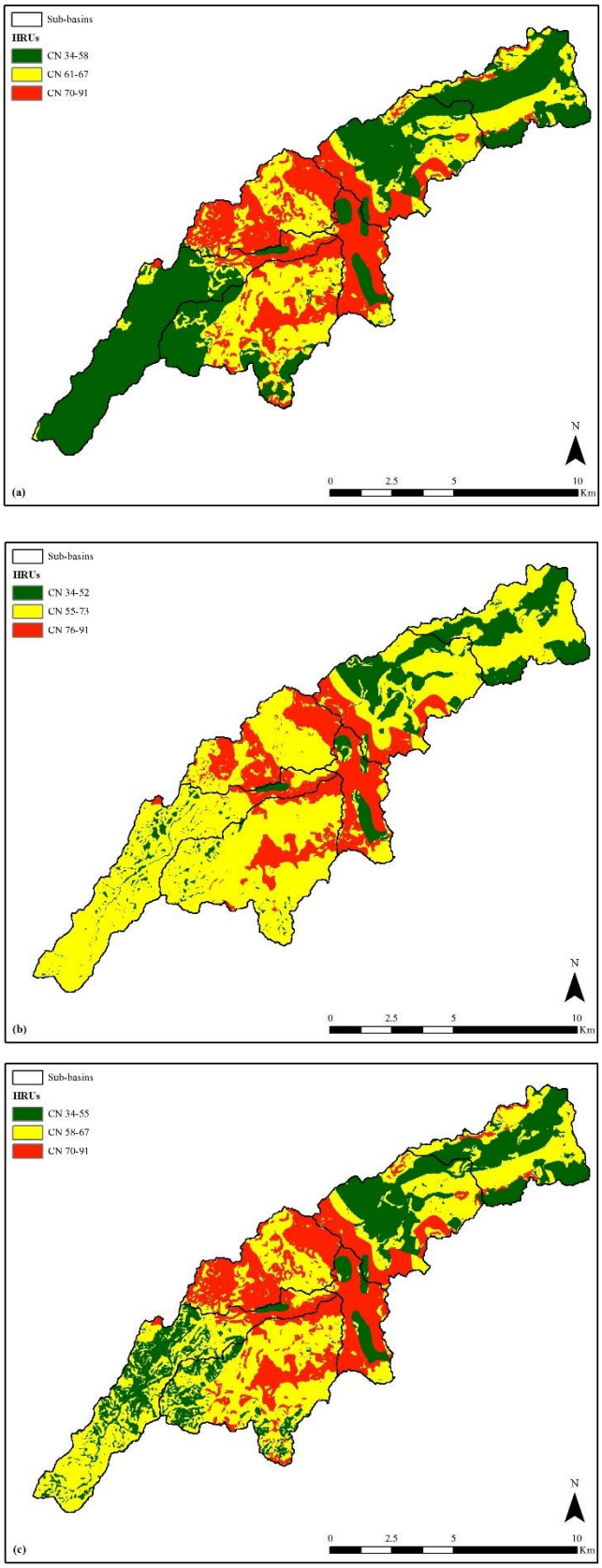


**Figure 33:** Yialias river basin HRU delineation using (a) quantile classification, (b) equal interval classification, and (c) natural breaks (jenks) classification.

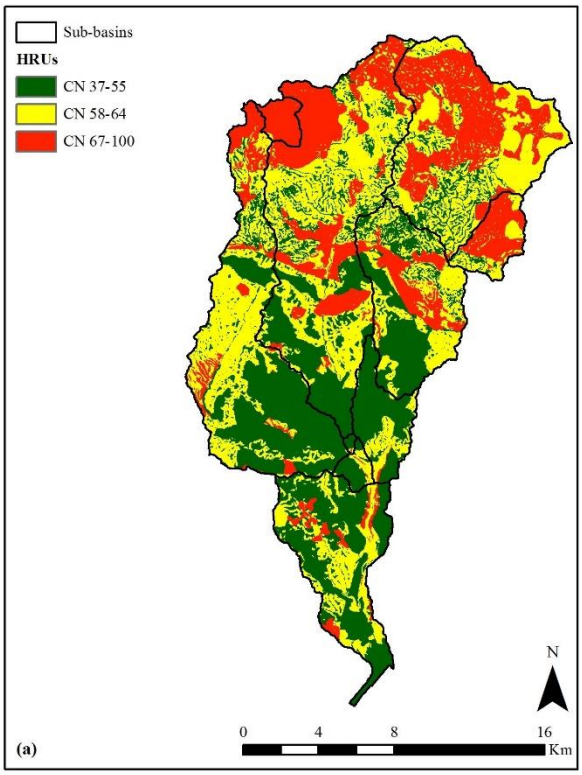
Sub-basins
HRUs
CN 37-55
CN 58-64
CN 67-100
N
0
4
8
16
Km
(a)

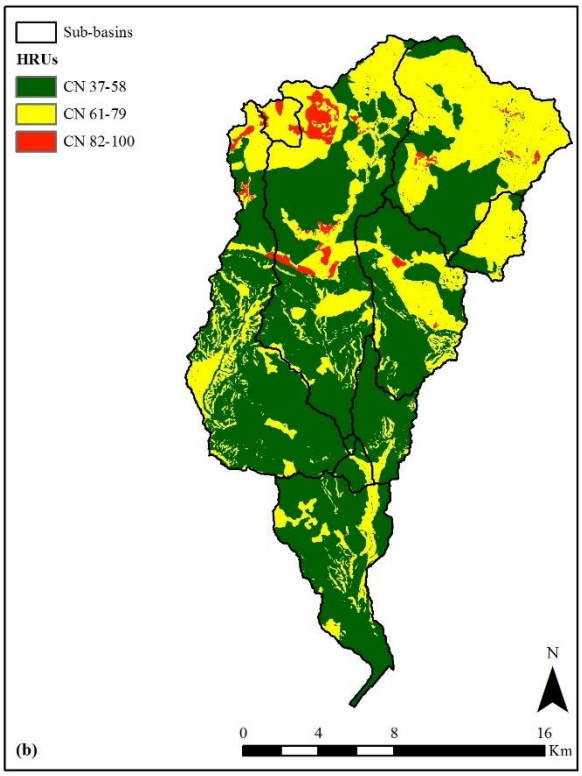
Sub-basins
HRUs
CN 37-58
CN 61-79
CN 82-100
N
0
4
8
16
Km
(b)

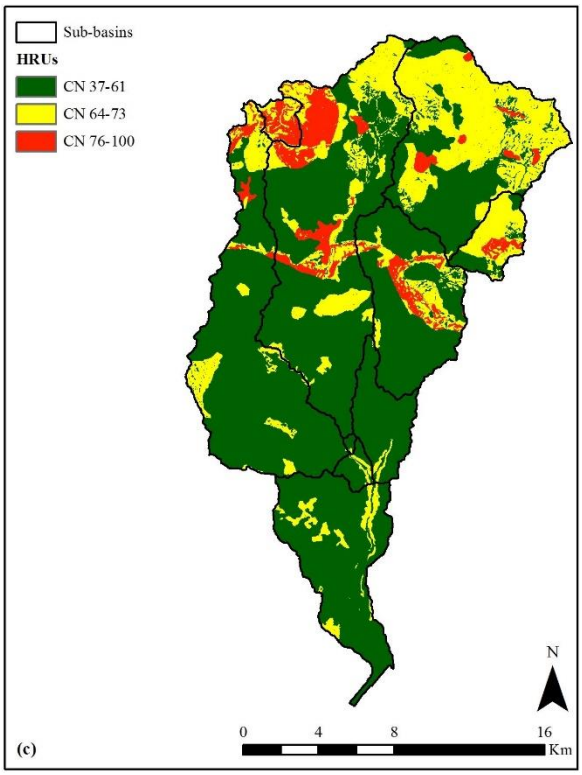


**Figure 34:** Kouris river basin HRU delineation using (a) quantile classification, (b) equal interval classification, and (c) natural breaks (jenks) classification.

Based on the three HRU delineations produced by the quantile, equal interval and natural breaks classification methods described above, three different simulation modes were set up in the HYDROGEIOS framework for the Yialias river basin and three different simulation models for the Kouris river basin.

### 5.5.1 Yialias river basin

The optimized statistical measures against the simulated runoffs are summarized in Table 23; Figures. 35-37 compare the observed hydrographs at the three monitoring sites against the ones simulated with the three HRU delineation methods: quantile, equal intervals, and natural breaks. Regarding the runoff at the Kotsiatis monitoring station (Fig. 35), a very good fit is achieved by all three models, for both the calibration and validation periods: the simulation with the HRU delineation based on the quantile classification achieving efficiency values of 75.5% and 51.1%, respectively, with the HRU delineation based on the equal interval classification achieving efficiency values of 75.6% and 51.3, respectively, and with the HRU delineation based on the natural breaks classification achieving efficiency values of 74.6% and 50.6%, respectively. As

shown in Fig. 28, the simulations preserve the important features of the hydrographs, such as the high flows over the winter and zero flows over the summer periods for the calibration periods. Although the high flow efficiency values are very good for the calibration period, none of the models succeeds to simulate well the high flows of February 2007 and 2010, and October 2009, leading to unsatisfactory prediction of high flows during the validation period.

For the Nisou monitoring station (Fig. 36), all models achieved higher efficiency values in calibration, but much lower in validation, compared to the Kotsiatis monitoring station, with 79.2 % in calibration and 27.9 % in validation for the simulation with the HRU delineation based on the quantile classification, 79.3 % and 26.3 %, respectively, with the HRUs based on the equal interval classification, and 80.4 % and 26.8 %, respectively, with the HRUs based on the natural breaks classification. Once again, the simulations preserve the important features of the hydrographs, such as the high flows over the winter and zero flows over the summer periods for the calibration periods (Fig. 29) but were unable to simulate the high flow of October 2009 leading to satisfactory high flow efficiency for the calibration period, but not for the validation.

Finally, for the Potamia monitoring station (Fig. 37), a very good fit is achieved by all three models for the calibration period, but a poor one for the validation periods: the simulation with the HRU delineation based on the quantile classification achieving efficiency values of 79.50% and 8.9%, respectively, with the HRU delineation based on the equal interval classification achieving efficiency values of 77.6% and 3.4%, respectively, and with the HRU delineation based on the natural breaks classification achieving efficiency values of 78.4% and 16.7% for the calibration and validation periods, respectively. High-flow efficiency was satisfactory for the calibration period, but not for the validation, following the same pattern of underestimating the high flows of October 2009.

The performance of all three models set up with the HRUs delineated based on the quantile, equal interval and natural break classification was satisfactory for the calibration period, with more or less the same efficiency and high-flow efficiency values. For the validation period however, the performance of the three models was satisfactory only for the Kotsiatis monitoring station, while it was unsatisfactory for the other two monitoring station (Nisou and Potamis). This may be attributed to the almost

zero flow from 2005 all the way up to 2010, except in 2007 when an isolated flow incident was recorded. Zero observed flow series for such a long period of time affected the models' performance in validation This is also indicated by the overall error index (F), which was calculated to be 1.797 for the calibration and 5.322 for the validation for the model with the HRUs delineated based on the quantile classification, 1.799 for the calibration and 5.420 for the validation for the model with the HRUs delineated based on the equal interval classification, 1.800 for the calibration and 5.371 for the validation for the model with the HRUs delineated based on the natural breaks classification, by applying a weight of 1 for both the efficiency and high-flow efficiency performance. The calibration performance of all three models is almost identical, while the model with the HRUs delineated based on the quantile classification performed best at the validation compared to the other two.

**Table 23:** Yialias river basin optimal values of efficiency, high flow efficiency and objective function error the calibration and validation periods for the simulations modes with HRU delineation based on quantile, equal interval, and natural breaks (jenks) classification.

| Daily runoff | Calibration period | | Validation period | |
|---|---|---|---|---|
| | Efficiency | High Flow Eff. | Efficiency | High Flow Eff. |
| | Quantile classification | | | |
| Kotsiatis monitoring station | 0.755 | 0.562 | 0.511 | 0.050 |
| Nisou monitoring station | 0.792 | 0.634 | 0.279 | 0.077 |
| Potamia monitoring station | 0.790 | 0.671 | 0.089 | -0.329 |
| | Equal intervals classification | | | |
| Kotsiatis monitoring station | 0.756 | 0.562 | 0.513 | 0.054 |
| Nisou monitoring station | 0.793 | 0.639 | 0.263 | 0.067 |
| Potamia monitoring station | 0.776 | 0.664 | 0.34 | -0.351 |
| | Natural breaks classification | | | |
| Kotsiatis monitoring station | 0.746 | 0.547 | 0.506 | 0.037 |
| Nisou monitoring station | 0.804 | 0.658 | 0.268 | 0.067 |
| Potamia monitoring station | 0.784 | 0.661 | 0.167 | -0.315 |

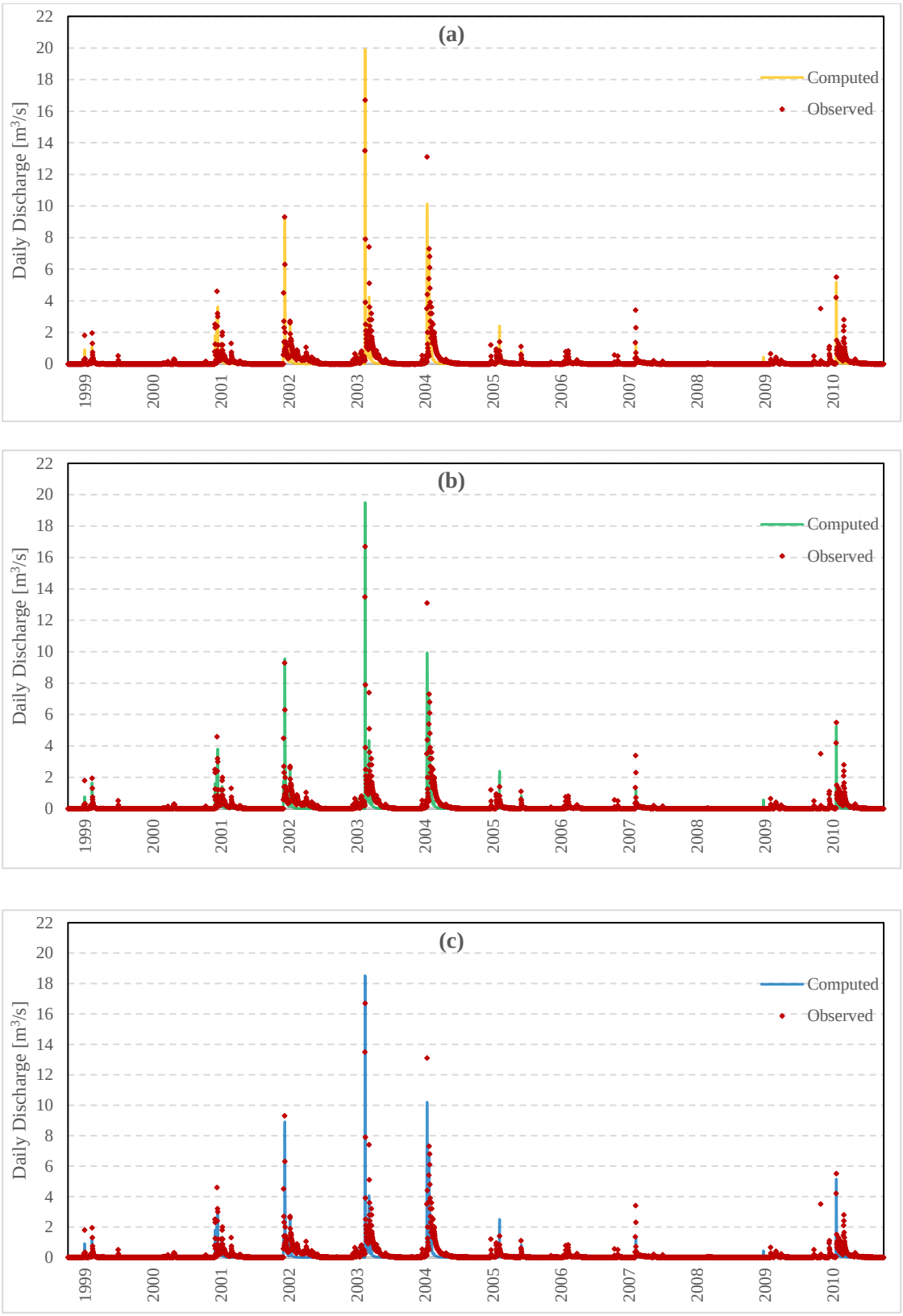


**Figure 35:** Yialias river basin computed vs. observed series at Kotsiatis monitoring station with HRU delineation based on (a) quantile classification (b) equal intervals classification, and (c) natural breaks (jenks) classification.

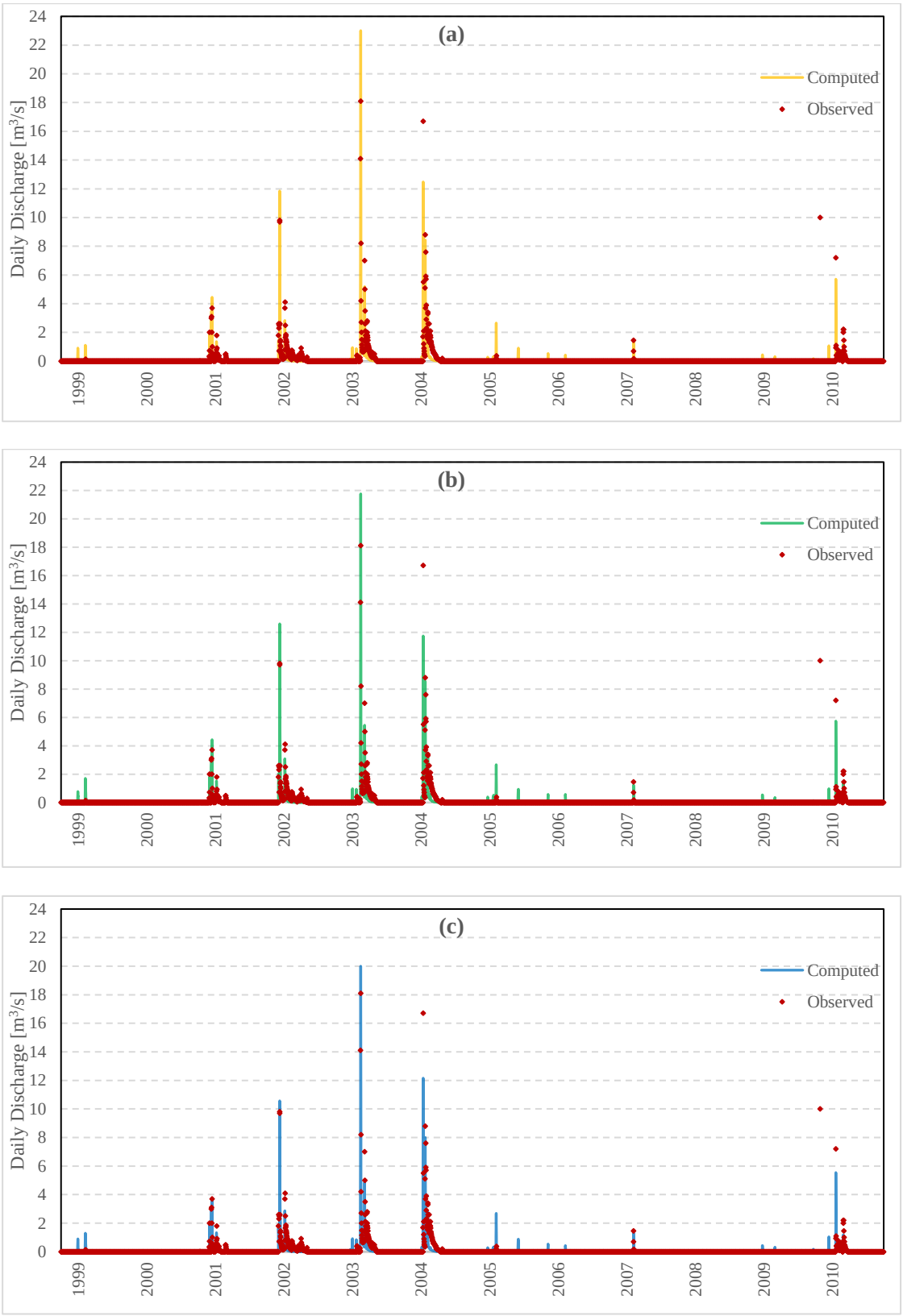


**Figure 36:** Yialias river basin computed vs. observed series at Nisou monitoring station with HRU delineation based on (a) quantile classification (b) equal intervals classification, and (c) natural breaks (jenks) classification.

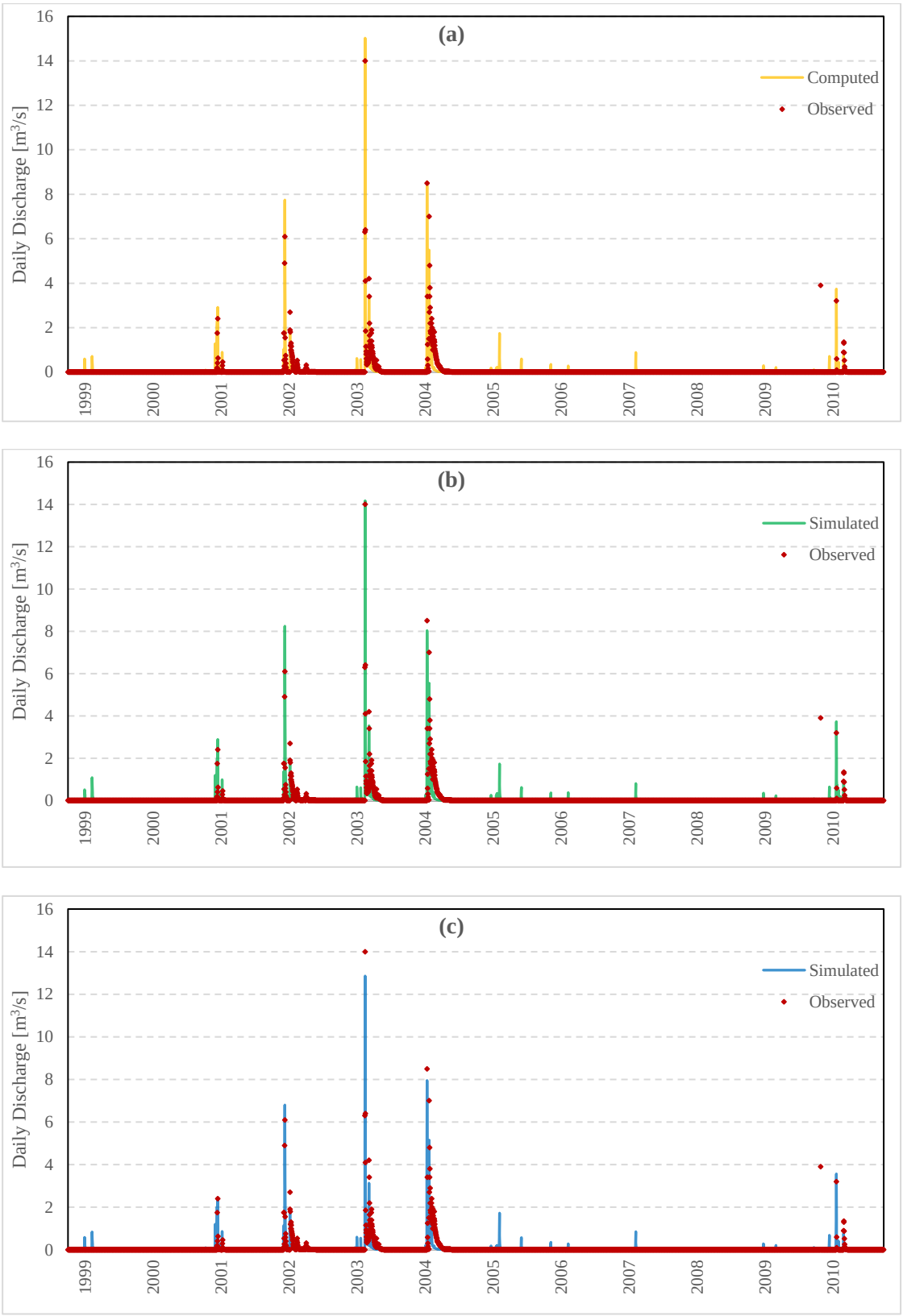


**Figure 37:** Yialias river basin computed vs. observed series at Potamia monitoring station with HRU delineation based on (a) quantile classification (b) equal intervals classification, and (c) natural breaks (jenks) classification.

Apart from the performance results obtained in terms of efficiency and high-flow efficiency, an important aspect of this implementation was to demonstrate the advantage of the CN approach in being less subjective and more parsimonious, by justifying each HRU runoff response and associated parameter values in terms of CNs; for instance, it is anticipated that an area with low CN values will generate less surface runoff than an area of moderate or high CN's. The correspondence of an HRU's response with CN is very advantageous, since the user can easily recognize whether the model parameters are physically consistent or not, and, consequently, evaluate the model robustness not only in terms of goodness-of-fit in validation, but also according to its physical grounds.

This was successfully demonstrated in Yialias river basin by all three models, where, according to the different CN sub-classes based on the different data classification methods, the HRU parameters followed the physical meaning of the CN parameter, i.e. a low CN value indicates areas of the basin with very high water permeability, dense vegetation and very low drainage capacity, which leads to minimum runoff, while a high CN value indicates areas of the basin with very low water permeability, no vegetation and a very high drainage capacity, leading to higher runoff values. As it can be seen in Table 24, the maximum infiltration ratio, which is directly associated with soil permeability properties, is higher for the HRUs with low CN range and decreases for the HRUs with higher CN value ranges. On the other hand, the soil capacity seems to be more explained by terrain slope characteristics. Thus, the flat plain areas of the basin have much larger capacities than the mountainous ones. Recession rates for percolation, as well as the percentage of infiltration to the lower zone, are also associated with permeability. Therefore, infiltration rates through the high-permeability soils are significant and their contribution to surface flow is limited. This is evident even when comparing model parameters of the CN sub-sets from HRU delineation based on different classification method. For example, when comparing the calibrated parameters of the first HRU from the quantile classification (CN 34-58, with a weighted-average value of 46) to those of the first HRU from the equal interval classification (CN 34-52, with a weighted-average value of 43) it can be observed that they are physically consistent.

**Table 24:** Yialias river basin calibrated HRU parameters produced from the delineation based on quantile, equal intervals, and natural breaks (jenks) classification.

| HRU quantile classification | CN 34-58 (46) | CN 61-67 (64) | CN 70-91 (80.5) |
|---|---|---|---|
| Total Area ($km^2$) | 49.2 | 34.4 | 29.1 |
| Max. infiltration ratio (mm/h) | 28.1 | 23.2 | 10.1 |
| Interception capacity (mm) | 441.4 | 264.5 | 136.0 |
| Soil capacity up to spill (mm) | 313.0 | 280.0 | 102.0 |
| Perc. of infiltration to the lower zone (%) | 40.0 | 10.0 | 5.0 |
| Soil capacity up to interflow (mm) | 301.0 | 298.2 | 282.2 |
| Recession rate for interflow (%) | 0.001 | 0.668 | 2.729 |
| Recession rate for percolation (%) | 0.235 | 0.109 | 0.030 |

| HRU equal intervals classification | CN 34-52 (43) | CN 55-73 (64) | CN 76-91 (83.5) |
|---|---|---|---|
| Total Area ($km^2$) | 18.0 | 73.0 | 21.7 |
| Max. infiltration ratio (mm/h) | 34.0 | 24.4 | 7.8 |
| Interception capacity (mm) | 589.0 | 314.5 | 134.3 |
| Soil capacity up to spill (mm) | 383.0 | 281.0 | 0.052 |
| Perc. of infiltration to the lower zone (%) | 46.0 | 10.0 | 5.0 |
| Soil capacity up to interflow (mm) | 457.0 | 298.2 | 89.0 |
| Recession rate for interflow (%) | 0.001 | 0.668 | 2.729 |
| Recession rate for percolation (%) | 0.235 | 0.109 | 0.030 |

| HRU natural breaks classification | CN 34-55 (44.5) | CN 58-67 (62.5) | CN 70-91 (80.5) |
|---|---|---|---|
| Total Area ($km^2$) | 31.9 | 51.7 | 29.1 |
| Max. infiltration ratio (mm/h) | 30.1 | 26.0 | 10.1 |
| Interception capacity (mm) | 450.0 | 345.0 | 135.8 |
| Soil capacity up to spill (mm) | 357.0 | 295.0 | 102.0 |
| Perc. of infiltration to the lower zone (%) | 45.0 | 12.0 | 5.0 |
| Soil capacity up to interflow (mm) | 357.0 | 30.70 | 282.2 |
| Recession rate for interflow (%) | 0.001 | 0.688 | 2.729 |
| Recession rate for percolation (%) | 0.235 | 0.109 | 0.030 |

### 5.5.1 Kouris river basin

The optimized statistical measures against the simulated runoffs are summarized in Table 25; Figures 38-41 compare the observed hydrographs at the three monitoring sites against the ones simulated with the three HRU delineation methods: quantile, equal intervals, and natural breaks. Regarding the runoff at the Loumata monitoring station simulated from October 1990 to September 2001 (Fig. 38), a very good fit is achieved by all three models, for the calibration and especially for the validation period: the simulation with the HRU delineation based on the quantile classification achieving efficiency values of 66.2% and 71.2%, respectively, with the HRU delineation based on the equal-interval classification achieving efficiency values of 66.7% and 70.8, respectively, and with the HRU delineation based on the natural-breaks classification achieving efficiency values of 66.1% and 69.1%, respectively. As shown in Fig. 31, the simulations preserve the important features of the hydrographs, such as the high flows over the winter and zero flows over the summer periods for the entire control period.

For the Limatis monitoring station simulated for the entire control period of October 1985 to September 2010 (Fig. 39), all models achieved higher efficiency values in calibration and lower in validation, compared to the other two monitoring stations. Specifically, 73.7 % in calibration and 55.9 % in validation for the simulation with the HRU delineation based on the quantile classification, 80.7 % and 49.8 % respectively with the HRUs based on the equal interval classification, and 77.5 % and 57.0% respectively with the HRUs based on the natural breaks classification. Once again, the simulations preserve the important features of the hydrographs, such as the high flows over the winter and zero flows over the summer periods for the entire period, underestimating by a small amount the high flows in January 1989 and 1995 (Fig. 39). Very satisfactory average-bias values were achieved by all models, especially for the validation period (Table 25).

Finally, the discharge series observed at the Kouris monitoring station were used for validation, as it was simulated only for the last three years of the control period, from October 2007 to September 2010 (Fig. 40 and 41). Very satisfactory efficiency values were achieved by all three models three models, with the HRU delineation based on the quantile classification achieving efficiency value of 82.5%, with the HRU delineation based on the equal interval classification achieving efficiency value of 81.1%, and with

the HRU delineation based on the natural breaks classification achieving a lower but still very satisfactory efficiency value of 68.6 %. Moreover, negligible average-bias values were achieved by all three models (Table 25). However, although the models preserved the overall behavior of the hydrographs, appear to have response difference compared to the observed series. Additionally, some of the high flow events were underestimated, more specifically, during the year 2008 and especially 2010, none of the models succeeds in simulating the high flows. This could be attributes to the fact that this monitoring station was used only for validation due to the lack of observed flow series in the previous years, and its validation results were based on the calibration performed on daily flow observation of two other monitoring stations of the network.

The performance of all three models set up with the HRUs delineated based on the quantile, equal interval and natural break classification was satisfactory with similar efficiency and average bias values. This is also indicated by the overall error index (F) which was calculated to be 0.819 for the calibration and 1.088 for the validation for the model with the HRUs delineated based on the quantile classification, 0.757 for the calibration and 1.186 for the validation for the model with the HRUs delineated based on the equal interval classification, 0.801 for the calibration and 1.176 for the validation for the model with the HRUs delineated based on the natural breaks classification, by applying a weight of 1 for both the efficiency and the average bias performance. The calibration performance was best for the model with the HRUs delineated based on the equal interval classification, while the model with the HRUs delineated based on the quantile classification performed best at the validation compared to the other two.

**Table 25:** Kouris river basin optimal values of efficiency, high flow efficiency and objective function error the calibration and validation periods for the simulations modes with HRU delineation based on quantile, equal interval, and natural breaks (jenks) classification.

| Daily runoff | Calibration period | | Validation period | | Overall |
|---|---|---|---|---|---|
| | Efficiency | Average Bias | Efficiency | Average Bias | Perc. Bias |
| | Quantile classification | | | | |
| Loumata monitoring station | 0.662 | 0.057 | 0.712 | 0.062 | -5.82% |
| Limnatis monitoring station | 0.737 | -0.161 | 0.559 | 0.031 | 7.92% |
| Kouris monitoring station | - | - | 0.825 | -0.090 | 9.10% |
| | Equal intervals classification | | | | |
| Loumata monitoring station | 0.667 | 0.036 | 0.708 | 0.039 | -3.65% |
| Limnatis monitoring station | 0.807 | -0.195 | 0.498 | -0.053 | 13.44% |
| Kouris monitoring station | - | - | 0.811 | -0.111 | 11.10% |
| | Natural break classification | | | | |
| Loumata monitoring station | 0.661 | 0.014 | 0.691 | 0.002 | -0.95% |
| Limnatis monitoring station | 0775 | -0.223 | 0.570 | -0.119 | 17.84% |
| Kouris monitoring station | - | - | 0.686 | -0.002 | 0.25% |

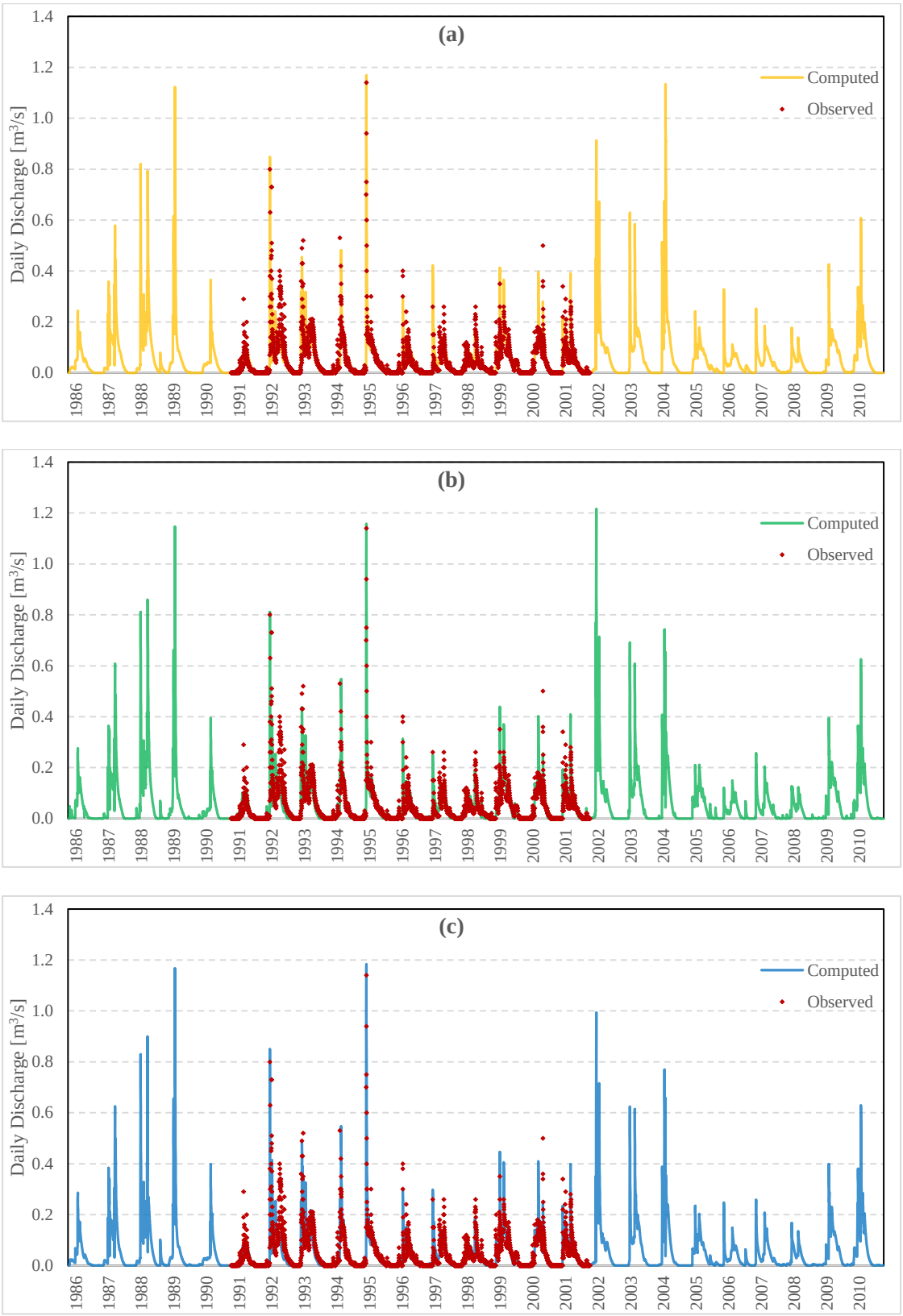


**Figure 38:** Kouris river basin computed vs. observed series at Loumata monitoring station with HRU delineation based on (a) quantile classification (b) equal intervals classification, and (c) natural breaks (jenks) classification.

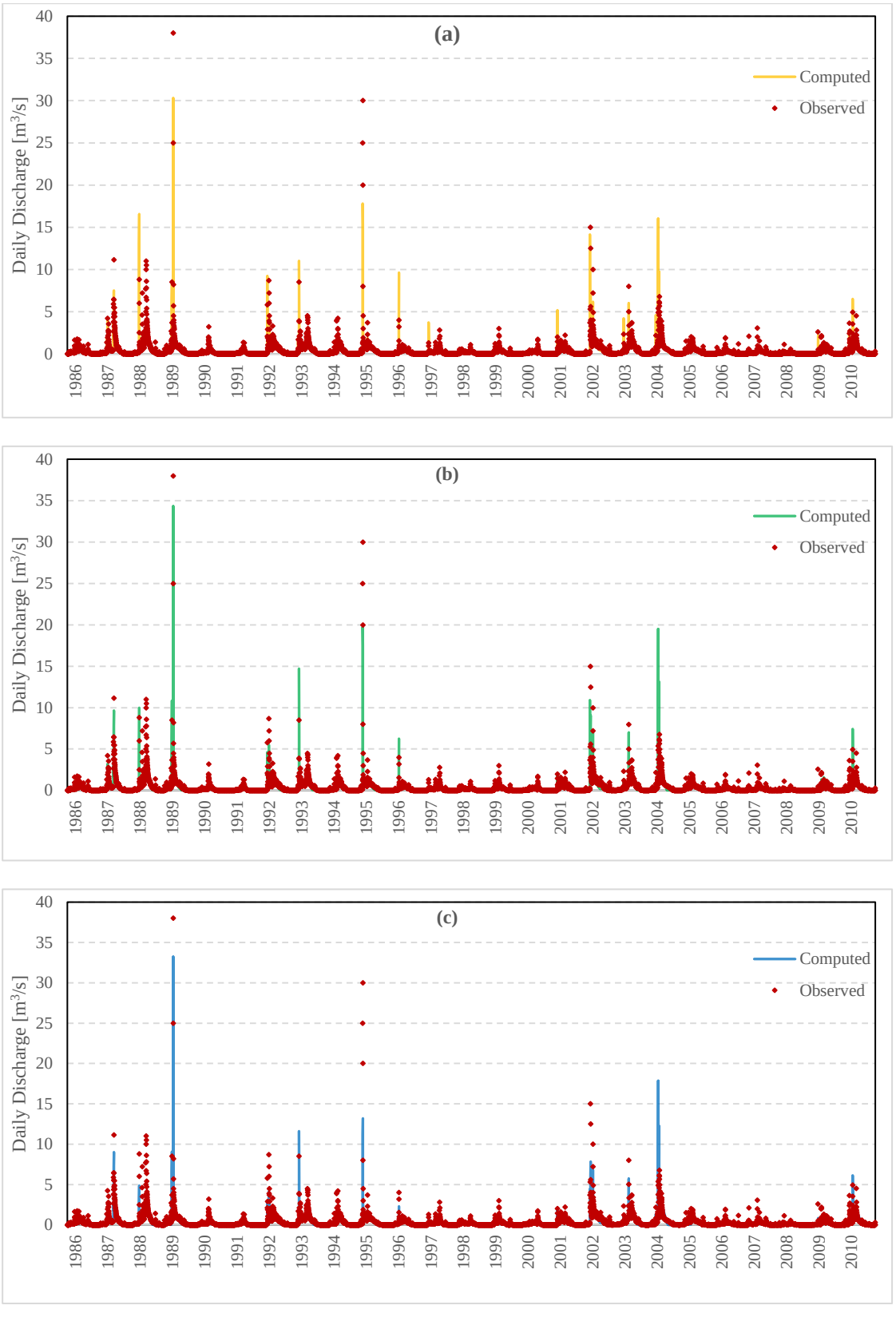


**Figure 39:** Kouris river basin computed vs. observed series at Limnatis monitoring station with HRU delineation based on (a) quantile classification (b) equal intervals classification, and (c) natural breaks (jenks) classification.

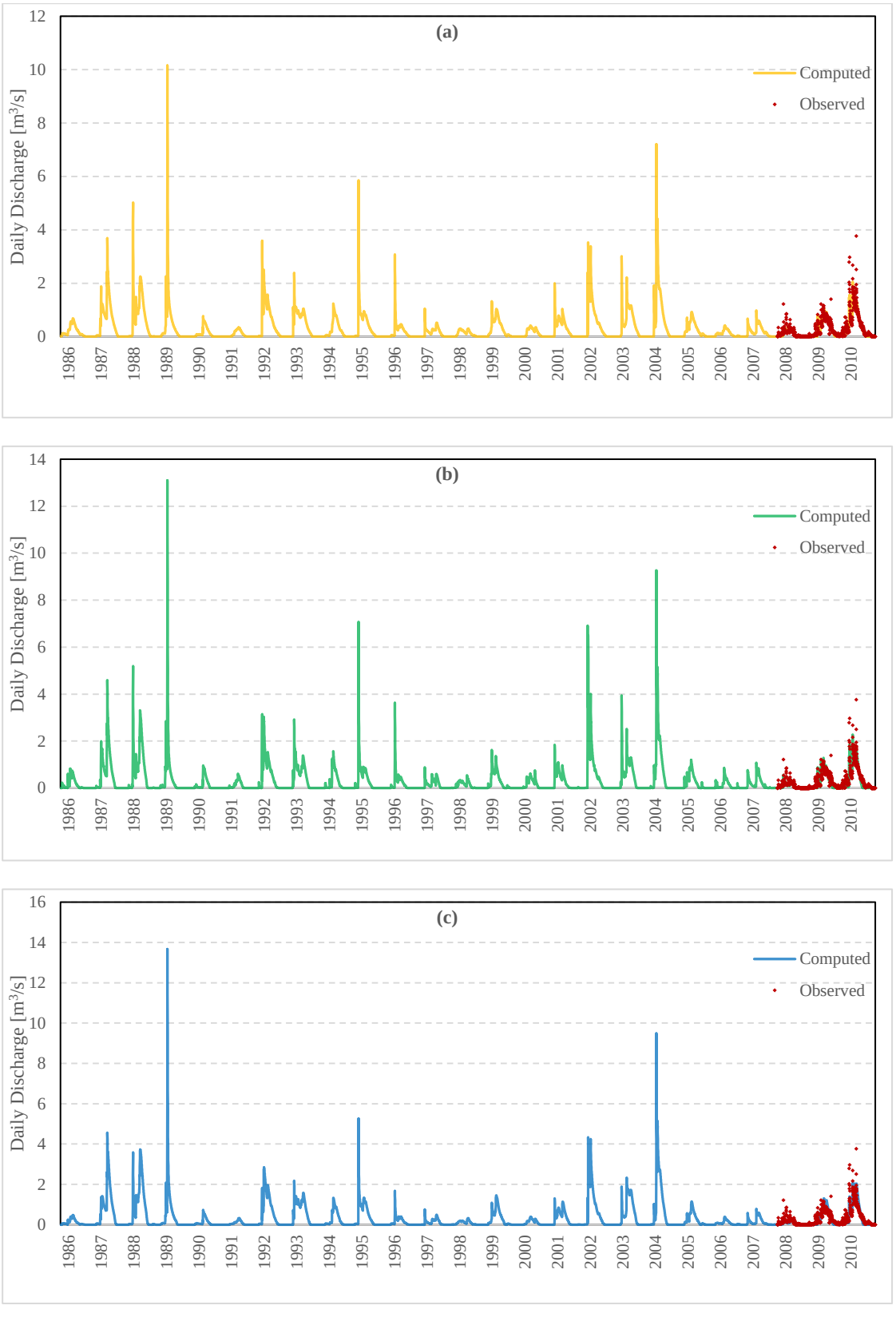


**Figure 40:** Kouris river basin computed vs. observed series at Kouris monitoring station with HRU delineation based on (a) quantile classification (b) equal intervals classification, and (c) natural breaks (jenks) classification.

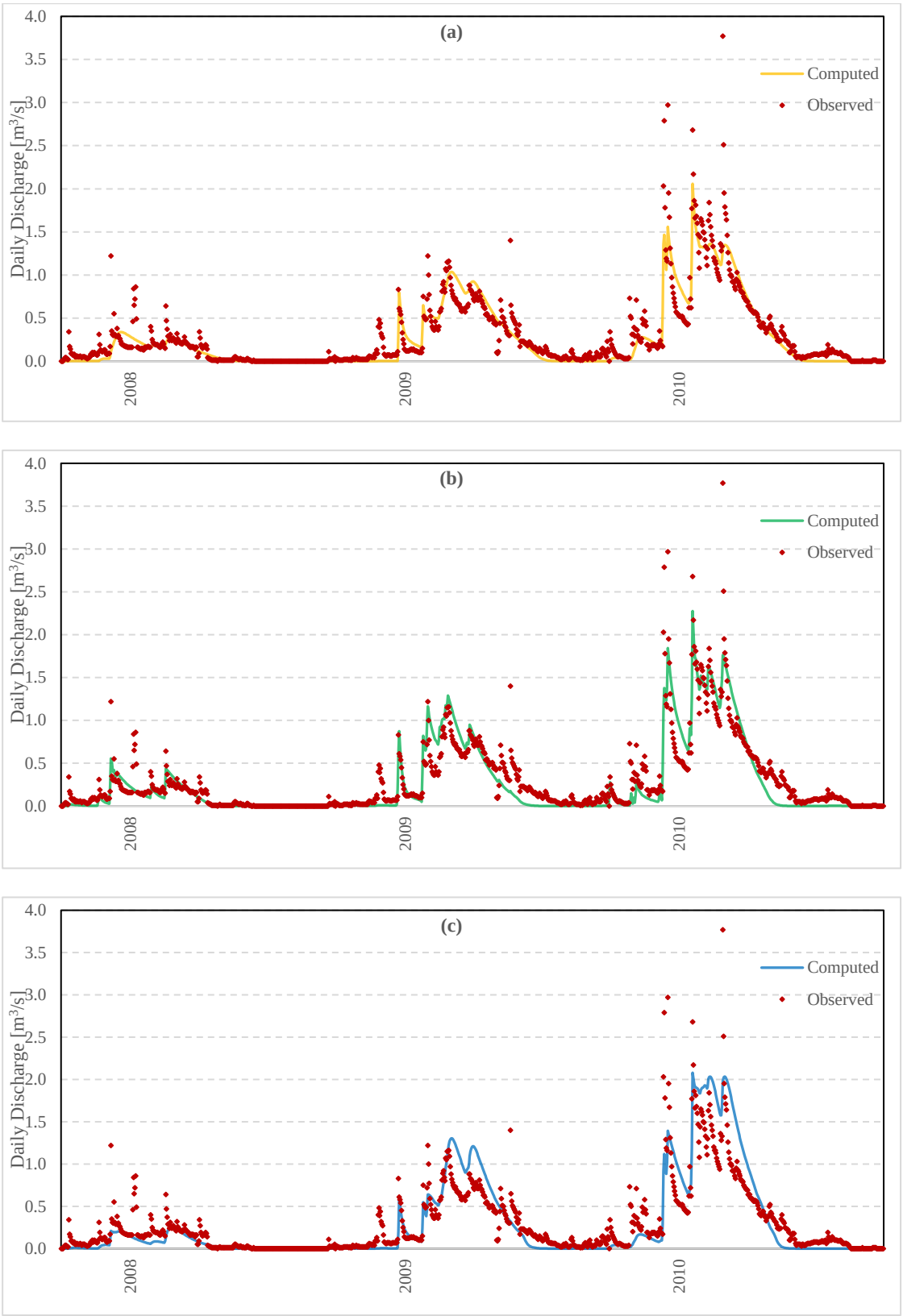


**Figure 41:** Kouris river basin computed vs. observed series at Kouris monitoring station detail with HRU delineation based on (a) quantile classification (b) equal intervals classification, and (c) natural breaks (jenks) classification.

Model parameters were also physically consistent for the Kouris river basin models (Table 26), with the low CN value indicating areas of the basin with very high permeability, dense vegetation and very low drainage capacity, leading to minimum runoff, while a high CN value indicates areas of the basin with very low water permeability, no vegetation and a very high drainage capacity, leading to higher runoff values. Similarly, with the calibrated model parameters of the Yialias river basin explained in Section 5.5.1, the maximum infiltration ratio, which is directly associated with soil permeability properties, is higher for the HRUs with low CN range and decreases for the HRUs with higher CN value ranges, while the soil capacity is higher for flatter areas of the basin and much lower for areas with high terrain slope. Recession rates for percolation, as well as the percentage of infiltration to the lower zone, are also associated with permeability, and therefore, infiltration rates are much higher for the HRUs with low CN range.

**Table 26:** Kouris river basin calibrated HRU parameters produce from the delineation based on quantile, equal intervals, and natural breaks (jenks) classification.

| HRU quantile classification | CN 37-55 (46) | CN 58-64 (61) | CN 67-100 (83.5) |
|---|---|---|---|
| Total Area ($km^2$) | 124.4 | 133.0 | 83.5 |
| Max. infiltration ratio (mm/h) | 148.3 | 103.9 | 49.8 |
| Interception capacity (mm) | 593.0 | 377.0 | 50.0 |
| Soil capacity up to spill (mm) | 614.0 | 429.0 | 317.0 |
| Perc. of infiltration to the lower zone (%) | 71.7 | 58.4 | 39.6 |
| Soil capacity up to interflow (mm) | 208.0 | 31.0 | 12.0 |
| Recession rate for interflow (%) | 1.000 | 1.996 | 2.016 |
| Recession rate for percolation (%) | 0.072 | 0.065 | 0.055 |

| HRU equal intervals classification | CN 37-58 (47.5) | CN 61-79 (70) | CN 82-1-- (91) |
|---|---|---|---|
| Total Area ($km^2$) | 206.2 | 127.9 | 7.6 |
| Max. infiltration ratio (mm/h) | 118.3 | 63.9 | 9.8 |
| Interception capacity (mm) | 303.0 | 127.0 | 30.0 |
| Soil capacity up to spill (mm) | 227.0 | 213.0 | 125.0 |
| Perc. of infiltration to the lower zone (%) | 64.0 | 40.4 | 11.7 |
| Soil capacity up to interflow (mm) | 108.0 | 29.0 | 2.0 |
| Recession rate for interflow (%) | 2.000 | 2.996 | 3.016 |
| Recession rate for percolation (%) | 0.062 | 0.055 | 0.045 |

| HRU natural breaks classification | CN 37-61 (49) | CN 64-73 (68.5) | CN 76-100 (88) |
|---|---|---|---|
| Total Area ($km^2$) | 232.4 | 87.4 | 21.9 |
| Max. infiltration ratio (mm/h) | 115.3 | 65.9 | 41.8 |
| Interception capacity (mm) | 293.0 | 227.0 | 40.8 |
| Soil capacity up to spill (mm) | 225.0 | 224.0 | 150.0 |
| Perc. of infiltration to the lower zone (%) | 50.0 | 42.1 | 41.9 |
| Soil capacity up to interflow (mm) | 78.0 | 27.0 | 2.0 |
| Recession rate for interflow (%) | 2.200 | 3.016 | 3.056 |
| Recession rate for percolation (%) | 0.059 | 0.049 | 0046 |

## 5.6 Verification Experiment 2: CN Equation Index Coefficient Sensitivity Analysis

In this section, the coefficients of the three indices used in Eq. (10) will be further investigated based on 28 different cases of index values combination, in order to test the sensitivity of the CN equation in terms of the final HRU delineation and thus, model efficiency, and apply changes necessary to the originally defined CN equation. A schematic layout of the processes followed in the verification experiment 2 is showed in Figure 42.

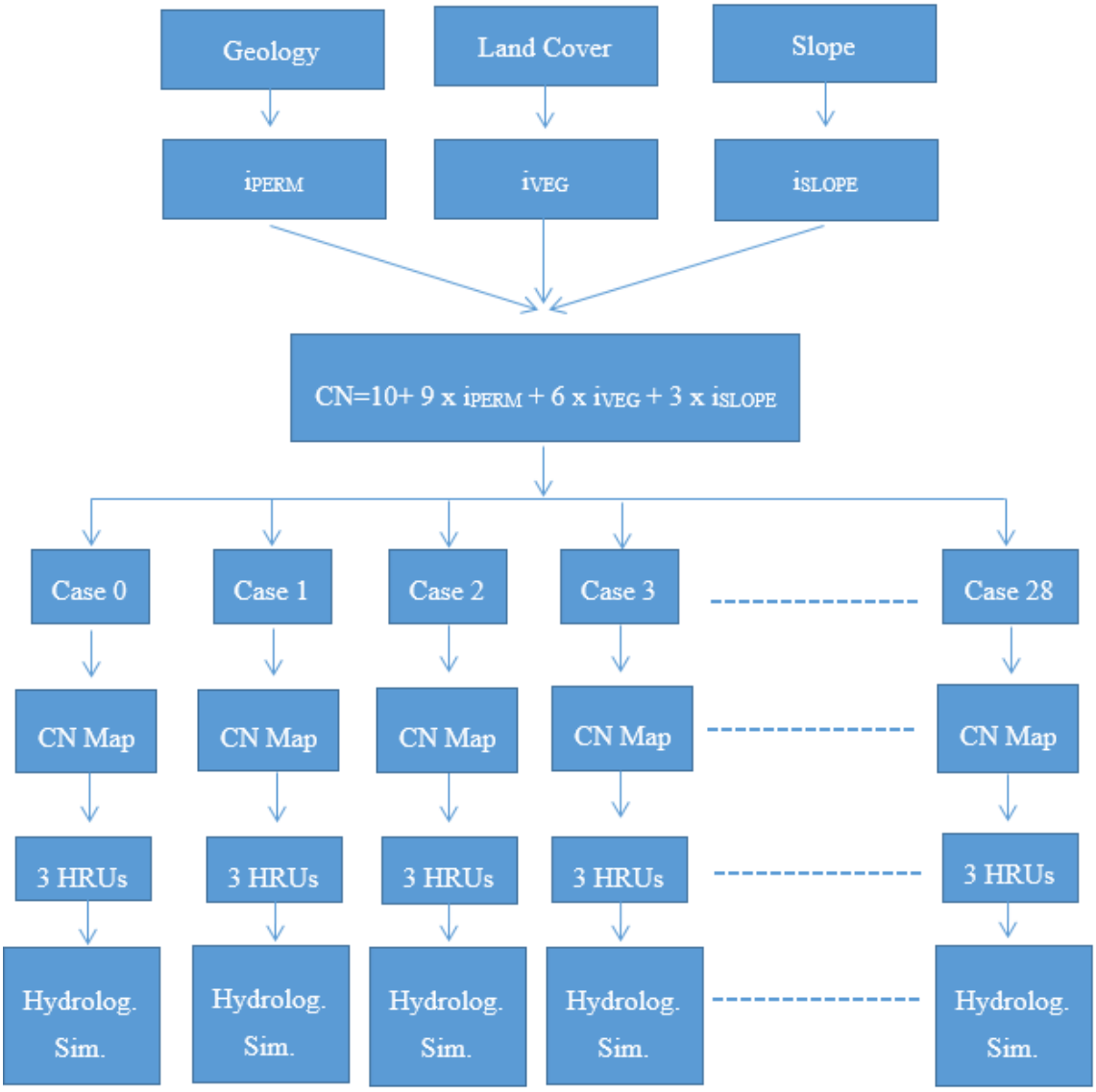


**Figure 42:** Schematic layout of the processes followed in the verification experiment 2

The same values ranging from 1 to 5 were assigned to the three indices, $i_{PERM}$, $i_{VEG}$, and $i_{SLOPE}$, as before (Section 5.5, Table 21, Table 22), producing the corresponding raster maps for Yialias river basin (Figs. 28a, 28b and 28c, respectively) and for Kouris river basin (Figs. 29a, 29b, and 29c, respectively). The CN-parameter map for each basin, however, was produced with the spatial overlay of the three classified raster maps according to Eq. (10), but with different index coefficients, thus producing different CN values, and consequently, different CN-parameter maps. The coefficient combination cases for the three indices that were used to produce different CN-parameter maps can be seen in Table 27, where Case 0 corresponds to the initially defined coefficients 9, 6, and 3 for $i_{PERM}$, $i_{VEG}$, and $i_{SLOPE}$, respectively (as stated in Eq. 10, Section 3.3).

**Table 27:** Index coefficient combinations

| | Coefficient combination cases | | | | | | | | | | | | |
|---|---|---|---|---|---|---|---|---|---|---|---|---|---|
| Index | 1 | 2 | 3 | 4 | *0* | 5 | 6 | 7 | 8 | 9 | 10 | 11 | 12 |
| $i_{PERM}$ | 7 | 7.5 | 8 | 8.5 | *9* | 9.5 | 10 | 10.5 | 11 | 11.5 | 12 | 12.5 | 13 |
| $i_{VEG}$ | 7 | 6.75 | 6.5 | 6.25 | *6* | 5.75 | 5.5 | 5.25 | 5 | 4.75 | 4.5 | 4.25 | 4 |
| $i_{SLOPE}$ | 4 | 3.75 | 3.5 | 3.25 | *3* | 2.75 | 2.5 | 2.25 | 2 | 1.75 | 1.5 | 1.25 | 1 |

| | 13 | 14 | 15 | 16 | *0* | 17 | 19 | 19 | 20 |
|---|---|---|---|---|---|---|---|---|---|
| $i_{PERM}$ | 10 | 9.75 | 9.5 | 9.25 | *9* | 8.75 | 8.5 | 8.25 | 8 |
| $i_{VEG}$ | 4 | 4.5 | 5 | 5.5 | *6* | 6.6 | 7 | 7.5 | 8 |
| $i_{SLOPE}$ | *4* | *3.75* | *3.5* | *3.25* | *3* | *2.75* | *2.5* | *2.25* | *2* |

| | 21 | 22 | 23 | 24 | *0* | 25 | 26 | 27 | 28 |
|---|---|---|---|---|---|---|---|---|---|
| $i_{PERM}$ | 10 | 9.75 | 9.5 | 9.25 | *9* | 8.75 | 8.5 | 8.25 | 8 |
| $i_{VEG}$ | 7 | 6.75 | 6.5 | 6.25 | *6* | 5.75 | 5.5 | 5.25 | 5 |
| $i_{SLOPE}$ | 1 | 1.5 | 2 | 2.5 | *3* | 3.5 | 4 | 4.5 | 5 |

For the first 12 coefficient combination cases, the $i_{PERM}$ coefficient varied from 7 to 13 by 0.5 intervals, with the other two coefficients adjusted accordingly from 7 to 4 for the $i_{VEG}$ coefficient and from 4 to 1 for the $i_{SLOPE}$ coefficient, so that the final CN-value computed would be in the 28-100 value range, which represents the basin behavior in runoff production, i.e., HRUs with lower CN value range are expected to produce less surface runoff than HRUs with higher CN value range. Moreover, for the cases 13 to 20, the $i_{VEG}$ coefficient varied from 4 to 8 by 0.5 intervals, with the other two coefficients adjusted accordingly from 10 to 8 for the $i_{PERM}$ coefficient and 4 to 2 for the $i_{SLOPE}$ coefficient; and for the cases 21 to 28, the $i_{SLOPE}$ coefficient varied from 1 to 5 by 0.5 intervals, with the other two coefficients adjusted accordingly from 10 to 8 for the $i_{PERM}$ coefficient and 7 to 5 for the $i_{SLOPE}$ coefficient.

Based on the 28 coefficient combination cases, 28 different CN-parameter maps were produced for each river basin, which were then used to delineate three HRUs in each case, based on the quantile classification method (Section 5.5).

Based on the HRU delineations produced by the quantile aggregation applied at each of the 28 CN-parameter maps, 28 different simulation modes were set up in the HYDROGEIOS framework for the Yialias and Kouris river, respectively, following the exact model set up described in Section 5.3, where the HRU configuration was based on

the quantile aggregation of the CN-parameter map produced with Eq. (10) with the initially defined coefficients, i.e. case 0. Moreover, the same model parameter values were used (Table 26 – quantile classification), and no calibration was performed.

### 5.6.1 Yialias river basin

The resulting statistical measures against the simulated runoffs are summarized in Table 28, whereas Figure 43 show the variation of those measures at the three monitoring sites produced from the 28 different delineation cases. In can be seen that for the Kotsiatis monitoring station, model efficiency in calibration varies from 69.8% for the simulation with the coefficient combination case 1, to 74.6% for the simulation with the coefficient combination case 27, while cases 9 to 15 seem to perform the best. In validation, model efficiency varies from 43.3% for the simulation with the coefficient combination case 1, to 51.0% for the simulations with the coefficient combination cases 17 and 18, while, except for cases 1, 19 and 20, all other cases performance was almost the same. In terms of high flow efficiency calibration, values vary from 44.7% for the simulation with the coefficient combination case 1, to 54.1% for the simulation with the coefficient combination case 14, while cases 9 to 15 seem to perform the best. In validation, high flow efficiency varies from three negative values -12.1%, -11.2% and -2.1% for the simulations with the coefficient combination cases 19, 1 and 20, respectively, to 4.6% for the simulations with the coefficient combination cases 17 and 18, while, except for cases producing the negative high flow efficiencies, all other cases performance was almost the same.

Similar results were obtained for the Nisou monitoring station, where model efficiency in calibration varied from 76.2% for the simulation with the coefficient combination case 1, to 78.5% for the simulations with the coefficient combination cases 12 and 15, while overall, all cases except 1, 19 and 20, performed equally well. In validation, model efficiency varies from 25.7% for the simulation with the coefficient combination case 11, to 28.1% for the simulation with the coefficient combination cases 20, with all cases performance being almost the same. In terms of high flow efficiency calibration, values vary from 56.8% for the simulation with the coefficient combination case 1, to 61.9% for the simulations with the coefficient combination cases 9-15, which seem to perform the best. In validation, high flow efficiency varies from 2.1% for the simulation

with the coefficient combination case 19, to 8.1% for the simulation with the coefficient combination case 18, while, except for cases 1, 19 and 20, all other cases performance was very similar.

The variation in the results obtained for the Potamia monitoring station was much more significant, compared to the results of the other two monitoring stations. Model efficiency in calibration varied from 71.9% for the simulation with the coefficient combination case 19, to 78.5% for the simulations with the coefficient combination cases 14 and 15, while overall, the best efficiencies were achieved from cases 5 to 16 and 25 to 28 and the worst from cases 17 to 21. In validation, model efficiency varies from -4.7% for the simulation with the coefficient combination case 27, to 18.1% for the simulation with the coefficient combination cases 1, with cases 5 to 8 performing the best, while cases 9 to 12, 14, 15, 27 and 28 produced negative efficiency values. In terms of high flow efficiency calibration, values vary from 62.1% for the simulation with the coefficient combination case 1, to 65.5% for the simulation with the coefficient combination case 27, completely the opposite when compared with the efficiency validation results. However, all cases seemed to performed equally well. In validation, high flow efficiency performance was unsatisfactory for all the cases, especially for cases 9-15.

Overall error index results in calibration were very similar for all cases, except for the simulations with coefficient combination cases 1, 19 and 20, while overall error index results in validation were the lowest for the cases 2 to 8, 16 to 18 and 21 to 24. Examining the results, one sees that there is an obvious lower performance by the simulations with coefficient combination cases 1, 19 and 20, which correspond to the combinations 7-7-4, 8.25-7.5-2.25 and 8-8-2 respectively (Table 27), all three cases having the same, or very close coefficients for the $i_{PERM}$ and $i_{VEG}$ indices. This is evidence that water permeability has a greater impact on the hydrologic response of a river basin and should therefore be weighted higher than it already is in the HRU delineation process.

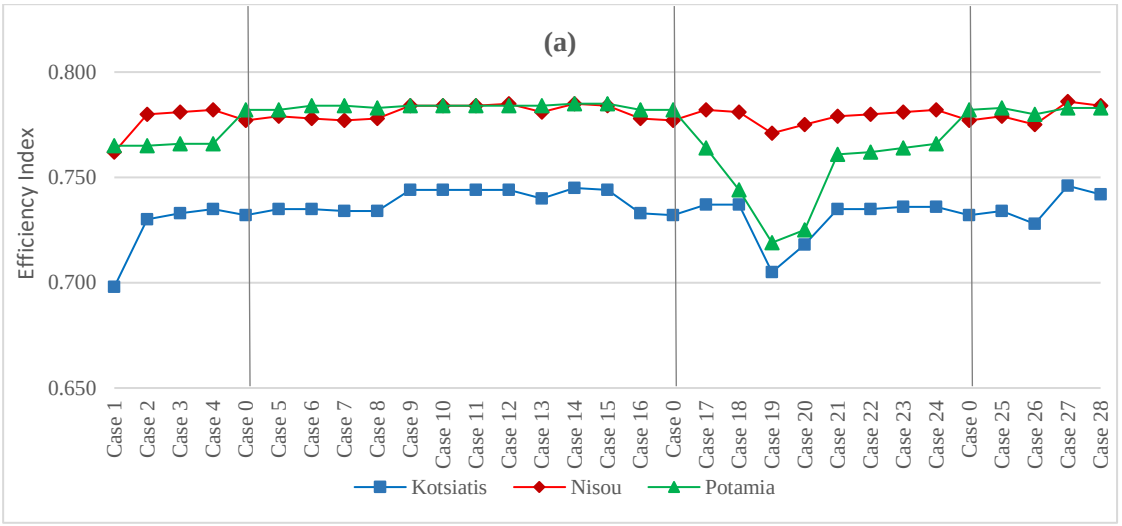
(a)
Efficiency Index
0.800
0.750
0.700
0.650
Case 1 Case 2 Case 3 Case 4 Case 0 Case 5 Case 6 Case 7 Case 8 Case 9 Case 10 Case 11 Case 12 Case 13 Case 14 Case 15 Case 16 Case 0 Case 17 Case 18 Case 19 Case 20 Case 21 Case 22 Case 23 Case 24 Case 0 Case 25 Case 26 Case 27 Case 28
Kotsiatis
Nisou
Potamia

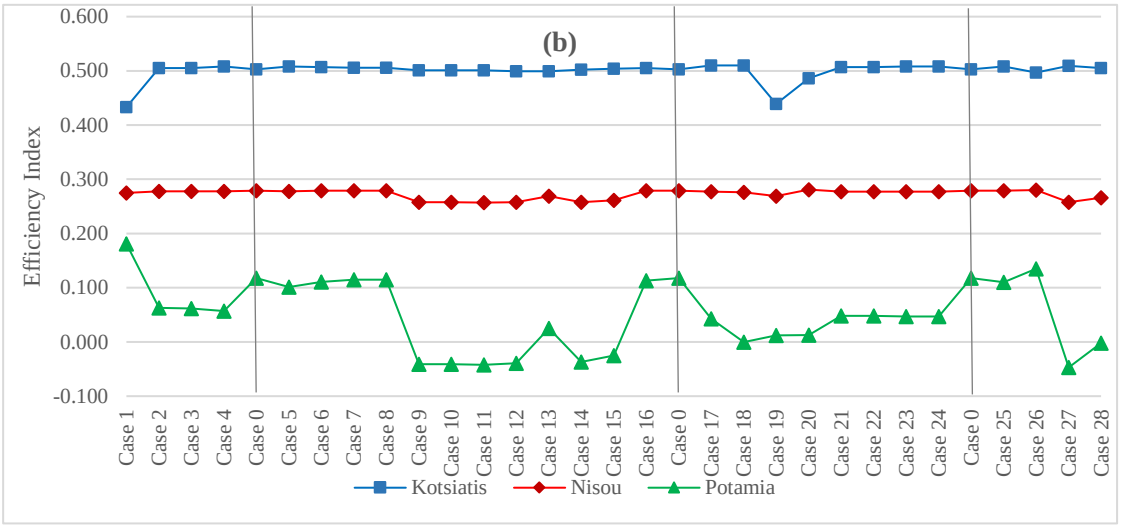
(b)
Efficiency Index
0.600
0.500
0.400
0.300
0.200
0.100
0.000
-0.100
Case 1 Case 2 Case 3 Case 4 Case 0 Case 5 Case 6 Case 7 Case 8 Case 9 Case 10 Case 11 Case 12 Case 13 Case 14 Case 15 Case 16 Case 0 Case 17 Case 18 Case 19 Case 20 Case 21 Case 22 Case 23 Case 24 Case 0 Case 25 Case 26 Case 27 Case 28
Kotsiatis
Nisou
Potamia

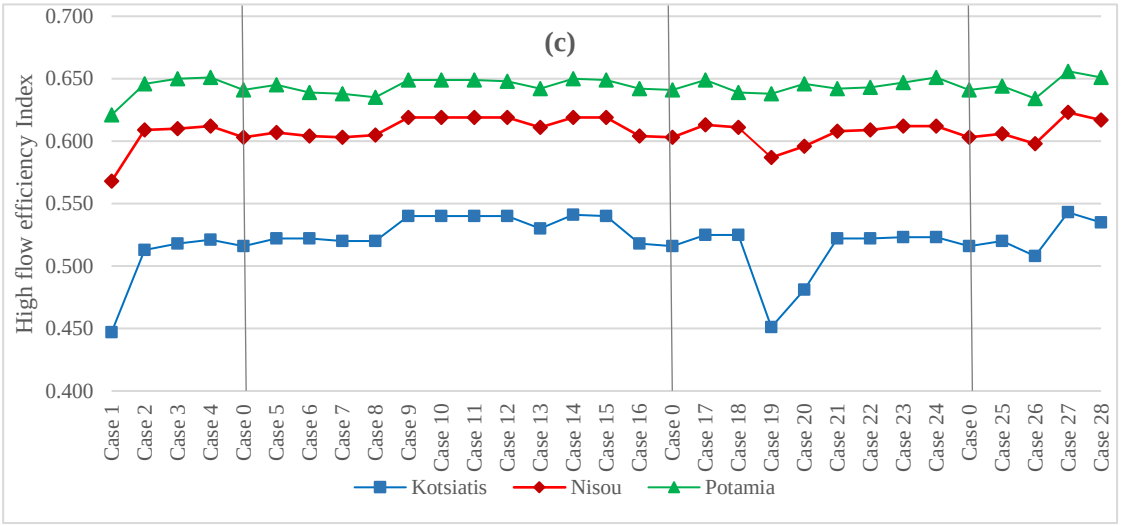
(c)
High flow efficiency Index
0.700
0.650
0.600
0.550
0.500
0.450
0.400
Case 1 Case 2 Case 3 Case 4 Case 0 Case 5 Case 6 Case 7 Case 8 Case 9 Case 10 Case 11 Case 12 Case 13 Case 14 Case 15 Case 16 Case 0 Case 17 Case 18 Case 19 Case 20 Case 21 Case 22 Case 23 Case 24 Case 0 Case 25 Case 26 Case 27 Case 28
Kotsiatis
Nisou
Potamia

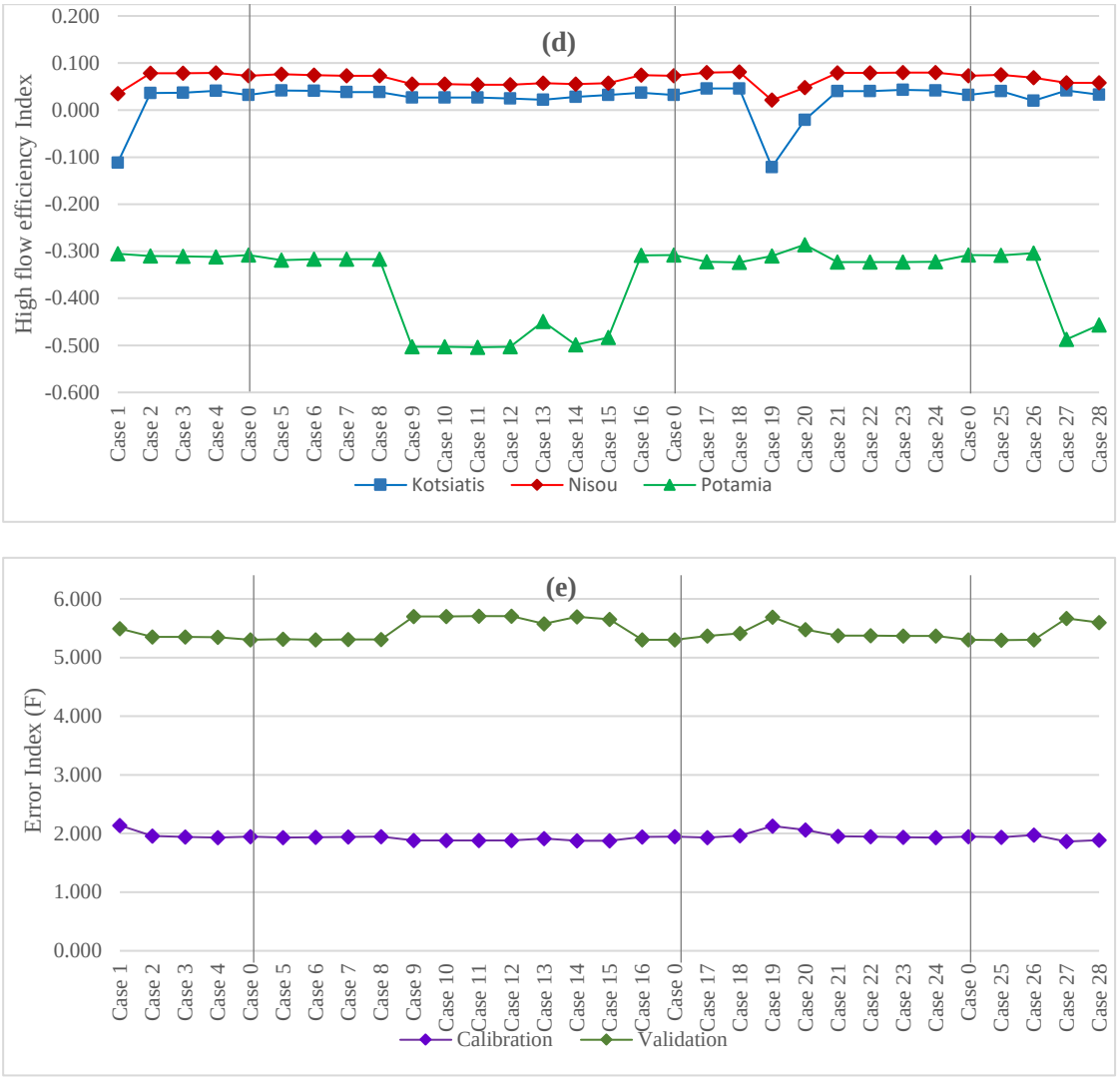


**Figure 43:** Yialias river basin sensitivity analysis results (a) model efficiency in calibration, (b) model efficiency in validation, (c) high flow efficiency in calibration, (d) high flow efficiency in validation, (e) overall error index in calibration and validation

**Table 28:** Yialias river basin sensitivity analysis results

| Case | Coefficient Combination | Kotsiatis | | | | Nisou | | | | Potamia | | | | Overall | |
|---|---|---|---|---|---|---|---|---|---|---|---|---|---|---|---|
| | | Efficiency | | High Flow Eff. | | Efficiency | | High Flow Eff. | | Efficiency | | High Flow Eff. | | Error Index (F) | |
| | $i_{PERM}$-$i_{VEG}$-$i_{SLOPE}$ | CAL | VAL | CAL | VAL | CAL | VAL | CAL | VAL | CAL | VAL | CAL | VAL | CAL | VAL |
| Case 0 | 9 - 6 - 3 | 0.732 | 0.503 | 0.516 | 0.032 | 0.777 | 0.279 | 0.603 | 0.073 | 0.782 | 0.118 | 0.641 | -0.308 | 1.949 | 5.303 |
| Case 1 | 7 - 7 - 4 | 0.698 | 0.433 | 0.447 | -0.112 | 0.762 | 0.275 | 0.568 | 0.035 | 0.765 | 0.181 | 0.621 | -0.305 | 2.139 | 5.493 |
| Case 2 | 7.5 - 6.75 - 3.75 | 0.730 | 0.505 | 0.513 | 0.036 | 0.780 | 0.278 | 0.609 | 0.078 | 0.765 | 0.063 | 0.646 | -0.310 | 1.957 | 5.350 |
| Case 3 | 8 - 6.5 - 3.5 | 0.733 | 0.505 | 0.518 | 0.037 | 0.781 | 0.278 | 0.610 | 0.078 | 0.766 | 0.062 | 0.650 | -0.311 | 1.942 | 5.351 |
| Case 4 | 8.5 - 6.25 - 3.25 | 0.735 | 0.508 | 0.521 | 0.041 | 0.782 | 0.278 | 0.612 | 0.079 | 0.766 | 0.057 | 0.651 | -0.312 | 1.933 | 5.349 |
| Case 5 | 9.5 - 5.75 - 2.75 | 0.735 | 0.508 | 0.522 | 0.042 | 0.779 | 0.278 | 0.607 | 0.076 | 0.782 | 0.101 | 0.645 | -0.319 | 1.930 | 5.314 |
| Case 6 | 10 - 5.5 - 2.5 | 0.735 | 0.507 | 0.522 | 0.041 | 0.778 | 0.279 | 0.604 | 0.074 | 0.784 | 0.111 | 0.639 | -0.317 | 1.938 | 5.305 |
| Case 7 | 10.5 - 5.25 - 2.25 | 0.734 | 0.506 | 0.520 | 0.038 | 0.777 | 0.279 | 0.603 | 0.073 | 0.784 | 0.115 | 0.638 | -0.317 | 1.944 | 5.306 |
| Case 8 | 11 - 5 - 2 | 0.734 | 0.506 | 0.520 | 0.038 | 0.778 | 0.279 | 0.605 | 0.073 | 0.783 | 0.115 | 0.635 | -0.317 | 1.945 | 5.306 |
| Case 9 | 11.5 - 4.75 - 1.75 | 0.744 | 0.501 | 0.540 | 0.027 | 0.784 | 0.258 | 0.619 | 0.055 | 0.784 | -0.041 | 0.649 | -0.503 | 1.880 | 5.703 |
| Case 10 | 12 - 4.5 - 1.5 | 0.744 | 0.501 | 0.540 | 0.027 | 0.784 | 0.258 | 0.619 | 0.055 | 0.784 | -0.041 | 0.649 | -0.503 | 1.880 | 5.703 |
| Case 11 | 12.5 - 4.25 - 1.25 | 0.744 | 0.501 | 0.540 | 0.027 | 0.784 | 0.257 | 0.619 | 0.054 | 0.784 | -0.042 | 0.649 | -0.504 | 1.880 | 5.707 |
| Case 12 | 13 - 4 - 1 | 0.744 | 0.499 | 0.540 | 0.025 | 0.785 | 0.258 | 0.619 | 0.054 | 0.784 | -0.039 | 0.648 | -0.503 | 1.880 | 5.706 |
| Case 13 | 10 - 4 - 4 | 0.740 | 0.499 | 0.530 | 0.022 | 0.781 | 0.269 | 0.611 | 0.057 | 0.784 | 0.025 | 0.642 | -0.449 | 1.912 | 5.577 |
| Case 14 | 9.75 - 4.5 - 3.75 | 0.745 | 0.502 | 0.541 | 0.028 | 0.785 | 0.258 | 0.619 | 0.055 | 0.785 | -0.037 | 0.650 | -0.499 | 1.875 | 5.693 |
| Case 15 | 9.5 - 5 - 3.5 | 0.744 | 0.504 | 0.540 | 0.032 | 0.784 | 0.261 | 0.619 | 0.057 | 0.785 | -0.025 | 0.649 | -0.483 | 1.879 | 5.654 |
| Case 16 | 9.25 - 5.5 - 3.25 | 0.733 | 0.505 | 0.518 | 0.037 | 0.778 | 0.279 | 0.604 | 0.074 | 0.782 | 0.113 | 0.642 | -0.309 | 1.943 | 5.301 |
| Case 17 | 8.75 - 6.5 - 2.75 | 0.737 | 0.510 | 0.525 | 0.046 | 0.782 | 0.277 | 0.613 | 0.080 | 0.764 | 0.043 | 0.649 | -0.322 | 1.930 | 5.366 |

| | | | | | | | | | | | | | | | |
|---|---|---|---|---|---|---|---|---|---|---|---|---|---|---|---|
| Case 18 | 8.5 - 7 - 2.5 | 0.737 | 0.510 | 0.525 | 0.046 | 0.781 | 0.276 | 0.611 | 0.081 | 0.744 | 0.000 | 0.639 | -0.324 | 1.963 | 5.411 |
| Case 19 | 8.25 - 7.5 - 2.25 | 0.705 | 0.439 | 0.451 | -0.121 | 0.771 | 0.269 | 0.587 | 0.021 | 0.719 | 0.012 | 0.638 | -0.310 | 2.129 | 5.690 |
| Case 20 | 8 - 8 - 2 | 0.718 | 0.486 | 0.481 | -0.021 | 0.775 | 0.281 | 0.596 | 0.048 | 0.725 | 0.013 | 0.646 | -0.286 | 2.059 | 5.479 |
| Case 21 | 10 - 7 - 1 | 0.735 | 0.507 | 0.522 | 0.040 | 0.779 | 0.277 | 0.608 | 0.079 | 0.761 | 0.048 | 0.642 | -0.323 | 1.953 | 5.372 |
| Case 22 | 9.75 - 6.75 - 1.5 | 0.735 | 0.507 | 0.522 | 0.040 | 0.780 | 0.277 | 0.609 | 0.079 | 0.762 | 0.048 | 0.643 | -0.323 | 1.949 | 5.372 |
| Case 23 | 9.5 - 6.5 - 2 | 0.736 | 0.508 | 0.523 | 0.043 | 0.781 | 0.277 | 0.612 | 0.080 | 0.764 | 0.047 | 0.647 | -0.323 | 1.937 | 5.368 |
| Case 24 | 9.25 - 6.25 - 2.5 | 0.736 | 0.508 | 0.523 | 0.042 | 0.782 | 0.277 | 0.612 | 0.080 | 0.766 | 0.047 | 0.651 | -0.322 | 1.930 | 5.368 |
| Case 25 | 8.75 - 5.75 - 3.5 | 0.734 | 0.508 | 0.520 | 0.040 | 0.779 | 0.279 | 0.606 | 0.075 | 0.783 | 0.110 | 0.644 | -0.309 | 1.934 | 5.297 |
| Case 26 | 8.5 - 5.5 - 4 | 0.728 | 0.497 | 0.508 | 0.020 | 0.775 | 0.280 | 0.598 | 0.069 | 0.780 | 0.135 | 0.634 | -0.304 | 1.977 | 5.303 |
| Case 27 | 8.25 - 5.25 - 4.5 | 0.746 | 0.509 | 0.543 | 0.042 | 0.786 | 0.258 | 0.623 | 0.058 | 0.783 | -0.047 | 0.656 | -0.487 | 1.863 | 5.667 |
| Case 28 | 8 - 5 - 5 | 0.742 | 0.505 | 0.535 | 0.033 | 0.784 | 0.266 | 0.617 | 0.058 | 0.783 | -0.002 | 0.651 | -0.457 | 1.888 | 5.597 |

### 5.6.2 Kouris river basin

The resulting statistical measures against the simulated runoffs are summarized in Table 29, whereas Figure 44 shows the variation of those measures at the three monitoring sites produced from the 28 different delineation cases. In can be seen that for the Loumata monitoring station, model efficiency in calibration varies from 65.6% for the simulations with the coefficient combination cases 9 to 15, to 67.7% for the simulation with the coefficient combination case 1, while overall all cases performance was almost the same. In validation, model efficiency varies from 70.3% for the simulations with the coefficient combination cases 7 to 15, to 73.5% for the simulation with the coefficient combination case 1, while, similarly with the calibration results, all cases performed the same. In terms of average bias in calibration, values vary from 0.4% for the simulation with the coefficient combination case 1, to 7% for the simulations with the coefficient combination cases 13 to 15, while in validation, average bias values varied from 0.4% for the simulation with the coefficient combination case 1, to 7.6% for the simulations with the coefficient combination cases 13 to 15. Overall, average bias results both in calibration and validation were very similar for all cases.

The variation in the results obtained for the Limnatis monitoring station was much more significant. Model efficiency in calibration varied from 66.5% for the simulation with the coefficient combination case 28, to 74.3% for the simulation with the coefficient combination case 8. In validation, model efficiency varies from 29.1% for the simulations with the coefficient combination cases 11 and 12, to 66.2% for the simulation with the coefficient combination cases 28, a completely opposite result of the calibration performance. In terms of average bias in calibration, values vary from -33.5% for the simulation with the coefficient combination case 28, to 0.1% and -0.1% for the simulations with the coefficient combination cases 16 and 6, respectively. In validation, average bias values varied from 30.2% for the simulations with the coefficient combination cases 11 and 12, to -0.7% for the simulation with the coefficient combination case 6. Overall, the results of the Limnatis monitoring station for both statistical measures for calibration and validation varied significantly.

The validation performance for the Kouris monitoring station in terms of model efficiency varied from 76.7% for the simulation with the coefficient combination case

24, to 82.7% for the simulations with the coefficient combination cases 8 and 12, while overall all cases performance was almost the same. In terms of average values, validation performance varied from-25.5% for the simulation with the coefficient combination case 1, to -0.6% for the simulation with the coefficient combination case 15, while overall the average bias result varied significantly, following the trend of the Limnatis monitoring station results.

Overall error index results followed the pattern of the Limnatis results, both in calibration and validation, producing opposite results, but with less variations. Overall best performance in calibration was achieved by simulations with coefficient cases 2 to 4, 13 to 16 and 26 and 27, while best performance in calibration was achieved by the default case 0. Not many conclusions can be drawn from these results, as there is no consistent pattern favoring specific coefficient combination cases. It is however evident that the overall model performance is mainly affected by the results of the Limnatis monitoring station, which leads to the conclusion that, although model statistical measures achieved satisfactory values (Table 25), perhaps the simulation needs further investigation.

**Table 29:** Kouris river basin sensitivity analysis results

| Case | Coefficient Combination | Loumata | | | | Limnatis | | | | Kouris | | | | Overall | |
|---|---|---|---|---|---|---|---|---|---|---|---|---|---|---|---|
| | | Efficiency | | Average Bias | | Efficiency | | Average Bias | | Efficiency | | Average Bias | | Error Index (F) | |
| | $i_{PERM}$-$i_{VEG}$-$i_{SLOPE}$ | CAL | VAL | CAL | VAL | CAL | VAL | CAL | VAL | CAL | VAL | CAL | VAL | CAL | VAL |
| Case 0 | 9 - 6 - 3 | 0.662 | 0.712 | 0.057 | 0.062 | 0.737 | 0.559 | -0.161 | 0.031 | - | 0.825 | - | -0.091 | 0.819 | 1.088 |
| Case 1 | 7 - 7 - 4 | 0.677 | 0.735 | 0.004 | 0.004 | 0.702 | 0.566 | -0.262 | -0.080 | - | 0.773 | - | -0.255 | 0.887 | 1.265 |
| Case 2 | 7.5 - 6.75 - 3.75 | 0.663 | 0.714 | 0.053 | 0.057 | 0.725 | 0.410 | -0.043 | 0.192 | - | 0.826 | - | -0.035 | 0.708 | 1.334 |
| Case 3 | 8 - 6.5 - 3.5 | 0.662 | 0.712 | 0.056 | 0.061 | 0.715 | 0.357 | -0.010 | 0.236 | - | 0.824 | - | -0.017 | 0.689 | 1.421 |
| Case 4 | 8.5 - 6.25 - 3.25 | 0.662 | 0.712 | 0.057 | 0.062 | 0.715 | 0.357 | -0.010 | 0.236 | - | 0.824 | - | -0.017 | 0.690 | 1.422 |
| Case 5 | 9.5 - 5.75 - 2.75 | 0.658 | 0.705 | 0.066 | 0.072 | 0.708 | 0.325 | -0.006 | 0.247 | - | 0.823 | - | -0.011 | 0.706 | 1.477 |
| Case 6 | 10 - 5.5 - 2.5 | 0.657 | 0.703 | 0.068 | 0.075 | 0.705 | 0.310 | -0.001 | -0.007 | - | 0.822 | - | 0.075 | 0.707 | 1.322 |
| Case 7 | 10.5 - 5.25 - 2.25 | 0.657 | 0.703 | 0.068 | 0.075 | 0.731 | 0.497 | -0.130 | 0.080 | - | 0.824 | - | -0.122 | 0.810 | 1.253 |
| Case 8 | 11 - 5 - 2 | 0.657 | 0.703 | 0.068 | 0.075 | 0.743 | 0.488 | -0.085 | 0.129 | - | 0.827 | - | -0.073 | 0.753 | 1.259 |
| Case 9 | 11.5 - 4.75 - 1.75 | 0.656 | 0.703 | 0.069 | 0.075 | 0.709 | 0.293 | 0.043 | 0.300 | - | 0.822 | - | -0.008 | 0.747 | 1.565 |
| Case 10 | 12 - 4.5 - 1.5 | 0.656 | 0.703 | 0.069 | 0.075 | 0.709 | 0.293 | 0.043 | 0.300 | - | 0.824 | - | -0.017 | 0.747 | 1.572 |
| Case 11 | 12.5 - 4.25 - 1.25 | 0.656 | 0.703 | 0.069 | 0.075 | 0.709 | 0.291 | 0.044 | 0.302 | - | 0.824 | - | -0.016 | 0.748 | 1.575 |
| Case 12 | 13 - 4 - 1 | 0.656 | 0.703 | 0.069 | 0.075 | 0.709 | 0.291 | 0.044 | 0.302 | - | 0.827 | - | -0.060 | 0.748 | 1.616 |
| Case 13 | 10 - 4 - 4 | 0.656 | 0.703 | 0.070 | 0.076 | 0.722 | 0.353 | 0.012 | 0.255 | - | 0.826 | - | -0.034 | 0.704 | 1.483 |
| Case 14 | 9.75 - 4.5 - 3.75 | 0.656 | 0.703 | 0.070 | 0.076 | 0.722 | 0.353 | 0.012 | 0.255 | - | 0.826 | - | -0.032 | 0.704 | 1.481 |
| Case 15 | 9.5 - 5 - 3.5 | 0.656 | 0.703 | 0.070 | 0.076 | 0.705 | 0.310 | 0.006 | 0.256 | - | 0.822 | - | -0.006 | 0.715 | 1.503 |
| Case 16 | 9.25 - 5.5 - 3.25 | 0.657 | 0.705 | 0.068 | 0.074 | 0.708 | 0.324 | 0.001 | 0.250 | - | 0.823 | - | -0.010 | 0.704 | 1.482 |
| Case 17 | 8.75 - 6.5 - 2.75 | 0.661 | 0.711 | 0.058 | 0.063 | 0.715 | 0.356 | -0.010 | 0.236 | - | 0.824 | - | -0.016 | 0.692 | 1.424 |

| | | | | | | | | | | | | | | | |
|---|---|---|---|---|---|---|---|---|---|---|---|---|---|---|---|
| Case 18 | 8.5 - 7 - 2.5 | 0.662 | 0.712 | 0.057 | 0.062 | 0.710 | 0.519 | -0.212 | -0.014 | - | 0.806 | - | -0.180 | 0.897 | 1.219 |
| Case 19 | 8.25 - 7.5 - 2.25 | 0.662 | 0.712 | 0.056 | 0.061 | 0.711 | 0.540 | -0.223 | -0.029 | - | 0.800 | - | -0.201 | 0.906 | 1.239 |
| Case 20 | 8 - 8 - 2 | 0.662 | 0.712 | 0.056 | 0.061 | 0.711 | 0.538 | -0.221 | -0.026 | - | 0.800 | - | -0.199 | 0.904 | 1.236 |
| Case 21 | 10 - 7 - 1 | 0.662 | 0.711 | 0.057 | 0.062 | 0.710 | 0.516 | -0.214 | -0.013 | - | 0.807 | - | -0.179 | 0.899 | 1.220 |
| Case 22 | 9.75 - 6.75 - 1.5 | 0.662 | 0.711 | 0.057 | 0.062 | 0.710 | 0.517 | -0.215 | -0.014 | - | 0.806 | - | -0.180 | 0.900 | 1.222 |
| Case 23 | 9.5 - 6.5 - 2 | 0.658 | 0.705 | 0.066 | 0.072 | 0.735 | 0.492 | -0.120 | 0.092 | - | 0.827 | - | -0.050 | 0.793 | 1.190 |
| Case 24 | 9.25 - 6.25 - 2.5 | 0.657 | 0.705 | 0.067 | 0.073 | 0.737 | 0.423 | -0.026 | 0.216 | - | 0.767 | - | 0.063 | 0.699 | 1.457 |
| Case 25 | 8.75 - 5.75 - 3.5 | 0.658 | 0.706 | 0.066 | 0.072 | 0.718 | 0.370 | -0.025 | 0.215 | - | 0.824 | - | -0.016 | 0.715 | 1.403 |
| Case 26 | 8.5 - 5.5 - 4 | 0.658 | 0.706 | 0.066 | 0.072 | 0.718 | 0.370 | -0.026 | 0.214 | - | 0.824 | - | -0.016 | 0.716 | 1.402 |
| Case 27 | 8.25 - 5.25 - 4.5 | 0.658 | 0.706 | 0.066 | 0.072 | 0.718 | 0.372 | -0.030 | 0.210 | - | 0.824 | - | -0.019 | 0.720 | 1.399 |
| Case 28 | 8 - 5 - 5 | 0.664 | 0.714 | 0.052 | 0.056 | 0.665 | 0.622 | -0.335 | -0.201 | - | 0.786 | - | -0.236 | 1.058 | 1.371 |

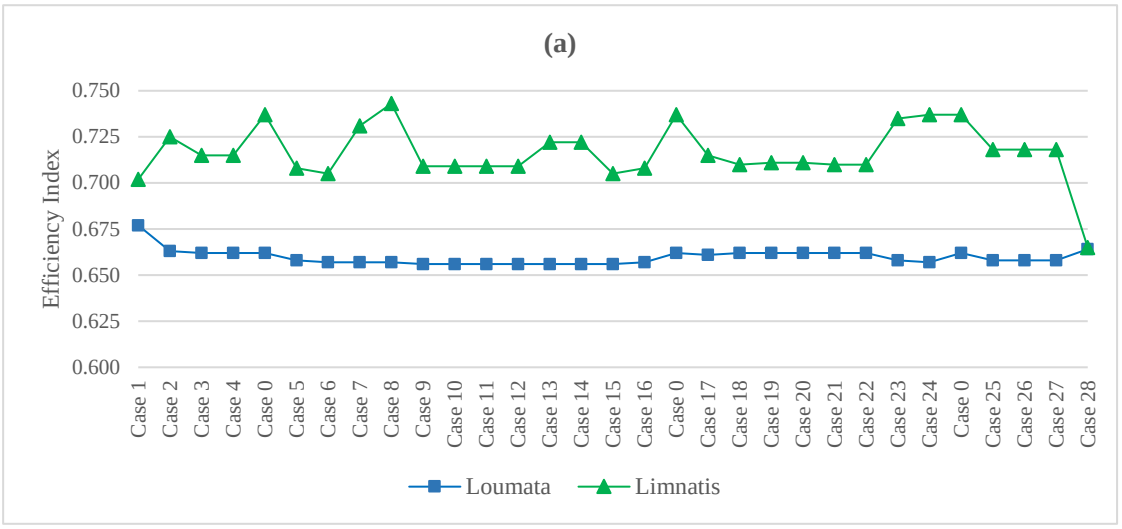
(a)
Efficiency Index
0.750
0.725
0.700
0.675
0.650
0.625
0.600
Case 1 Case 2 Case 3 Case 4 Case 0 Case 5 Case 6 Case 7 Case 8 Case 9 Case 10 Case 11 Case 12 Case 13 Case 14 Case 15 Case 16 Case 0 Case 17 Case 18 Case 19 Case 20 Case 21 Case 22 Case 23 Case 24 Case 0 Case 25 Case 26 Case 27 Case 28
Loumata
Limnatis

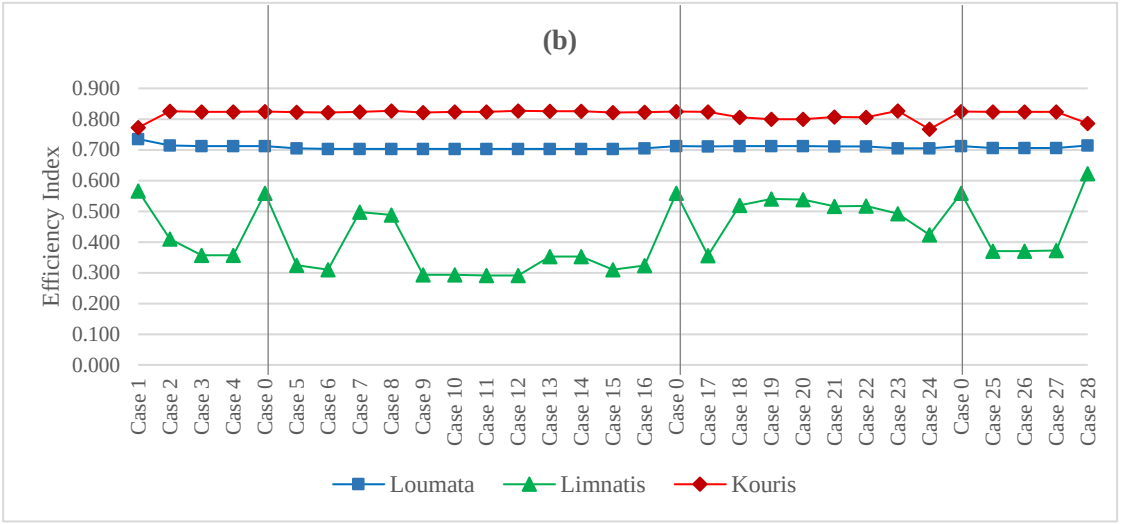
(b)
Efficiency Index
0.900
0.800
0.700
0.600
0.500
0.400
0.300
0.200
0.100
0.000
Case 1 Case 2 Case 3 Case 4 Case 0 Case 5 Case 6 Case 7 Case 8 Case 9 Case 10 Case 11 Case 12 Case 13 Case 14 Case 15 Case 16 Case 0 Case 17 Case 18 Case 19 Case 20 Case 21 Case 22 Case 23 Case 24 Case 0 Case 25 Case 26 Case 27 Case 28
Loumata
Limnatis
Kouris

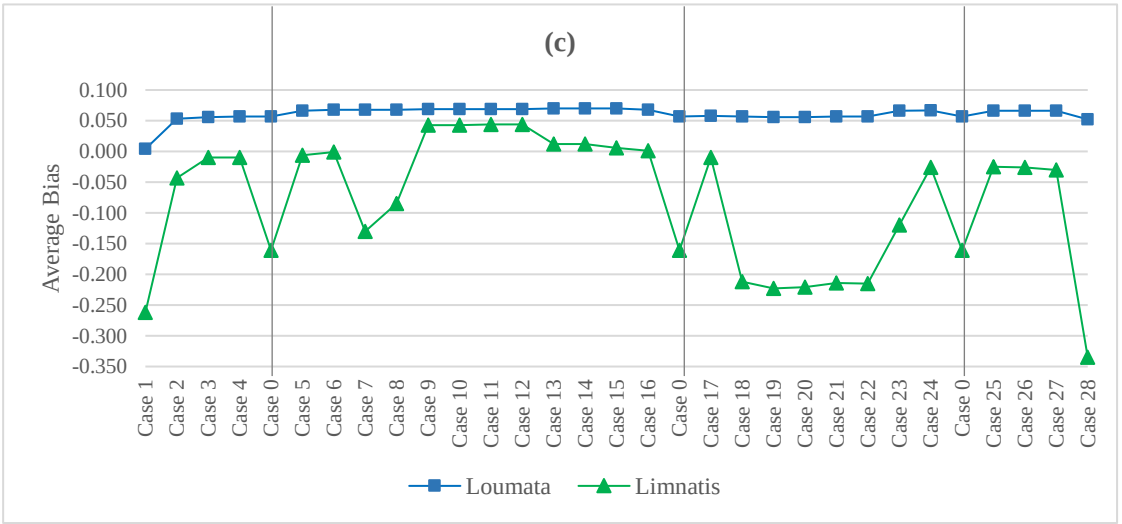
(c)
Average Bias
0.100
0.050
0.000
-0.050
-0.100
-0.150
-0.200
-0.250
-0.300
-0.350
Case 1 Case 2 Case 3 Case 4 Case 0 Case 5 Case 6 Case 7 Case 8 Case 9 Case 10 Case 11 Case 12 Case 13 Case 14 Case 15 Case 16 Case 0 Case 17 Case 18 Case 19 Case 20 Case 21 Case 22 Case 23 Case 24 Case 0 Case 25 Case 26 Case 27 Case 28
Loumata
Limnatis

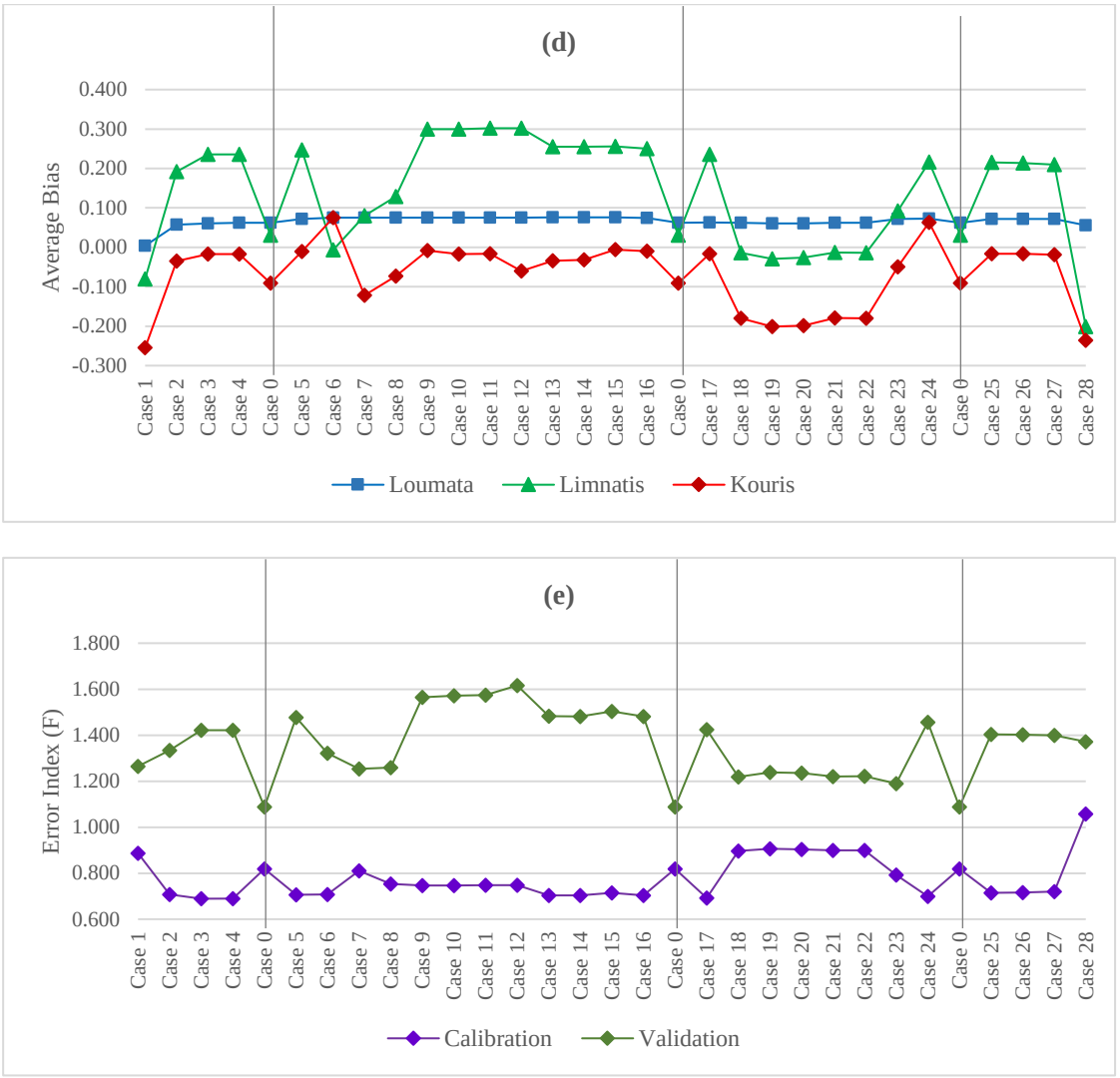


**Figure 44:** Kouris river basin sensitivity analysis results (a) model efficiency in calibration, (b) model efficiency in validation, (c) average bias in calibration, (d) average bias in validation, (e) overall error index in calibration and validation

# CONCLUSIONS

In the context of distributed hydrological modelling, the configuration of HRUs is subject to the conflict between two topics: the accuracy in the representation of process heterogeneity, dictating the required number of HRUs; and model parsimony, associated with the number of parameters to be inferred through calibration. To reduce the subjectivity introduced by the definition of a small number of HRUs in a parsimonious modelling structure, this research provides a systematic and physically-consistent procedure for formulating HRUs in the context of hybrid semi-distributed hydrological modeling, based on the widespread known curve number concept. Key innovations of this work are:

(1) the formulation of CN maps within a GIS, based on a proposed relationship to estimate the representative value of CN, accounting for three major physiographic characteristics of the river basin, namely soil permeability, vegetation density and drainage capacity, within a GIS;
(2) the use of these maps as input layers for delineating HRUs within hydrological models of various levels of complexity;
(3) the use of CN classes within model parameterization as a guide for configuring a specified number and spatial extent of HRUs, in semi-distributed models.

The raster map of CN values may have several applications, since this parameter is commonly used in watershed hydrology. For instance, it can provide information on potential maximum soil moisture retention at the grid-scale, in the context of the well-known NRCS-CN model. However, the emphasis here was on the use of CN data as a proxy for delineating HRUs in the context of fully- or semi-distributed hydrological models of any structure, provided that parameters associated with the modelled processes are mapped at the HRU scale. As the level of detail of the model parameterization depends on the number of HRUs, one can determine a specific number of CN classes to be used as the basis for HRU configuration, through aggregating cells of similar CN values.

A very important issue highlighted is that the model complexity, expressed in terms of the number of CN classes and, consequently, the number of HRUs, should be consistent with the context of available hydrological information. Therefore, a general

recommendation is to provide as many HRUs as the number of available discharge observation stations in the basin. This ensures a satisfactory balance between process realism and modelling parsimony and also allows taking advantage of all available information in order to avoid over-parameterized schemes.

The CN-based approach for HRU delineation was tested in HYDROGEIOS modelling framework, built on the HRU concept, following the union of layers delineation approach. A shortcoming of this method is the configuration of a specific number of HRUs, i.e., the product of different layer classes. In contrast, in the CN-based delineation, the number of HRUs is determined a priori. Therefore, the new approach is more objective, more flexible and, ultimately, more parsimonious. Furthermore, it allows explaining the HRU response and associated parameter values in terms of CNs; for instance, it is anticipated that an area with low CN values will generate less surface runoff, and vice versa. The correspondence of an HRU's response with CN is very advantageous, since the user can easily recognize whether the model parameters are physically consistent or not, which in return facilitates the evaluation of the model robustness both in terms of goodness-of-fit and physical representation.

The new CN approach for HRU delineation was demonstrated in the hydrological simulation of Nedontas River Basin, Greece, where parameterizations of different levels of complexity were employed within HYDROGEIOS. In this context, two calibration experiments are employed.

In the first experiment, the CN map of the basin was used to delineate from one up to five HRUs, thus providing configurations of varying complexity. The efficiency and high flow efficiency values achieved by the simulation with the three HRUs were higher, further confirming the fundamental hypothesis that the best compromise, in terms of model performance against computational effort, is ensured by considering the parameterization with three HRUs, which equals the number of available hydrographs.

The proposed CN-based method was then contrasted with two other well-established HRU delineation strategies, i.e., the unique combination and the union of layers. Results showed that the optimal performance was achieved by the most parsimonious parameterization, i.e., the CN approach with three HRUs, as dictated by the number of monitoring stations across the basin. Experiments showed that the calibration effort (in terms of time needed for manual interventions, as well as the number of individual

optimizations considering small sub-sets of parameters), for achieving acceptable model performance and ensuring realistic hydrological behavior, varied markedly with the different HRU configuration approaches. An important conclusion is that the CN approach resulted in optimal parameter values across the three HRUs that are in agreement with their physical interpretation, as also quantified in terms of associated CN classes. Hence, it is anticipated that through a proper classification of CNs, the user will be able to determine a priori a reasonable and relatively narrow range of feasible parameter bounds, thus substantially facilitating the calibration effort.

The CN approach is further tested in the hydrological simulations of Yialias and Kouris river basins, Cyprus, two watersheds of different sizes that vary in terms of physiographic characteristics and meteorological stresses, ideal to evaluate the performance of the method in diverse environments. Two verification experiments were performed.

Initially, different classification schemes were implemented in creating the CN sub-sets to delineate the final HRUs in an attempt to emphasize the advantage of the association of each HRU response to the corresponding parameter values in terms of CN, thus, allowing for a more efficient and objective model set up, assuring the user of the parameters physical meaning and realistic representation of the hydrological behaviour of the basin. Model performance was very satisfactory in calibration but less satisfactory in validation, with the simulations preserving the overall behaviour of the hydrograph but underestimating a number of high flow events in validation. The resulted HRU parameters demonstrated the advantage of the CN approach in being less subjective and more parsimonious, by justifying each HRU runoff response and associated parameter values in terms of CNs; i.e. a low CN value indicates areas of the basin with very high water permeability, dense vegetation and very low drainage capacity, which leads to minimum runoff, while a high CN value indicates areas of the basin with very low water permeability, no vegetation and a very high drainage capacity, leading to higher runoff values. The correspondence of an HRU's response with CN is very advantageous, since the user can easily recognize whether the model parameters are physically consistent or not, and, consequently, evaluate the model robustness not only in terms of goodness-of-fit in validation, but also according to its physical grounds.

In the second experiment the sensitivity of the proposed equation that estimates the CN value was examined, by varying the coefficients of the three indices, (permeability, vegetation and slope), forming the equation, to provide further insight as to what impact each index has on the HRU delineation processes, and thus, model performance. Based on the 28 coefficient combination cases, 28 different CN-parameter maps were produced for each river basin, which were then used to delineate three HRUs in each case. For the Yialias case study, cases were the permeability and vegetation indices were very similar produced the highest overall error index, providing further that water permeability has a greater impact on the hydrologic response of a river basin compared to vegetation, and should therefore be weighted higher than it already is in the HRU delineation process. For the Kouris case study, the overall model performance was dictated by the mainly unstable performance of Limnatis monitoring station throughout the cases. Therefore, no insights to the index weight impact were given.

While the Kouris case study could be investigated further, future research steps could involve testing this approach in a representative number of river basins varying in physiographic characteristics as well as climatic conditions. This should provide the opportunity to test and potentially improve the applicability of the approach to global level. Moreover, the approach should be implemented in different modelling schemes, besides HYDROGEIOS, to test its adaptability.

# REFERENCES


Abbott, M.B. et al., 1986a. An introduction to the European Hydrological System — Systeme Hydrologique Europeen, “SHE”, 1: History and philosophy of a physically-based, distributed modeling system. *Journal of Hydrology*, 87(1–2), pp.45–59.

Abbott, M.B. et al., 1986b. An introduction to the European Hydrological System — Systeme Hydrologique Europeen, “SHE”, 2: Structure of a physically-based, distributed modelling system. *Journal of Hydrology*, 87(1–2), pp.61–77.

Agrawal, R.K. & Singh, J.K., 2003. Application of a genetic algorithm in the development and optimization of a non-linear dynamic runoff model. *Biosystems Engineering*, 86, pp.87–95.

Ajami, N.K. et al., 2004. Calibration of a semi-distributed hydrologic model for streamflow estimation along a river system. *Journal of Hydrology*, 298(1–4), pp.112–135.

Al-Qurashi, A., Macintyre, N. & Wheater, H., 2007. Rainfall-runoff modelling using KINEROS model. *Geophysical Research Abstracts*, 9(804).

Aqauveo, 2014. Watershed Modeling System (WMS).

AquaTerra, 2011. Development of WinHSPF - An Independent, Fully Integrated Component of a Compehensive Modelling System. *AquaTerra Concultants*.

Arabi, M. et al., 2006. Role of Watershed Subdivision on Modeling the Effectiveness of Best Management Practices With Swat 1. *Journal of the American Water Resources Association*, 45268, pp.513–528.

Argent, R.M. et al., 2007. *E2 Catchment Modelling Software*, Australia.

Arnold, J.G., Allen, P.M. & Bernhardt, G., 1993. A comprehensive surface-groundwater flow model. *Journal of Hydrology*, 142(1–4), pp.47–69.

Baginska, B., Milne-Home, W. & Cornish, P.S., 2003. Modelling nutrient transport in Currency Creek, NSW with AnnAGNPS and PEST. *Environmental Modelling & Software*, 18(8–9), pp.801–808.

Bai, H. et al., 2004. Applicability of ANSWERS-2000 to estimate sediment and runoff

from Canagagigue Creek watershed in Ontario.

Banasik, K., Rutkowska, A. & Kohnová, S., 2014. Retention and curve number variability in a small agricultural catchment: The probabilistic approach. *Water*, 6, pp.1118–1133.

Bärlund, I. et al., 2007. Assessing the SWAT model performance in the evaluation of management actions for the implementation of the water framework directive in a Finnish catchment. *Environmental Modelling & Software*, 22(5), pp.719–724.

Bathurst, J.C., 1986. Sensitivity analysis of the Systeme Hydrologique Europeen for an upland catchment. *Journal of Hydrology*, 87(1–2), pp.103–123.

Beasly, D.B., Huggins, L.F. & Monke, E.J., 1980. ANWERS: A model for watershed planning. *Transactions of the ASAE*, 23(4), pp.938–944.

Bennie, D.T. et al., 1997. Occurrence of alkylphenols and alkylphenol mono- and diethoxylates in natural waters of the Laurentian Great Lakes basin and the upper St. Lawrence River. *Science of the Total Environment*, pp.263–275.

Beven, K., 2006. A manifesto for the equifinality thesis. *Journal of Hydrology*, 320(1–2), pp.18–36.

Beven, K., 2001. How far can we go in distributed hydrological modelling? *Hydrology and Earth System Sciences*, 5(1), pp.1–12.

Beven, K.J., 1989. Changing ideas in hydrology – The case of physicallybased models. *Journal of Hydrology*, 105(1–2), pp.157–172.

Beven, K.J., 1993. Prophecy, reality and uncertainty in distributed hydrological modelling. , 16. Available at: http://www.sciencedirect.com/science/journal/03091708.

Beven, K.J., 2000. *Rainfall-runoff modeling: the primer*, New York: John Wiley and Sons Ltd.

Beven, K.J.. & Binley, A.M., 1992. The future of distributed models: Model calibration and uncertainty prediction. *Hydrological Processes*, 6(3), pp.279–298.

Bingner, R.L. et al., 1997. Effect of watershed subdivision on simulation runoff and fine sediment yield. *Transactions of the Americal Society of Agricultural Engineers*,

40(5), pp.1329–1335.

Bogaart, P.W. & Troch, P.A., 2006. Curvature distribution within hillslopes and catchments and its effect on the hydrological response. *Hydrology and Earth System Sciences*, 10(6), pp.925–936.

Bongartz, K., 2003. Applying different spatial distribution and modelling concepts in three nested mesoscale catchments of Germany. *Physics and Chemistry of the Earth*, 28(33–36), pp.1343–1349.

Borah, D.K. & Bera, M., 2003. Watershed-scale hydrologic and nonpoint source pollution models: Review of mathematical bases. *Transactions of the ASAE*, 46(6), pp.1553–66.

Borah, D.K., Demissie, M. & Keefer, L., 2002. AGNPS-based assessment of the impact of BMPs on nitrate-nitrogen discharging into an Illinois water supply lake. *International Water Resources Association*, 27(2), pp.255–265.

Bosch, D. et al., 1998. Evaluation of the AnnAGNPS water quality model. ASAE Paper No.982195. Presented at ASAE Annual Meeting, St. Joseph, Mich., ASAE.

Bouraoui, F. et al., 2005. Application of the SWAT model on the Medjerda River basin. *Application of the SWAT model on the Medjerda River basin*, 30(8–10), pp.497–507.

Boyd, M.J., Pilgrim, D.H. & Cordery, I., 1979. A storage routing model based on catchment geomorphology. *Journal of Hydrology*, 42(3–4), pp.209–230.

Boyle, D.P. et al., 2001. Towards improved streamflow forecasts: The value of semidistributed modeling. *Water Resources Research*, 37(11), pp.2749–2759.

Boyle, D.P., Gupta, H. V. & Sorooshian, S., 2000. Toward improved calibration of hydrologic models: combining the strengths of manual and automatic methods. *Water Resources Research*, 36(12), pp.3663–3674.

Bruneau, P. et al., 1995. Sensitivity to space and time resolution of a hydrological model using digital elevation data. *Hydrological Processes*, 9(1), pp.69–81.

Butts, M.B. et al., 2004. An evaluation of the impact of model structure on hydrological uncertainty for streamflow simulation. *Journal of hydrology*, 298, pp.242–266.

Chaplot, V. et al., 2004. Predicting water, sediment and NO3-N loads under scenarios of land-use and management practice. *Water, Air, and Soil Pollution*, 154(1), pp.271–293.

Chen, E. & Mackay, D.S., 2004. Effects of distribution-based parameter aggregation on a spatially distributed agricultural nonpoint source pollution model. *Journal of Hydrology*, 295(1–4), pp.211–224.

Cho, H. & Olivera, F., 2009. Effect of the Spatial Variability of Land Use, Soil Type, and Precipitation on Streamflows in Small Watersheds. *Journal of the American Water Resources Association*, 45(3), pp.673–686.

Cho, J. et al., 2010. Effect of watershed subdivision and filter width on swat simulation of a coastal plain watershed1. *Journal of the American Water Resources Association*, 46(3), pp.586–602.

Christensen, F.D., 2004. Coupling between the river basin management model (MIKE BASIN) and the 3D hydrological model (MIKE SHE) with use of OpenMI system. In *6th International Conference on Hydroinformatics*. Singapore: Danish Hydraul Institude.

Connolly, R.D., Silburn, D.M. & Ciesiolka, C.A.A., 1997. Distributed parameter hydrology model (ANSWERS) applied to a range of catchment scales using rainfall simulator data. III. Application to a spatially complex catchment. *Journal of Hydrology1997*, 193(1–4), pp.183–203.

Croley, T.E. & He, C., 2005a. Distributed-parameter large basin runoff model. I: Model development. *Journal of Hydrologic Engineering*, 10(3), pp.173–181.

Croley, T.E. & He, C., 2005b. Great Lakes spatially distributed watershed model of water and materials runoff. Ecological Environment. In *International Conference on Poyang Lake Wetland Ecological Environment*. Jiangxi Normal University, Nanchang, Jiangxi, P.R. China, p. 12.

Daniel, E.B. et al., 2011. Watershed modeling and its applications : A state-of-the-art review. *The Open Hydrology Journal*, 5(5), pp.26–50.

Das, S. et al., 2004. Application of AnnAGNPS Model under Ontario condition.

Dehotin, J. & Braud, I., 2008. Which spatial discretization for distributed hydrological

models? Proposition of a methodology and illustration for medium to large scale catchments. *Hydrology and Earth System Sciences*, 12, pp.769–796.

Demetriou, C. & Punthakey, J.F., 1999. Evaluating sustainable groundwater management options using the MIKE SHE integrated hydrogeological modelling package. *Environmental Modelling & Software*, 14(2), pp.129–140.

Deshmukh, D.S. et al., 2013. Estimation and comparison of curve numbers based on dynamic land use land cover change, observed rainfall-runoff data and land slope. *Journal of Hydrology*, 492, pp.89–101.

Dillaha, T.A. et al., 2004. ANSWERS-2000: Agricultural Non-Point Source Water Quality Models, Their Use and Application.

Donigian, A.S.J., Bicknell, B.R. & Imhoff, J.C., 1995. Hydrological simulation program - FORTRAN (HSPF). In V. P. Singh, ed. *Computer models of watershed hydrology*. Highlands Ranch, Colorado: Water Research Publications.

Donnelly, C., Andersson, J.C.M. & Arheimer, B., 2016. Using flow signatures and catchment similarities to evaluate the E-HYPE multi-basin model across Europe. *Hydrological Sciences Journal*, 61(2), pp.255–273.

Downer, C.W. & Ogden, F.L., 2004. GSSHA: A model for simulating diverse streamflow generating processes. *Journal of Hydrologic Engineering*, 9(3), pp.161–174.

Du, B. et al., 2005. Development and application of SWAT to landscapes with tiles and potholes. *Transactions of the ASAE*, 48(3), pp.1121–1133.

Duru, J.O. & Hjelmfelt, J.A.T., 1994. Investigating prediction capability of HEC-1 and KINEROS kinematic wave runoff models. *Journal of Hydrology*, 157(1–4), pp.87–103.

Eckhardt, K. & Arnold, J.G., 2001. Automatic calibration of a distributed catchment model. *Journal of Hydrology*, 251(1–2), pp.103–109.

Eckhardt, K. & Ulbrich, U., 2003. Potential impacts of climate change on groundwater recharge and streamflow in a central European low mountain range. *Journal of Hydrology*, 284(1–4), pp.244–252.

Efstratiadis, A., Koukouvinos, A., Michaelidi, E., et al., 2014. *Description of regional*

*approaches for the estimation of characteristic hydrological quantities, DEUCALION - Assessment of flood flows in Greece under conditions of hydroclimatic variability: Development of physically-established conceptual-probabilistic*, Department of Water Resources and Environmental Engineering - National Technical University of Athens, National Observatory of Athens, Athens.

Efstratiadis, A., Koussis, A.D., et al., 2014. Flood design recipes vs. reality: can predictions for ungauged basins be trusted? *Natural Hazards and Earth System Science*, 14(6), pp.1417–1428.

Efstratiadis, A. et al., 2013. Hydrometeorological network for flood monitoring and modeling. In *Proceedings of First International Conference on Remote Sensing and Geoinformation of Environment*. Paphos, Cyprus: (SPIE), Society of Photo-Optical Instrumentation Engineers, 8795, 10-1–10-10.

Efstratiadis, A., Koukouvinos, A., Dimitriadis, P., et al., 2014. *Theoretical documentation of hydrological-hydraulic simulation model, DEUCALION - Assessment of flood flows in Greece under conditions of hydroclimatic variability: Development of physically-established conceptual-probabilistic framework and computational*, Department of Water Resources and Environmental Engineering - National Technical University of Athens, National Observatory of Athens, Athens.

Efstratiadis, A. & Koutsoyiannis, D., 2002. An evolutionary annealing-simplex algorithm for global optimisation of water resource systems. In *Proceedings of the Fifth International Conference on Hydroinformatics*. Cardiff, UK: International Water Association, pp. 1423–1428.

Efstratiadis, A. & Koutsoyiannis, D., 2010. One decade of multiobjective calibration approaches in hydrological modelling: a review. *Hydrological Sciences Journal*, 55(1), pp.58–78.

Efstratiadis, a. et al., 2008. HYDROGEIOS: a semi-distributed GIS-based hydrological model for modified river basins. *Hydrology and Earth System Sciences*, 12(4), pp.989–1006.

ERDC, 2013. GSSHA - Gridded Surface Subsurface Hydrologic Analysis. *Engineer Research and Development Center, Coastal and Hydraulics Laboratory*.

Fatichi, S. et al., 2016. An overview of current applications, challenges, and future trends in distributed process-based models in hydrology. *Journal of Hydrology*, 537, pp.45–60.

Feldman, A.D., 1995. HEC-1 flood hydrograph package. In V. P. Singh, ed. *Computer models of watershed hydrology*. Highlands Ranch, Colorado: Water Resources Publications, p. 1144.

Fenicia, F. et al., 2014. Catchment Properties, Function, and Conceptual Model Representation: Is there a Correspondence? *Hydrological Processes*, 28(4), pp.2451–2467.

Fenicia, F. et al., 2016. From spatially variable streamflow todistributed hydrological models: Analysis of key modeling decisions. *Water Resources Research*, 52(2), pp.1–36.

FitzHugh, T.. & Mackay, D.., 2001. Impact of subwatershed partitioning on modeled source-and transport-limited sediment yields in an agricultural nonpoint source pollution model. *Journal of Soil and Water Conservation*, 56(2), pp.137–143.

FitzHugh, T.W. & Mackay, D.S., 2000. Impacts of input parameter spatial aggregation on an agricultural nonpoint source pollution model. *Journal of Hydrology*, 236(1–2), pp.35–53.

Flügel, W.-A., 1997. Combining GIS with regional hydrological modelling using hydrological response units (HRUs): An application from Germany. *Mathematics and Computers in Simulation*, 43, pp.297–304.

Flügel, W.-A., 1995. Delineating hydrological response units by geographical information system analyses for regional hydrological modelling using PRMS/MMS in the drainage basin of the river Brosl, Germany. *Hydrological Processes*, 9(1994), pp.423–436.

Foster, G.R. & Meyer, L.D., 1972. Transport of soil particles by shallow flow. *Transactions of the ASAE*, 15(1), pp.99–102.

Freer, J., Beven, K.J. & Ambroise, B., 1996a. Bayesian estimation of uncertainty in runoff prediction and the value of data: An application of the GLUE approach. *Water Resources Management*, 32(7), pp.2161–2173.

Freer, J., Beven, K.J. & Ambroise, B., 1996b. Bayesian estimation of uncertainty in runoff prediction and the value of data: an application of the GLUE approach,. *Water Resources Research*, 32(7), pp.2161–2173.

Garen, D.C. & Moore, D.S., 2005. Curve number hydrology in water quality modeling: uses, abuses, and future directions. *Journal of the American Water Resources Association*, 41(1), pp.377–388.

Gassman, P.W., 2008. *A Simulation Assessment of the Boone River Watershed: Baseline Calibration/Validation Results and Issues, and Future Needs*. Iowa State University, Ameas, Iowa.

Gassman, P.W. et al., 2007. The soil and water assessment tool: Historical development, applications, and future research directions. *Transactions of the Asabe*, 50(4), pp.1211–1250.

Gebremeskel, S., Rudra, R.P. & Gharabaghi, B., 2005. Assessing the performance of various hydrological models in the Canadian Great Lakes Basin. In P. W. Gassmann, ed. *Watershed management to meet water quality standards and emerging TMDL (Total Maximum Daily Load)*. Atlanta, GA: ASAE Publication No. 701P0105.

Gharari, S. et al., 2011. Hydrological landscape classification: investigating the performance of HAND based landscape classifications in a central European meso-scale catchment. *Hydrology and Earth System Sciences*, 15(11), pp.3275–3291.

Giandotti, M., 1934. Previsione delle piene e delle magre dei corsi d'acqua. *Istituto Poligrafico dello Stato*, 8, pp.107–117.

Gikas, G.D., Yiannakopoulou, T. & Tsihrintzis, V.A., 2005. Modeling of nonpoint-source pollution in a Mediterranean drainage basin. *Environmental Modelling and Assessment*, 11(3), pp.219–233.

Gitau, M.W., 2003. *A Quantitative Assessment of BMP Effectiveness for Phosphorus Pollution Control: The Town Brook Watershed, NY*. The Pennsylvannia State University, Pennsylvannia, USA.

Githui, F. & Thayalakumaran, T., 2011. The effect of discretization of hydrologic response units on the performance of SWAT model in simulating flow and

evapotranspiration. *19th International Congress on Modelling and Simulation*, (December), pp.3412–3418.

Gong, Y. et al., 2010. Effect of Watershed Subdivision on SWAT Modeling with Consideration of Parameter Uncertainty. *Journal of Hydrologic Engineering*, 15(12), pp.1070–1074.

Goodrich, D.C., 1992. An Overview of the USDA-ARS Climate Change and Hydrology Program and Analysis of Model Complexity as a Function of Basin Scale. In *Proceedings of the Workshop on the Effects of Global Climate Change on Hydrology and Water Resources at Catchment Scale*. Tsukuba, Japan, pp. 233–242.

Goodrich, D.C., Woolhiser, D.A. & Sorooshian, S., 1988. Model complexity required to maintain hydrologic response. In S. A. Abt & J. Gessler, eds. *Proceedings ASCE National Conference on Hydraulic Engineering*. Colorado Springs CO, USA, pp. 431–463.

Gosain, A.K., Rao, S. & Basuray, D., 2006. Climate change impact assessment on hydrology of Indian river basins. *Current Science*, 90(3), pp.346–353.

Graham, D.N. & Butts, M.B., 2005. Flexible integrated watershed modeling with MIKE SHE. In V. P. Singh & D. K. Frevert, eds. *Watershed Models*. CRC Press, p. 678.

Guertin, D.P. et al., 2008. Automated Geospatial Watershed Assessment (AGWA): A GIS-Based Tool for Watershed Assessment and Planning. In *Soil and Water Conservation Society Annual Conference*. Tucson, AZ.

Hammond, R. & McCullagh, P.S., 1989. *Quantitative techniques in geography: an introduction*, Oxford: Clarendon Press.

Han, J.-C. et al., 2014. Effects of watershed subdivision level on semi-distributed hydrological simulations: case study of the SLURP model applied to the Xiangxi River watershed, China. *Hydrological Sciences Journal*, 59(1), pp.108–125.

Hao, F.H., Zhang, X.S. & Yang, Z.F., 2004. A distributed nonpoint source pollution model: Calibration and validation in the Yellow River basin. *Journal of Environmental Sciences*, 16(4), pp.646–650.

Harvey, D., 1967. Models of the evolution of spatial patterns in human geography. In R.

J. Chorley & P. Haggett, eds. *Models in Geography*. London: Methuen & Co. Ltd., pp. 549–597.

Haverkamp, S. et al., 2003. Subwatershed spatial analysis tool: Discretization of a distributed hydrologic model by statistical criteria. *Journal Of The American Water Resources Association*, 38(6), pp.1723–1733.

Hawkins, R.H., 1979. Runoff curve numbers from partial area watersheds. *Journal of Irrigation and Drainage Engineering - ASCE*, 120(3), pp.573–590.

Haykin, S., 1999. *Neural Networks, a comprehensive foundation*, New Jersey: Prentice Hall.

Hilberts, A.G.J. et al., 2007. Low-dimensional modeling of hillslope subsurface flow: relationship between rainfall, recharge, and unsatu- rated storage dynamics. *Water Resources Research*, 43(3).

Hobson, A.N., 2005. *Use of a stochastic weather generator in a watershed model for streamflow simulation*. University of Colorado, Boulder.

Hromadka, T. V., 1986. *San Bernardino county Hydrology Manual,* Irvine, California.

Huang, M. et al., 2006. A modification to the Soil Conservation Service curve number method for steep slopes in the Loess Plateau of China. *Hydrological Processes*, 20(3), pp.579–589.

Huggins, L.F. & Monke, E.J., 1966. *The mathematical simulation of the hydrology of small watersheds. Technical Report No. 1*, West Lafayette, Indiana.

Hunt, R.J. & Steuer, J.J., 2000. *Simulation of the recharge area for Federick Spring, Dane County, Wisconsin. Water-Resources Investigations Report 00–4172.*, Middleton, Wisconsin.

Jakeman, A.J. & Hornberger, G.M., 1993. How much complexity is warranted in a rainfall-runoff model? *Water Resources Research*, 29(8), pp.2637–2649.

Jakeman, A.J. & Hornberger, G.M., 1993. How much complexity is warranted in a rainfall-runoff model? *Water Resources Research*, 29(8), pp.2637–2649.

Jayatilaka, C.J., Storm, B. & Mudgway, L.B., 998. Simulation of water flow on irrigation bay scale with MIKE SHE. *Journal of Hydrology1*, 208(2), pp.108–130.

Jha, M. et al., 2004. Effect of Watershed Subdivision on SWAT Flow, Sediment, and Nutrient Predictions. *Journal of the American Water Resources Association*, 40(3), pp.811–825. Available at: http://doi.wiley.com/10.1111/j.1752-1688.2004.tb04460.x.

Julien, P.Y. & Saghafian, B., 1991. *CASC2D user's manual : a two-dimensional watershed rainfall-runoff model*, Colorado.

Kalin, L., Govindaraju, R.S. & Hantush, M.M., 2003. Effect of geomorphologic resolution on modeling of runoff hydrograph and sedimentograph. *Journal of Hydrology*, 276(1–4), pp.89–111.

Kalin, L. & Hantush, M.M., 2003. *Evaluation of sediment transport models and comparative application of two watershed models*, Cincinnati, Ohio.

Kamp, R.G. & Savenije, H.H.G., 2007. Hydrological model coupling with ANNs. *Hydrology and Earth System Sciences*, 11, pp.1869–1881.

Kang, M.S. et al., 2006. Applying SWAT for TMDL programs to a small watershed containing rice paddy fields. *Agricultural Water Management*, 79(1), pp.72–92.

Karvonen, T. et al., 1999. A hydrological model for predicting runoff from different land use areas. *Journal of Hydrology*, 217(3–4), pp.253–265.

Kaur, R. et al., 2004. Comparison of a subjective and a physical approach for identification of priority areas for soil and water management in a watershed: A case study of Nagwan watershed in Hazaribagh District of Jharkhand, India. *Environmental Modeling & Assessment*, 9(2), pp.115–127.

Kawkins, R.H., 1978. Runoff curve number relationships with varying site moisture. *Journal of Irrigation and Drainage Engineering*, 104, pp.389–398.

Khan, U., Tuteja, N. & Sharma, A., 2011. Evaluation of hydrologic response units by soil moisture simulations, in-situ observations and high resolution aerial photographs. *Geophysical Research Abstracts*, 13.

Khan, U., Tuteja, N.K. & Sharma, A., 2013. Delineating hydrologic response units in large upland catchments and its evaluation using soil moisture simulations. *Environmental Modelling & Software*, 46, pp.142–154.

Kite, G.W., 1994. Hydrological modelling using remotely sensed data and geographic

information systems. *Trends in Hydrology*, 1, pp.191–208.

Kite, G.W., 1997. *Manual for the SLURP hydrological model*, Saskatoon, Canada.

Kottegoda, N.T., 1980. *Stochastic water resources technology*, Hong Kong: McMillan Press.

Koussis, A.D., 2009. Assessment and review of the hydraulics of storage flood routing 70 years after the presentation of the Muskingum method. *Hydrological Sciences Journal*, 54(1), pp.43–61.

Koussis, A.D., 2010. Reply to the Discussion of "Assessment and review of the hydraulics of storage flood routing 70 years after the presentation of the Muskingum method" by M. Perumal. *Hydrological Sciences Journal*, 55(8), pp.1431–1441.

Koutsoyiannis, D., 2011. *Design of Urban Sewer Networks* Edition 4., National Technical University of Athens, Athens.

Koutsoyiannis, D. et al., 2008. *National Programme for the Management and Protection of Water Resources*, Athens.

Kowalik, T. & Walega, A., 2015. Estimation of CN Parameter for Small Agricultural Watersheds Using Asymptotic Functions. *Water*, 7, pp.939–955.

Kuczera, G. & Parent, E., 1998. Monte Carlo assessment of parameter uncertainty in conceptual catchment models: the Metropolis algorithm,. *Journal of hydrology*, 211, pp.69–85.

Kumar, S. & Merwade, V., 2009. Impact of watershed subdivision and soil data resolution on swat model calibration and parameter uncertainty. *Journal of the American Water Resources Association*, 45(5), pp.1179–1196.

Lacroix, M.P., 1999. *Spatial scale and hydrological model response*. University of Saskatchewan.

Lajili-Ghezal, L., 2004. Use of the KINEROS model for predicting runoff and erosion in a tunisian semi-arid region. *Journal of Water Science*, 17(2), pp.227–244.

Leavesley, G.H. et al., 1983. *Precipitation-Runoff Modeling System: User's Manual.*, Denver, Colorado, USA.

Leavesley, G.H., Markstrom, S.L. & Viger, R.G., 2000. USGS modular modeling (MMS) - precipitation-runoff modeling system (PRMS). In V. P. Singh & D. K. Frevert, eds. *Watershed models*. Boca Raton, Florida: Taylor and Francis, p. 678.

Leavesley, G.H. & Stannard, L.G., 1995. The precipitation-runoff modeling system-PRMS. In V. P. Singh, ed. *Computer models of watershed hydrology*. Highlands Ranch, Colorado: Water Resources Publication, p. 1144.

Li, Z. et al., 2014. Effect of watershed subdivision on confluence parameter. *Journal of Hohai University*, 42(4), pp.283–288.

Di Luzio, M. & Arnold, J.G., 2004. Formulation of a Hybrid Calibration Approach for a Physically Based Distributed Model With NEXRAD Data Input. *Journal of Hydrology*, 298(1–4), pp.136–154.

Lyon, S.W. & Troch, P.A., 2007. Hillslope subsurface flow similarity: real-world tests of the hillslope Péclet number. *Water Resources Research*, 43(7).

Madsen, H., 2003. Parameter estimation in distributed hydrological catchment modelling using automatic calibration with multiple objectives. *Advances in Water Resources*, 26, pp.205–216.

Mahabir, C., Hicks, F.E. & Fayek, A.R., 2003. Application of fuzzy logic to forecast seasonal runoff. *Hydrological Processes*, 17, pp.3749–3762.

Mamillapalli, S. et al., 1991. Effect of Spatial Variability on Basin Scale Modeling. , (1994).

Manguerra, H.B. & Engel, B. a., 1998. Hydrologic Parameterization of Watersheds for Runoff Prediction Using SWAT. *Journal of the American Water Resources Association*, 34(5), pp.1149–1162. Available at: http://doi.wiley.com/10.1111/j.1752-1688.1998.tb04161.x.

Mazi, K. et al., 2004a. A groundwater-based, objective-heuristic parameter optimisation method for the PRMS model: The Akrotiri Basin, Cyprus application. *Journal of Hydrology*, 290(3), pp.243–258.

Mazi, K. et al., 2004b. Erratum: A groundwater-based, objective-heuristic parameter optimisation method for the PRMS model: The Akrotiri Basin, Cyprus application. *Journal of Hydrology*, 299(1–2), pp.160–161.

Melone, F., Barbetta, S. & Diomede, T., 2005. Review and selection of hydrological models – Integration of hydrological models and meteorological inputs. *Contract No. 12*.

Merheb, M. et al., 2016. Hydrological Response Characteristics of Mediterranean Catchments at Different Time Scales: A Meta-Analysis. *Hydrological Sciences Journal*, 61(14), pp.2520–2539.

Miller, S.N. et al., 2007. The Automated Geospatial Watershed Assessment Tool. *Environmental Modelling & Software*, 22, pp.365–377.

Mishra, A., Froebrich, J. & Gassman, P.W., 2007. Evaluation of the SWAT model for assessing sediment control structures in a small watershed in India. *Transactions of the ASAE*, 50(2), pp.469–477.

Mishra, A., Singh, R. & Raghuwanshi, N.S., 2005. Development and application of an integrated optimization-simulation model for major irrigation projects. *Journal of Irrigation and Drainage Engineering*, 131(6), pp.504–513.

Molnár, D.K. & Julien, P.Y., 2000. Grid-Size Effects on Surface Runoff Modeling. *Journal of Hydrologic Engineering*, 5(1), pp.8–16.

Montgomery, D.R. & Dietrich, W.E., 2002. Runoff generation in a steep, soil-mantled landscape. *Water Resources Management*, 38(9), p.1168.

Moriasi, D.N. et al., 2007. Model evaluation guidelines for systematic quantification of accuracy in watershed simulations. *Transactions of the American Society of Agricultural and Biological Engineers*, 50, p.885–900.

Muleta, M.K. & Nicklow, J.W., 2005. Sensitivity and uncertainty analysis coupled with automatic calibration for a distributed watershed model. *Journal of Hydrology*, 306, pp.127–145.

Muleta, M.K., Nicklow, J.W. & Bekele, E.G., 2007. Sensitivity of a Distributed Watershed Simulation Model to Spatial Scale. *Journal of Hydrologic Engineering*, 12(2), pp.163–172.

Nalbantis, I. et al., 2011. Holistic versus monomeric strategies for hydrological modelling of human-modified hydrosystems. *Hydrology and Earth System Sciences*, 15(3), pp.743–758.

Nash, J.E. & Sutcliffe, J. V., 1970. River flow forecasting through conceptual models part I - A discussion of principles. *Journal of Hydrology*, 10(3), pp.282–290.

Neitsch, S.L. et al., 2002. *Soil and Water Assessment Tool Theoretical Documentation, Version 2000*, Temple, Texas, USA.

Neitsch, S.L. et al., 2005. *Soil and Water Assessment Tool Theoretical Documentation, Version 2005*, Temple, Texas, USA.

Norris, G.R., 1992. *A proccess for interfacing a hydrologic model to a geographic information system*. Oklahoma State University - Stillwater.

Norris, G.R. & Haan, C.T., 1993. Impact of subdivining watersheds on estimated hydrographs. *Americal Society of Agricutlural Engineers*, 9(5), pp.443–445.

Nour, M.H. et al., 2008. Effect of watershed subdivision on water-phase phosphorus modelling: An artificial neural network modelling application. *Journal of Environmental Engineering and Science*, 7(S1), pp.95–108.

NRCS, 1972. *SCS National Engineering Handbook, Section 4*, Washington, DC.

NRCS, U., 2004. *National Engineering Handbook: Part 630—Hydrology.*, Washington, USA.

Ogden, F.L. et al., 2001. GIS and distributed watershed models. II: Modules, interfaces, and models. *Journal of Hydrologic Engineering*, 6(6), pp.515–523.

Oogathoo, S., 2006. *Runoff simulation in the Canagagigue Creek watershed using the MIKE SHE model*. Montreal, Canada: McGill University.

Pai, N., Saraswat, D. & Srinivasan, R., 2012. Field_SWAT: A tool for mapping SWAT output to field boundaries. *Computers and Geosciences*, 40, pp.175–184. Available at: http://dx.doi.org/10.1016/j.cageo.2011.07.006.

Pollacco, J.A.P., Mohanty, B.P. & Efstratiadis, A., 2013. Weighted Objective Function Selector Algorithm for Parameter Estimation of SVAT Models with Remote Sensing Data. *Water Resources Research*, 49(10), pp.6959–6978.

Ponce, V.M. & Hawkins, R.H., 1996. Runoff Curve Number: has is reach maturity? *Journal of Hydrologic Engineering*, 1(1), pp.11–19.

Refsgaard, J.C., 1997. Parameterisation, calibration and validation of distributed

hydrological models. *Journal of Hydrology*, 198(1–4), pp.69–97.

Refsgaard, J.C., 1996. Terminology, modelling protocol and classification of hydrological model codes. In M. B. Abbott & J. C. Refsgaard, eds. *Distributed Hydrological Modelling*. pp. 17–39.

Reggiani, P. et al., 1999. A unifying framework for watershed thermodynamics: constitutive relationships. *Advances in Water Resources*, 23(1), pp.15–39.

Reggiani, P. & Rientjes, T.H.M., 2005. Flux parameterization in the representative elementary watershed approach: application to a natural basin. *Water Resources Research*, 41(4), pp.1–18.

Reggiani, P., Sivapalan, M. & Hassanizadeh, S.., 2000. Conservation equations governing hillslope responses: exploring the physical basis of water balance. *Water Resources Research*, 36(7), pp.1845–1863.

Reggiani, P., Sivapalan, M. & Hassanizadeh, S.M., 1998. A unifying framework for watershed thermodynamics: balance equations for mass, momentum, energy and entropy, and the second law of thermodynamics. *Advances in Water Resources*, 22(4), pp.367–398.

Rennó, C.D. et al., 2008. HAND, a new terrain descriptor using SRTM-DEM: Mapping terra-firme rainforest environments in Amazonia. *Remote Sensing of Environment*, 112(19), pp.3469–3481.

Rouhani, H., Willems, P. & Feyen, J., 2009. Effect of watershed delineation and areal rainfali distribution on runoff prediction using the SWAT modei Hamed Rouhani , Patrick Willems and Jan Feyen. *Hydrology Research*, 40(6), pp.505–519.

Rozos, E. et al., 2004. Calibration of a semi-distributed model for conjunctive simulation of surface and groundwater flow. *Hydrological Sciences Journal*, 49(5), pp.819–842.

Rozos, E. & Koutsoyiannis, D., 2006. A multicell karstic aquifer model with alternative flow equations. *Journal of Hydrology*, 325(1–4), pp.340–355.

Rozos, E. & Koutsoyiannis, D., 2005. Application of the Integrated Finite Difference Method in groundwater flow, EGU General Assembly. In *EGU General Assembly 2005, Geophysical Research Abstracts*.

Sahoo, G.B., Ray, C. & DeCarlo, E.H., 2006. Calibration and validation of a physically distributed hydrological model, MIKE SHE, to predict streamflow at high frequency in a flashy mountainous Hawaii stream. *Journal of Hydrology*, 327(1–2), pp.94–109.

Saleh, A. & Du, B., 2004. Evaluation of SWAT and HSPF within BASINS program for the Upper North Bosque River watershed in Central Texas. *Transactions of the ASAE*, 47(4), pp.1039–1049.

Santhi, C. et al., 2006. A modeling approach to evaluate the impacts of water quality management plans implemented in a watershed in Texas. *Environmental Modeling & Assessment*, 21(8), pp.1141–1157.

Sanzana, P. et al., 2013. Computer-assisted mesh generation based on hydrological response units for distributed hydrological modeling. *Computers & Geosciences*, 57, pp.32–43.

Sasowsky, K.C. & Gardner, T.W., 1991. Watershed configuration and geographic information system parameterization for SPUR model hydrologic simulations. *Journal of The American Water Resources Association*, 27(1), pp.7–18.

Savenije, H.H.G., 2010. HESS Opinions "Topography driven conceptual modelling (FLEX-Topo)." *Hydrology and Earth System Sciences*, 14(12), pp.2681–2692.

Scharffenberg, B., 2008. Introduction to HEC-HMS. Technical workshop on watershed modeling with HEC-HMS. (US Army Corps of Engineers, Hydrologic Engineering Center's Hydrologic Modeling System).

Schneiderman, E.M. et al., 2007. Incorporating variable source area hydrology into a curve-number-based watershed model. *Hydrological Processes*, 21, pp.3420–3430.

Setegn, S.G., Srinivasan, R. & Dargahi, B., 2008. Hydrological Modelling in the Lake Tana Basin, Ethiopia Using SWAT Model. *The Open Hydrology Journal*, 2(1), pp.49–62.

Sharpley, A.N. & Williams, J.R., 1990. *EPIC—Erosion/Productivity Impact Calculator: 1. Model Documentation*, Washington, DC: US Department of Agriculture Technical Bulletin No. 1768. US Government Printing Office.

Shrestha, S. et al., 2005. Evaluation of annualized agricultural nonpoint source model

for a watershed in the Siwalik Hills of Nepal. *Environmental Modelling & Software*, 21(7), pp.961–975.

Silvestro, F. et al., 2015. Uncertainty Reduction and Parameter Estimation of a Distributed Hydrological Model with Ground and Remote-Sensing Data. *Hydrology and Earth System Science*, 19, pp.1727–1751.

Singh, R., Subramanian, K. & Refsgaard, J.C., 1999. Hydrological modelling of a small watershed using MIKE SHE for irrigation planning. *Agricultural Water Management*, 41(3), pp.149–166.

Singh, V.P., 1995. *Computer Models of Watershed Hydrology*, Colorado, USA: Water Resources Publications.

Singh, V.P., 1999. *Elementary hydrology*, Englewood Cliffs, NJ: Prentice- Hall.

Singh, V.P. et al., 2006. Hydrologic modeling inventory: Cooperative research effort. *Journal of Irrigation and Drainage Engineering*, 132(2), pp.98–103.

Singh, V.P., 1988. *Hydrologic Systems, Volume I: Rainfall-Runoof Modeling*, Englewood Cliffs, New Jersey: Prentice-Hall Inc.

Singh, V.P., 1989. *Hydrologic Systems, Volume II: Watershed Modeling*, Englewood Cliffs, New Jersey: Prentice-Hall Inc.

Singh, V.P. & Woolhiser, D.A., 2002. Mathematical modeling of watershed hydrology. *Journal of Hydrologic Engineering*, 7(4), pp.270–292.

Soulis, K.X. & Valiantzas, J.D., 2012. SCS-CN Parameter Determination Using Rainfall-Runoff Data in Heterogeneous Watersheds—The two-CN System Approach. *Hydrology and Earth System Science*, 16, pp.1001–1015.

Srinivasan, R. et al., 2000. *Hydrologic unit model for the United States (HUMUS)*, Temple, TX.

Steuer, J.J. & Hunt, R.J., 2001. *Use of a watershed modeling approach to assess hydrologic effects of urbanization urbanization, North Folk Pheasant Branch near Middleton, Wisconsin. Water Resources Investigations Report 01-4113*, Middleton, Wisconsin.

Stone, M.C. et al., 2001. Impacts of climate change on Missouri river basin water yield.

*Journal of the American Water Resources Association*, 37(5), pp.1119–1130.

Sui, J., 2005. Estimation of design flood hydrograph for an ungaged watershed. *Water Resources Management*, 19, pp.813–830.

Suttles, J.B. et al., 2003. Watershed-scale simulation of sediment and nutrient loads in Georgia coastal plain streams using the annualized AGNPS model. *Transactions of the ASAE*, 46(5), pp.1325–1335.

Tao, T. & Kouwen, N., 1989. Remote sensing and fully distributed modelling for flood forecasting B. C. Yen, ed. *Journal of Water Resources Planning and Management*, 115(6), pp.809–823.

Tegos, A., Efstratiadis, A. & Koutsoyiannis, D., 2013. A parametric model for potential evapotranspiration estimation based on a simplified formulation of the Penman-Monteith equation. In S. G. Alexandris, ed. *Evapotranspiration - An Overview*. InTech, p. 24.

Thieken, A.H. et al., 1999. Scaling input data by GIS for hydrological modelling. *Hydrological Processes*, 13(4), pp.611–630.

Thiemann, M. et al., 2001. Bayesian recursive parameter estimation for hydrologic models. *Water Resources Research*, 37(10), pp.2521–2536.

Thompson, J.R. et al., 2004. Application of the coupled MIKE SHE/MIKE 11 modelling system to a lowland wet grassland in southeast England. *Journal of Hydrology2*, 293(2), pp.151–179.

Thomson, A.M. et al., 2003. Simulated impacts of El Nino/southern oscillation on United States water resources. *Journal of the American Water Resources Association*, 39(1), pp.137–148.

Tripathi, M.P., Raghuwanshi, N.S. & Rao, G.P., 2006. Effect of watershed subdivision on simulation of water balance components. *Hydrological Processes*, 20(5), pp.1137–1156.

Tsoukalas, I. et al., 2016. Surrogate-enhanced evolutionary annealing simplex algorithm for effective and efficient optimization of water resources problems on a budget. *Environmental Modelling & Software*, 77, pp.122–142.

USACE, 2013. Hydrologic Modeling System (HEC-HMS). *Hydrologic Engineering*

*Center*.

USDA, 1986. *Urban Hydrology for Small Watersheds, TR-55* Second Edi.,

USEPA, 2015. BASINS 4.1 (Better Assessment Science Integrating point & Non-point Sources) Modeling Framework. *National Exposure Research Laboratory, PTP, North Carolina*.

USEPA, 2008. *Hydrological Simulation Program - FORTRAN (HSPF)*,

USGS, 2014. Shuttle Radar Topography Mission, 1 Arc Second scene. *Global Land Cover Facility, University of Maryland, College Park, Maryland*.

Valeo, C. et al., 2007. Climate change impacts in the Elbow River watershed. *Canadian Water Resources Journal*, 32(4), pp.285–302.

Verma, S. et al., 2017. A Revisit of NRCS-CN Inspired Models Coupled with RS and GIS for Runoff Estimation. *Hydrological Sciences Journal*, 62(12), pp.1891–1930.

Vrugt, J.A. et al., 2004. Inverse modeling of large-scale spatially distributed vadose zone properties using global optimization. *Water Resources Research*, 40(W06503).

Vrugt, J.A. et al., 2002. oward improved identifiability of hydrologic model parameters: the information content of experimental data. *Water Resources Research*, 38(2), p.1312.

Wagener, T., Boyle, D.P., et al., 2001. A framework for development and application of hydrological models. *Hydrology and Earth System Sciences*, 5(1), pp.13–26.

Wagener, T., Boyle, D.P., et al., 2001. A framework for development and application of hydrological models. *Hydrology and Earth System Science*, 5(1), pp.13–26.

Wheater, H.S., Bishop, K.H. & Beck, M.B., 1986. he Identification of Conceptual Hydrological Models for Surface Water Acidification. *Hydrological Processes*, 1, pp.89–109.

White, E.D. et al., 2011. Development and application of a physically based landscape water balance in the SWAT model. *Hydrological Processes*, 25(6), pp.915–925.

White, E.D. et al., 2009. Improving daily water yield estimates in the Little River watershed: SWAT adjustments. *Transactions of the American Society of*

*Agricultural and Biological Engineers*, 52(1), pp.69–79.

Winchell, M. et al., 2013. *ArcSwat Interface For SWAT 2012: Users Guide*, Temple, Texas, USA.

Wingfield, M.T., 2008. Effect of watershed of watershed subdivision and parameter selection on modeling results. , p.114.

Wischmeier, W.H. & Smith, D.D., 1978. *Predicting rainfall erosion losses. Agricultural Handbook No. 537*, Washington, D.C.

Wood, E.F. et al., 1988. Effects of spatial variability and scale with implications to hydrologic modeling. *Journal of Hydrology*, 102(1–4), pp.29–47.

Woolhiser, D.A., Smith, R.E. & Goodrich, D.C., 1990. *KINEROS, A Kinematic Runoff and Erosion Model: Documentation and User Manual*,

Xu, Y. et al., 2011. Watershed discretization based on multiple factors and its application in the Chinese Loess Plateau. *Hydrology and Earth System Sciences*, 8(5), pp.9063–9087.

Yates, D.N., Warner, T.T. & Leavesley, G.H., 2000. Prediction of a flash flood in complex terrain. Part II: A comparison of flood discharge simulation using rainfall input from radar, a dynamic model, and an automated algorithmic system. *Journal of American Meteorological Society*, 39(6), pp.815–25.

Young, R.A., Onstad, C.A. & Bosch, D.D., 1995. AGNPS: An agricultural nonpoint source model. In V. P. Singh, ed. *Computer models of watershed hydrology*. Highlands Ranch, Colorado: Water Resources Publications, p. 1130.

Yuan, Y., Bingner, R.L. & Rebich, R.A., 2001. Evaluation of AnnAGNPS on Mississippi Delta MSEA watersheds. *Transactions of the ASAE*, 44(5), pp.1183–1190.

Zadeh, L.A., 1965. Fuzzy sets. *Information and Control*, 8(3), pp.338–353.

Zhang, H.L. et al., 2013. The effect of watershed scale on HEC-HMS calibrated parameters: A case study in the Clear Creek watershed in Iowa, US. *Hydrology and Earth System Sciences*, 17(7), pp.2735–2745.

Zhang, W. & Montgomery, D.R., 1994. Digital elevation model grid size, landscape

representation, and hydrologic simulations. *Water Resources Research*, 30(4), pp.1019–1028.

Zhang, Z. et al., 2004. Use of Next Generation Weather Radar Data and Basin Disaggregation to Improve Continuous Hydrograph Simulations. *Journal of Hydrologic Engineering*, 9(2), pp.103–115.